University of East Anglia

Dietary isothiocyanates for cancer combination therapy: Synergistic anticancer activity of phenethyl isothiocyanate and dasatinib

Gabriele Strusi

A thesis submitted for the degree of Doctor of Philosophy

University of East Anglia

Norwich Medical School

July 2023

Declaration

I declare that the thesis entitled “Dietary isothiocyanates for cancer combination therapy: Synergistic anticancer activity of phenethyl isothiocyanate and dasatinib” was completed by myself unless otherwise acknowledged. The present thesis has been submitted to the University of East Anglia for the degree of Doctor of Philosophy and has not been submitted in an application for another degree or qualification in this or any other university or institution.

Parts of this thesis have been published and are referenced in the List of Publications.

Word count: 55,635

Gabriele Strusi

Abstract

Combination therapies exploit multiple drugs to synergistically target key pathways to reduce tumour growth and metastatic potential. Isothiocyanates (ITCs) have been shown to have anticancer capabilities and may complement the anticancer activity of clinically approved chemotherapeutic agents. Hepatocellular carcinoma (HCC) is the most common type of liver cancer, which is second most lethal tumour. Thus, there is a continuous need for the development of new therapeutic solutions, and the use of ITCs in combination therapy seems to be a promising strategy for treatment of HCC progression.

The research presented in this thesis aimed to assess the potential of phenethyl isothiocyanate (PEITC) to improve the activity of dasatinib in HCC. A murine syngeneic subcutaneous model was used to assess the combination efficacy *in vivo* and the MTT cell viability assay was used to assess the anticancer effect *in vitro*. Furthermore, the effect on HCC metastatic potential and angiogenesis was assessed using adhesion, scratch wound healing, invasion, colony formation, chorioallantoic membrane (CAM), and yolk sac membrane assays. Flow cytometry, RT-qPCR, HPLC and Western blot were used to elucidate the mechanism of action of the drug combination.

PEITC and dasatinib showed a synergistic anticancer effect *in vitro* and *in vivo*. By inducing oxidative stress, through the production of reactive oxygen species (ROS), PEITC and dasatinib combination promoted the formation of a premature CDK1-Cyclin B1 complex, leading to mitotic catastrophe and activating oxeiptosis, a novel programmed cell death. Furthermore, the inhibition of FAK/STAT3 signalling led to increased E-cadherin expression and diminished secretion of pro-angiogenic factors, reducing HCC metastatic potential.

Phenethyl isothiocyanate can complement dasatinib's action in treating HCC, inducing cell cycle arrest and oxeiptosis and decreasing metastatic potential and tumour-induced angiogenesis. This thesis highlights the role of ITCs in cancer therapy to complement clinically approved chemotherapeutic drugs.

Acknowledgements

I express my gratitude to my supervisors, Professor Yongping Bao and Professor Andrea Münsterberg, for their support and the invaluable opportunity they provided me to develop my scientific thinking and shape the researcher I aspired to become.

I would like to extend special thanks to Dr Rachel Hurst for meticulously proofreading this manuscript and offering indispensable comments and advice. Her contributions have significantly enhanced the quality and clarity of this work.

I am grateful to Jasmine, Catherine, and Chris, whose unwavering support has been indispensable in facilitating the research conducted at the BCRE laboratory. Their contributions have been instrumental in the successful execution of this project. I extend my gratitude to the group members Wei Wang and Qi Wang for their lab support.

I would like to express my heartfelt appreciation to the Cancer Prevention Research Trust London for generously funding this project. Their financial support has played a pivotal role in the realisation of this research.

I am indebted to my family for their constant love and unwavering support, which have been the pillars that have consistently enriched my life and guided me on this journey, even from places we don't fully comprehend. Their belief in me has been a source of inspiration and motivation.

A special acknowledgment goes to my future fiancée, Caterina, for her boundless love and incredible support, which have extended beyond personal boundaries and even reached the laboratory. Her unwavering encouragement has made the writing of this thesis possible, and her presence has been a source of strength throughout this process.

List of Publications

Strusi, G., Suelzu, C.M., Horwood, N., Munsterberg, E.A., Bao, Y. Phenethyl isothiocyanate and dasatinib combination synergistically reduces hepatocellular carcinoma growth via cell cycle arrest and oxeiptosis.
Frontiers in Pharmacology, 2023. *https://doi.org/10.3389/fphar.2023.1264032*

Strusi, G., Suelzu, C.M., Weldon S., Giffin J., Munsterberg, E.A., Bao, Y. Combination of phenethyl isothiocyanate and dasatinib inhibits hepatocellular carcinoma metastatic potential through FAK/STAT3/Cadherin signalling and reduction of VEGF secretion. Pharmaceutics, 2023. *https://doi.org/10.3390/pharmaceutics15102390*

Access Condition and Agreement

Table of Contents

List of Figures

List of Tables

List of Abbreviations

AIF	Apoptosis inducing factor
AITC	Allyl isothiocyanate
AKR1C1	Aldo-keto reductase family 1 member C1
Ang-1/2	Angiopoietin 1/2
ANOVA	Analysis of variance
ARE	Antioxidant responsive element
BITC	Benzyl isothiocyanate
CAM	Chorioallantoic membrane
CDK	Cyclin-dependent kinase
Chk2	Checkpoint kinase 2
CI	Combination index
CM	Conditioned medium
DAPI	4′,6-diamidino-2-phenylindole
DCFDA	Dichlorofluorescein diacetate
DLS	Dynamic light scattering
DMEM	Dulbecco's Modified Eagle Medium
DMSO	Dimethyl sulfoxide
DNMT	DNA methyltransferase
DPX	Dibutylphthalate polystyrene xylene
DSBs	Double strand breaks
DSPC	1,2-distearoyl-sn-glycero-3-phosphocholine
DTPA	Diethylenetriaminepentaacetic acid
DTT	Dithiothreitol
ECM	Extracellular matrix
EDTA	Ethylenediaminetetraacetic acid
ELISA	Enzyme-linked immunosorbent assay
EMA	European Medicines Agency
EMT	Epithelial-mesenchymal transition
EPG	L-α-phosphatidyl-glycerol
ERK	Extracellular signal-regulated kinases

ESP	Epithiospecifier protein
FA	Focal adhesion
FAK	Focal adhesion kinase
FBS	Fetal bovine serum
FDA	Food and Drug Administration
FGFR	Fibroblast growth factor receptor
FIH	Factor inhibiting HIF1
FITC	Fluorescein isothiocyanate
GL	Glucosinolate
GSH	Glutathione
GSSG	Glutathione disulfide
GST	Glutathione S-transferase
HAT	Histone acetylase
HVB	Hepatitis B virus
HVC	Hepatitis C virus
HCC	Hepatocellular carcinoma
HDAC	Histone deacetylase
HEPES	N-2-hydroxyethylpiperazine-N'-2-ethanesulfonic acid
HPLC	High performance liquid chromatography
HRP	Horseradish peroxidase
HUVECs	Human umbilical vein endothelial cells
ITC	Isothiocyanate
Keap1	Kealch-like ECH-associated protein 1
MAPK	Mitogen-activated protein kinase
MMP	Matrix metalloproteinases
MTT	3-(4,5-Dimethylthiazol-2-yl)-2,5-diphenyltetrazolium bromide
NAC	N-acetyl cysteine
NADH	Nicotinamide adenine dinucleotide (NAD) + hydrogen (H)
NEM	N-ethylmaleimide
NF-κB	Nuclear factor κ-light-chain-enhancer of activated B cells
NNK	Nicotine-derived nitrosamine ketone
NOAEL	No-observed-adverse-effect-level

NOEL	No-observed-effect-level
NPs	Nanoparticles
NQO1	NAD(P)H quinone reductase 1
Nrf2	Nuclear factor erythroid 2-related factor 2
OCT	Optimal cutting temperature
PARP	Poly (ADP-ribose) polymeras
PBS	Phosphate buffered saline
PCa	Prostate cancer
PDc	Phenethyl isothiocyanate and dasatinib combination
PDGF	Platelet-derived growth factor
PEITC	Phenethyl isothiocyanate
PHD	Prolyl hydroxylases
PlGF	Placental growth factor
PSA	Prostate-specific antigen
PVDF	Polyvinylidene fluoride
ROS	Reactive oxygen species
RT-qPCR	Real time quantitative polymerase chain reaction
RTK	Receptor tyrosine kinase
SEM	Standard error of mean
SFN	Sulforaphane
STAT3	Signal transducer and activator of transcription 3
TAMRA	5-Carboxytetramethylrhodamine
TBHP	Tert-Butyl hydroperoxide
TBS	Tris-buffered saline
Tie-2	Tyrosine-protein kinase receptor
TKI	Tyrosine kinase inhibitor
TNF-α	Tumour necrosis factor α
TrxR1	Thioredoxin reductase
VEGF	Vascular endothelial growth factor
VEGFR	Vascular endothelial growth factor receptor
WHO	World Health Organization
YSM	Yolk sac membrane

Chapter 1: Introduction

1.1 Cancer and chemoprevention

Cancer is the second leading cause of death worldwide; in 2020, it led to nearly ten million deaths, and this number is predicted to increase over time as reported by the World Health Organisation (WHO) [1]. The main causes of cancer development may include factors, such as are lack of physical activity, unhealthy diet, and use of tobacco and alcohol. Indeed, the most influential cause is the environmental exposure to carcinogens [1]. Carcinogens lead to a multistep process with genetic alterations that culminate in cell transformation. The result of this process is the formation of a group of cells that are distinguishable from normal ones because of a set of acquired biological capabilities [2]. Tumour cells can produce their own growth signals to avoid the mechanisms that regulate the cell cycle, activate the invasive capacity, avoid senescence through increased telomerase activity, induce angiogenesis to help the tumour expansions and avoid cell programmed death [2]. The transformation process can be divided into three fundamental steps: initiation, promotion, and progression. The initiation step consists of different intra- and extracellular mechanisms that start from an insult or contact with a carcinogenic agent that may cause a mutation. Consequently, the cell tries to internalise the carcinogen for metabolisation or detoxification [3]. The promotion step is reversible and slow, during which neoplastic cells grow with the formation of a population of precancerous cells [3]. The final progression step is irreversible characterised by the development of a population of cells with invasive capacities [4].

1.1.1 Hepatocellular carcinoma

Hepatocellular carcinoma (HCC) is the most common type of liver cancer, which accounted for around 800 thousand deaths in 2020 as the second most lethal tumour worldwide [5]. Cancer incidence has not changed in the last few decades, and the mortality rate increases every year (**Figure 1.1**). Since 1970, the mortality rate of liver cancer in the UK increased by 228% [6], and only in the last decade has it increased by 40%. More than 6,000 people are diagnosed with liver cancer every year, and the five years survival rate is 13%. The prediction is that there will be 1.3 million death liver cancer-related in 2040 [7]. The only curative treatment modalities are tumour resection and liver transplant at early stages. However, HCC diagnosis usually presents only after admission to the emergency

room due to severe symptoms that indicate an advanced stage of cancer. The first drug approved for the treatment of HCC was sorafenib in 2007, and for a decade it was the only systemic therapy available [7]. Nevertheless, sorafenib showed severe adverse effects and lack of efficacy after treatment interruption, in addition several patients demonstrated both primary and acquired resistance [7].

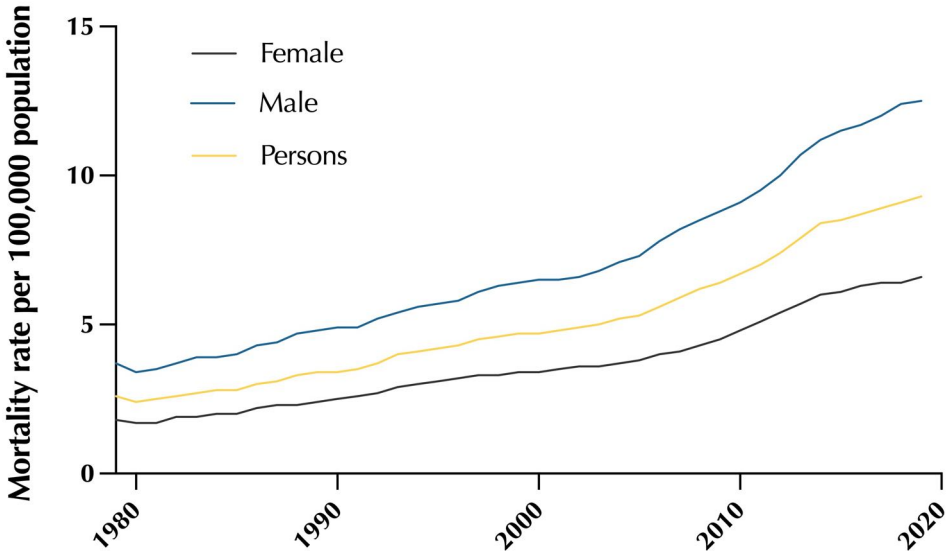

FIGURE 1.1 | Incidence of liver cancer death over time (UK) [6].

1.1.1.1 Risk factors

Risk factors can be categorised into infectious and toxins, behavioural, and underlying conditions. Hepatitis B (HBV) virus is responsible for the initiation of a chronic necro-inflammatory disease that can lead to HCC [5]. HBV DNA is found integrated into the genome of patients affected by HCC and HBV, and the possibility of developing HCC in HBV carriers is around 10-25% in a lifetime with an increased of HCC incidence of 11-fold [8]. On the other hand hepatitis C virus (HVC) increases the risk of HCC development by 10-20 fold [9]. As an RNA virus, HVC is not found integrated into the genome but it is likely that repetitive damage, fibrosis and induced cirrhosis lead to tumour development [5]. Aflatoxin B1 has been recognised as a group 1 carcinogen with an increased risk of HCC of 6-fold, while when combined with HBV infection the risk factor goes to 54-fold [5]. Behavioural factors also have a great impact in the incidence of cancer. Alcohol consumption and cigarette smoking are well known to be associated with increased risk of cancer development and in particular they are associated with increased risk of HCC development of 16 and 70%, respectively [5]. As it will be discussed in the next section, diet has a fundamental

role in chemoprevention, indeed certain type of diets that prefer the consumption of high volumes of vegetables, wholegrains, fish, poultry, with high vitamins and mono-unsaturated fats, have been associated with reduced risk of HCC development [10]. Underlying conditions such as diabetes, obesity and non alcoholic fatty liver disease also have an impact on HCC development [11]. Diabetes can lead to chronic hepatitis and increase up to 4 fold the incidence of HCC [11]. Overweight subjects have a 4 fold increased chance of HCC development [11]. Obesity is often associated with different hepatobiliary diseases such as non-alcoholic fatty liver disease, that can culminate with the development of HCC [11].

1.1.1.2 Driver mutations

As other solid tumours, HCC presents with a series of genetic mutations that confer a number of cancer hallmarks that allow the uncontrolled growth and tumour progression [2]. Some mutations are not responsible for the increased tumorigenesis and are defined "passenger mutations", while the tumorigenic mutations are defined as "driver mutations" [12]. The main driver mutations identified in HCC are found in different genes involved in diverse fundamental cellular processes [12]. Telomere length maintenance, for example, is achieved with a mutation found in TERT, which is the most occurring in HCC tissues [12]. Cell cycle is controlled with mutation in TP53 a well known tumour suppressor, CCND1 involved in cell proliferation, and CDKN2A that regulate the cell cycle [12]. The control of the oxidative stress is achieved with mutations on NFE2L2 (transcriptional regulator) and KEAP1 (proteinase adaptor) [12]. ARID1A and ARID2 are mutate to control chromatin remodelling, and angiogenesis is controlled with mutation of VEGF-A, which is fundamental for the growth of a tumour mass [12]. Several major pathways hare altered in HCC in particular the Wnt-β-catenin signalling pathway is controlled with CTNNb1 and AXIN1 mutations, AKT-mTOR-MAPK pathway with RPS6KA3, PTEN, FGF19, and PI3KCA, mutations while the JAK/STAT signalling JAK1 mutation [12].

1.1.1.3 Cellular origin

The cellular origin of HCC is still debated and different players have been proposed as responsible for the tumour initiation [13]. Hepatocytes represent the most common cellular active type in the liver parenchyma followed by the duct epithelial cells [13]. The duct epithelial cells are hepatic progenitor cells (HPCs) that originate from the

Hering canal which is considered the hepatic stem cells niche [13]. In case of liver damage HPCs emerge from the niche to form new hepatocytes and maintain the normal liver function and structure [13]. Increased expansion of HPCs has been observed in HCC and different studies suggest HPCs as the origin of liver tumours [14]. Indeed, different mice models showed that HPCs are responsible for the formation of masses into the liver [15-17]. By contrast, some researchers ruled out the participation of HPCs in carcinogenesis as the evidences are mainly based on animal models, thereby not easily translatable to humans [14]. More recent studies suggest that HCC may originate directly from adult hepatocytes that after an insult such as genomic damage can differentiate into precursor cells and finally transform in cancerous cells [18]. On the other hand, considering the high heterogeneity of solid tumours the concept of liver cancer stem cells has been considered even if it is complicated to distinguish between normal stem cells and tumour stem cells [14]. Therefore, it is necessary to better understand the process of HCC initiation to develop tumour markers and more specific target therapies.

1.1.1.4 Treatment

Surgical resection is considered the first-line treatment of HCC with a 5 year survival between 41 and 74 %, but this is limited to non-cirrhotic patients and is dependent on tumour size and, liver function [11]. Liver resection can be preceded by the portal vein embolisation that causes hypertrophy of the liver, allowing a more extensive resection [11]. The best curative option is liver transplantation and HCC is the only solid cancer that can be treated in this way. Other non-surgical approaches to diminish the volume of the tumour are the trans-arterial chemo-embolisation to reduce the angiogenesis on which HCC particularly rely, radiation, local percutaneous or microwave ablations [11].

As the majority of the patients presents with advanced disease, systemic therapy is the most used approach. Currently, the HCC systemic treatment is related to molecular targeted therapy and the administration of immune checkpoint inhibitors [19]. Several drugs failed to show positive results in HCC, such as erlotinib [20], brivanib [21], sunitinib [22], linifanib [23], everolimus [24], and tivantinib [25], because of a lack of efficiency at phase III trials. Lenvantinib, an inhibitor of vascular endothelial growth factor receptor 1 (VEGFR1), fibroblast growth factor receptor (FGFR) and platelet-derived growth factor (PDGF), showed non-inferiority to sorafenib treatment, and it

was approved as the second first-line treatment in 2018 [7]. After 2016, several drugs have been approved as second and third-line treatments of HCC, such as the oral inhibitor regorafenib (2017), the monoclonal antibodies that target programmed death-ligand 1 (PD-L1) nivolumab (2017) and pembrolizumab (2018), the tyrosine kinase inhibitor cabozantinib (2019), and the VEGFR2 monoclonal antibody ramucirumab (2019) [7]. The combination therapy strategy started to gain success with an improved therapeutic response with a combination of different immune checkpoint inhibitors and combined with tyrosine kinase inhibitors (TKIs). For example, nivolumab and ipilimumab combination showed positive long-term results, and it was approved in 2020 as a further second-line treatment for HCC [26]. The latest addition to the approved treatment strategies is the combination of atezolizumab and bevacizumab. These two antibodies target PD-L1 and vascular endothelial growth factor (VEGF) respectively, and their combination has been approved as the third first-line treatment in 2020 [7]. Despite the recent advances in HCC treatment of the last years [7], the efficacy of the newly developed drugs in HCC is not comparable to the treatments approved for the treatment of other types of cancer [7]. Thus, new therapy solutions are required, and combination therapy is a viable treatment strategy.

1.1.2 Chemotherapy

The term "chemotherapy" has been coined in the early 1900s but the first systemic treatment approved arrived in 1949 [27]. The approved agents for treatment of cancer had a broad action associated with high toxicity. In 1990s and early 2000s the first targeted agents were approved for a more precise treatment of the only cancer cells and reduced off site toxicity [27]. Different classes oncology therapeutics have been approved by the FDA and can be included in 3 main categories: targeted drugs, mainly small molecules that interfere with defined molecular targets in cancerous cells; targeted biologics, which are biological products such as antibodies that target amino acids sequences specific of cancerous cells; cytotoxic drugs, small molecules that induce cellular toxicity [27]. The total approvals for targeted drugs is the highest and the amount of approved targeted biologics has been growing rapidly in the last 10 years, whilst the cytotoxic drug class has not grown significantly since the early 2000s [27].

1.1.2.1 Protein kinase inhibitors

Protein kinase inhibitors belong to a class of chemotherapeutics that counts the majority of drugs approved with the broadest application [27]. Most of protein kinase inhibitors are tyrosine kinase inhibitors (TKIs), that inhibit kinases that specifically add a phosphate to a tyrosine residue on their substrate [28]. The first protein kinase inhibitor approved was Imatinib, a TKI used for treatment of chronic myeloid leukaemia arrived in clinical use in 2001 [27]. Most of the signal transduction processes occur through a cascade of phosphorylations, indicating that protein kinase inhibitors are multiple nodes involved in numerous aberrant biological processes such as cancer [29]. In fact, regulation of kinases activity is one of the mechanisms that cancerous cells exploit to increase their growth and avoid growth suppression [30]. Protein kinase inhibitors action is linked to the inhibition of the phosphorylative ability of protein kinases, blocking the downstream signalling [31]. Sorafenib and lenvatinib are two multi-kinase inhibitors approved as first-line treatment of HCC, while regorafenib and cabozantinib are approved as second-line treatment [32]. The main mechanism of these molecules in HCC is the inhibition of angiogenesis and reduction of the epithelial-mesenchymal transition (EMT) [32].

Dasatinib is an oral TKI that has been approved for the treatment of chronic myeloid leukaemia and deregulates the enzymatic activity of the protein BCR-ABL responsible for onset of leukaemia [33]. As dasatinib is a multi-kinase inhibitor it also inhibits several other targets (e.g. Scr, c-Kit, ephrin receptors) [28]. Among the different side effects observed dasatinib can also lead to liver injury [28]. Dasatinib showed to inhibit proliferation, adhesion, migration, and invasion of HCC cells *in vitro*, affecting several pathways such as SFK/FAK and PI3K/PTEN/Akt [34]. Chang *et al*. study evaluated the effect of different chemotherapeutics on HCC *in vitro* and showed that dasatinib was the most effective agent in synergising with other compounds, providing the future research directions for combination therapy in HCC [35]. Indeed, other studies showed that dasatinib synergises with other drugs, to suppress HCC growth [36, 37]. Therefore, dasatinib has potential for treatment of HCC and combination therapy may be a promising approach to improve its anticancer activity.

1.1.3 Chemoprevention

The complete elimination of carcinogenic agents exposure is not possible, and often the source is unknown [4]. A radical lifestyle change can help prevent cancer development but is insufficient to eliminate its risk. Consequently, the most adopted strategy is chemoprevention [4]. The term chemoprevention was first proposed by Sporn *et al.* as a strategy that exploits natural or synthetic agents to inhibit tumour development [38]. Based on the simplified cancer expansion process, Lee Wattenberg classified chemopreventive agents into two main categories: blocking and suppressing agents [39]. The first can block a carcinogenic agent from reaching sensible structures (i.e. DNA), whereas the second category comprises all the agents that can suppress tumour growth during the promotion and progression steps [39]. The chemopreventive agents' classification is an oversimplification of a complex mechanism. Moreover, chemopreventive agents can influence numerous biological processes, such as detoxification through cellular enzymes, repair of genetic material, apoptosis, cell-cycle arrest, and activation of oncogenes [3]. The totality of these processes could be intended as chemoprevention.

Chemoprevention can be firstly achieved with diet. Richard Doll and Richard Peto reported that the highest cancer mortality may be attributed to and related to the diet [3]. Guidelines from the WHO explained that to reduce the cancer risk, the increase in fruit and vegetable consumption could be beneficial [1]. Evidence shows that a vegetable-rich diet is inversely proportional to cancer incidence [3]. Identifying the compounds found in fruit and vegetables that positively affect human health is necessary. The National Cancer Institute identified over 1,000 different phytochemicals that have a role in chemoprevention [40]. Phytochemicals are non-nutritive compounds that influence several processes responsible for cancer development. Due to these compounds' potential and easy availability, several clinical trials have evaluated and are currently evaluating the human response to these molecules [41-43]. Phytochemicals showed the ability to inhibit the tumour expansion either by blocking the initiation or reversing the promotion phases, stimulating intracellular-signalling cascades within the major pathways involved in cancer progression [3]. Phytochemicals are classified as terpenoids, phenolic metabolites, alkaloids, and a class of nitrogen-containing compounds which comprise glucosinolates (GLs) [44]. GLs, and more precisely their metabolites isothiocyanates (ITCs), are mainly known as activators of detoxification enzymes. GLs are found abundant in cruciferous vegetables of the Brassicaceae family (e.g. broccoli, cabbage, horseradish, mustard) [45]. Several studies

reported their efficacy against various tumour types such as lung [46], gastric [47], breast [48], bladder [49], and prostate cancer [50]. A recent umbrella review of 41 systematic reviews and meta-analyses of 303 observational studies showed a correlation between consumption of cruciferous vegetables and beneficial effects on different types of cancer [51]. Moreover, ITCs showed *in vitro* anticancer activity against liver cancer [52] and appear to inhibit different cellular processes involved in the hyper-proliferation of tumour cells. For this reason, ITCs represent an interesting group of anticancer compounds to be investigated with regard to liver cancer to contribute to understand and determine the complex pathways involved in tumour inhibition.

1.2 Isothiocyanates

ITCs are biologically active compounds derived from GLs' hydrolysis. GLs are glucose and sulfur-containing organic anions [53]. The *B. oleracea* species has the highest diversity in terms of different GLs chain structures [54]. GLs are categorised depending on their amino acid precursor, and around 200 unique structures have been identified to date [45]. Consequently, different GLs structures correspond to the same amount of different ITCs structures. ITCs are responsible for the pungent taste of certain types of cruciferous vegetables. A clear example of that taste is found in mustard and wasabi, produced from seeds of the genus *Brassiceae* and the rhizome of the genus *Eutremeae*, respectively. The consumption of an average portion of cruciferous vegetables can lead to the intake of around 10 mg of ITCs [55]. **FIGURE 1.2** presents some of the most studied ITCs.

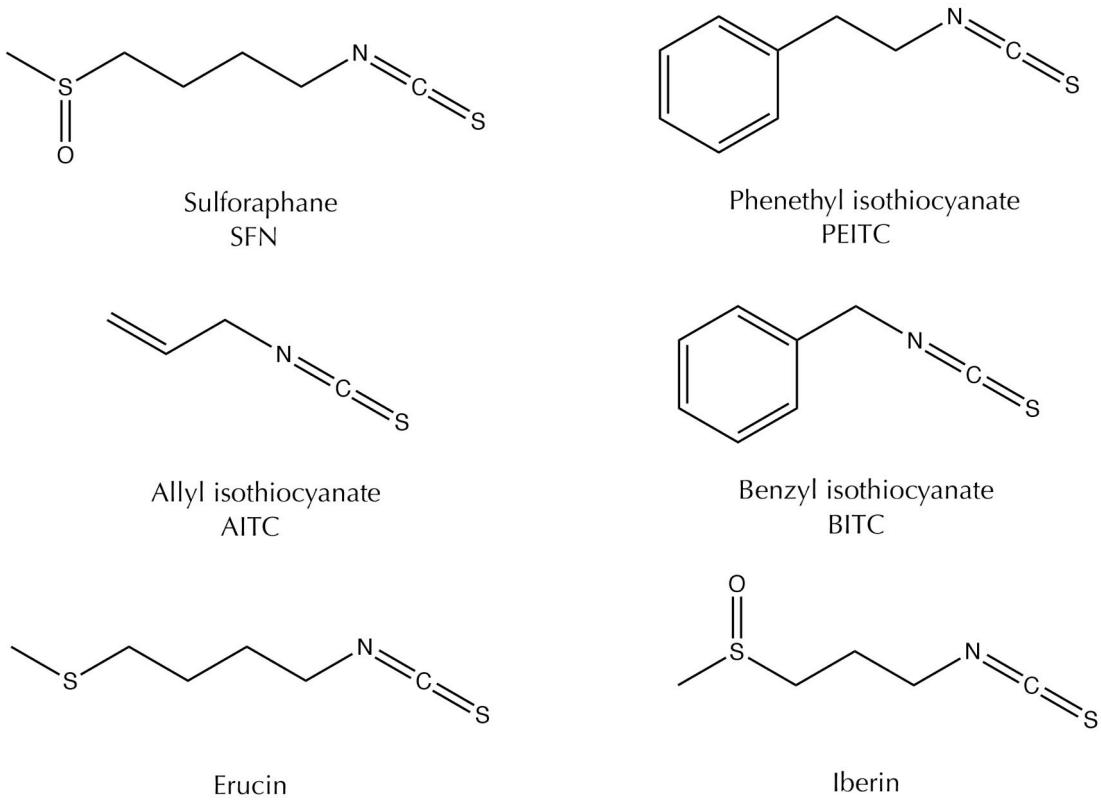

FIGURE 1.2 | Structures of most common isothiocyanates

1.2.1 Absorption of ITCs

The production of ITCs is due to the action of the enzyme myrosinase that hydrolyses GLs [54]. The enzyme myrosinase (β-thioglucosidase glucohydrolase) and GLs are located in two different compartments of the plant cell; only when the plant tissues are damaged, the enzyme contacts its substrate and the hydrolysis take place with the removal of the β-thioglucose moiety [56]. Different products are generated from this reaction (**FIGURE 1.3**), including ITCs and nitriles; however, if the reaction happens in a controlled environment with neutral pH, ITCs represent the only products obtained [56]. The parameters that determine the fate of the reaction are pH, ferrous ions, epithiospecifier proteins (ESPs), and temperature [57-59]. For this reason, preparation and cooking of these vegetables is crucial to optimise the reaction and increase the intake of bioactive compounds. The plant ESPs are responsible for the hydrolysis shift to nitriles; consequently, their denaturation due to a mild heat treatment moves the reaction to the production of ITCs [54]. On the other hand, excessive heating would denature ESPs and myrosinase without hydrolysis, leaving GLs intact [54]. Thus, short cooking times such as boiling, steam, and microwaving represent the best way to achieve a high intake of ITCs [59].

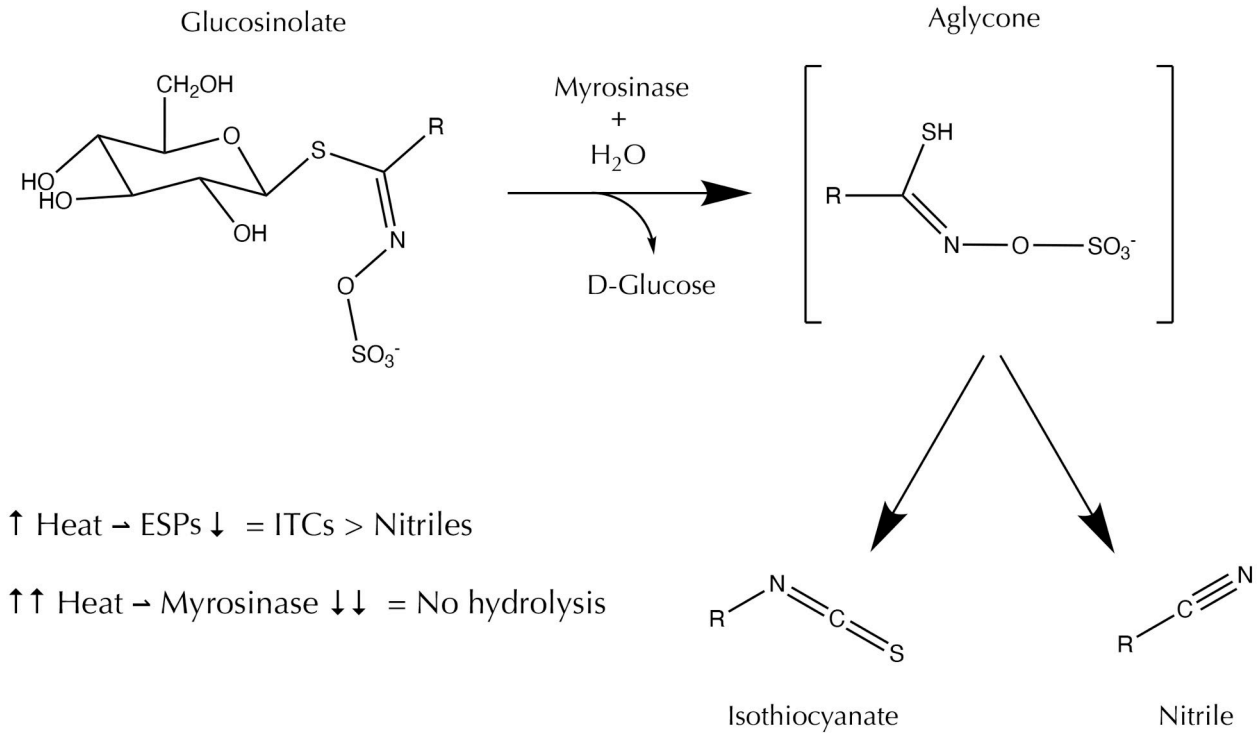

FIGURE 1.3 | Hydrolysis of glucosinolates by myrosinase action
Myrosinase enzyme metabolises the glucosinolates in Brassicaceae's vegetables to produce an intermediate that can be converted into isothiocyanates and nitriles.

Non-hydrolysed GLs are inactive in the human body and excreted unmodified, even though intact GLs are hydrolysed by the bacterial thioglucosidase of the colon microflora, producing a low yield of ITCs [54]. Indeed, Liou *et al*. showed the biochemical mechanism by which GLs are metabolised by a particular bacteria species in the gut microflora called *Bacteroides thetaiotaomicron,* present in the gut microflora [60]. Either way, ITCs are passively absorbed into epithelial cells of the small and large intestines and are conjugated with glutathione (GSH) by the glutathione S-transferase (GST) [54]. Then the GSH-ITC conjugate is transported to the bloodstream through the multidrug resistance protein-1 (**FIGURE 1.4**) [61], before being metabolised through the mercapturic acid pathway in the liver. The GSH-ITC conjugate is cleaved firstly to ITC-cysteine, then into ITC-cysteine glycine. Finally, the last metabolite, a dithiocarbamate called N-acetyl cysteine-(NAC-)conjugate, is translocated to the kidneys for excretion [45]; the measure of this final metabolite concentration in the urine is used to determine the amount of ITC metabolised [59]. Furthermore, a study showed that sulforaphane (SFN) was also found as a free form in blood samples [62], which may be related to a possible dissociation in the blood plasma or a

GST cleavage, allowing an association with serum albumins and other proteins [54, 63]. In this way, ITCs could be released in other tissues.

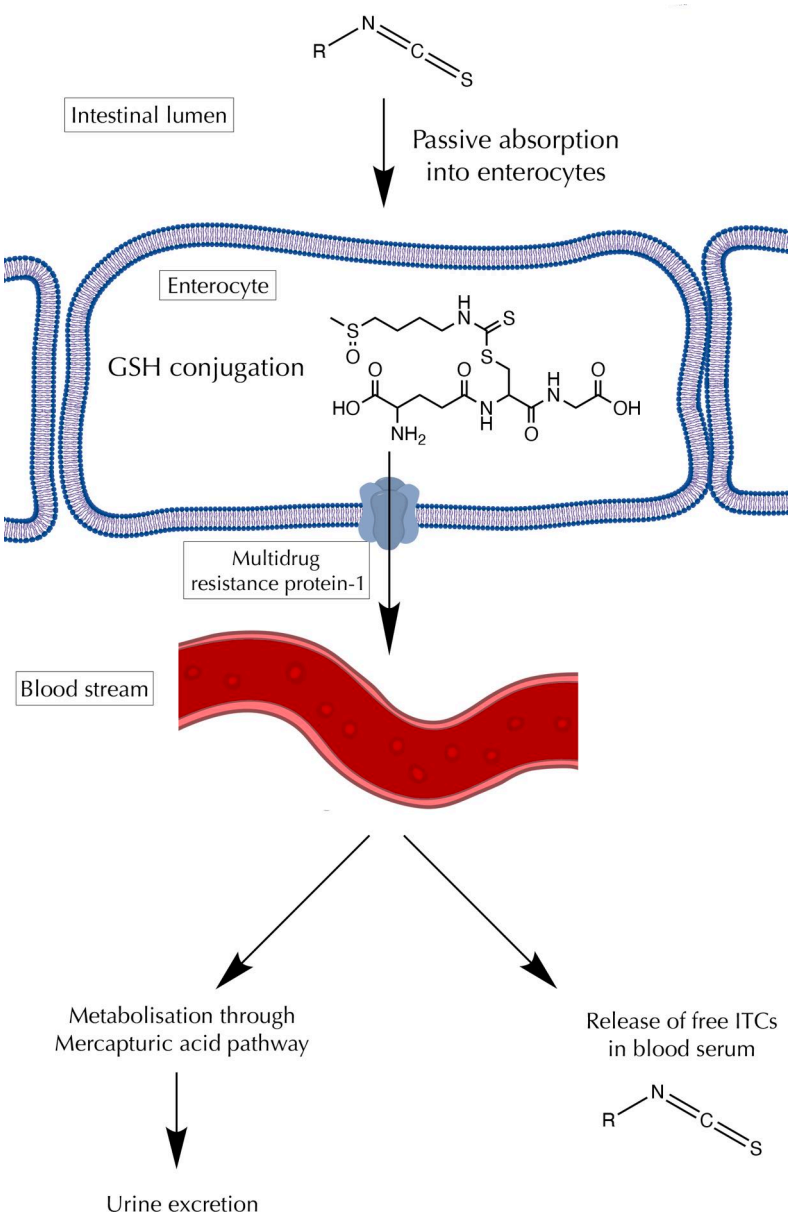

FIGURE 1.4 | Metabolism of isothiocyanates.
ITCs are absorbed passively into enterocytes, where they are readily conjugate with GSH. Then, ITCs reach the bloodstream, passing through the multidrug resistance protein-1. ITCs are metabolised through the mercapturic acid pathway and excreted with urine, or a part of free ITCs are released into the blood serum.

Understanding the ITCs' absorption into the body is fundamental to exploit these compounds for chemoprevention. ITCs activity is characterised by a biphasic effect that stimulates cell viability at low doses, while at high doses, inhibits a range of cellular processes involved in the anticancer activity [64]. Generally defined as hormesis, this

behaviour could represent an undesirable risk factor. In this regard, the results of the Bao *et al*. study indicate that the action of ITCs may prevent tumour development and promote healthy cellular processes. However, it could also promote tumour growth [64]. Since determining the precise hormetic window is fundamental for cancer therapy, and consideration of the ITCs' hormetic effect and human bioavailability in clinical trials is essential.

1.2.2 Hormetic effect

Hormesis is an ancient Greek term meaning "to excite" [65]. This term is used to describe a biphasic dose-response of a compound that can stimulate or inhibit particular biological processes if used at low or high concentrations, respectively [65]. This phenomenon is probably related to an evolutionary mechanism that allows the cell to adapt to a particular minor stress, elaborating a biochemical response to face a more severe stress [66]. Indeed, the cell can respond with different signalling activities and reparative processes [65], which help the cells to also cope with other types of stress [66]. Understanding hormesis is crucial in drug development to obtain the requested cellular response rather than the opposite one. For example, low-dose anxiolytic drugs have a positive effect, but high doses increase anxiety [65]. The hormetic effect is described in **FIGURE 1.5** as a diagram of the inverted U hormetic dose-response curve. When the response reaches a peak, identified as the maximum cellular response around 130-160% higher than the control, the curve declines to the NOAEL, which represents the no-observed-adverse-effect-level point [65]. Then, following the NOAEL, the compound starts to have a toxic effect on cell viability [65].

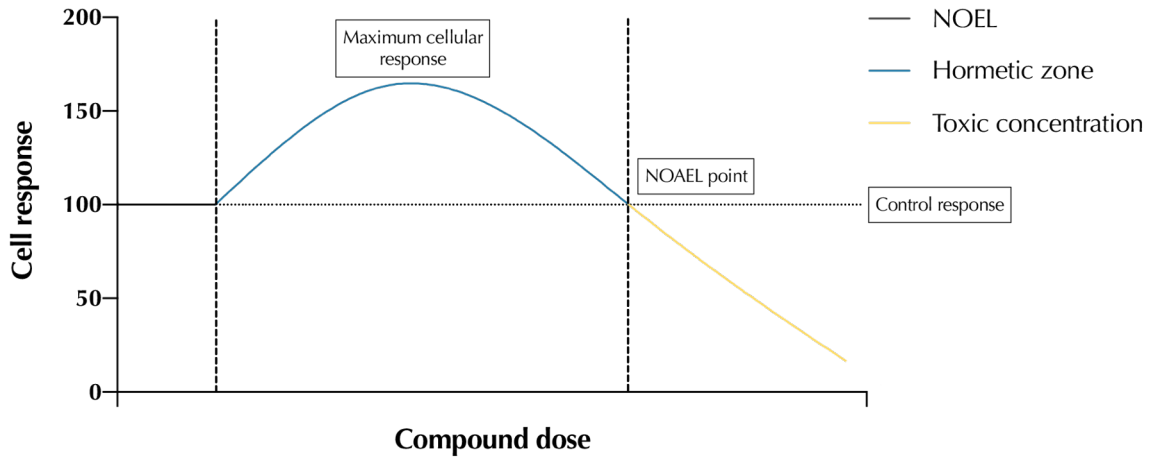

FIGURE 1.5 | Hormetic effect diagram.
ITCs exhibit a hormetic effect due to their dual effect depending on the concentration used. At low doses ITCs elicit a maximum cellular response with the activation of reparative processes, facilitating cell proliferation. Increasing the dose, the cell response reaches the NOAEL point, after which the concentration elicits a toxic effect. Adapted from the work of Bao *et al.* [64].

The exact mechanism by which the hormetic effect elicits two completely different cellular responses is unclear. Calabrese *et al.* analysed several studies in which different cell types and compounds were studied to better understand the hormesis mechanism [67, 68]. Every cell type and set of compounds investigated had a specific and unique mechanism and there was not a general rule that predicted cellular response. The mechanism could probably be explained with the pharmacological model of natural receptor-based responses involving two receptor subtypes, one at high affinity and the other with low affinity but high capacity in terms of simultaneously occupied receptors [67]. Consequently, the first receptor is activated at low doses and the second one at high doses, with two separate cell responses [67].

Several studies showed that different ITCs, i.e. allyl isothiocyanate (AITC), SFN, and phenethyl isothiocyanate (PEITC), elicit a hormetic effect in different cell types [64, 66, 69]. The levels that ITCs can reach in the human blood after a meal of vegetables rich in this type of compound should not reach concentrations higher than the nM level in the NOAEL zone (**FIGURE 1.5**), being far from the hormesis zone [64]. However, different human trials demonstrated that in particular conditions, such as the increased consumption of cruciferous vegetables or the intake of ITCs supplements, the blood ITCs value could reach the level of active biological stimulation [64]. For this reason, it is important to consider the bioavailability of these compounds to understand better how ITCs can be exploited for

chemotherapy, avoiding the undesired stimulation of tumour cells and reaching the desired anticancer activity.

1.2.3 Bioavailability of ITCs

There are no extensive data about the oral human bioavailability of ITCs. Encapsulated benzyl isothiocyanate (BITC) and watercress were administered to subjects in a trial study, and the BITC-NAC metabolite was evaluated in the urine with a peak after 2-4 hours after ingestion [63]. A dose of 1.8 μmol/kg of BITC produced a peak in urine excretion of the BITC-NAC metabolite after 2-6 hours [70, 71]. Platz *et al*. found that after the ingestion of 10 g of Indian cress, the subjects showed a high concentration of four different BITC metabolites in the blood, with BITC-NAC as the prominent metabolite [72]. The concentration peak was reached after 3h with BITC-CysGly at 1 μmol/L [72]. Also, they found that the presence of BITC metabolites in the urine occurred 24 h later, with a peak at 6 h of BITC-NAC that reached 2.063 μM [72]. Oral administration of 3.5 μmol/kg PEITC led to a peak in plasma concentration of 1 μmol/L after 4.6 hours [73]. In a different study, the consumption of watercress with an estimated content of 25 mg of PEITC led to a concentration peak in plasma of 0.93 μmol/L [74]. SFN was found in plasma at a concentration between 0.943 and 2.27 μmol/L after 1h of ingestion of 200 μmol broccoli sprout extract [75]. Gasper *et al*. also found that the plasma SFN concentration after a soup of "SuperBroccoli" reached 7.3 μmol/L [62]. Song *et al*. conducted a study on five subjects with oral administration of raw broccoli [76]. The results showed an ITCs plasma concentration of 0.55 μmol/L 3 h post the consumption of 200 g of raw broccoli [76]. Considering that several human studies highlighted that the blood concentration of ITCs could easily reach the hormetic window levels, it is necessary to consider the risks associated with consuming these compounds in subjects that are affected by tumours. Therefore, focusing the inhibitory ITCs' activity on targeted tumour cells is fundamental.

1.2.4 Clinical trials with ITC dietary interventions

A search on ClinicalTrials.gov made on the 19th May 2023, using the keywords cancer, sulforaphane, isothiocyanate, and PEITC generated a list of 40 registered clinical trials that investigate the effects of ITCs on different types of cancer. In this list, six trials are registered as active, two terminated or withdrawn, three unknown, and thirty-two completed, of which nine with results (**TABLE 1.1**). A phase II trial showed that the administration of PEITC

to smokers subjects could act as an inhibitor of carcinogenesis with a reduction of nicotine-derived nitrosamine ketone (NNK) metabolism, which has a particular role in carcinogenesis [77]. In a different study, 200 μmol of SFN were administered to prostate adenocarcinoma-positive patients and the level of prostate-specific antigen (PSA) was monitored [78]. The results were not as expected as it was hypothesised that the PSA levels would decrease by more than 50%, compared to the baseline PSA, but this was observed in just one patient [78]. The investigators suggested that the study needed to be revised with treatment optimisation with a higher dose of SFN [78]. Moreover, another phase II clinical trial considered the effect of SFN broccoli sprout extract on women affected by ductal carcinoma in situ (breast cancer) [79]. The results highlighted the increase of expression of NAD(P)H quinone reductase 1 (NQO1), which has a detoxification role, and the decreased expression of Aldo-keto reductase family 1 member C1 (AKR1C1), involved in metastasis [79]. Furthermore, Zhang *et al*. published the results of a randomised controlled trial that evaluated the SFN activity on prostate cancer (PCa) prevention [80]. The subjects were administered with 100 μmol of SFN in capsules [80]. The results showed a non-significant reduction in the expression of the principal PCa biomarkers assessed and it was suggested that the treatment pattern and dosage should be revised for further studies [80]. Atwell *et al*. evaluated cancer biomarkers and histone deacetylase (HDAC) activity levels in women scheduled for breast biopsy after an administration of SFN capsules [81]. The study showed decreased HDAC activity and the expression of the Ki-67 cell proliferation marker, which is usually over-expressed in breast and prostate cancer [81]. Recently results of a randomised trial of broccoli seed and sprout extract administration to current smokers have been published [82]. The main finding of this study was the increased detoxification of tobacco carcinogens benzene, acrolein, and crotonaldehyde. Finally, a randomised clinical trial in China revealed that the administration of a broccoli sprout beverage could increase the rapid detoxification of pollutants, such as benzene and acrolein metabolites [83]. They also concluded that further studies are necessary to optimise the delivery of SFN and to evaluate its bioavailability even at low doses [83]. The aforementioned clinical trials demonstrated that ITCs may affect the metabolism of carcinogens and the expression of cytoprotective mechanisms.

The main conclusion of the studies mentioned above is that the dose and the treatment pattern for dietary supplementation with ITCs need further investigation. ITCs may represent valid compounds for chemoprevention and chemotherapy, but additional studies are required to understand their bioavailability, taking into consideration the hormetic

effect. Combination therapy might be the right solution to exploit the ITCs' potential to achieve an effective result, as ITCs could act as adjuvants to clinically approved chemotherapeutics.

TABLE 1.1 | ITCs clinical trials with results list retrieved from *ClinicalTrials.gov*.

	Condition	Results	Identifier
PEITC	Lung cancer/tobacco use disorders	Inhibition of lung carcinogen (NNK) metabolism	NCT00691132
SFN	Prostate adenocarcinoma	No significant decrease in PSA levels (> 50%)	NCT01228084
SFN	Breast cancer	NQO1 expression ↑ AKR1C1 expression ↓	NCT00982319
SFN	Prostate cancer prevention	No significant change in PCa biomarkers	NCT01265953
SFN	Breast cancer	HDAC activity ↓ Ki-67 expression ↓	NCT00843167
SFN	Environmental carcinogenesis	Detoxification of benzene and acrolein metabolites	NCT01437501
SFN	Environmental carcinogenesis	Detoxification of benzene and acrolein metabolites	NCT02656420
SFN	Tobacco use disorders	Detoxification of benzene, crotonaldehyde, and acrolein metabolites	NCT03402230

1.3 Anticancer activity of isothiocyanates

Verhoeven *et al*. highlighted an inverse association between the consumption of Brassica vegetables and the risk of cancer development [84]. As mentioned, ITCs play a dual role in cancer depending on their concentration. At low doses, ITCs promote the expression of antioxidant genes, promoting chemoprevention. On the other hand, higher concentrations of ITCs elicit an anticancer activity through the activation of anti-proliferative pathways, inhibiting cancer growth at all three stages of the tumour development process [85]. Cancer cells present a modified equilibrium with increased proliferation and uncontrolled growth, many pathways and mechanisms occurring in normal cells are inactivated or down-regulated, allowing cancer cell survival. ITCs have been shown to exert anticancer activity through different mechanisms, affecting several cellular processes simultaneously. In particular, ITCs showed potential benefits in the treatment of HCC, reducing the activation of different pathways involved in tumour growth and metastasis [86]. The following section will highlight some of the mechanisms of action of ITCs' in the reduction of tumour growth, metastatic potential, and inhibition of angiogenesis.

1.3.1 Anti-proliferative action of ITCs

The anticancer activity of ITCs can be exploited to reduce the proliferation and inhibit cancerous cells, targeting multiple pathways. The primary effect of ITCs is their influence on cell metabolism and redox state. ITCs induce the expression of antioxidant phase II enzymes that (i) detoxify and prepare molecules for excretion and (ii) inhibit the production of phase I enzymes that could activate pro-carcinogens [45]. Therefore, ITCs can regulate the balance of oxidants and antioxidants, perturbing cellular homeostasis. ITCs also exert an anti-proliferative action through directly regulating gene expression and by induction of DNA damage in cancerous cells. ITCs may act as histone deacetylase (HDAC) inhibitors [87], epigenetically controlling gene expression. ITCs can also induce DNA damage as consequence of DNA replication blockage [88], and control the machinery of DNA damage response, leading cancerous cells to cell cycle arrest and apoptosis [89-91]. Furthermore, ITCs can control the regulators of the cell cycle to reduce uncontrolled cancer growth [89, 92, 93,] and to regulate the formation of microtubules [94], which are cellular structures that play a fundamental role in numerous cellular processes. In addition, ITCs have been shown to exert their anticancer activity through the control and induction of programmed cell death. Indeed, ITCs reactivate or up-regulate the normal cellular mechanisms overridden by aberrant cancerous cells.

1.3.1.1 Metabolism and oxidative stress

Compounds that enters the organism are metabolised to absorb useful molecules and excrete non-functional ones. In this process, the metabolism comprises two fundamental phases, I and II. Phase I regards the functionalisation of exogenous compounds to increase reactivity and facilitate phase II reactions [95]. Phase II is characterised by excretion enzymes that reduce the reactivity of phase I products and introduce more hydrophilic functions, allowing the final excretion of exogenous compounds [95]. In most cases, carcinogens after the phase I reaction become highly reactive and may interact with nucleophilic centres in various macromolecules, generating an insult [96]. Highly reactive carcinogens are detoxified by phase II enzymes [96]. Both phases I and II are inducible. Consequently, an effective cancer prevention strategy could be the balance of the two metabolism phase reactions [96]. ITCs showed the ability to up-regulate phase II, confirmed by human studies of

cruciferous vegetables feeding, and down-regulate phase I enzymes, mainly through the binding of Keap1 to avoid Nrf2 degradation [97].

The most studied pathway in ITCs' anticancer activity is the nuclear factor erythroid 2-related factor 2 (Nrf2) (**FIGURE 1.6**). This pathway is involved in the transcriptional regulation of numerous antioxidant genes, thus typically associated with a protective function. Nrf2 is usually situated in the cytoplasm bond by kelch-like ECH-associated protein 1 (Keap1), which mediates its degradation through ubiquitination [56]. The phosphorylation of the cofactor Cul3 leads to the translocation of Nrf2 into the nucleus, where it can bind a region called antioxidant responsive element (ARE) with the aid of Maf proteins [56, 98]. ARE is situated in the promoter region of different antioxidant genes and regulates gene expression [56]. ITCs may stimulate the release of Nrf2 and the inhibition of its ubiquitination. It has been hypothesised that ITCs can directly conjugate with the cysteine residues on Nrf2 or Keap1 to alter the interaction of these two proteins [99]. This hypothesis is corroborated by the fact that generally ARE inducers can react with the cysteine residues on Keap1 to induce expression of ARE-controlled genes [100]. SFN has been shown to increase detoxification with the up-regulation of genes such as NQO1, GSTs, and thioredoxin reductase (TrxR1) [56]. On the other hand, SFN may inhibit different enzymes of the cytochromes P450 family that commonly activate pro-carcinogens [101]. Therefore, ITCs control the cell redox state through the control of cellular metabolism.

The balance between oxidants and antioxidants is fundamental for cellular health. Reactive oxygen species (ROS) are excited molecules that can react with biomolecules of the organism damaging structures and interfering with normal biological processes [102]. The cell has an antioxidant system that controls the production and elimination of ROS, protecting itself from oxidative damage [103]. The imbalance created between the produced and eliminated ROS may lead to oxidative stress. ITCs possess ability to protect the cell from oxidative stress or to induce cell death through oxidative imbalance (**FIGURE 1.6**) [54, 104], which may be explained by the hormetic effect. The protective mechanism is related to the induction of the expression of antioxidant genes through the Nrf2 pathway [54] after induction of mild oxidative stress [64]. ITCs deplete free intracellular GSH generating an oxidative imbalance that leads the cell to respond with increased production of GSH. However, if the concentration of ITCs increases, the level of depleted GSH is too

severe, and the cell cannot cope with the higher oxidative imbalance. The result is cell death due to ROS damage [104]. Indeed, ITCs at low doses increase cell viability, which is a defensive response against mild oxidative stress, but high doses correspond to decreased cell viability [64]. In this context, ITCs-induced oxidative stress can be exploited to enhance the activity of other chemotherapeutic agents, working in synergy. Xu *et al*. demonstrated that the nano-encapsulation of SFN is an effective way to increase the sensitivity of tumour cells to anticancer drug cisplatin due to increased sequestration of intracellular GSH [105].

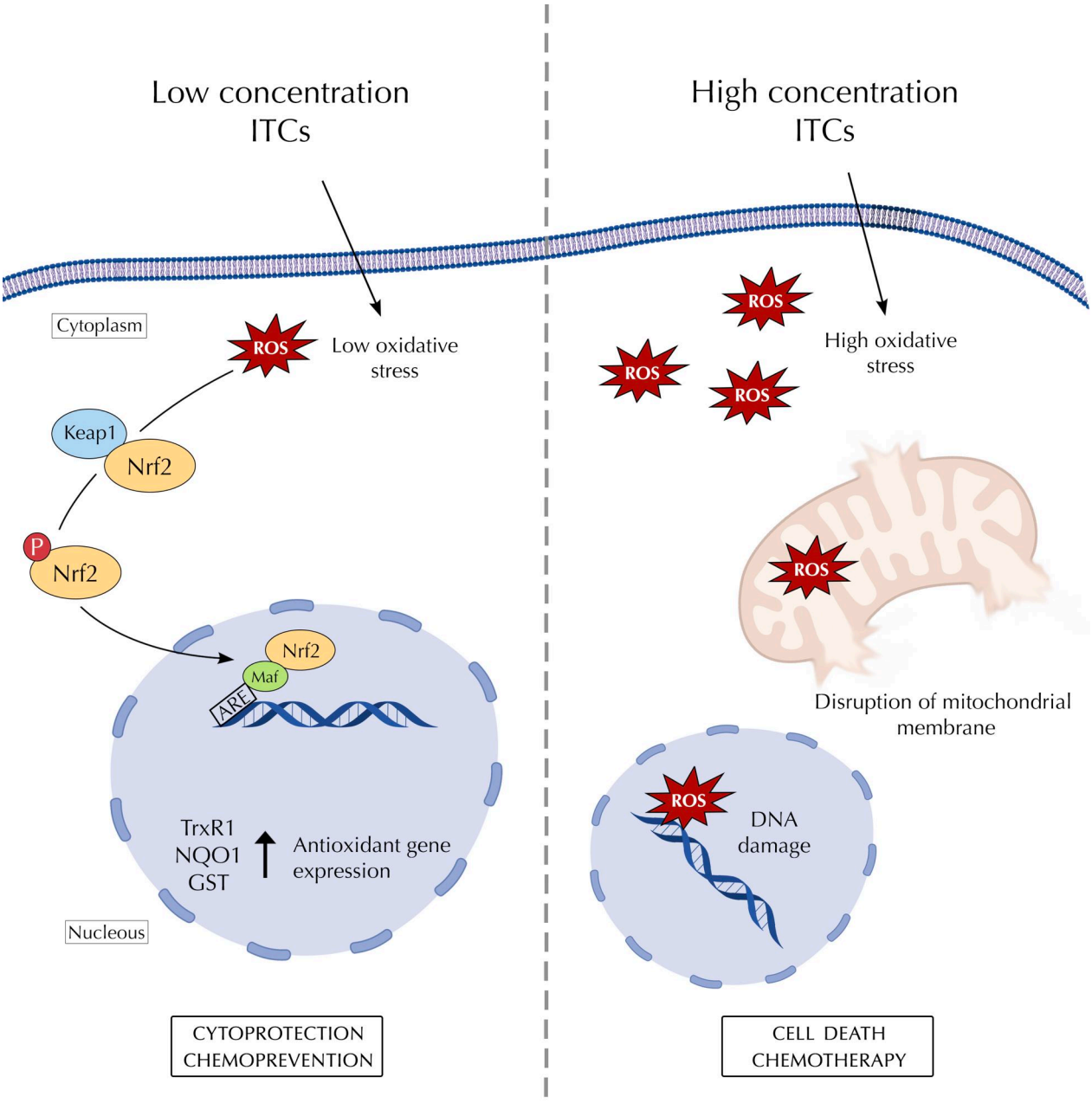

FIGURE 1.6 | Dual role of ITCs in chemoprevention and chemotherapy.
Low doses of ITCs elicit a cytoprotective effect through the Nrf2 pathway. The release of Nrf2 from Keap1 allows the activation of the transcription factor ARE, which activates the transcription of antioxidant genes (i.e. TrxR1, NQO1, GST) with the aid of Maf proteins. High doses of ITCs induce an oxidative imbalance. Uncontrolled ROS cause DNA and organelles damages, leading to cell death, thus playing a role in chemotherapy.

1.3.1.2 Epigenetic regulation and DNA damage

Epigenetic modifications are responsible for controlling gene expression without changes in the genetic sequence. It is well documented in literature how these alterations are involved in the development of cancerous diseases [106]. Different mechanisms can alter the structure and the organisation of chromatin and DNA filaments, influencing the expression of specific genes. Tumours can exploit these naturally occurring mechanisms to enhance the expression of oncogenes while inhibiting oncosuppressor genes [106]. An effective anticancer strategy targets the enzymes responsible for epigenetic modifications, and ITCs have also demonstrated to alter the machinery of epigenetic control.

The over-expression of HDACs is a common trait in cancer cells, so the inhibition of these has been identified as a cancer therapy strategy [107]. Histones are responsible for chromatin packing, a gene expression regulatory mechanism. HDACs and histone acetyltransferases (HATs) are responsible for the acetylation and deacetylation of chromatin histones, representing the mechanism of chromatin packing and unpacking. Consequently, the activity of these two enzymes results in transcriptional control of specific genes. In tumour cells, the up-regulation of the activity and the expression of HDACs is common, allowing the expression of oncogenes and the inhibition of their silencing [107]. ITCs appear to inhibit the activity of HDACs in different tumour types, with increased acetylation of histones, and increased expression of protein p21, blocking DNA repair mechanisms in tumour cells, thus inducing DNA damage and stimulating apoptosis and cell cycle arrest (**FIGURE 1.7**) [45]. Furthermore, SFN seems to inhibit the acetylation of histones related to the pro-apoptotic Bax gene, thus having a role in apoptosis induction [108].

Uncontrolled DNA methylation is another common trait for cancer development. DNA methyltransferases (DNMTs) are responsible for adding or removing methyl groups to the DNA structure [109]. Mutated cells exploit the function of these enzymes to silence oncosuppressor genes and to activate the expression of pro-metastatic genes [109]. Saito *et al.* showed that the increased expression of DNMT1 in human hepatocellular carcinoma is related to a poor prognosis [110]. Indeed, the inhibition of DNMTs is considered a feasible anticancer strategy. Several studies showed that the inhibition of DNMTs, combined with the inhibition of HDAC, prevents or attenuates the growth of different types of cancer, such as lung cancer [111] mammary [112] cancer

types resulting in resistant tumours being more sensitive to chemotherapy [113]. ITCs inhibit DNMTs and other molecular targets, performing a broad anticancer activity in different types of tumour [98, 104].

Cancer cells are characterised by genomic instability that leads to the accumulation of DNA damage. Conventional radiotherapy and chemotherapy exploit this fact to increase DNA damage accumulation, leading to cell cycle arrest and programmed cell death [114]. A fundamental pathway involved in DNA damage response is ATM-Chk2, which is a signalling cascade that responds to double-strand breaks (DSBs) [115]. Specifically, ATM phosphorylates p53 (Ser-15) and tumour suppressor checkpoint kinase 2 (Chk2) (Thr-68), regulating cell cycle and programmed cell death [116]. ITCs have been shown to target different types of cancer with increased DNA damage mediated by the ATM-p53-Chk2 pathway, leading to cell cycle arrest and apoptosis (FIGURE 1.7) [90, 91]. In particular, the increased DNA damage induced by PEITC showed to be related to an increase in ROS production that was reversible with an antioxidant pre-treatment [91].

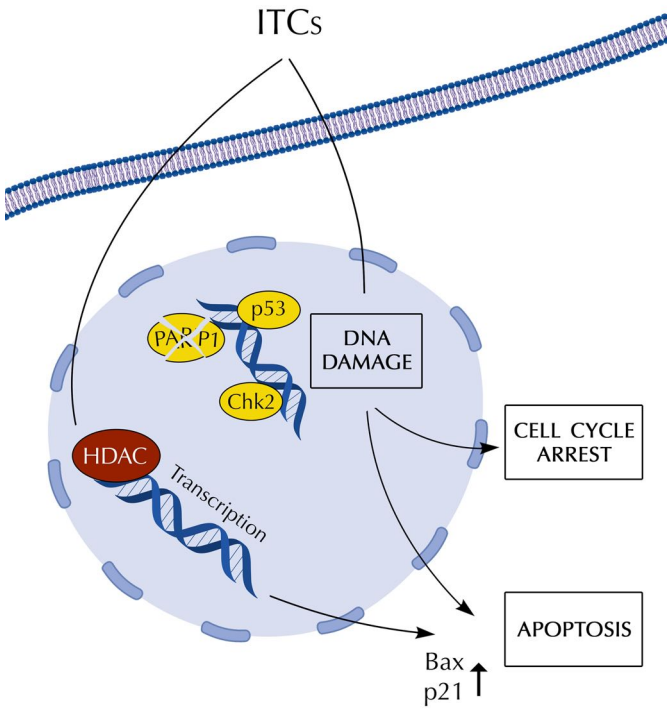

FIGURE 1.7 | ITCs epigenetic regulation and DNA damage.
ITCs inhibit HDAC activity, increasing the expression of different proteins such as bcl-2-like protein 4 (Bax) and p21, controlling the apoptosis. ITCs induce DNA damage with activation of the ATM-p53-Chk2 pathway.

1.3.1.3 Cell cycle and microtubule dynamics

Throughout the cell cycle, there are a few checkpoints at which the cell can be repaired or undergo programmed death. The cell can be blocked at these points if the conditions are not adequate for the next phase of the cycle. In tumour development, this control system is bypassed, allowing uncontrolled growth with the perpetration of deleterious DNA mutations [117], which give the tumour cell genomic instability, increasing its proliferative capacity [118]. The mammalian cell cycle is controlled by cyclin-dependant kinases (CDKs) that are activated by cyclins and deactivated by inhibitors [118]. Generally, cyclin phosphorylation results in the deactivation of its activity, while the phosphorylation of inhibitors leads to its activation. ITCs have been found to regulate the expression of both inhibitors and cyclins (FIGURE 1.8). PEITC down-regulated cyclins A, D, and E with cell cycle arrest at G1 [92]. Arrest at G2/M was associated with the reduction in expression of CDK1 and accumulation of phosphorylated CDK1 [119]. Also, BITC activated Chk2, leading to G2/M phase cell cycle arrest [119]. Furthermore, SFN acts as a cell cycle modulator, decreasing levels of cyclin B1 and increasing levels of phosphorylated CDK1 [89].

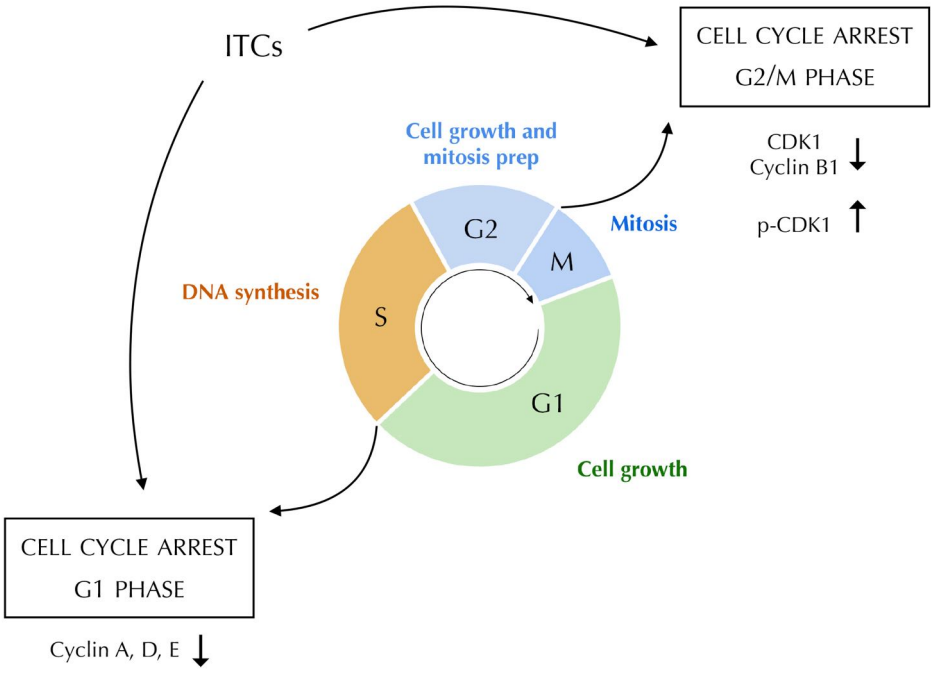

FIGURE 1.8 | Effect of ITCs on cell cycle.
ITCs induce cell cycle arrest at the G1 phase through the deregulation of Cyclin A, D, and E while inducing cell cycle arrest at the G2/M phase with deregulation of CDK1, Cyclin B1 and up-regulation of p-CDK1.

Microtubules are dynamic structures, part of the cytoskeleton, formed by the polymerisation of α/β-tubulin heterodimers. Microtubules play a fundamental role in numerous cellular processes. In particular, their role in cell division makes them attractive targets for cancer therapy [120]. Microtubules are highly dynamic structures that reorganise depending on the cellular growth phase. During interphase, they play a role in cell shape, motility and intracellular trafficking [120]. During mitosis, microtubules reorganise to form the mitotic spindle fibres responsible for chromosome segregation. Chemotherapeutic agents target tubulin directly to destabilise microtubule formation, leading to mitotic arrest and consequent cell death [120]. Therefore, tubulin-targeting agents reduce cancer cell proliferation, blocking the formation of a functional mitotic fuse. ITCs may bind directly tubulins to block the microtubule polymerisation as investigation of binding sites of ITCs on tubulins showed that their cysteine residues are accessible to ITCs [121]. In particular Grzywa *et al*. showed that the ITCs' modification of the residue Cys347 on α-tubulin may be responsible for the inhibition of microtubule polymerisation [122]. ITCs were shown to induce cell cycle arrest and apoptosis in bladder cancer cells through tubulin binding (**FIGURE 1.9**), leading to the disintegration of microtubules [121]. The effects of BITC and PEITC also lead to the degradation of α/β-tubulin [94]. SFN and PEITC have been shown to bind to α/β-tubulin to disrupt the formation of microtubules, inhibiting angiogenesis [94].

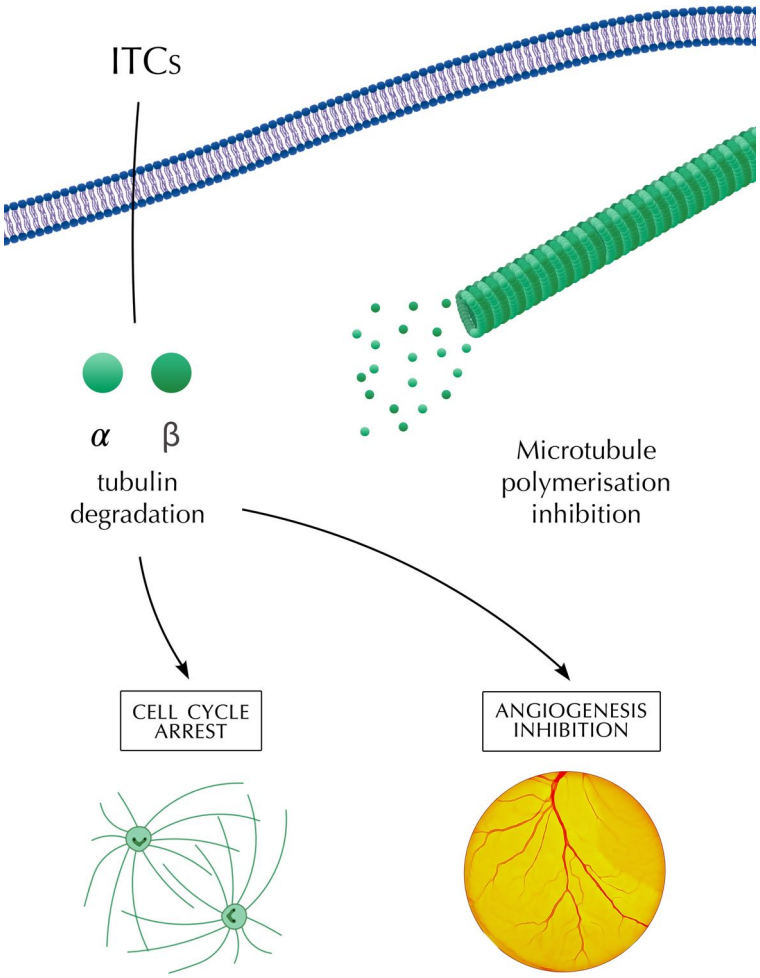

FIGURE 1.9 | ITCs and α/*β*-tubulin degradation.

ITCs are known to control the expression of tubulins, affecting the polymerisation of microtubules. Microtubules are involved in numerous cellular processes, such as apoptosis, cell cycle regulation, and angiogenesis.

1.3.1.4 Programmed cell death

Programmed cell death is a conserved controlled mechanism that cells use to eliminate superfluous and damaged cells that could cause harm to the organism [123]. Different types of programmed cell death have been identified so far, some of which are widely described in the literature [124]. Since 2005, the Nomenclature Committee on Cell Death (NCCD) regularly publishes guidelines for defining and interpreting cell death [123]. The last update was published in 2018, counting twelve different types of programmed cell death (**FIGURE 1.10**). In the last years, other types of programmed cell death were identified, such as oxeiptosis and alkaliptosis [124]; therefore, a new update from the NCCD is expected. In particular, oxeiptosis is a form of apoptosis independent from caspases activation that is linked to an increased production of

ROS. Oxeiptosis is a mechanism of response to an increase of oxidative stress from which the cell cannot recover, undergoing programmed cell death. The main factors involved in this process are Keap1, PGAM5, and AIFM1 [125]. Briefly, Keap1 releases PGAM5 that translocates into the mitochondria where it de-phosphorylate AIFM1 to activate oxeiptosis death [126]. Interestingly, Keap1 and PGAM5 form a complex with Nrf2 that has been identified as a sensor for ROS levels [125]. ITCs are known to bind Keap1-Nrf2 complex but there is no known correlation between ITCs and oxeiptosis. Therefore, the relation between ITCs and oxeiptosis markers is worth exploring.

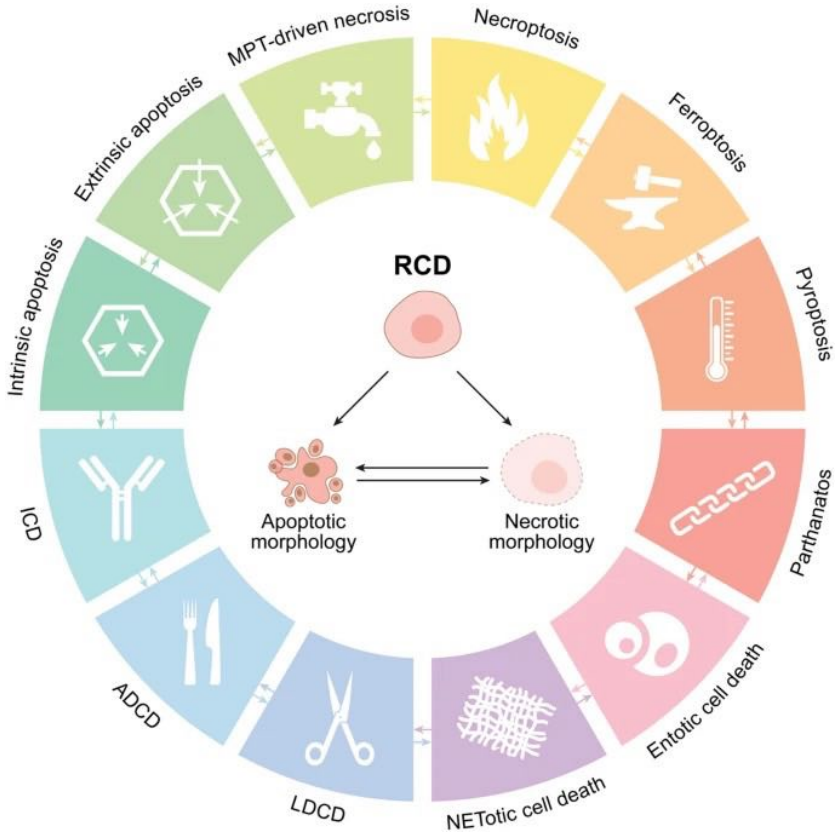

FIGURE 1.10 | Different types of programmed cell death from NCCD.
Intrinsic apoptosis is activated by caspases; Extrinsic apoptosis extracellular perturbations are detected and then propagated by caspase-8 to caspase-3; MPT-driven necrosis is initiated by oxidative stress and Ca^{2+} overload that lead to a necrotic morphotype; Necroptosis characterised by RIPK1 kinase activity; Ferroptosis is initiated by oxidative stress controlled by GPX4; Pyroptosis is induced by formation of pores from gasdermin proteins; Parthanatos is induced by PARP1 hyperactivation leading to AIF-dependent DNA degradation; Entotic cell death is characterised by cell-in-cell entosis followed by lysosomes execution; NETotic cell death is typical of hematopoietic derived cells dependent on ROS; LDCD lysosome-dependent cell death; ADCD autophagy-dependent cell death; ICD immunogenic cell death. Image reused under Creative Commons license from L. Galluzzi *et al.* [123].

Among various programmed cell death mechanisms, apoptosis or type I cell death are the most studied, counting more than 3,500,000 results in a Google Scholar search in June 2023. Apoptosis is a conserved mechanism that allows complex organisms to eliminate cells in excess or remove aberrant cells that can represent a risk for a specific tissue and the entire organism [127]. One of the primary mechanisms beyond apoptosis is the activation of the caspases pathway. This family of proteases is specifically activated in apoptotic cells [127]. The activity of caspases is regulated by other factors, such as apoptotic peptidase activating factor 1 and cytochrome c, required to activate the caspase pathway [127]. Cytochrome c is transported out of the mitochondria to the cytoplasm and may allow the activation of caspases [127]. The B-cell lymphoma-2 (Bcl-2) family has a role in the induction and inhibition of apoptosis. Indeed, inhibitors such as Bcl-2 and stimulators of apoptosis such as Bax compete to block or allow the translocation of cytochrome c to the cytoplasm through a mechanism that is not completely understood [127].

The anticancer activity of ITCs is also strictly related to the ability of these compounds to induce apoptosis. ITCs have been shown to induce these natural cell mechanisms both *in vivo* and *in vitro*. Several pathways are involved in apoptosis induction, and the main ones are discussed here. First of all, ITCs down-regulate several anti-apoptotic proteins such as Bcl-2 and Bcl-XL and, on the contrary, stimulate the production of pro-apoptotic protein Bax [98] (**FIGURE 1.11**). SFN appears to induce apoptosis through the production of ROS. SFN is one of the more potent ROS inducers among different ITCs [98]. Indeed, SFN-induced ROS production disrupts mitochondrial membrane potential and consequently releases cytochrome c in the cytoplasm, leading to apoptosis [98]. Furthermore, Xu *et al*. highlighted the implication of the Mitogen-activated protein kinases (MAPK) signalling pathways in apoptosis induction [128]. PEITC was shown to bind tubulin, generating the cleavage of caspase -3/-8/-9 inducing apoptosis [119].

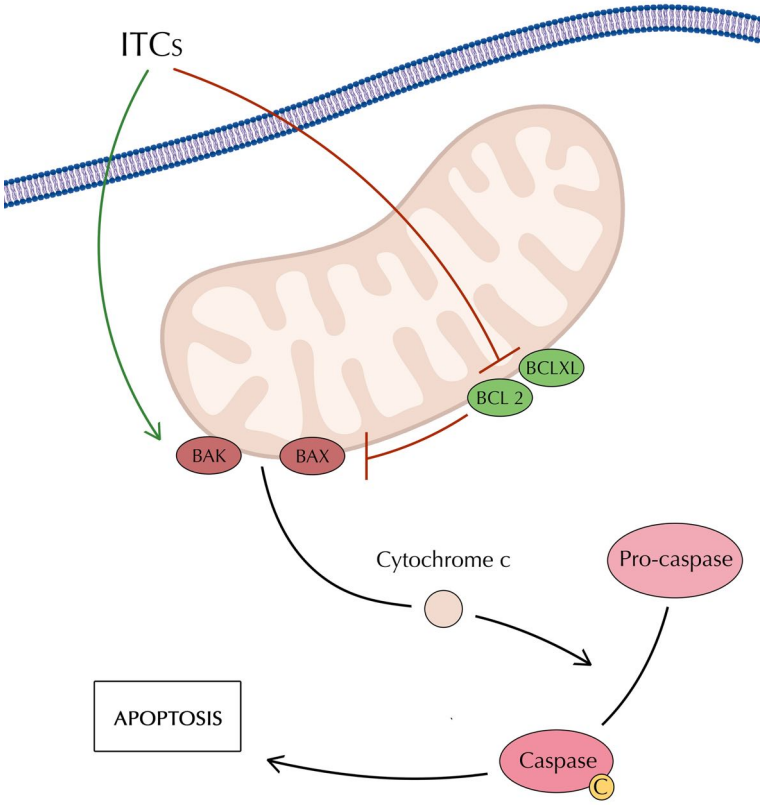

FIGURE 1.11 | ITCs and induction of apoptosis

ITCs control the induction of apoptosis, affecting mitochondrial homeostasis. The inhibition of anti-apoptotic proteins (i.e. Bcl2, B-cell lymphoma-extra large (Bcl-XL) and the stimulation of Bax proteins allow the formation of pores to release cytochrome c into the cytosol. Finally, cytochrome c triggers the cascade of caspases' activation/cleavage that culminates with apoptosis induction.

1.3.2 Anti-metastatic action

Most cancer-associated deaths correlate with metastatic tumours, as there is often no efficient therapeutic solution for metastatic diseases [129]. Once the cells from a primary tumour disseminate to form tumours into secondary sites of the body, the probability of a successful treatment decreases drastically. Therefore, it is vital to explore new therapeutic regimens to fight the metastatic potential of HCC. Metastatic potential is enabled by the activation of traits that give the cancerous cells the ability to migrate from a primary site, invade neighbouring tissues, adhere to a new site, and generate a metastatic colony starting with a group of just a few cells [129]. Several studies underlined the ability of ITCs to suppress cancer cell migration and invasion [130-132], thus reducing the metastatic potential of cancerous cells.

1.3.2.1 Epithelial to mesenchymal transition

Epithelial to mesenchymal transition (EMT) is a process in which epithelial cells are reprogrammed during stages of embryonic development, with the activation of several transcription factors [133]. The transition process allows epithelial cells to gain migratory and invasive capabilities. Therefore, cells can migrate to allow tissue-specific development. The activated transcription factors (i.e. Snail, Twist families) modulate the expression of the cadherin family, which are proteins involved in the modulation of cell adhesion and migration [133]. Cancerous cells exploit this mechanism to migrate and colonise sites to produce metastasis. ITCs are able to inhibit the EMT process in cancerous cells [134]. BITC inhibited the EMT in breast cancer cells *in vivo* through the expression of E-cadherin and the suppression of vimentin and fibronectin [135] and through suppression of Forkhead box protein O1 (FOXQ1) [136]. PEITC synergised with platinum-based chemotherapy to reduce the proliferation of several cancer cell lines that showed stem-cell-like EMT properties through GSH depletion [137], and to reduce the transforming growth factor β (TGF-β)-induced EMT in colorectal cancer through the Smad pathway [138].

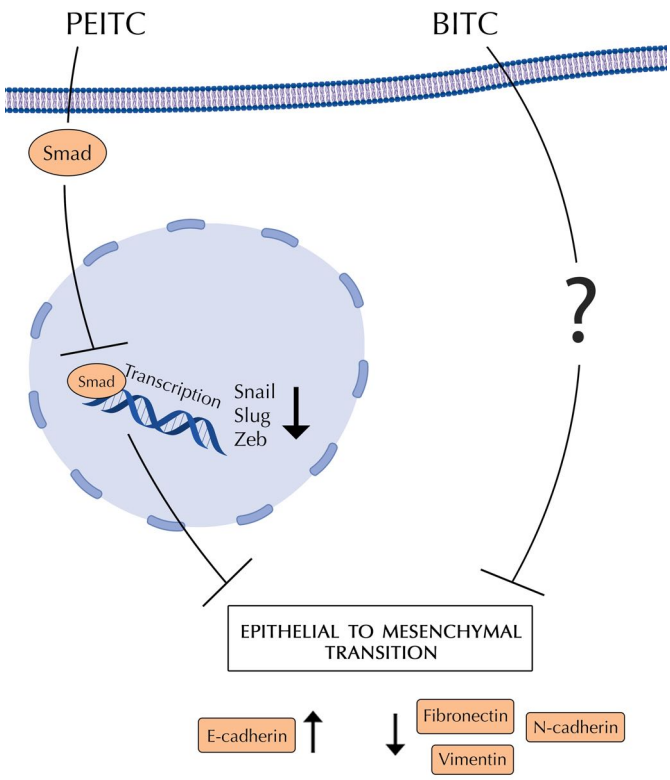

FIGURE 1.12 | ITCs inhibition of EMT.
PEITC inhibits EMT through the inactivation of the Smad pathway that decreases the expression of Snail, Slug, and Zeb genes, leading to increased expression of E-cadherin and reduced expression of N-cadherin and vimentin. BITC inhibits EMT through increased expression of E-cadherin and reduced expression of fibronectin and vimentin, but the mechanism remains unknown.

1.3.2.2 Focal adhesion kinase and actin remodelling

Focal adhesion kinase (FAK) is a non-receptor tyrosine kinase often over expressed in solid cancers [139]. In particular, FAK and its phosphorylated residue Tyr-397 were found over-expressed in HCC [140]. The silencing of FAK expression substantially reduced HCC cell adhesion, migration, and invasion with a reduction of matrix metalloproteinases (MMPs) [140]. Moreover, FAK promotes tumour progression and metastasis, being often associated with advanced-stage malignant tumours [139]. Indeed, FAK control cell motility and invasion, promoting the EMT process in cancerous cells. FAK is involved in expressing MMPs to promote invasion of the extracellular matrix (ECM) and in forming focal adhesions and actin remodelling to allow cell motility and adhesion to the ECM. Focal adhesions provide an anchorage link between the ECM and the cytoskeleton and act as signal transmitters for

downstream pathways, pivotal in cell proliferation and survival [141]. The actin cytoskeleton has a pivotal role in numerous biological processes. The forces generated by actin filaments are responsible for motility processes, therefore playing a role in cancer metastasis [142]. Cytoskeleton structures such as microfilaments, microtubules, and intermediate filaments are also crucial for morphogenesis and the formation and maintenance of new blood vessels [143]. ITCs are known for their anti-metastatic capability through the inactivation of FAK, reducing invasion and metastasis in different types of tumours [144, 145]. The inactivation of FAK leads to reduced expression of MMP-9 and thus reduced tumour invasion. Moreover, ITCs are able to target actin filaments [146, 147]; in particular, PEITC led to disrupted actin fibres organisation and contributed to cell death in lung cancer cells [147] (**FIGURE 1.13**).

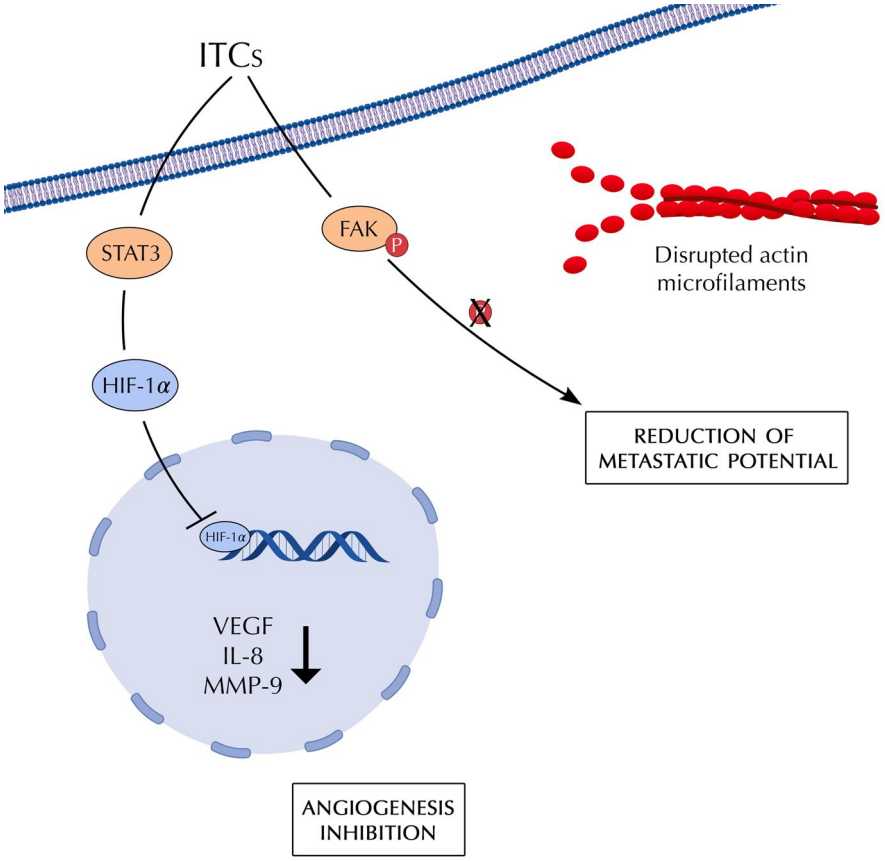

FIGURE 1.13 | ITCs reduction of metastatic potential and angiogenesis.
ITCs have been shown to reduce the cancer metastatic potential by inhibiting cell migration and invasion through deactivation of FAK signalling, as well as targeting actin microfilaments. ITCs also control angiogenesis through HIF-1α via the STAT3 pathway. HIF-1α activates the transcription of genes involved in angiogenesis and cancer cell invasion (i.e. VEGF, IL-8, MMP-9).

1.3.3 Anti-angiogenic action

Angiogenesis plays a fundamental role in tumour development. The growth of blood vessels is under the influence of various angiogenic factors and inhibitors in which equilibrium plays a pivotal role [148]. During development and wound repair, the physiological process could be damaged and become pathological, allowing tumours to grow and develop other diseases [148]. Indeed, different studies showed that oncogenes could increase the expression of pro-angiogenic factors, such as VEGF and bFGF, while suppressing the expression of angiogenesis inhibitors, such as THBS1 [149, 150]. A tumour requires new angiogenesis to grow beyond 1-2 mm in diameter [94] thus an oncogene unable to stimulate the formation of a new network of vessels may be responsible for a harmless microscopic tumour instead of a macroscopic and potentially lethal one [151]. Various molecules are involved in the complex equilibrium that regulates the angiogenesis process. In this equilibrium, tumour cells interact with endothelial cells, immune cells, and ECM [94]. The pathological angiogenesis switch may occur when tumour pro-angiogenic factors modify the equilibrium and overtake the production of natural anti-angiogenic factors [94]. The activity of pro-angiogenic growth factors is accompanied by the action of MMPs that are crucial to prepare the ECM for the outgrowth of new blood vessels [152].

The VEGF family involved in tumour angiogenesis is the most characterised together with their binding domain, the family of receptors tyrosine kinases VEGFR. The main family component involved in tumour angiogenesis is VEGF-A, which binds the receptor VEGFR-2 [153] and VEGFR-1 with much more affinity but weaker signal transduction [154]. Tumour cells usually produce VEGF to stimulate angiogenesis through the binding of VEGFR-2 situated on endothelial cells. However, in rare cases, tumour cells also express this receptor, stimulating angiogenesis with an autocrine mechanism [154]. Furthermore, there is evidence of tumours that express VEGFR-1 inside the cell, stimulating angiogenesis in an intracrine way [155]. The binding between VEGF-VEGFR-2 results in the activation of different pathways culminating with the up-regulation of genes that promote proliferation and migration of endothelial cells, such as MAPK pathway and phosphatidylinositol 3′–kinase (PI3K)–Ak strain transforming (Akt) pathway, which stimulates cell growth and endothelial-cell survive respectively [153]. Other important factors involved in the angiogenesis process are the angiopoietin 1 and 2 (Ang-1, Ang-2) that cooperate with VEGF to produce mature capillaries [154]. Ang-1 and Ang-2 bind the Tyrosine-protein kinase receptor TEK (Tie-2),

expressed on the membrane of endothelial cells [154]. Moreover, the hypoxia-inducible transcription factor 1α and 2α (HIF-1 1α/2α) are potent inducers of VEGF in tumours [156].

Since 1980 a broad range of angiogenesis inhibitors have been developed and approved by the Food and Drug Administration (FDA) [148]. The problem with this type of therapy is that not all tumours respond to it, and side effects include hypertension and bowel perforation [148]. A proposed solution might be the combination of an angiogenesis inhibitor agents with a chemotherapy drug, allowing increased sensitivity to the latter [148]. ITCs showed the ability to reduce the production of pro-angiogenic factors *in vivo*, inhibit cellular migration, and to reduce the formation of blood vessels in cultured human endothelial cells (HUVECs) models [94]. SFN was able to decrease the intratumoral neovascularisation of xenografted liver tumours in mice [132]. BITC inhibited pancreatic tumour angiogenesis in both rat aorta and chorioallantoic membrane models, by reducing the activation of signal transducer and activator of transcription 3 (STAT3) pathway [157]. PEITC inhibited angiogenesis *in vitro* and *ex vivo* with down-regulation of VEGFR-2 and inactivation of Akt [130]. The mechanisms by which ITCs inhibit the expression of pro-angiogenic factors are not completely clear. Different mechanisms and pathways involved are discussed here.

SFN has been shown to influence the expression of VEGF and MMP-9 by inhibiting the transcriptional factors HIF-1α [56]. HIF is a family of 3 transcription factors, but only HIF-1 and HIF-2 are involved in angiogenesis. These factors are formed by two subunits, α and β. The subunit alpha is the hypoxia-inducible factor that, in normoxia conditions, is hydroxylated by oxygen-sensitive prolyl hydroxylases (PHD) [158]. This hydroxylation triggers the bond of VHL protein and ubiquitin ligase, which leads to the ubiquitylation and degradation of the α subunit [158]. On the other hand, hypoxic conditions lead to the inhibition of PHD's action. Consequently, the α subunit is stabilised and, once accumulated, translocates into the nucleus and associates with the β subunit and the hypoxia response element, activating the transcription of pro-angiogenic genes [158]. Also, in normoxia conditions, the factor inhibiting HIF1 (FIH) is hydroxylated in an oxygen-dependent reaction [94]. Indeed, in hypoxia conditions, even the action of the FIH is decreased, increasing the transcription of angiogenic factors. PEITC appeared to influence the translation activity of HIF and SFN to decrease VEGF in hypoxic conditions [94] (**FIGURE 1.13**). BITC down-regulated HIF-1α through the STAT-3 dependent pathway [157].

1.4 Hypothesis, aims, and objectives

As mentioned before, new therapeutic solutions for HCC treatment are required. Single-drug treatment seems insufficient for the treatment of advanced HCC. Considering the results of the latest clinical trials, it seems that combination therapy is the most promising strategy for HCC treatment [7]. ITCs exert an anticancer activity through numerous mechanisms that lead to the prevention and therapy of various types of cancer. ITCs showed promising results in HCC and to be viable candidates to improve the anticancer activity of other chemotherapeutic agents [86]. Therefore, the anticancer activity of ITCs can be exploited to increase the efficacy of clinically approved chemotherapeutic agents. Clinically approved drugs that did not show efficacy in HCC, such as TKIs, may be repurposed for the treatment of HCC in combination with ITCs.

The primary project hypothesis is that ITCs, through their anticancer potential, can enhance the efficacy of TKIs in hepatocellular carcinoma. This PhD research project aimed to evaluate if the ITC-TKI combination have a greater anticancer effect, evaluating if they may work in synergy and to investigate the biochemical and molecular mechanisms behind the synergistic anticancer activity.

The objectives of the project can be summarised as follows:

1. Identify the most effective ITC-TKI combination;
2. Determine the effect of the ITC-TKI combination on cell growth, DNA damage, cell cycle, and programmed cell death;
3. Test the effect of the ITC-TKI combination on metastatic potential i*n vitro* and *in vivo* with tumour xenograft chorioallantoic membrane (CAM) assay;
4. Assess the influence of the ITC-TKI combination on tumour-induced angiogenesis *in vitro* and *in vivo* with yolk sac membrane assay;
5. Evaluate the efficacy of the ITC-TKI combination *in vivo* with a syngeneic mouse model.

Chapter 2: Materials and Methods

2.1 Materials, chemicals, instruments, and software

Generic cell culture plastics were bought from as follows: flasks and dishes (ThermoFisher Scientific UK Ltd, Loughborough, UK), plates (Greiner Bio-One, Kremsmünster, Austria), cell scrapers, strippettes, conical tubes, syringes and filters (Sarstedt, Nümbrecht, Germany).

Generic chemicals such as buffered 10% formalin, methanol, ethanol, EDTA, Tris-Base, NaCl, HEPES, NaOH, HCl, glycerol, CaCl, acetic acid, sucrose where obtained from Fisher Scientific (ThermoFisher Scientific, Loughborough, UK), Tween 20, GSH, N-acetylcysteine (NAC), monobromobimane (mBBr), N-ethylmaleimide (NEM), diethylenetriaminepentaacetic acid (DTPA), methanesulfonic acid (MsOH), Nonidet-NP40, corn oil, dithiothreitol (DTT), Dimethyl sulfoxide (DMSO), and Triton X-100 were purchased from Merck Life Science (Gillingham, UK).

Table 2.1 | Key resources

Product	Supplier	Identifier
Materials		
CELLSTAR® cell repellent U bottom 96-well plates	Greiner Bio-One, Kremsmünster, Austria	650970
ThinCert™ 24 well 8 µm	Greiner Bio-One, Kremsmünster, Austria	662638
Amicon® Ultra-15 3 kDa	Merck Life Science, Gillingham, UK	UFC900396
Leukosilk tape	Health Care Equipment and Supplies Ltd, Ipswich, UK	HCP1309
Round glass coverslips 15 mm	Scientific Laboratory Supplies, Nottingham, UK	MIC3338
Square glass coverslips 18 mm	Chance Propper Ltd., West Midlands, UK	N/A
Teflon rings	Eastern Seals, Ashington, UK	BS013PTFE
Mice feeding tubes 20 gauge x 30 mm	Instech Laboratories, Plymouth Meeting, USA	FTP20-30-50
MX35 Ultra low profile blades	Epredia, Portsmouth, New Hampshire, USA	3053835
Plastic cryomoulds	Agar Scientific Ltd, Stansted, UK	AGG4580
Menzel-Glaser Superfrost plus slides	ThermoFisher Scientific, Loughborough, UK	J1810AMNZ
Menzel-Glaser cover glasses	ThermoFisher Scientific, Loughborough, UK	12342118

Product	Supplier	Identifier
CHEMICALS		
DMEM	Gibco, ThermoFisher Scientific, Loughborough, UK	10938-025
DMEM phenol red free	Gibco, ThermoFisher Scientific, Loughborough, UK	21063-029
MEM	Gibco, ThermoFisher Scientific, Loughborough, UK	32561029
Endothelial Cell Growth Medium 2 (EGM2)	PromoCell GmbH, Heidelberg, Germany	C-22011B
SupplementMix/Endothelial	PromoCell GmbH, Heidelberg, Germany	C-39216
Cryo-SFM	PromoCell GmbH, Heidelberg, Germany	C-29910
FBS	Gibco, ThermoFisher Scientific, Loughborough, UK	10500-064
L-glutamine (200 mM)	Gibco, ThermoFisher Scientific, Loughborough, UK	25030081
Penicillin 100 U/ml Streptomycin (100 µg/ml)	Gibco, ThermoFisher Scientific, Loughborough, UK	15070-063
Trypsin EDTA 0.25%, 0.05%	Gibco, ThermoFisher Scientific, Loughborough, UK	25200-056
Goat serum	Merck Life Science, Gillingham, UK	G9023
Collagen 4 mg/mL	Gibco, Franklin Lakes, New Jersey, USA	A1048301
Matrigel®	Corning, Somerville, Massachusetts, USA	354230
ECM Gel	Merck Life Science, Gillingham, UK	E6909
Cultrex Basement Membrane Extract, Type 3	Bio-Techne Ltd, Abingdon, UK	3632-005-02
SFN	Toronto Research Chemicals, Toronto, Canada	S699115
BITC	Alfa Aesar, ThermoFisher Scientific, Loughborough, UK	A15008
PEITC	Alfa Aesar, ThermoFisher Scientific, Loughborough, UK	A11596
PEITC *in vivo*	Merck Life Science, Gillingham, UK	253731
Lapatinib	Merck Life Science, Gillingham, UK	SML2259
Gefitinib	Merck Life Science, Gillingham, UK	SML1657
Dasatinib	Merck Life Science, Gillingham, UK	SML2589
Sorafenib tosylate	Advanced ChemBlock Inc., Burlingame, California, USA	G-6085

Product	Supplier	Identifier
STAINING AND HISTOLOGY		
Crystal violet	Merck Life Science, Gillingham, UK	V5265
Calcein AM	Merck Life Science, Gillingham, UK	C1359
Ethidium homodimer-1	Merck Life Science, Gillingham, UK	E1903
ProLong™ Gold Antifade Mountant with DAPI	ThermoFisher Scientific, Loughborough, UK	P36931
OCT compound	Agar Scientific Ltd, Stansted, UK	AGR1180
Haematoxylin	Merck Life Science, Gillingham, UK	HHS32
Eosin	Merck KGaA, Darmstadt, Germany	HX884852
Shandon Xylene substitute	ThermoFisher Scientific, Loughborough, UK	FIS9999122
DPX mountant	VWR, Radnor, Pennsylvania, USA	MERC1.00579.0500_P
COMMERCIAL ASSAYS		
DCFDA - Cellular ROS Assay Kit	abcam Inc., Cambridge, UK	ab113851
BD Pharmingen™ PI/RNase staining	BD Biosciences, Franklin Lakes, New Jersey, USA	550825
Annexin V PI staining kit	Invitrogen, ThermoFisher Scientific, Loughborough, UK	V13242
Apoptosis Human Proteome Profiler™	Bio-Techne Ltd, Abingdon, UK	ARY009
Angiogenesis Human Proteome Profiler™	Bio-Techne Ltd, Abingdon, UK	ARY007
DuoSet® ELISA Ancillary kit	Bio-Techne Ltd, Abingdon, UK	DY008
DuoSet® ELISA VEGF kit	Bio-Techne Ltd, Abingdon, UK	DY293B
ELISA PlGF/VEGF heterodimer kit	Bio-Techne Ltd, Abingdon, UK	DY297
WESTERN BLOTTING		
Bradford reagent	Merck Life Science, Gillingham, UK	B6916
Protease Inhibitor Cocktail (100X)	Cell Signaling Technologies, Leiden, NL	5871S
Pierce™ Phosphatase Inhibitor Mini Tablets	ThermoFisher Scientific, Loughborough, UK	A32957
4x NuPage LDS sample buffer	Invitrogen, ThermoFisher Scientific, Loughborough, UK	NP0007
TruPAGE™ TEA-Tricine SDS Running Buffer	Merck Life Science, Gillingham, UK	PCG30001
PageRuler™ Plus	Invitrogen, ThermoFisher Scientific, Loughborough, UK	26619 26616

Product	Supplier	Identifier
Immobilon FL PVDF	Merck Life Science, Gillingham, UK	IPFL00010
TBS blocking buffer	LI-COR Biotechnology, Cambridge, UK	927-60001
IRDye® 800CW Streptavidin	LI-COR Biotechnology, Cambridge, UK	926-32230
Antibodies	Santa Cruz Biotech, Dallas, Texas, USA R&D Systems, Bio-Techne Ltd, Abingdon, UK Cell Signaling Technologies, Leiden, NL ECM Biosciences, Aurora, Colorado, USA Upstate, Merck Life Science, Gillingham, UK LI-COR Biotechnology, Cambridge, UK	TABLE 2.6 TABLE 2.7
PCR		
Quick-DNA Microprep Kit	Zymo Research, Irvine, USA	D3021
MassRuler™ DNA Ladder	ThermoFisher Scientific, Loughborough, UK	SM0403
SYBR safe DNA gel stain	ThermoFisher Scientific, Loughborough, UK	S33102
Mammalian Total RNA Miniprep	Merck Life Science, Gillingham, UK	RTN70
qScript cDNA SuperMix	Quantabio, Beverly, Massachusetts, USA	95048
Precision-LR qPCR Mastermix	Primerdesign Ltd, York, UK	Precision-LR
Primers and probes	Merck Life Science, Gillingham, UK	TABLE 2.8
EXPERIMENTAL MODELS: CELL LINES AND ORGANISMS		
HepG2 cell line	American Type Culture Collection (ATCC), Manassas, Virginia, USA	HB-8065
HHL-5 cell line	Kind gift from Prof. Arvind Patel	Clayton *et al.* [159]
Hepa 1-6 cell line	American Type Culture Collection (ATCC), Manassas, Virginia, USA	CRL-1830
HUVECs cell line	PromoCell GmbH, Heidelberg, Germany	C-12200
C57BL/6NHsd 6-7 Weeks	Envigo RMS, Bicester, UK	11204F
Fertilised Shaver Brown chicken eggs	Henry Stewart & Co Ltd, UK	N/A
CRITICAL INSTRUMENTS		
EVOS M5000 Imaging System	ThermoFisher Scientific, Loughborough, UK	N/A
Leica DMI3000 B	Leica Biosystems Nussloch GmbH, Nußloch, Germany	N/A
Stemi SV11	ZEISS, Germany	N/A

Product	Supplier	Identifier
IM IC5500	Ricoh Company Ltd, Tokyo, Japan	N/A
iPhone 11 Pro	Apple, Cupertino, California USA	N/A
FLUOstar Omega	BMG Labtech Ltd., Bucks, UK	N/A
BD FACSymphony A1™	BD Biosciences, Franklin Lakes, New Jersey, USA	N/A
Cube 6	Sysmex Partec GmbH, Goerlitz, Germany	N/A
GBOX Chemi XRQ	Syngene, Cambridge, UK	N/A
Odyssey CLx Imaging System	LI-COR Biotechnology, Cambridge, UK	N/A
Nanodrop 2000	ThermoFisher Scientific, Loughborough, UK	N/A
Veriti 96 well thermal cycler	ThermoFisher Scientific, Loughborough, UK	N/A
Mini Protean Tank	Bio-Rad Laboratories, Hercules, California, USA	N/A
Trans-Blot® Turbo™ Transfer System	Bio-Rad Laboratories, Hercules, California, USA	N/A
QuantStudio 5	ThermoFisher Scientific, Loughborough, UK	N/A
Gilson HPLC-306 Laboratory system	Gilson, Middleton, Wisconsin, USA	N/A
HiChrom ACE-AR C18	Phenomenex, Torrance, California, USA	N/A
Jasco FP-920	Oklahoma City, Oklahoma, USA	N/A
Leica CM1850 UV	Leica Biosystems Nussloch GmbH, Nußloch, Germany	N/A
SOFTWARE AND ALGORITHMS		
GraphPad Prism 9	GraphPad software, San Diego, California USA	v9.1.1
Compusyn	ComboSyn Inc., Paramus, New Jersey USA	N/A
ModFit LT	Verity Software House, Topsham, Maine, USA	v6.0.11
FlowJo 10.4	BD Biosciences, Franklin Lakes, New Jersey, USA	v10.4
Image Studio Lite 5.2.5	LI-COR Biotechnology, Cambridge, UK	v5.2.5
Clarity 2.6	DataApex, Prague, Czech Republic	v2.6
Adobe Photoshop 22.4.3	Adobe, San Jose, California, USA	v22.4.3
ChemDraw 16.0.1.4	ParkinElmer, Waltham, Massachusetts,, USA	v16.0.1.4

Product	Supplier	Identifier
ImageJ 1.53k	National Institute of Health, Bethesda, Maryland, USA	v1.53k
Colony area	ImageJ macro, GitHub	Guzmán *et al.* [160]
MRI Wound Healing Tool	ImageJ macro, GitHub	Cormier *et al.* [161]
Colour Threshold method	ImageJ macro	O'Brien *et al.* [162]
Angiogenesis Analyzer	ImageJ macro, NIH	Carpentier *et al.* [163]

2.2 Cell culture

HepG2, a carcinoma cell line taken from a primary hepatocellular carcinoma, was cultured in DMEM$^+$, composed of DMEM supplemented with 10% (v/v) FBS, 1% (v/v) L-glutamine (200 mM), penicillin (100 U/ml) and streptomycin (100 μg/ml), at 37 °C, 5% (v/v) CO_2, and cultured to a maximum of 20 passages.

HHL-5, an immortalised human hepatocyte-derived line 5, was provided by Professor Arvind Patel from the Department of Infection, Immunity & Inflammation, University of Glasgow [159], and cultured in DMEM$^+$, composed of DMEM supplemented with 10% (v/v) FBS, 1% (v/v) L-glutamine (200 mM), penicillin (100 U/ml) and streptomycin (100 μg/ml), at 37 °C, 5% (v/v) CO_2, and cultured to a maximum of 20 passages.

HUVECs, human umbilical vein endothelial cell line, was cultured in EGM2$^+$, composed of EGM2 supplemented with SupplementMix/Endothelial, (EGM2$^-$ refer to medium without SupplementMix) penicillin (100 U/ml) and streptomycin (100 μg/ml), at 37 °C, 5% (v/v) CO_2. HUVECs were cultured in flasks pre coated with 2% (v/v) collagen solution (4 mg/mL) and cultured to a maximum of 8 passages as specified by the supplier (15 doublings). Cells were sub-cultured using T75 flasks with 10 ml of DMEM$^+$, which was replaced every 2 days.

Hepa1-6, a murine carcinoma cell line generated from the BW7756 mouse hepatoma that arose in a C57BL6 mouse [164], was cultured in DMEM$^+$, composed of DMEM supplemented with 10% (v/v) FBS, 1% (v/v) L-glutamine (200 mM), penicillin (100 U/ml) and streptomycin (100 μg/ml), at 37 °C, 5% (v/v) CO_2, and cultured to a maximum of 10 passages.

Cell lines actively growing in flasks were kept at 37°C, 5% CO_2 and all the processes were conducted in conditions of sterility in a Class II Biological Safety Cabinet. The

subculturing process was carried out once the confluence reached 80%. The medium was removed and flasks washed twice with PBS. Then, 2 ml of 0.25% (v/v) trypsin-EDTA (0.05% for HUVECs) was added and the flask incubated at 37 °C, 5% CO_2 for 5 minutes (3 minutes for HHL-5) (2 minutes RT for HUVECs) to detach all the cells from the plastic surface. Once the trypsin was neutralised with 8 ml of complete medium with 10% FBS, the solution containing the cells was centrifuged for 5 minutes at 250 x g (220 x g for HUVECs). Cells were seeded either in new T75 flasks for subculture or in various plastic culture vessels for incubation with different test compounds in medium. Cell lines were preserved by resuspension in a freezing medium made of 10% (v/v) DMSO 90% (v/v) FBS, or Cryo-SFM for HUVECs and then subject to controlled temperature reduction to -80 °C. For all experiments with ITCs or other compounds 0.1% DMSO was used as vehicle control (unless otherwise stated) as no difference was observed between 0.1% (v/v) and 0.2% (v/v) of DMSO in the assays employed (**FIGURE A1**).

2.3 Cell growth

2.3.1 Cell viability - MTT assay

MTT is the acronym for (3-(4,5-dimethylthiazol-2-yl)-2,5-diphenyltetrazolium bromide) tetrazolium and it is the most used assay to study cell viability. Cells reduce MTT to formazan through an electron transfer involving cellular cofactors such as NADH and mitochondrial succinate dehydrogenase. This product is deposited near the cell membrane or it is secreted into the extracellular environment. Formazan is produced only by viable cells and it gives purple colour to the solution. This type of analysis is considered an endpoint assay because the cytotoxic nature of this compound, which deprives cofactors to the cellular metabolism, leads to cell death. To quantify the amount of formazan produced, the solution needs to be analysed with a spectrophotometer to calculate the absorbance at 570 nm (the formazan maximum absorbance value). Before reading the absorbance, the formazan needs to be solubilised using various solutions such as DMSO [165].

Cells were seeded in 96-well plates (HepG2 7×10^3 cells/well, HHL-5 5×10^3 cells/well, Hepa1-6 5×10^3 cells/well) and once reached 70% of confluency, DMEM$^+$ with test compounds was added (**FIGURE 2.1**). After 24 h, 100 µL of 10% (w/v) 5 mg/mL MTT in DMEM$^+$ was added to each well and incubated at 37 °C for 1 h. The MTT solution was removed and the formazan crystals formed were then dissolved in 100 µL of DMSO per

well. The absorbance was determined using a FLUOstar omega plate reader at 550 nm. Cell viability was calculated as follows:

$$\text{Cell viability \%} = \frac{\text{Test}_{A550nm}}{\text{Control}_{A550nm}} \times 100$$

Values of IC_{50} were calculated using Prism 9.1.1 using a Nonlinear fit with the equation "Inhibitor vs response, variable slope (four parameters)", while combination index (CI) values were calculated using Compusyn software that employ the Chou-Talalay method, based on the median-effect equation.

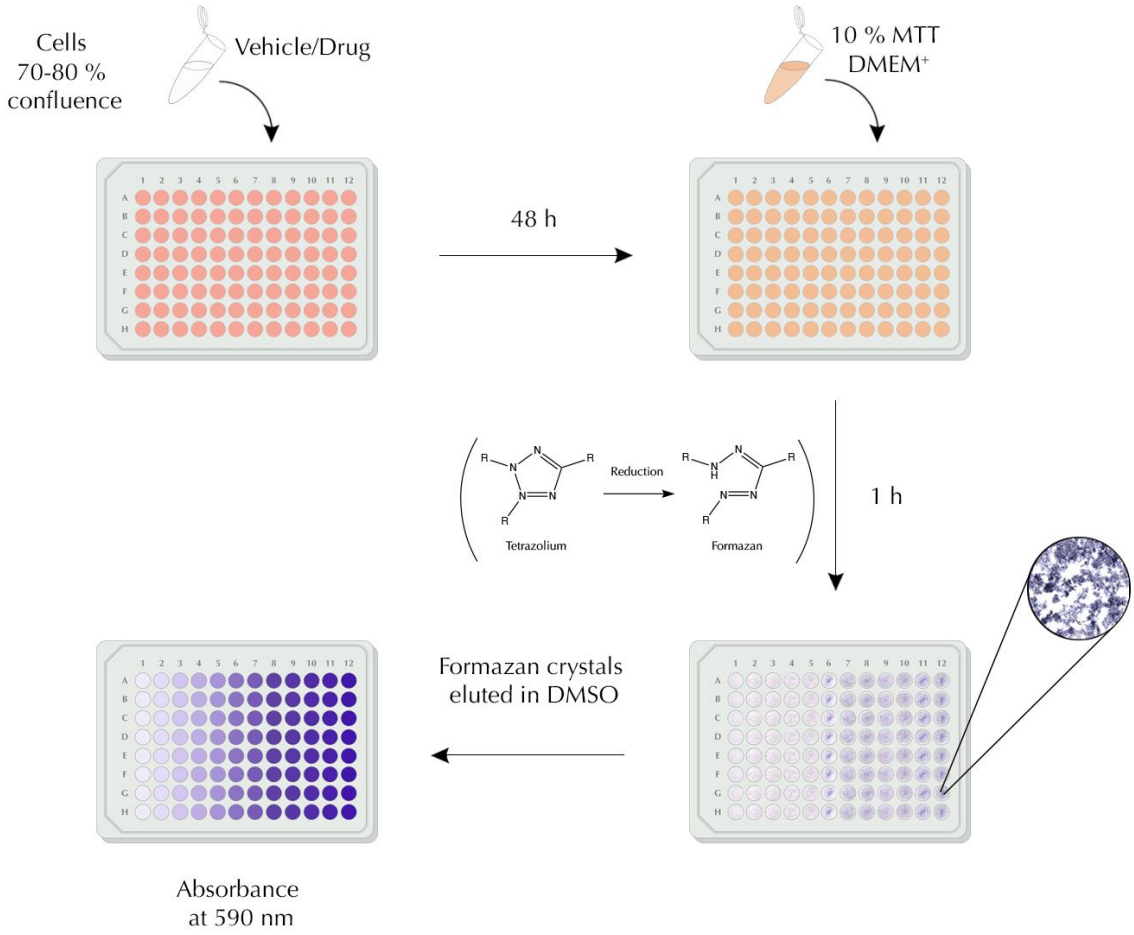

FIGURE 2.1 | Diagram of MTT assay

2.3.2 Cell clonogenic capacity - Colony formation assay

The clonogenic or colony formation assay evaluates the ability of single cells to grow and form a colony formed at least by 50 cells. The assay studies the cell division capacity of a given population. This assay is often used to test the cytotoxicity radiation of cytotoxic

agents. Cells were seeded at low density, or reseeded at low density after treatment. After initial treatment, cells were cultured for 1-3 weeks then fixed and stained and the number of colonies are counted [166].

Cells were seeded in 6-well plates (HepG2 $5x10^3$ cells/well) and incubated for 24 h. Then DMEM+ containing test compounds was added to the cells and incubated for a further 24 h (**FIGURE 2.2**). After 24 h the medium was replaced without test compounds. Cell cultures were maintained for 18 days with medium changed every 5 days. The colonies formed were fixed with 10% buffered formalin for 20 minutes and stained with 0.1% Crystal violet for 20 minutes. Macroscopic images were acquired using a document scanner IM IC5500 with 600 dpi glossy colour image settings. The colony area was evaluated using ImageJ 1.53k software with the macro "Colony area" described in *Guzmán et al.* [160].

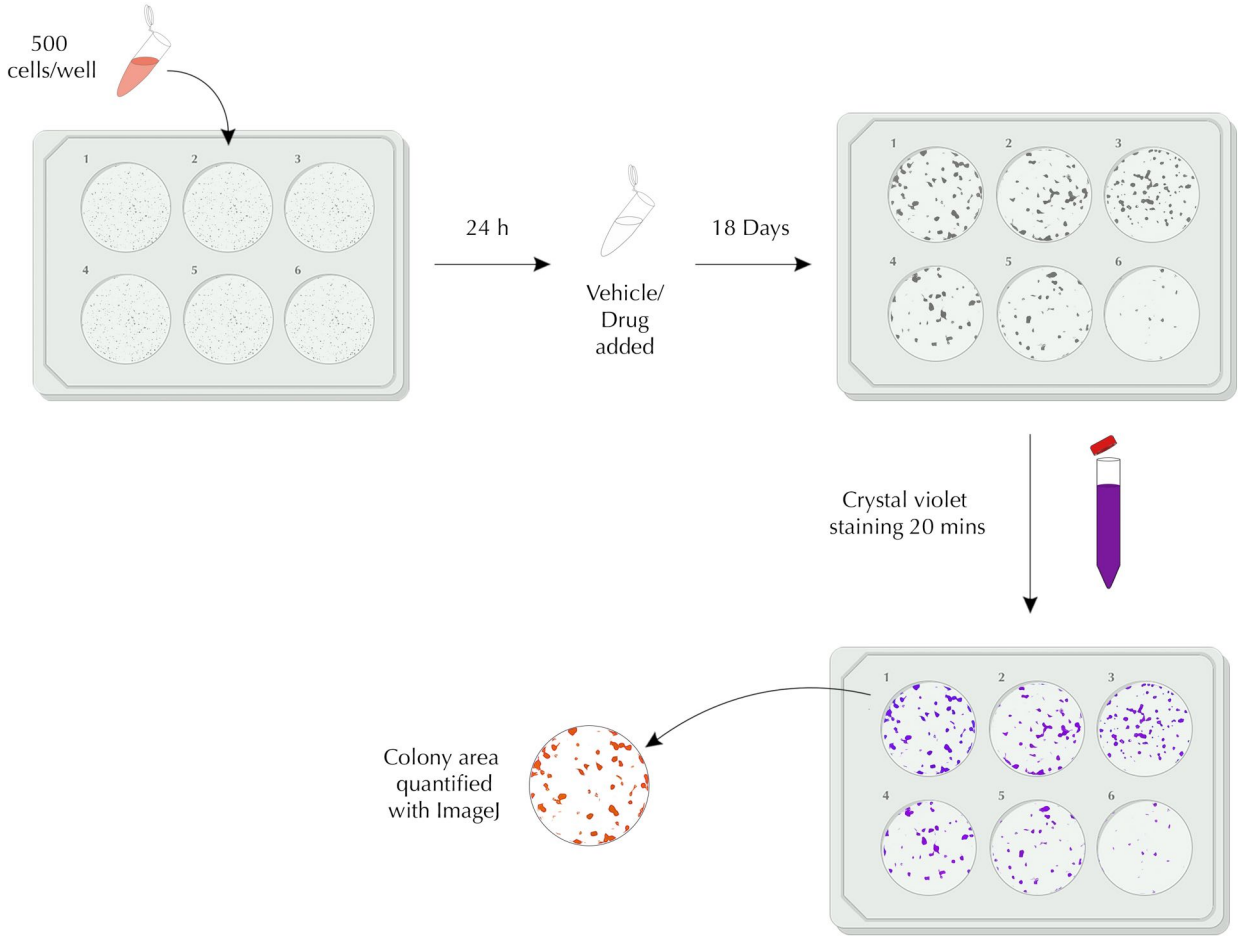

FIGURE 2.2 | Diagram of colony formation assay

2.3.3 3D spheroids model

Canonical 2D cell culture models are not able to accurately mimic the complexity of the tumour structure. Therefore, 3D spheroids are employed to better mimic the architecture of tumour cells organised in a solid mass [167].

On day 0 cells were seeded in 96-well plates CELLSTAR® cell repellent U bottom (HepG2 1.25x10^3 cells/well, Hepa 1-6 500 cells/well) with addition of ECM Gel without phenol red (8 mg/mL) at a final concentration of 0.1 mg/mL with 50 µL/well as total volume (**FIGURE 2.3**). The plates were immediately centrifuged for 5 minutes at 210 x g at room temperature. After that the plates were incubated for 3 days to allow the formation of the spheroids. On day 3 images of the cell spheroids were taken then 50 µL of DMEM+ containing test compounds were added. On day 6 spheroids were ready for further analysis.

2.3.3.1 Spheroids size growth - Area quantification

For the size quantification images of the spheroids were taken with a EVOS M5000 Imaging System on day 3 before the addition of the test compounds and on day 6 after 72 h of treatment. The size of the spheroids was analysed using ImageJ 1.53k software as follows:

Analyse > Set scale (Set appropriate scale px to µm)

Image > Adjust > Brightness and contrast

Image > Adjust > Threshold

Analyze Particles > 50000-infinity

The size growth was calculated as follows:

$$\text{Growth size} = At_1 - At_0$$

where At_1 is the spheroid on day 6, and At_0 is the spheroid on day 3. The images shown are representative of a set of three spheroids for each conditions. The quantitative results presented are the mean of a minimum of three independent experiments with 6 spheroids for each experiment.

2.3.3.2 Viability determination - Calcein AM and ethidium homodimer staining

For the viability staining on day 6, spheroids were washed by removing 100 µL of media and adding 100 µL of PBS containing 2.5% (v/v) FBS twice, and then after removal of 100 µL of volume from the well, 100 µL of2x staining solution were added (Calcein AM 2 µM , Ethidium homodimer-1 6 µM final, to give a final concentration of 1 µM and 3 µM respectively, in PBS containing 0.5% (v/v) FBS). Images were taken using appropriate filters with a Leica DMI3000 B at 10x magnification.

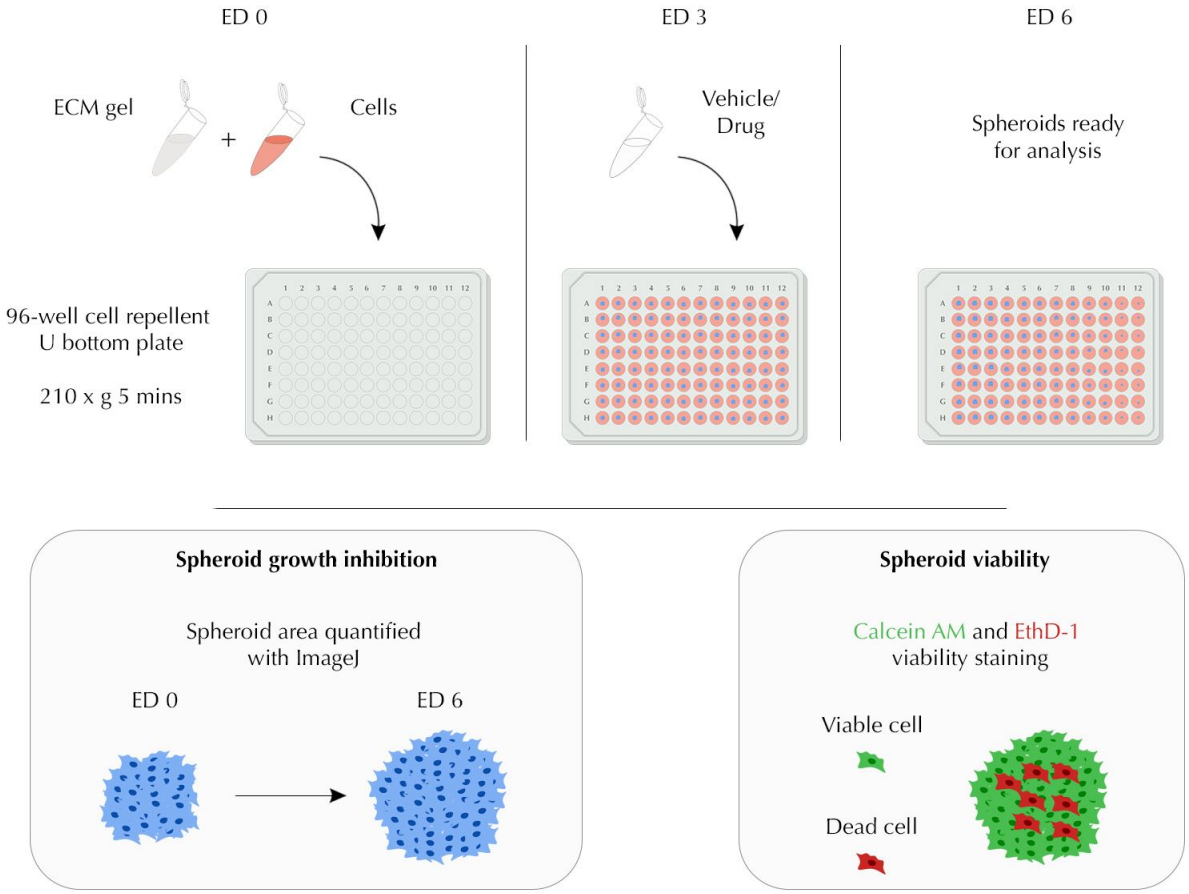

FIGURE 2.3 | Diagram of establishment of 3D spheroids model

2.4 Cell death and apoptosis

2.4.1 Apoptotic DNA assessment - DNA fragmentation assay

A typical hallmark of apoptosis is the formation of DNA fragments. There are several types of DNA fragmentation such as inter-nucleosomal DNA cleavage, fragmentation into large DNA fragments, and single strand cleavage [168]. DNA fragments can be observed using a

conventional agarose gel electrophoresis that allow visualisation of the fragmented DNA that appear as a smear commonly referred as DNA ladder [169].

Cells were seeded in 6-well plates (HepG2 1.8x10^5 cells/well) and grown to confluence, DMEM$^+$ with different test compounds were added. After 24 h cells were washed twice with PBS and then DNA was extracted with Quick-DNA Microprep Kit. DNA samples were quantified with Nano drop and 2 ng of DNA were mixed with 3 µL of 6X loading dye. Samples were loaded into an agarose gel 1.2% (w/v), with 4 µL of SYBR safe DNA gel stain, together with MassRuler™ DNA Ladder, and run at 120 V for 120 minutes. DNA fragmentation was observed with a transilluminator GBOX Chemi XRQ.

2.4.2 Cell cycle analysis - Propidium iodide staining flow cytometry

During the life of a single cell numerous external stresses can arise and lead to DNA damage. Intracellular checkpoints have the aim to check for possible errors in DNA replication to ensure proper development of daughter cells [170]. In case of identification of an error, the error it can be repaired or the cells goes into a cell cycle arrest with a consequent induction of apoptosis. In this assay propidium iodide was used as a DNA staining dye, and flow cytometry used to quantify stained cells. The resultant signal distribution was analysed with a mathematical model to fit a curve to quantify the number of cells in a specific cell cycle phase.

Cells were seeded in 6-well plates (HepG2 3.2x10^5 cells/well) and once reached confluence, DMEM$^+$ with different test compounds was added (**FIGURE 2.4**). After 24 h, cells were detached with 350 µL of trypsin-EDTA (0.25% (v/v)) and centrifuged at 300 x g for 5 minutes. The cell solution was washed (300 x g for 5 minutes) in 10 ml of cold PBS and after that were fixed in 5 mL of 70% Et OH added drop by drop while vortexing the pellet. Cells were fixed at -20 °C for at least 2 h. Fixed cells were washed once in 1 mL of PBS and once in 2% (v/v) FBS PBS. Washed cells were stained with 500 µL of BD Pharmingen™ PI/RNase staining buffer. After 15 minutes, samples were analysed with the flow cytometer BD FACSymphony A1™ and 10,000 events were collected. Finally, the data were analysed using ModFit LT 6.0.11 software to quantify the cells present in each phase of the cell cycle.

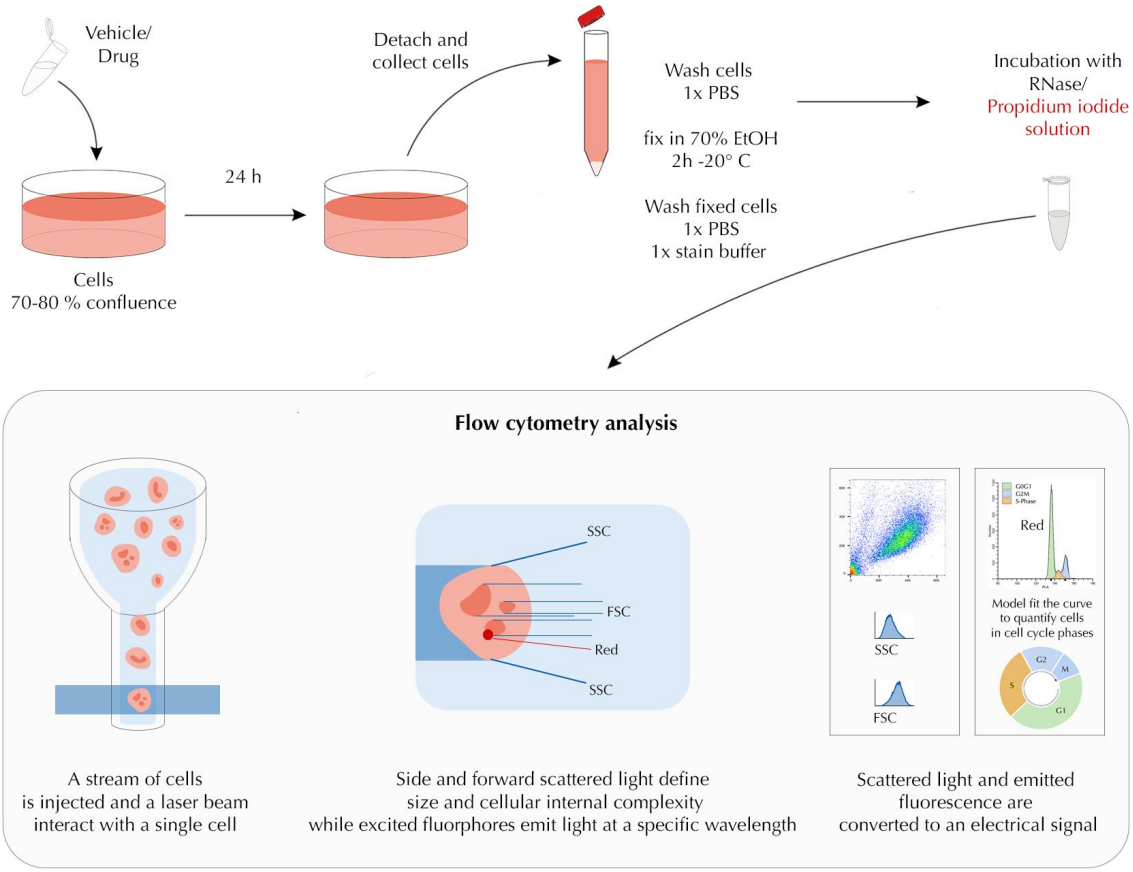

FIGURE 2.4 | Diagram of cell cycle phases analysis by flow cytometry

2.4.3 Apoptosis detection - Annexin V and propidium iodide staining flow cytometry

Annexin V is a Ca^{2+} dependent phospholipid-binding protein that has a high affinity for phospholipid phosphatidylserine (PS). PS is a particular phospholipid which is usually present in the inner leaflet of the phospholipid membrane. When a cell goes into the apoptosis process, PS is translocated into the outer leaflet to be exposed to the extracellular environment, to label the cell for disposal. Annexin V binds PS to label all the cells that are going to apoptosis. The addition of a fluorescent label (i.e. FITC - green) allows to identify and quantify all the PS labelled cells. On the other hand, Propidium iodide (PI) can only enter dead cells and stain the DNA, fluorescing in red. PI penetrates only damaged or destroyed cell membranes. Consequently, viable cells are negative for both dyes: dead cells are stained by PI, late apoptotic are stained by both the dyes, and early apoptotic cells are stained by Annexin V only [171].

Cells were seeded in 12-well plates (HepG2 $1.5x10^5$ cells/well, Hepa 1-6 $9x10^5$ cells/well) and once reached confluence, DMEM+ with different test compounds was added

(FIGURE 2.5). After 24 h, exhausted medium and PBS, used to wash the wells, were collected and the cells were detached with 200 µL of trypsin-EDTA (0.25% (v/v)) and centrifuged at 300 x g for 5 minutes. The cell solution was washed (300 x g for 5 minutes) in 1 ml of cold PBS and after that in 1 ml of cold binding buffer (0.1 M HEPES (pH 7.4), 1.4 M NaCl, 25 nM $CaCl_2$). Then, cells were resuspended in binding buffer at a density of $1x10^6$ cells/ml. 100 µL of cell solution was added with 5 µL of Annexin V and samples were incubated for 15 minutes in the dark. After, cells were washed (300 x g for 5 minutes) adding 900 µL of binding buffer to remove excess of Annexin V. The pellet was resuspended in 200 µL of binding buffer with addition of 5 µL of propidium iodide. After 15 minutes, 900 µL of binding buffer were added and each sample was analysed with the flow cytometer Cube 6 and 10,000 events were collected. Finally, the data were analysed using FlowJo 10.4 software. H_2O_2 treated well was used as apoptosis positive control, flow cytometry compensation was carried out with samples added with Annexin V or propidium iodide only. Results are expressed as a percentage of healthy, early apoptotic, late apoptotic, and necrotic cells.

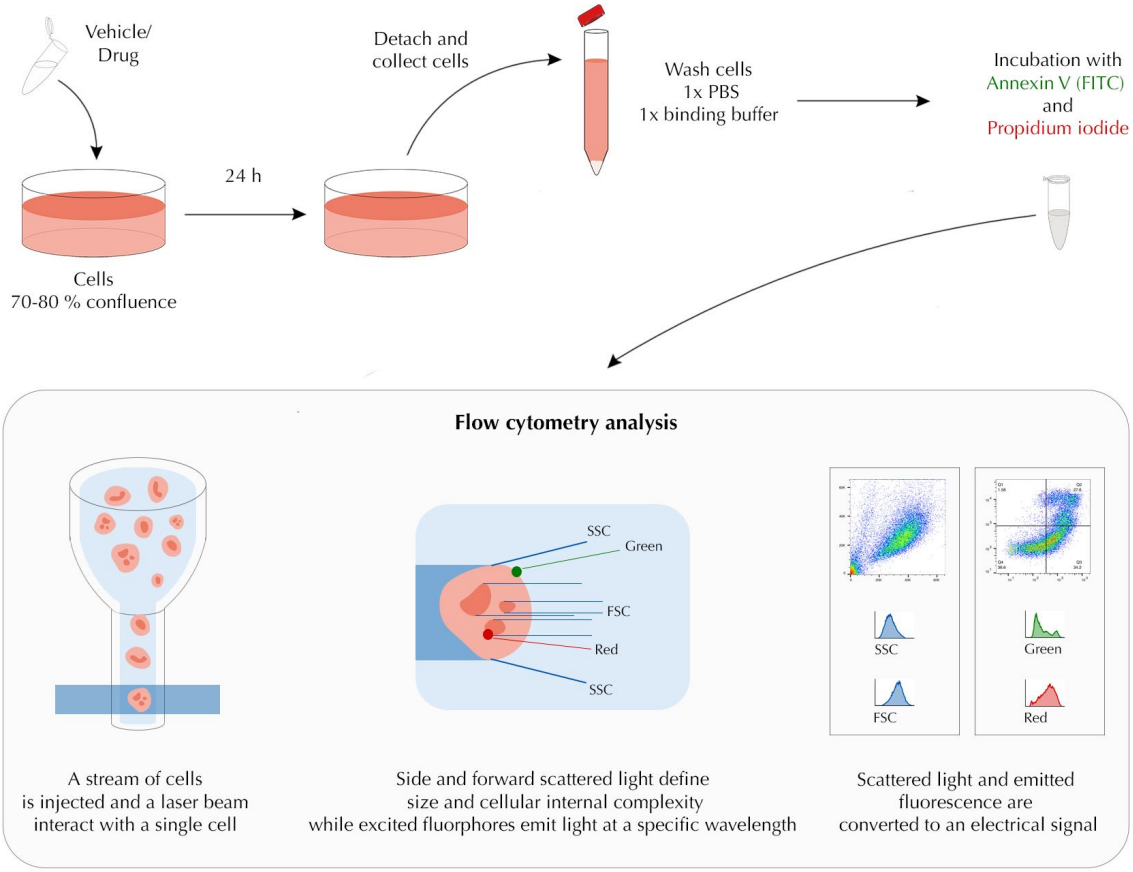

FIGURE 2.5 | Flow cytometry-based apoptosis detection

2.4.4 Apoptosis morphological assessment - DAPI staining

DAPI (4,6-diamidino-2-phenylindole-dihydrochloride) is a fluorescent stain that allows the visualisation of DNA in live and fixed cells. DAPI binds strongly to adenosine-thymidine rich regions of DNA through electrostatic interactions [172]. During apoptosis the cell DNA is fragmented and chromatin appears condensed due to a loss of structural organisation. Furthermore, as the cell loses contact from the ECM it shrinks and starts to form blebs due to loss of the cytoskeleton structure [173]. DAPI staining is often used to image apoptotic cells as the stain allows to distinguish the modifications in terms of DNA structure and organisation. Nuclear fragmentation and cell blebbing can be observed and shrunken nuclei with dense chromatin appears brighter [173].

Cells were seeded on coverslips placed inside 6-well plates (HepG2 $1.5x10^5$ cells/well) and once the monolayer reached confluence, DMEM+ with different test compounds was added (**FIGURE 2.6**). After 24 h cells were washed with PBS and then fixed with 10% (v/v) buffered formalin for 15 mins and permeabilised with Triton X-100 (0.1% (v/v) in PBS) for 30 mins. After that, the coverslips were transferred to a glass slide with 25 µL of ProLong™ Gold Antifade Mountant with DAPI and incubated for 30 mins in the dark. Finally, morphological changes were observed using fluorescence microscope Leica DMI3000 B with a 100x magnification.

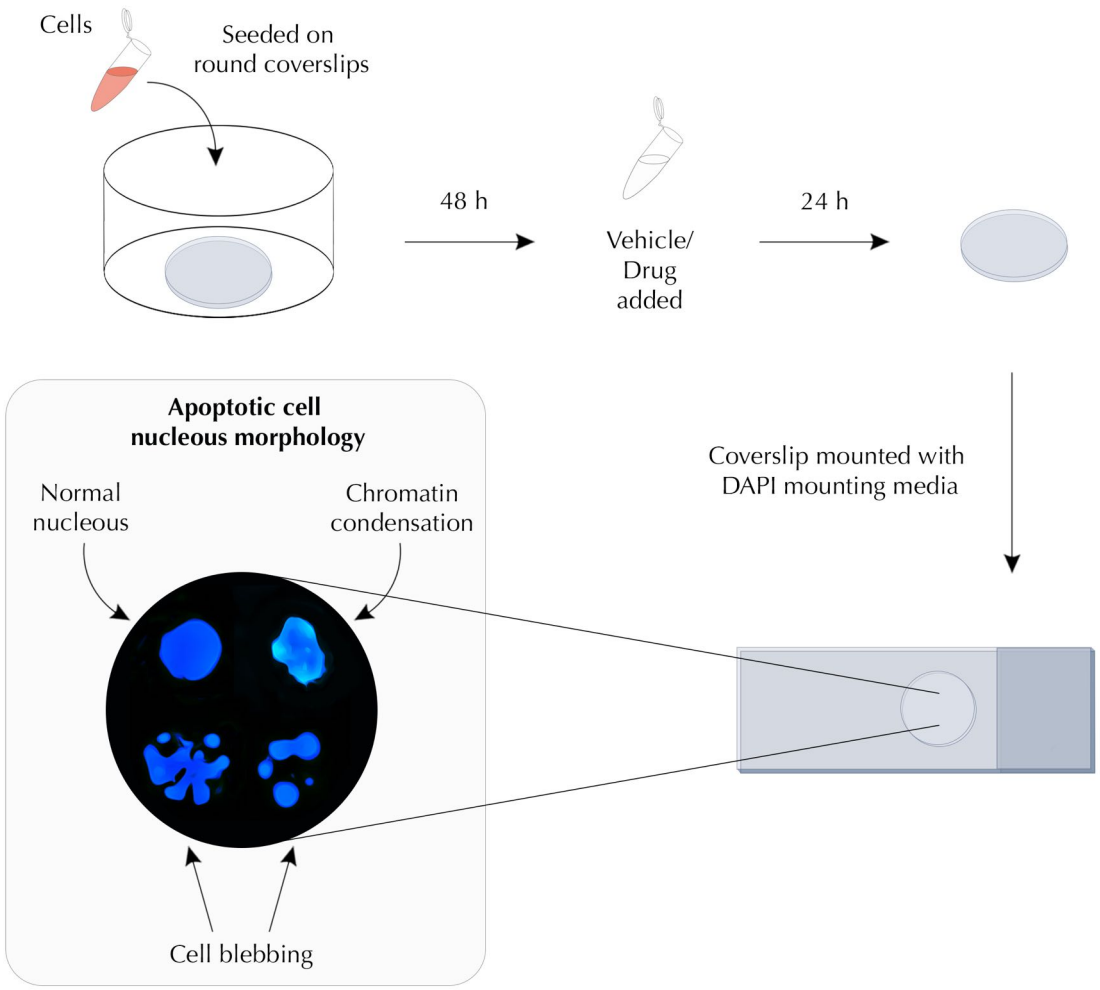

FIGURE 2.6 | DAPI staining for apoptosis morphological assessment

2.4.5 Apoptotic protein expression analysis - Antibody array

In order to identify the apoptotic factors involved in the PDc anti-apoptotic action, the Proteome Profiler™ Human Apoptosis Antibody Array was used to analyse lysate samples. Antibody arrays allow the multiplexed use of antibodies to analyse several targets using low amount of sample [174]. The Proteome Profiler™ is a membrane-based sandwich immunoassay. A cocktail of detection antibodies is mixed with the sample and then incubated with a membrane that contain multiple antibodies captured in dots on the membrane. Therefore, every dot correspond to a specific target of interest. The detection antibodies are biotinylated, allowing the quantification of the membrane bound antibodies using streptavidin conjugated with a fluorophore. The signal generated is relatively proportional to the amount of analyte and it is compared to a control.

As per manufacturer instructions the membranes were blocked with blocking buffer for 1 h at room temperature. In the meantime, 300 µg cell lysates were diluted and mixed with blocking buffer to a final volume of 1.5 mL. The membrane were incubated with the sample solution over night at 4 °C on a rocking platform. After that the membranes were washed three times 10 minutes each and incubated with a detection antibody cocktail for 1 h at room temperature on a rocking platform. Then the membranes were washed three times 10 minutes each and incubated with IRDye® 800CW Streptavidin for 30 minutes at room temperature. After 3 further washes of 10 minutes each the membranes were imaged with Odyssey CLx Imaging System. The dot density was quantified using Image Studio Lite 5.2.5 software and compared to the signal of a control membrane.

2.5 Cell redox state analysis

2.5.1 ROS levels quantification - DCFDA staining

ROS play a fundamental role in redox signalling but can also lead to cell damage. Consequently, ROS have a dual role in physiological and patophysiological processes [175]. Increased production of ROS is often used in chemotherapy to induce DNA damage and cell death as cancer cells are susceptible due to their imbalanced redox status [176]. ROS levels were measured with a DCFDA cellular ROS assay kit. The protocol was adapted from Brandolini *et al* [177] and also optimised following Reiniers *et al* [178].

Cells were seeded in a 96-well plate at a density of 25,000 cells/well in triplicates and incubate overnight to allow cells to adhere (**FIGURE 2.7**). The day after the medium was removed and wells were washed with 100 µL of 1x buffer. 100 µL of a solution of DCFDA staining 25 µM in 1X buffer was added and the plate was incubated for 45 mins 37 °C. DCFDA solution was then removed and the wells were washed with 100 µL 1X buffer. Treatment and positive control (TBHP) were diluted in DMEM High Glucose, 25 mM HEPES, phenol red free, L-glutamine, 10% (v/v) FBS and 100 µL were added to the wells. The plate was incubated in a plate reader FLUOstar omega at 37 °C 5% (v/v) CO_2 for 4 h with readings (Ex/Em = 485/535) every 30 mins. Fluorescent intensity values were normalised to T_0 readings. Representative images were taken after 4 h of incubation with a Leica DMI3000 B at 20x magnification with same exposure levels for all conditions.

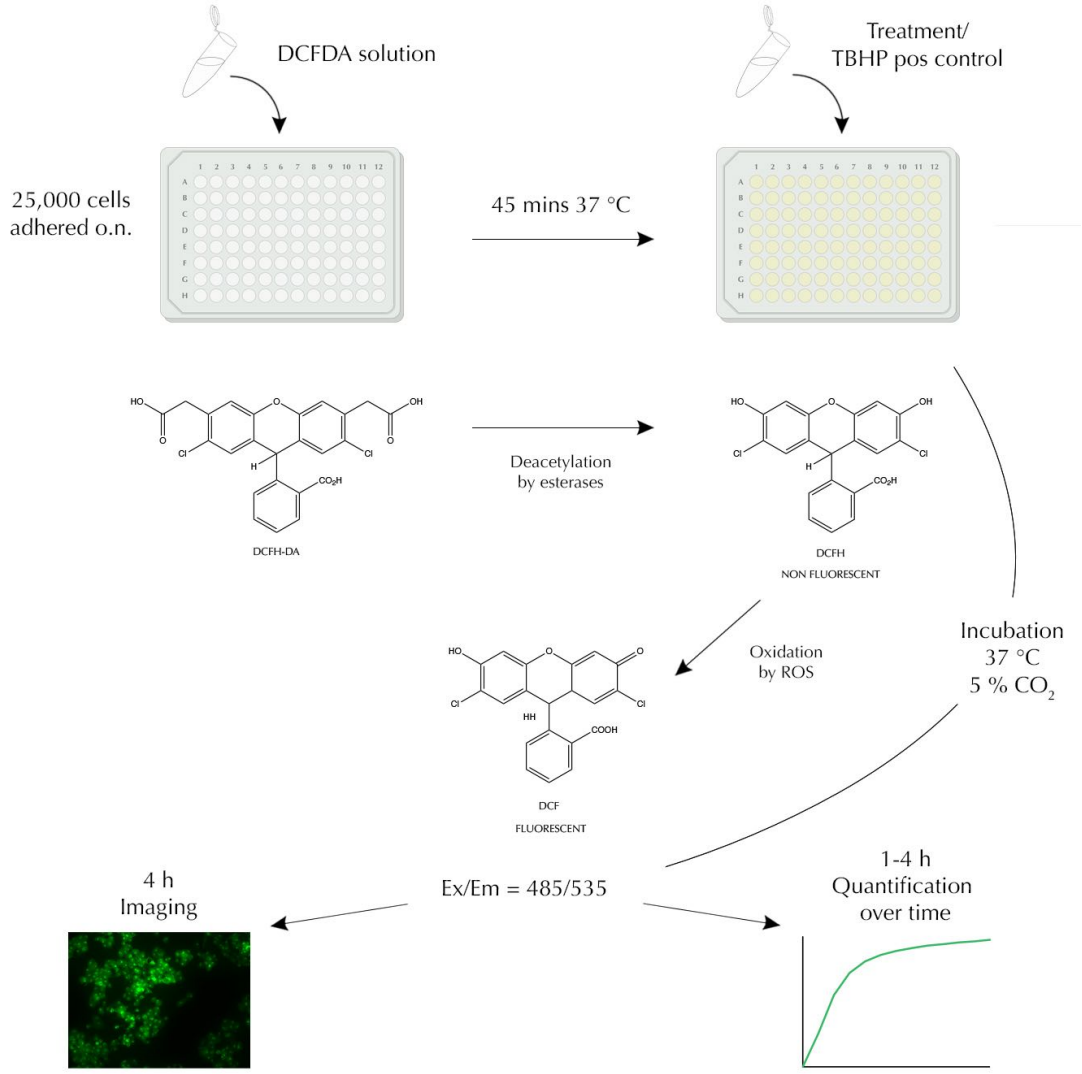

FIGURE 2.7 | DCFDA staining for ROS relative quantification

2.5.2 GSH/GSSG levels quantification - HPLC assay

Glutathione (GSH) is an antioxidant molecule that represent the major system for redox regulation in the cell environment [179]. It is mainly found in its reduced form GSH while the oxidised form glutathione disulphide (GSSG) is less abundant. The usual ratio GSH/GSSG in mammalian cells is between 1:10 and 1:100 [180]. GSH is kept at its reduced state by the glutathione reductase and this system is responsible for the detoxification of ROS that could damage cell structures. The levels of GSH were determined by HPLC using monobromobimane (mBBr) a weakly fluorescent reagent that conjugate with GSH molecules. Evaluation of GSSG concentration was carried out first neutralising GSH with N-ethylmaleimide (NEM), then GSSG was reduced using DTT to be conjugated with mBBr for HPLC detection [181]. The assay was adapted from Quievryn and Zhitkovich [182].

2.5.2.1 GSH/GSSG samples preparation

Cells were seeded on 6-well plates (HepG2 $1.8x10^5$ cells/well) and once reached confluence DMEM+ with different test compounds was added. After different incubation time points cells were detached and washed twice in PBS then resuspended in 75 µL of 5 mM diethylenetriaminepentaacetic acid (DTPA) in PBS. Samples were then acidified by addition of 300 µl 50 mM methanesulfonic acid (MsOH), and then subjected to three freeze-thaw cycles alternating between dry ice and a 37 °C heat block for 6 minutes and vortexed 10 seconds max speed. GSH/GSSG-containing supernatants were obtained after centrifugation at 12,000 x g for 10 min at room temperature and then kept in ice. Protein content was measured with Bradford assay.

2.5.2.2 GSH derivatization

GSH was derivatized with monobromobimane by mixing 75 µl of sample with 25 µl of reaction buffer composed of 50 mM HEPES pH 8, 5 mM EDTA, 15 mM NaOH, 2 mM mBBr, in acetonitrile. The reaction was vortexed immediately and incubated for 15 min in the dark at room temperature. The reaction was stopped through acidification with 1 µl 5 M MsOH and samples were stored at -20 °C after three-fold dilution with 10 mM MsOH.

2.5.2.3 GSSG conversion and derivatization

Samples were removed of GSH through a reaction with N-ethylmaleimide. 150 µl of sample was mixed with 50 µl reaction buffer composed of 50 mM HEPES pH 8, 5 mM EDTA, 15 mM NaOH, 2 mM NEM, in acetonitrile. The reaction was vortexed immediately and incubated for 15 min in the dark at room temperature. After that disulfides were reduced for 20 min at room temperature with 3 mM DTT. Reduced thiols from disulfides were derivatised in 7 mM mBBr for 15 min the in dark at room temperature. The reaction was halted through acidification with 2 µl 5 M MsOH and samples were stored at -20 °C.

2.5.2.4 GSH/GSSG quantification

The GSH/GSSG-mBBr complexes were separated by HPLC using a Gilson HPLC-306 Laboratory system with fluorescence detector Jasco FP-920 using the software Clarity 2.6. A HiChrom ACE-AR C18 4.6 × 250 mm, 5 µm column was equilibrated at 37°C

with Solvent A (0.25% v/v acetic acid and 10% methanol, pH 4 NaOH). Samples were eluted with a gradient of Solvent B (90% methanol) at 1.0 ml/min flow rate as follow: 0-5 mins 0%, 5-15 mins 20%, 15-20 100% followed by 5 mins re-equilibration. The peak of GSH and reduced GSSG were observed at 7.9 min (FIGURE 2.8). Concentrations derived from interpolation from the standard curves were normalised to total protein concentration in initial sample considering the amount of sample injected in 10 µl (FIGURE 2.8).

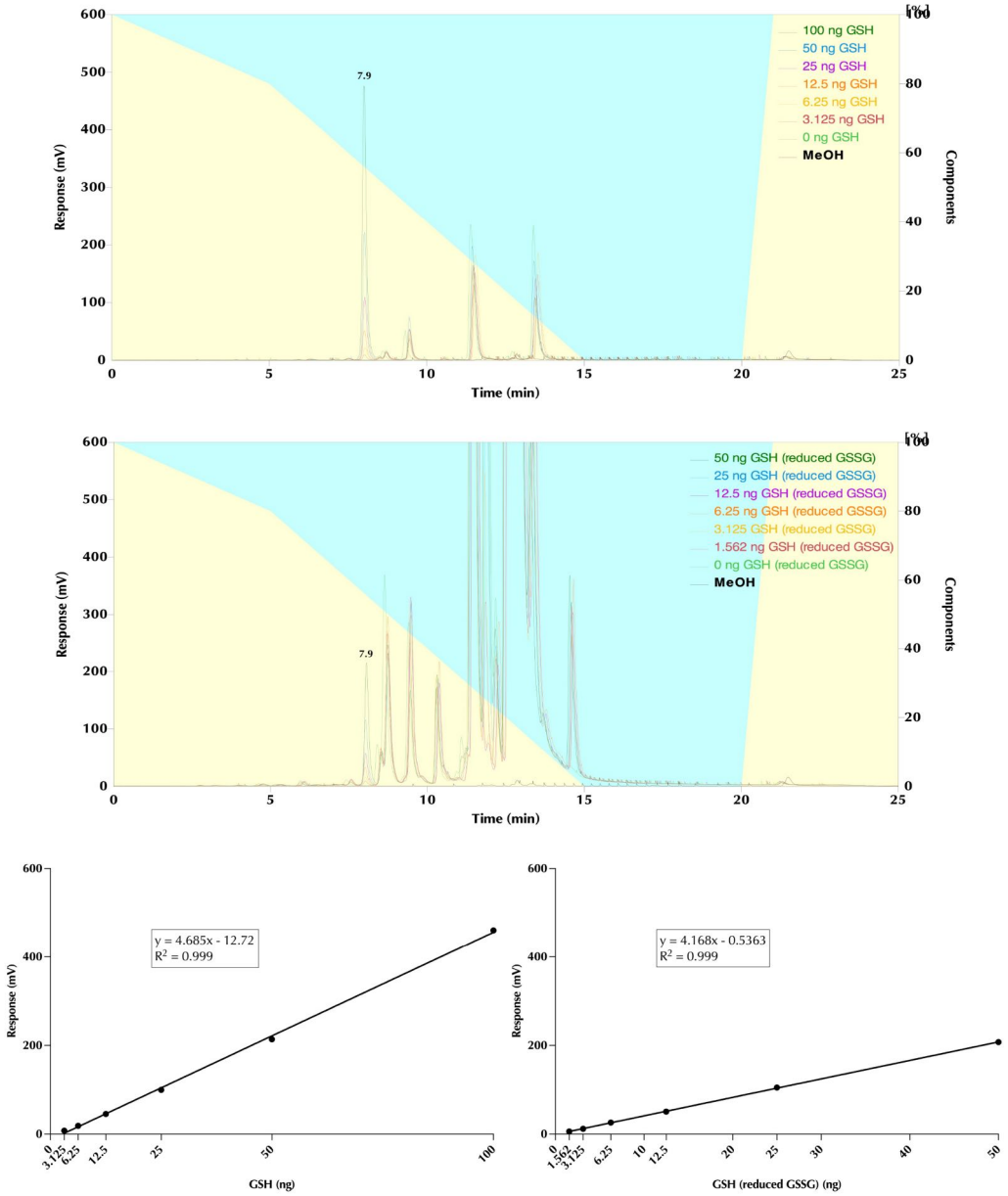

FIGURE 2.8 | Chromatograms and standard curve of GSH and GSSG quantification by HPLC assay

2.6 Interaction of tumour cells with their microenvironment

2.6.1 Cell adhesion - Matrigel® coated plate assay

The adhesion between cells and cells-ECM is regulated by numerous proteins such as cadherins, integrins, immunoglobulins and selectins. Integrins regulate the cell anchorage and with other adhesion molecules are attached to actin filaments of the cytoskeleton forming focal adhesion complexes (FA). The formation of the FA leads to a cascade of signals which are implicated in numerous cell processes such as differentiation, migration, and growth [183]. Moreover, cell adhesion is crucial for development of tumours that have to establish strong interactions with the ECM and other cells to form a solid mass and metastasise. Therefore, the study of cell adhesion is fundamental to evaluate the efficacy of cancer treatments.

96-well plates were coated with 50 µL of 2% (v/v) Matrigel® (10 mg/mL) in DMEM FBS free and incubated at 4 °C overnight (**FIGURE 2.9**). The Matrigel® solution was removed and the wells washed once with PBS to remove unbound proteins. Cells (HepG2, Hepa 1-6 $1x10^5$ cells/well) were seeded with DMEM FBS free media with test compounds added. After 3 h, medium was removed and the wells were washed three times with PBS to remove non adhered cells. 100 µL of 10% (v/v) buffered formalin was added for 20 minutes to fix the adhered cells. After that, wells were washed once with PBS and 100 µL of 0.1% (w/v) crystal violet was added and incubated for 20 minutes. Finally, the wells were washed three times with dH_2O and left in a fume hood to air dry. Single wells were imaged with a Leica DMI3000 B. Quantification of adhesion rate was calculated using ImageJ 1.53k software using a method derived from O'Brien *et al*. [162]. The area occupied by adhered cells was calculated as follows:

Image > Type > 32-bit
Image > Adjust > Threshold (Set background pixel to NaN)
Analyze Particles (0-infinity)

Adhesion rate was calculated with the following formula:

$$\text{Adhesion rate } \% = \frac{\text{Adhered cells area}}{\text{Adhered cells area control}} \times 100$$

The images shown are representative of a set of two pictures/well with three well/conditions.

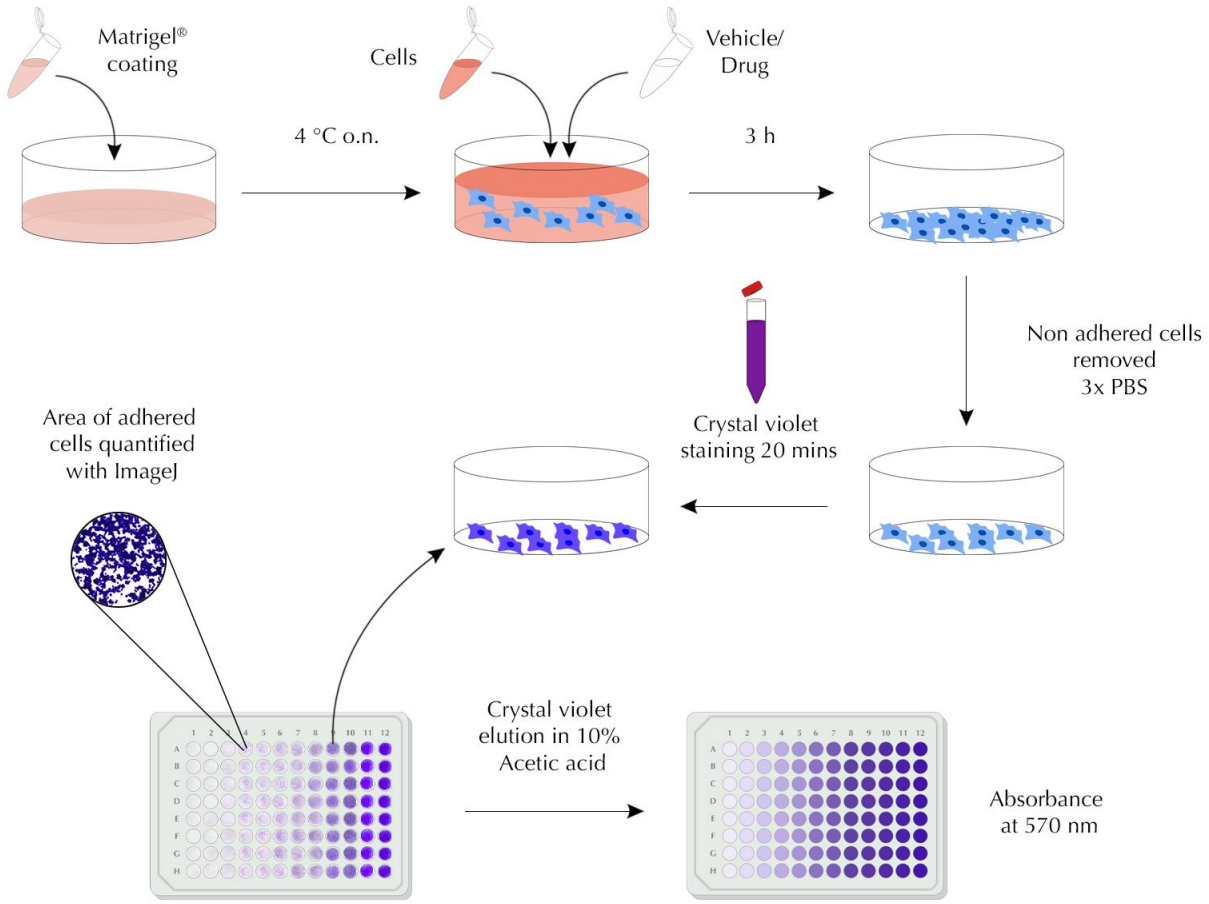

FIGURE 2.9 | Matrigel® coated plate-based adhesion assay

2.6.2 2D cell migration - Scratch wound healing assay

The scratch assay is an easy and economical way to assess cell migration *in vitro*. Once a monolayer of cells reaches the maximum confluence, a tip is used to create an artificial gap defined scratch. After that, the cells on the edges of the gap will start to migrate to occupy the free available surface. Consequently, it is useful to capture pictures at regular intervals of the same scratched area to evaluate the cell migration rate [184].

Cells were seeded in 24-well plates (HepG2 2.5x10^5 cells/well, Hepa 1-6 1.5x10^5 cells/well) and once reached 100% of confluence scratches were made with a 200 µL pipette tip across the centre of the well (**FIGURE 2.10**). Wells were then washed twice with 1% (v/v) FBS medium and then added with DMEM 1% (v/v) FBS containing test compounds. Wells were imaged at 3 experimental times, 0 h, 24 h, 48 h, and 72 h. Three pictures were taken from each well using a Leica DMI3000 B with a 5x magnification. Pictures were taken from the same spot determined by a permanent marker sign at the bottom of the plate. The wound

area was evaluated using ImageJ 1.53k software with the macro "MRI Wound Healing Tool" described in *Cormier et al.* [161]. Wound closing rate rate was calculated with the following formula:

$$\text{Wound closing rate \%} = \frac{At_0 - At_1}{At_0} \times 100$$

where At_0 is the wound area at time 0, and At_1 is the correspondent wound area at 24 h, 48 h or 72 h. The images shown are representative of a set of three pictures/well with three well/conditions.

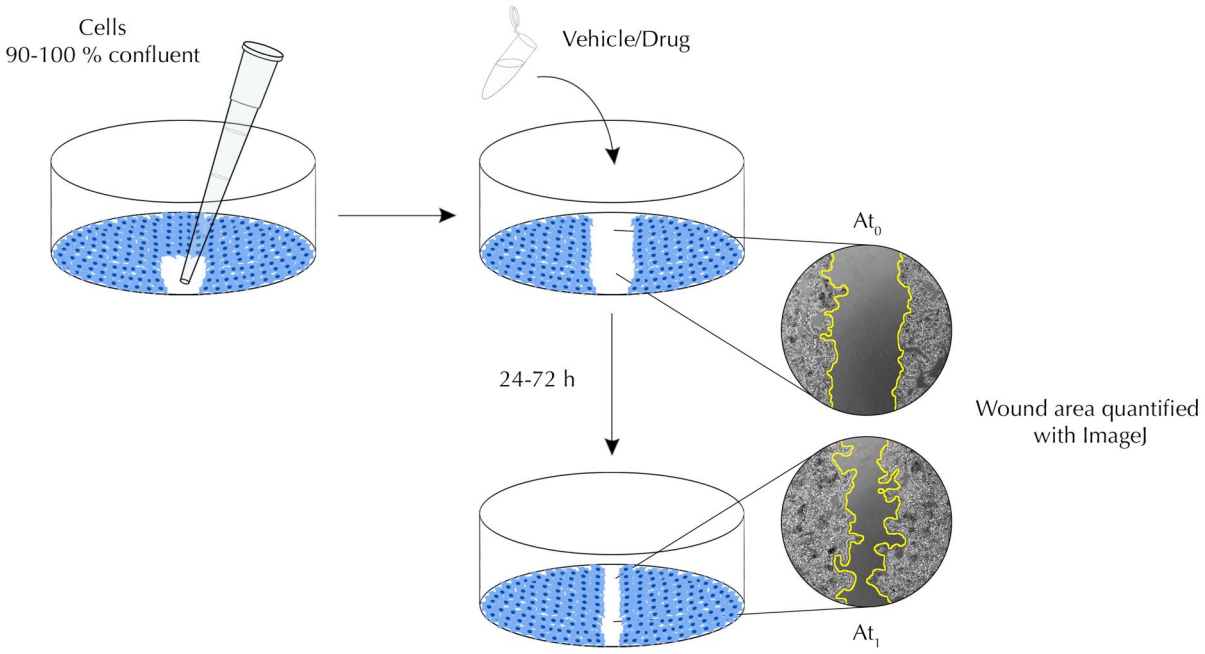

FIGURE 2.10 | Diagram of scratch wound healing assay

2.6.3 3D cell migration/invasion - Boyden chamber assay

The Boyden chamber assay evaluate the ability of cells to migrate through a porous membrane attracted by a chemoattractant [185]. The Boyden insert is a hollow plastic chamber sealed at one end with a porous membrane. The size of the pores can vary from 2 to 12 µm. The plastic insert is placed into a larger well that contain a chemoattractant. The migratory cells will move from the top side of the membrane to the under side of the membrane passing through the pores. The migrated cells that have attached to the membrane lower side are stained and quantified.

Harvested cells were seeded on the top chamber of the Boyden chamber ThinCert™ 8 µm with a density of 1x10^6/mL in 100 µL FBS free DMEM with addition of test compounds (**FIGURE 2.11**). The lower chamber was filled with 500 µL of DMEM with 10% (v/v) of FBS. After incubation at 37 °C for 48 h the solution from the top chamber was discarded and the non migrated cells removed with a cotton swab. The inserts were washed twice with PBS and placed in a new 24-well with 500 µL of 10% (v/v) buffered formalin for 20 minutes to fix the cells migrated into the under side of the porous membrane. After that, the inserts were washed twice with PBS and placed in a new well with 500 µL of 0.1% (w/v) crystal violet to stain the cells that had migrated for 20 minutes. Finally, the inserts were washed twice with dH_2O and left in a fume hood to air dry. Macroscopic images of the membranes were taken with an iPhone 11 Pro. Dry inserts were imaged with a Leica DMI3000 B 5 pictures were taken from each insert from random fields.Migrated/invaded cells were counted by an independent operator.

The migration/invasion rate was calculated as follows:

$$\text{Migration rate \%} = \frac{M}{C_m} \times 100 \qquad \text{Invasion rate \%} = \frac{I}{C_i} \times 100$$

where M and I are the average number of migrated and invaded cells respectively, while C_m and C_i are migrated and invaded cells respectively in control inserts.

The invasion assay was performed as the migration assay but with the addition of 100 µL of 1% (v/v) Matrigel® (10 mg/mL) in DMEM FBS free media in the top chamber and DMEM with 30% (v/v) FBS added in the bottom chamber. The matrix coated inserts were incubated at 37 °C overnight to allow complete polymerisation of the matrix.

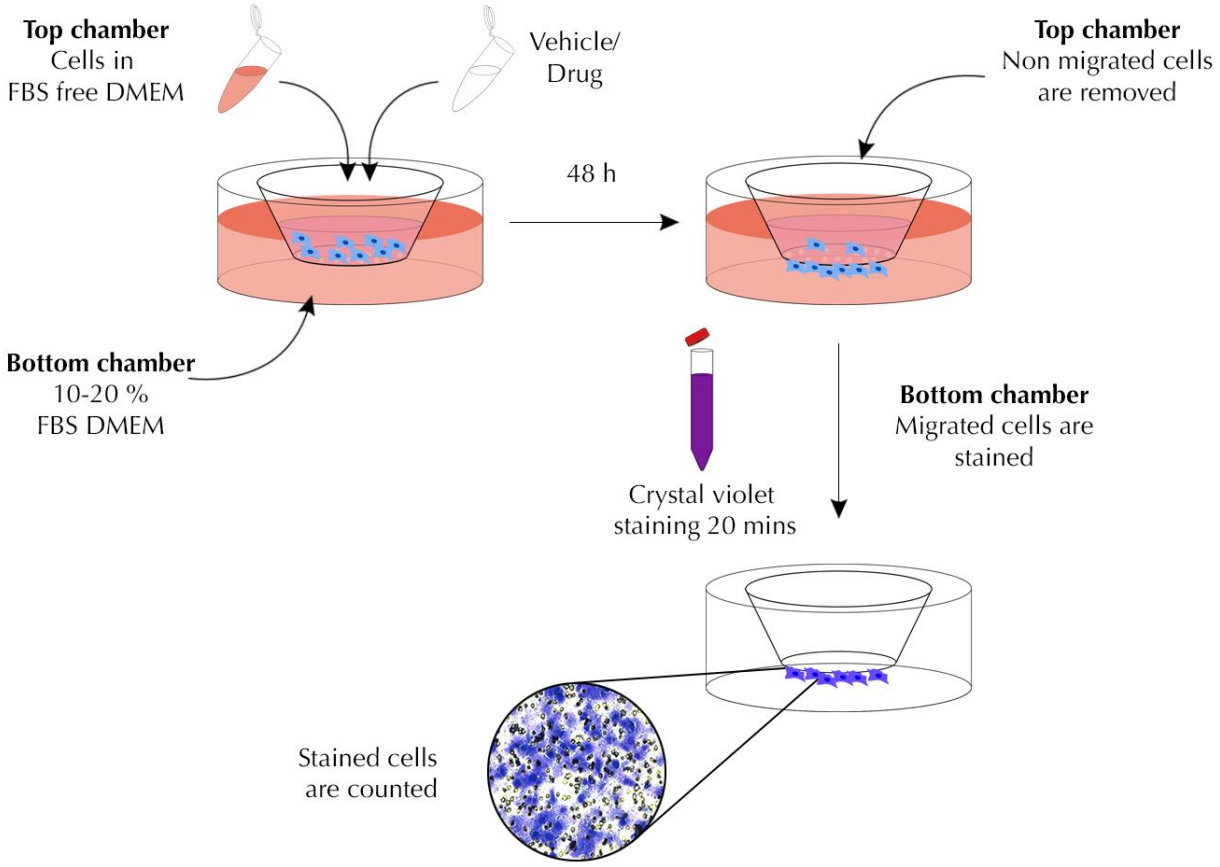

FIGURE 2.11 | Diagram of Boyden chamber assay

2.6.4 Tumour invasiveness *in vivo* - Chorioallantoic tumour xenograft in ovo assay

The chick chorioallantoic membrane (CAM) assay is a well established method to study angiogenesis and tumour development *in vivo*. Advantages of this technique are a high reproducibility and reduced costs compared with other animal models. Furthermore, there is no need for ethical approval as the experiment do not lead to pain as the membrane is not innervated and also the experiment is terminated before the complete animal development. Disadvantages are related to low egg viability and low tumour uptake rate. This model allows the growth of tumours as the CAM mimics the physiological cancer environment and the absence of an immune system permits the xenograft of human tumour cells [186].

The CAM assay was run at the UEA Cell & Developmental Biology Münsterberg lab. The CAM assay is adapted from Kunz P. *et al* with some modifications [186]. Opened eggs were managed inside a sterile hood to reduced mortality rate. Fertilised Shaver Brownchicken eggs were incubated at 37 °C. On day 1 (ED1) 6 ml albumen were removed at the wider

end of the egg with a syringe (**FIGURE 2.12**). Eggs were incubated in a horizontal positioning until ED7. On ED6 40 µL of Cultrex Basement Membrane Extract, Type 3 mixed with vehicle or drug treatment with $1x10^6$ HepG2 were pipetted on a petri dish and incubated at 37 °C to solidify for 1 h and then covered with DMEM+. On ED7 the side of the egg was covered with Leukosilk tape and a window of 1.5 cm was opened into the eggshell. The cut eggshell was not completely removed in order to close the window after cell transplantation. A plastic ring of 8 mm internal diameter and 11 mm external diameter was placed onto the CAM and the area within was lacerated with a 30 gauge needle. The pre formed cell pellet was placed onto the CAM delimited by the plastic ring using a pair of curved forceps. The eggshell window was sealed with Leukosilk and the eggs incubated for further 7 days at 37 °C. On ED14 the eggs were opened and the developed xenograft tumours resected and measured. The tumour relative volume (V_r) was calculated as follows:

$$r_t = \frac{1}{2}\sqrt{D_1+D_2}$$

$$V_r = \frac{4}{3} \times \pi \times r_t^3$$

where r_t is the radius calculate using the two perpendicular diameters D_1 and D_2. The results presented are the mean of a minimum of three biological replicates with representative images. All experiments were performed on chicken embryos younger than 14 days of development and therefore were not regulated by the Animal Scientific Procedures Act 1986.

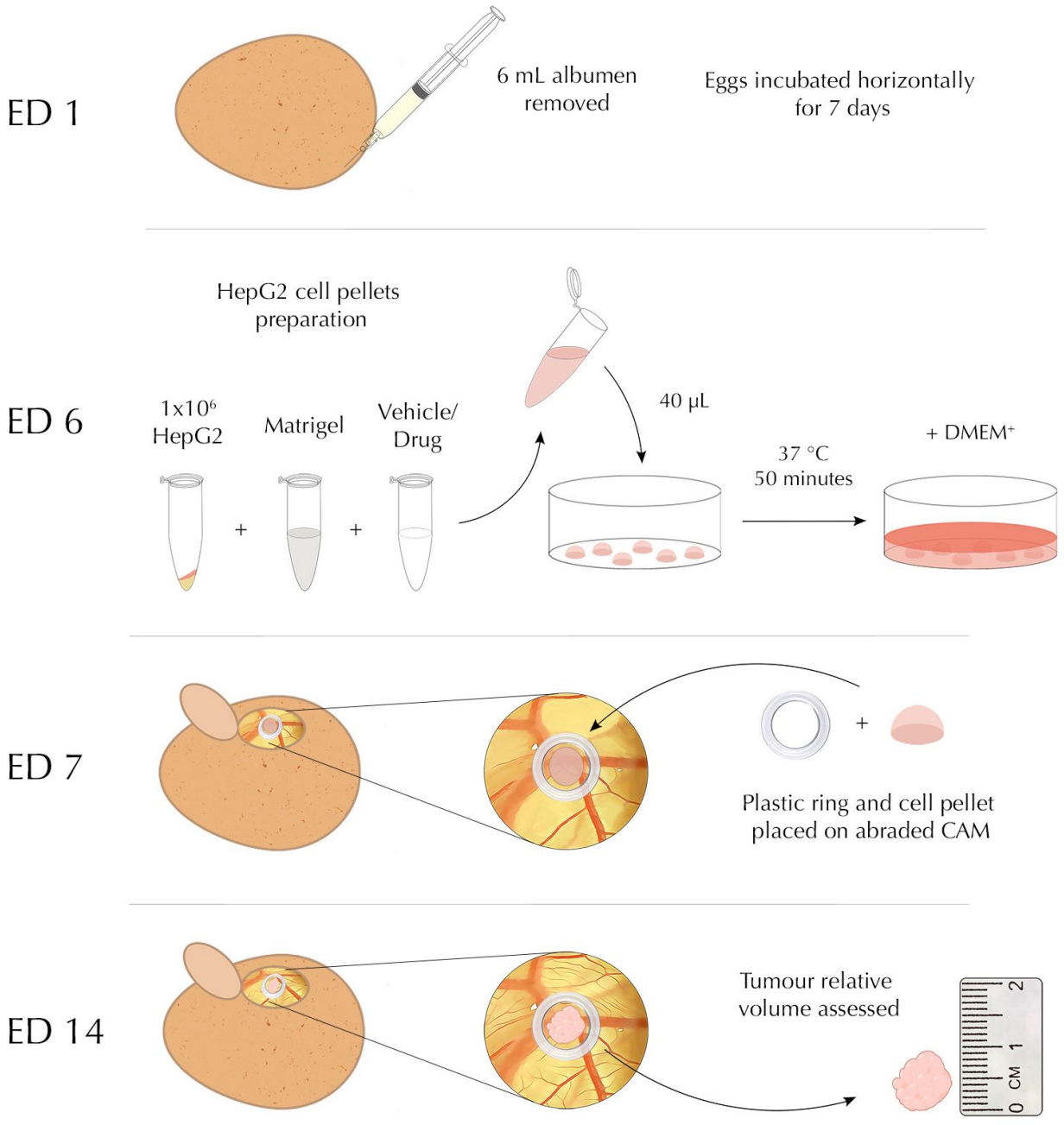

FIGURE 2.12 | In ovo CAM assay for xenograft model of HCC

2.7 Tumour-induced angiogenesis

During tumour development the relation between cancer cells and non-tumour cells is fundamental. Tumour cells recruit several cellular types to support their growth. Furthermore, tumour cells release numerous growth factors to recruit endothelial cells (ECs) for the formation of new vessels to support the tumour growth [187]. Also, this relationship plays a crucial role in early development of metastasis, due to the extravasation process [188]. Therefore, the effect of the conditioned medium, obtained from

tumour cells treated with dasatinib, PEITC, or their combination, on ECs has been evaluated.

2.7.1 Conditioned medium preparation

HepG2 cells (1x10^6) were seeded in 15 cm dishes and once reached confluence were washed with FBS free DMEM (FIGURE 2.13). Different drug treatment in 30 mL FBS free DMEM were added to the plates. The conditioned medium from each plates was collected and centrifuged at 1000 x g 10 mins to remove cells. The supernatant was collected, filtered with a 0.45 µM filter and added to Amicon® Ultra-15 3 kDa Centrifugal Filter Unit. One column was filled with FBS free DMEM only as blank control. Filter tubes were centrifuged at 4 °C for 3000 x g at steps of 30 minutes until the volume reached roughly 500 µL achieving an average concentration of 30X. Samples were aliquoted, the protein concentration was quantified using Bradford assay, and stored at -80 °C. Conditioned medium was then diluted with EGM2$^+$ prior HUVECs treatment for different assays or subjected to analysis using the Proteome Profiler Human Angiogenesis Array Kit.

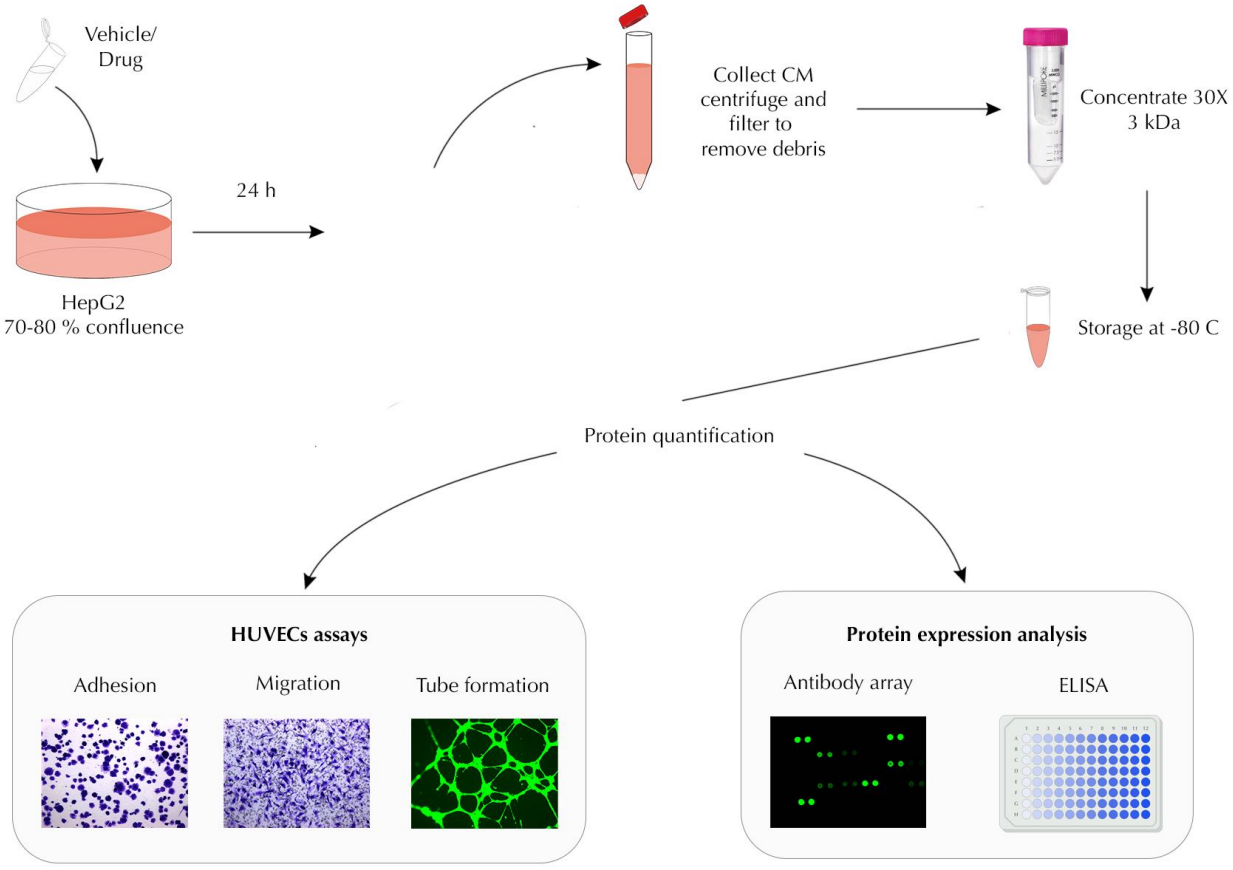

FIGURE 2.13 | Diagram of CM preparation and analysis

2.7.2 Angiogenesis protein expression analysis - Antibody array

In order to identify the angiogenic factors involved in the PDc anti-angiogenic action, an antibody array (Proteome Profiler™ Human Angiogenesis Antibody Array, Bio-Techne Ltd, Abingdon, UK) was used to analyse CM samples.

As per manufacturer instructions the membranes were blocked with blocking buffer for 1 h at room temperature. In the meantime, 500 µL of CM (300 µg) and the antibody detection cocktail were incubated for 1 h at room temperature. The membranes were incubated with the sample/antibody detection solution over night at 4 °C on a rocking platform. After that the membranes were washed three times 10 minutes each and incubated with IRDye® 800CW Streptavidin for 30 minutes at room temperature on a rocking platform. After 3 further washes of 10 minutes each the membranes were imaged with Odyssey CLx Imaging System. The dot density was quantified using Image Studio Lite 5.2.5 software and compared to the signal of a control membrane.

2.7.3 VEGF and PlGF/VEGF heterodimer quantification in CM - ELISA assay

An enzyme-linked immunosorbent assay (ELISA) is a widely used technique to quantify a specific analyte in a given solution. The most commonly used type of ELISA is the solid phase sandwich assay where the target of interest is detected using a primary antibody and then the secondary antibody that has an indicator enzyme is used to allow the quantification the antigen of interest [189]. To quantify VEGF and PlGF/VEGF heterodimers in the conditioned medium of combination-treated cells, two ELISA assays were employed.

Reagents were prepared at room temperature as per manufacturer instructions (**TABLE 2.5**). 96-well plate strips were coated with 100 µL of capture antibody diluted in coating buffer (1X PBS) and incubated overnight. 96-well plate strips were washed 3X with washing buffer using a squirt bottle and liquid was completely removed blotting against clean paper towel. The wells were blocked with 300 µL of blocking buffer and incubated for 1 h at room temperature. The strips were washed again as previously described and then added with 100 µL of sample/standard diluted in blocking buffer and incubated for 2 h at room temperature (HepG2 CM PlGF/VEGF heterodimer 1X dilution, VEGF 3X dilution). The strips were washed again as previously described and then 100 µL of detection antibody diluted in blocking buffer was added and incubated for 2 h at room temperature. The strips were washed again as previously described and then 100 µL of streptavidin-HRP diluted in

blocking buffer was added and incubated for 20 mins at room temperature. The strips were washed again as previously described and then incubated for 20 mins at room temperature in the presence of 100 µL of substrate A/B diluted in blocking buffer. 50 µL of stop solution was added to the strips and then the absorbance was read at 450 nm with a FLUOstar omega plate reader. The generated standard curves were used to establish the samples analyte concentrations (FIGURE 2.14).

TABLE 2.2 | Stock and working concentration of VEGF and PlGF/VEGF heterodimer ELISA kits

	VEGF		PlGF/VEGF heterodimer	
	Stock	**Working**	**Stock**	**Working**
Capture antibody	120 µg/mL	1 µg/mL	240 µg/mL	2 µg/mL
Detection antibody	6 µg/mL	100 ng/mL	3 µg/mL	50 ng/mL
Standard	120 ng/mL	31.2-2000 pg/mL	140 ng/mL	93.8-6000 pg/mL
Streptavidin-HRP		40X		40X

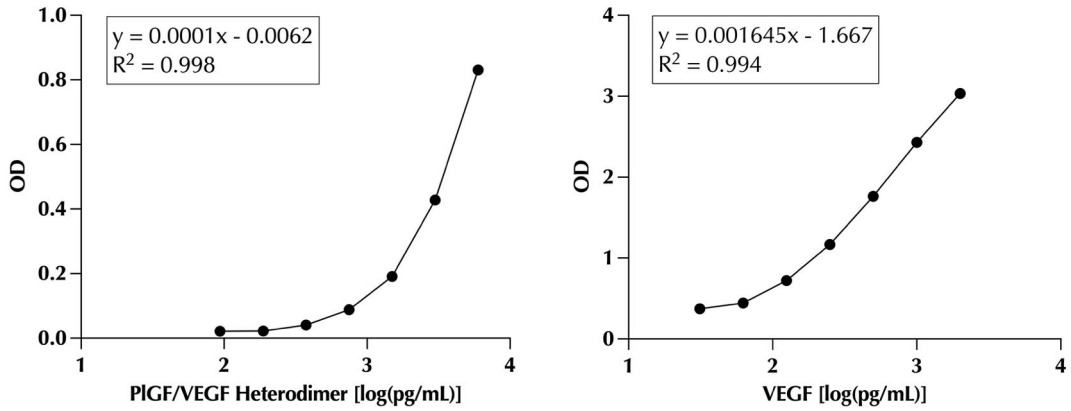

FIGURE 2.14 | ELISA standard curves for CM VEGF and CM PlGF/VEGF heterodimer

2.7.4 HUVECs proliferation - MTT assay

The MTT assay was used to determine the toxicity of PDc and CM on HUVECs as previously described with minor modifications (FIGURE 2.1). Cells were seeded in 96-well plates (3×10^3 cells/well) and once reached 70% of confluency, 100 µL of EGM2+ with 25 µL of CM at different concentrations was added. After 24 h, 100 µL of 5 mg/mL MTT 10% in EGM2+ was added to each well and incubated at 37 °C for 4 h. The MTT solution was removed and the formazan crystals formed were then dissolved by the addition of 100 µL of DMSO to each well. The absorbance was determined using FLUOstar Omega plate reader at 550 nm. Cell viability was calculated as follows:

$$\text{Cell viability \%} = \frac{\text{Test}_{A550nm}}{\text{Control}_{A550nm}} \times 100$$

2.7.5 HUVECs adhesion - ECM gel coated plate assay

The adhesion assay was performed with HUVECs cells as previously described with some minor modifications (**FIGURE 2.15**). 96-well plates were added with 50 µL of 5% (v/v) ECM Gel without phenol red (8 mg/mL) in $EGM2^+$ and incubated at 4 °C overnight. The ECM Gel solution was removed and $2x10^4$ cells/well were seeded with $EGM2^+$ added with 25 µL of CM 0.1 mg/mL. After 30 minutes, medium was removed and the well were washed three times with PBS to remove non-adhered cells. 100 µL of 10% (v/v) buffered formalin was added for 20 minutes to fix the adhered cells. After that, wells were washed once with PBS and added with 100 µL of 0.1% crystal violet for 20 minutes. Finally, the wells were washed three times with dH_2O and left in a fume hood to air dry. Macroscopic images were taken with an iPhone 11 Pro and single wells were imaged with a Leica DMI3000 B at 10x magnification. The images shown are representative of a set of two pictures/well with three well/conditions.

Quantification of adhesion rate was calculated using ImageJ 1.53k software using a method derived from O'Brien *et al*. [162]. The area occupied by adhered cells was calculated as follows:

Image > Type > 32-bit
Image > Adjust > Threshold (Set background pixel to NaN)
Analyze Particles (0-infinity)

$$\text{Adhesion rate \%} = \frac{\text{Adhered cells area}}{\text{Adhered cells area control}} \times 100$$

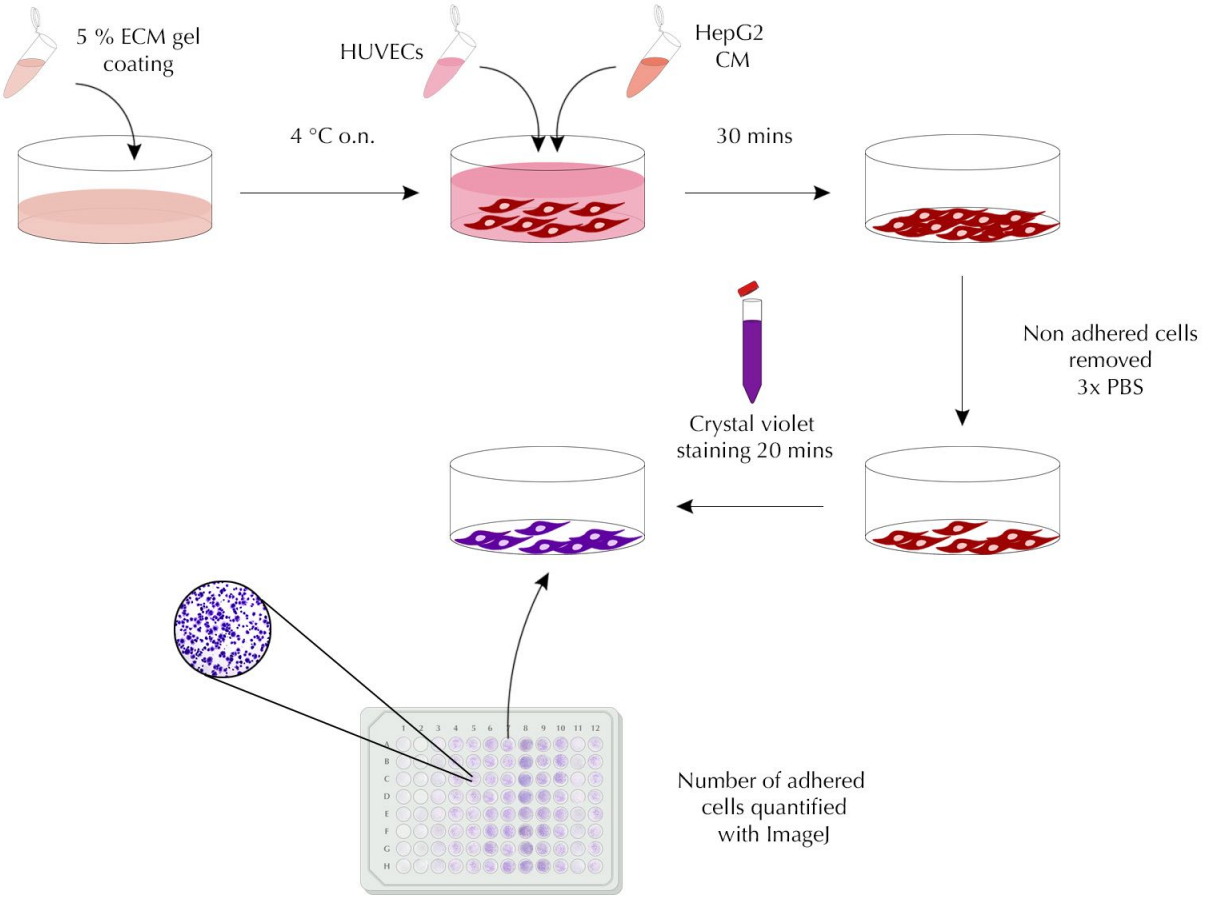

FIGURE 2.15 | HUVECs ECM gel plate adhesion assay

2.7.6 HUVECs migration - Boyden chamber assay

Harvested cells were seeded on the top chamber of the Boyden chamber ThinCert™ 8 µm with a density of 2x10^5/mL in 100 µL of EGM2$^-$ added with 25 µL of CM 0.1 mg/mL (**FIGURE 2.16**). After incubation at 37 °C for 6 h the solution from the top chamber was discarded and the cells that had not migrated were removed with a cotton swab. The inserts were washed twice with PBS and placed in a new 24-well with 500 µL of 10% (v/v) buffered formalin for 20 minutes to fix the cells migrated into the underside of the porous membrane. After that, the inserts were washed twice with PBS and placed in a new well with 500 µL of 0.1% (w/v) crystal violet to stain the migrated cells for 20 minutes. Finally, the inserts were washed twice with dH_2O and left in a fume hood to air dry. Macroscopic images of the membranes were taken with an iPhone 11 Pro. Dry inserts were imaged with a Leica DMI3000 B 5 pictures were taken from each insert from random fields. Migrated/ invaded cells were counted and the migration/invasion rate was calculated as follows:

$$\text{Migration rate } \% = \frac{M}{C_m} \times 100$$

where M is the average number of migrated cells, while C_m are migrated cells in control inserts.

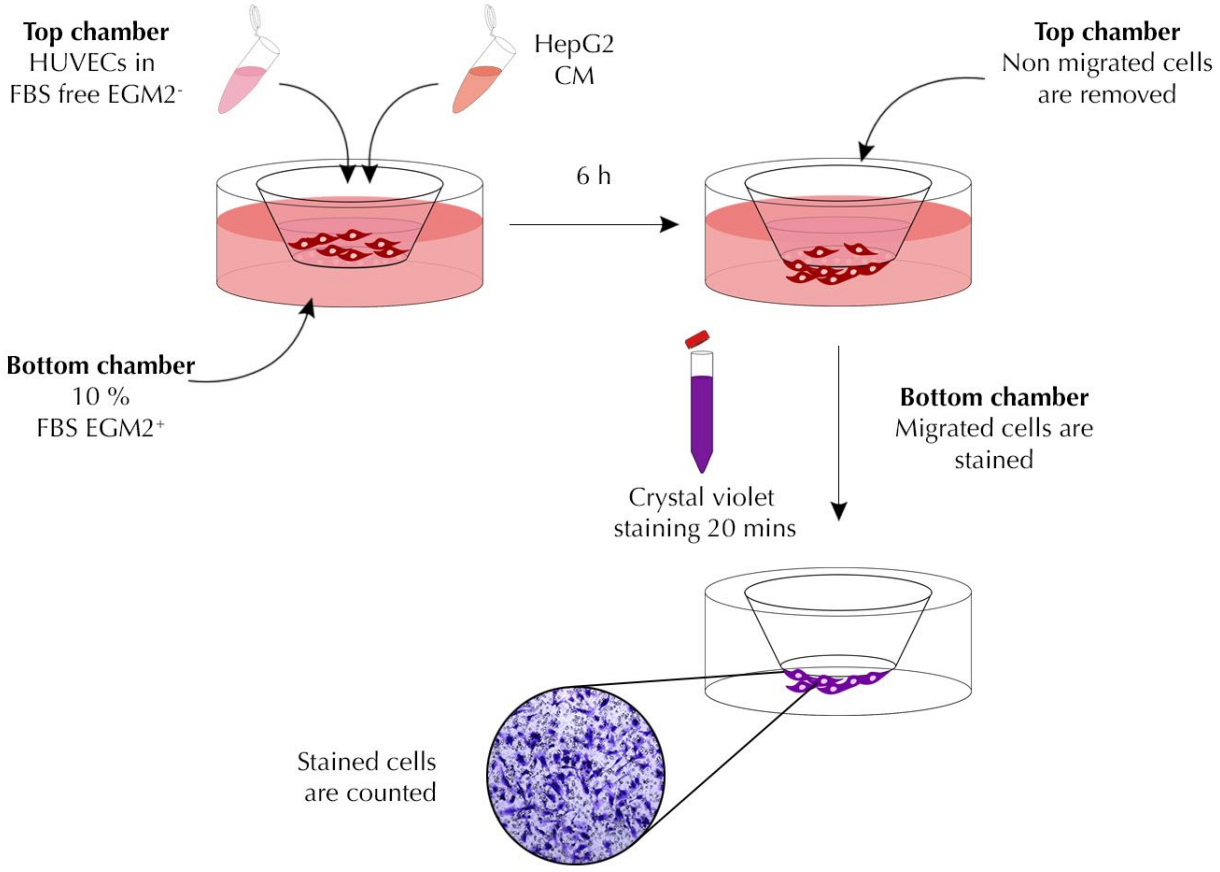

FIGURE 2.16 | HUVECs Boyden chamber assay

2.7.7 Angiogenesis *in vitro* - Matrigel® tube formation assay

The tube formation assay is an *in vitro* assay that mimics the process of angiogenesis. This method is simple and rapid and it is widely used mainly to evaluate the efficacy of angiogenesis inhibitors [190]. Endothelial cells are seeded on or within an extra cellular matrix such as collagen or Matrigel®. Matrigel® is a mixture of basement membrane proteins isolated from Engelbreth-Holm-Swarm mouse sarcoma cells that mimic a favourable environment for the tubes development and is the most used for the tube formation assay. HUVECs are plated on top of a thick layer of Matrigel® and after 12-16 h tubules can be observed through light microscopy in bright field or with a cell live fluorescent staining. Quantitative data are generated through image digital analysis and

several parameters can be considered such as tubules number, tubules length, number of meshes and meshes area.

96-well plates were added with 50 µL of 10 mg/mL Matrigel® (10 mg/mL) and incubated at 37 °C for 40 minutes. HUVECs cells were harvested and resuspended at $2x10^5$ cells/mL, 100 µL of cell solution were added with CM diluted in $EGM2^+$ for a final volume of 125 µL loaded onto the gelified Matrigel® (FIGURE 2.17). After 16 h the tubular structures were stained with a solution of 8 µg/mL Calcein AM in PBS. The media was removed and the gels were washed once with PBS and then 50 µL of staining solution were added. The plates were incubated for 30 minutes at 37 °C and then the staining solution was removed and the wells were washed once with PBS. Single wells were imaged with EVOS M5000 Imaging System with a 470/525 nm light filter at 4x magnification. One image per well was taken with both phase contrast, for quantitative analysis, and fluorescence filter for results presentation. The images were analysed using ImageJ 1.53k software with the macro Angiogenesis Analyzer described in Carpentier *et al* [163].

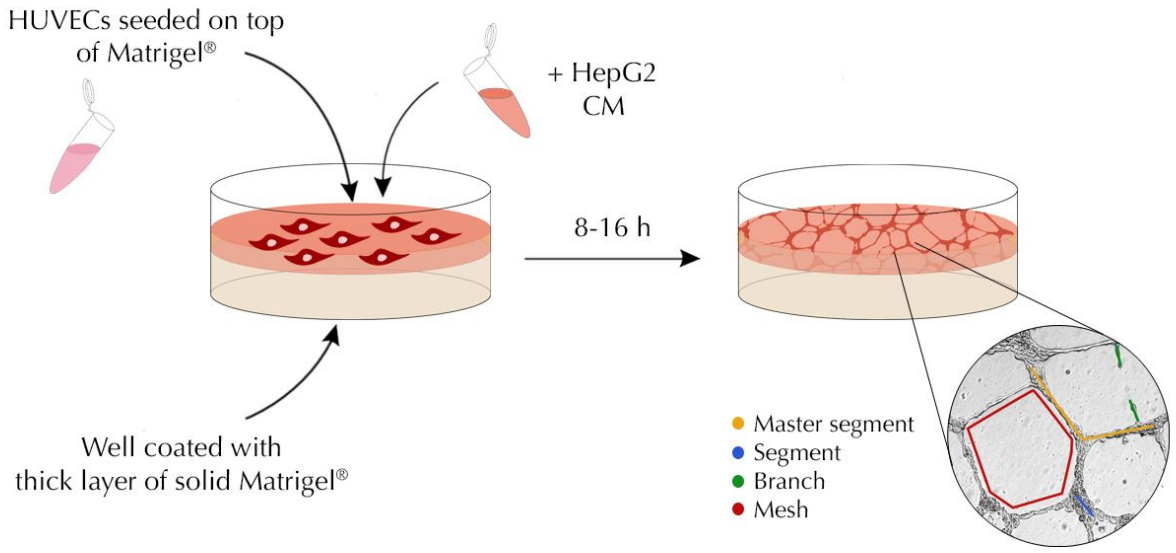

FIGURE 2.17 | HUVECs Matrigel® tube formation assay

2.7.8 Angiogenesis *in vivo* - Ex ovo yolk sac membrane assay

The yolk sac membrane (YSM) of the chick egg is exploited to study the ability of a compound to inhibit the formation of new vessels. The membrane that surround the yolk plays a fundamental role because is responsible for the nutrition of the chick embryo,

providing the nutrients stored in the yolk [191]. Therefore, the yolk membrane become widely vascularised in just 36 hours and this time frame can be exploited to study the ability of a compound to inhibit the process of angiogenesis *in vivo* [192]. In this study the conditioned medium of combination-treated HepG2 has been applied to the YSM to evaluate if the drug combination can reduce the secretion of important angiogenic factors responsible for the increased tumour-induced angiogenesis.

The YSM assay was run at the UEA Cell & Developmental Biology Münsterberg lab. The YSM assay was adapted from and Wang *et al.* with some modifications [192]. Opened eggs were managed inside a sterile hood to reduced mortality rate. Fertilised Shaver Brown chicken eggs were incubated at 37 °C for 2.5 days (**FIGURE 2.18**). Eggs were crack opened and the content carefully placed on a paper boat previously sterilised. A teflon ring of 10 mm internal diameter was placed onto the yolk sac membrane on top of a main branch of blood vessels and 20 µL of CM 2.5 mg/mL were pipetted inside. The egg in boat was covered with a petri dish lid and incubated at 37 °C for 36 h. Pictures were taken every 12 h to check the blood vessels development using a stereomicroscope Stemi SV11. The developed blood vessels at 36 h were classified in primary, secondary, tertiary, and quaternary and quantified as described in Datar P. *et al* [193]. The results presented are the mean of a minimum of three biological replicates with representative images. All experiments were performed on chicken embryos younger than 14 days of development and therefore were not regulated by the Animal Scientific Procedures Act 1986.

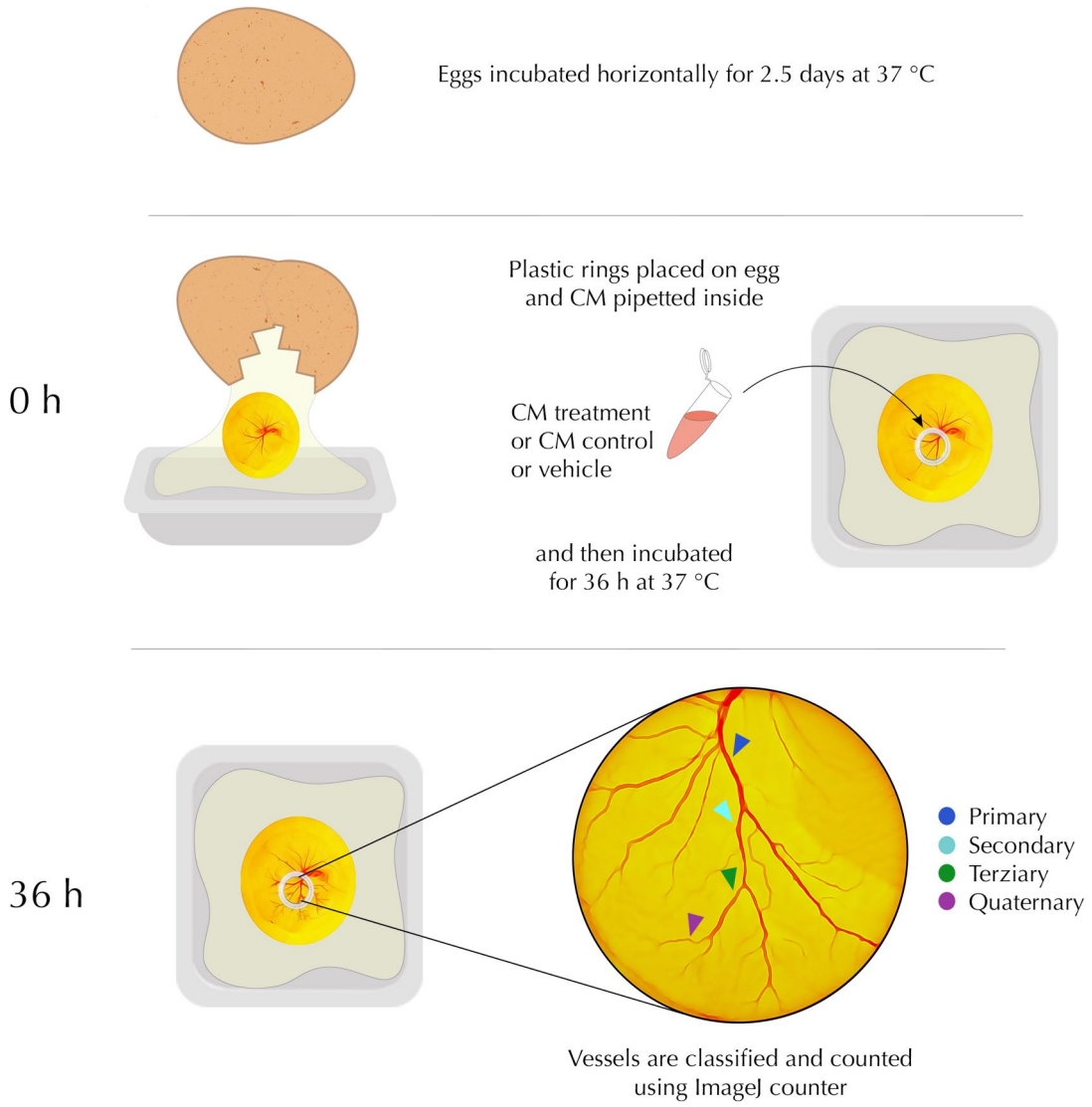

FIGURE 2.18 | Ex ovo yolk sac membrane assay

2.8 Cell morphology and cytoskeleton - Immunocytochemistry

Immunocytochemistry is a widely used technique that exploits antibodies to visualise specific antigens *in vitro*. In an indirect immunofluorescence technique, a primary antibody is raised against a specific target of interest and then a secondary antibodies raised on the same host of the primary antibody is used to detect the antigen-primary antibody complex [194]. The secondary antibody is usually a fluorophore that is able to emit light at specific wavelength generating a signal that can be also quantified. This technique is helpful for protein localisation and to study the structures in specific cell compartments. In the current study immunocytochemistry techniques have been used to study cell

morphology with a stain of f-actin, and to investigate the effect on the cell cycle progression with staining of α-tubulin.

Cells were seeded on 15 mm coverslips in 24 well plates at density of $5x10^4$ cells/well. After desired time and treatment the wells were washed once with PBS and the cells fixed with 10% formalin for 15 minutes at room temperature (**FIGURE 2.19**). After that the wells were rinsed with PBS and then washed twice with PBS for 5 minutes on a rocker. The cells were permeabilised with 0.1% (v/v) Triton X-100 in PBS for 15 minutes at room temperature. The wells were rinsed with PBS and then washed twice with PBS for 5 minutes on a rocker. The cells were blocked with a Blocking buffer (5% goat serum PBS) for 2 h on a rocker at room temperature. Primary antibody (**TABLE 2.6**) solution was added and incubated over night on rocker at 4 °C. The wells were rinsed in washing buffer (0.1% Tween 20 PBS) and then washed twice for 10 minutes with washing buffer on a rocker at room temperature. From this point the plates were covered from direct light. The cells were incubated with secondary antibody solution for 1 h on a rocker at room temperature. The wells were rinsed in washing buffer (0.1% Tween 20 PBS) and then washed twice for 5 minutes with washing buffer on a rocker at room temperature. Cell masking for actin filaments was added for 30 minutes at room temperature. After a rinse in PBS coverslips were carefully removed from the plate and added to glass slide with 10 µL of ProLong™ Gold Antifade Mountant with DAPI. Protein localisation and cell morphology were observed using fluorescence microscope Leica DMI3000 B.

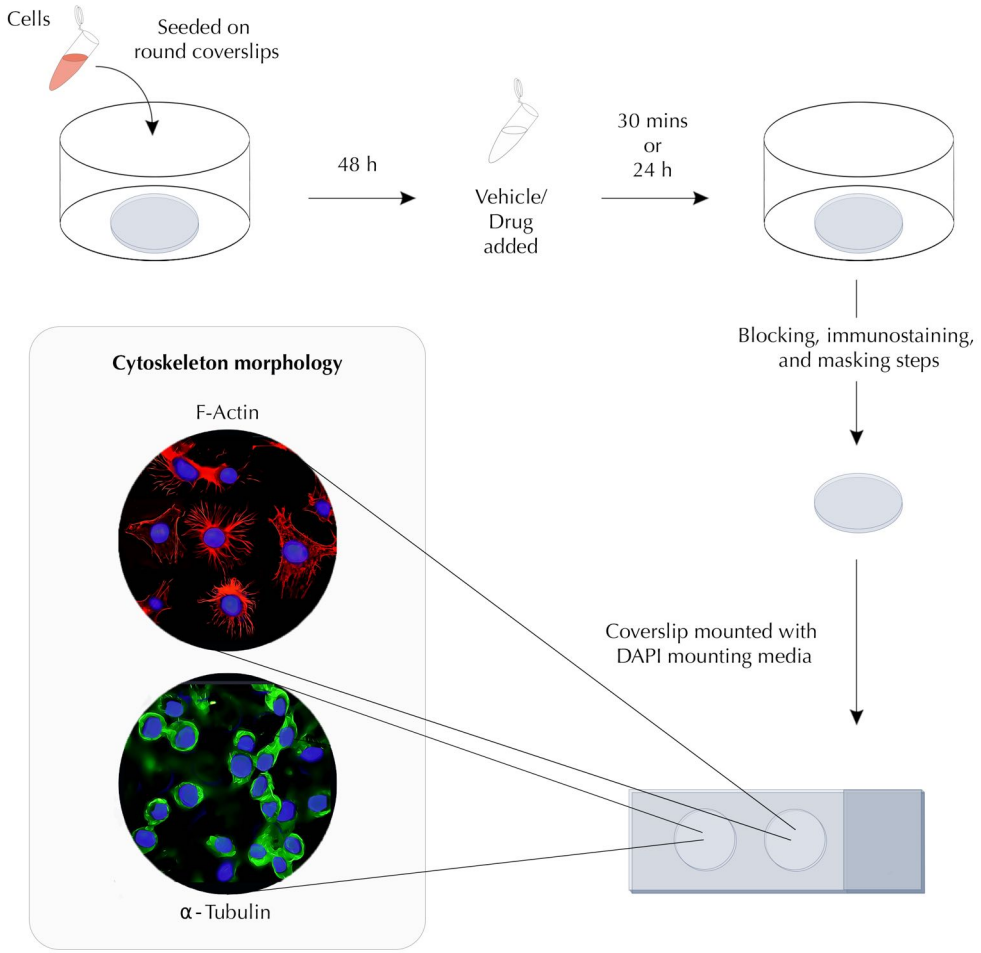

FIGURE 2.19 | Immunocytochemistry assay

TABLE 2.3 | List of antibodies used in immunocytochemistry

	Antigen	Dilution	Supplier	Catalogue number
Primary antibodies	α-Tubulin	1:200	Santa Cruz Biotech	sc-5286
F-Actin masking	Rhodamine Phalloidin	1:200	Thermo Fisher Scientific	R415
Secondary antibodies	AlexaFluor 488	1:500	Thermo Fisher Scientific	A-21202

2.9 Protein expression analysis - Western blot

Western blot allows the identification of specific proteins from a mixture of total cell protein. The first step consists of the protein separation based on size trough electrophoresis. After electrophoresis, separated proteins are transferred from the gel to a membrane of nitrocellulose or polyvinylidene difluoride (PVDF) through an electrophoretic transfer in wet or semi-dry conditions. After the transfer, the membrane is blocked with a

blocking buffer to avoid non-specific antibody-membrane interactions. Then the membrane is incubated firstly with the primary antibody and secondly with the secondary antibody. Wash steps are useful to remove unbound antibodies. The secondary antibody tipically labelled with a fluorophore is exploited to visualise the bands and determine the amount of protein [195].

2.9.1 Protein extraction and quantification

Total protein content was extracted from treated cells using a solution of 20 mM Tris-HCl (pH 8), 150 mM NaCl, 2 mM EDTA, 10% (v/v) glycerol, 1% (v/v) Nonidet P40 added with Protease Inhibitor Cocktail (100X) and Pierce™ Phosphatase Inhibitor Mini Tablets at the moment of the cell lysis. Cells were firstly washed twice with ice-cold PBS, incubated with lysis solution for 30 minutes at 4 °C on a rocker, and then harvested and centrifuged at 13,600 x g for 15 minutes at 4 °C. The supernatant was collected and stored at -80 °C. The protein quantification was performed using Bradford reagent, with bovine serum albumin as a standard. The protein concentration was assessed with a FLUOstar omega plate reader at 595 nm, assuring the loading of an equal amount of protein.

2.9.2 Protein separation - SDS-PAGE

Total protein samples were mixed with 4x NuPage LDS sample buffer and 1 M DTT in a mixture of 70% (v/v) Protein, 25% (v/v) sample buffer, 5% (v/v) DTT. The loading samples were denatured at 95 °C for 5 minutes and between 20-40 µg separated onto 8%/10%/12% (v/v) SDS-polyacrylamide gels, depending on the target size, with a 4% (v/v) stacking gel. The electrophoresis was run at 60 V for the first 20 minutes and then 100 V for the rest of the run using a Mini Protean Tank filled with TruPAGE™ TEA-Tricine SDS Running Buffer. Molecular weight was determined by PageRuler™ Plus.

2.9.3 Protein transfer and immunoblotting

Separated proteins were transferred into a PVDF membrane using a semi dry Trans-Blot® Turbo™ Transfer System. After that, the membrane was blocked with Intercept TBS blocking buffer for 1 h. The membrane was then incubated with the primary antibody solution with appropriate dilution (**TABLE 2.7**) on low rocker speed overnight at 4 °C. After three washes with TBST (0.1% Tween 20), the membrane was incubated with a secondary antibody IRDye® solution (**TABLE 2.7**) with appropriate dilution for 1 h on low rocker speed at room

temperature. After other three washes with TBST (0.1% Tween 20), the membrane was rinsed with TBS and immediately scanned with Odyssey CLx Imaging System. The protein band density was quantified using Image Studio Lite 5.2.5 software and normalised to the signal of a housekeeping protein.

TABLE 2.4 | List of antibodies used in Western blot

	Antigen	Host	Dilution	Molecular weight	Supplier	Catalogue number
Primary antibodies	PARP-1	Mouse	1:2000 (0.1 µg/mL)	116 kDa	Santa Cruz Biotech	sc-74470
	Chk2	Rabbit	1:2000 (0.5 µg/mL)	65 kDa	R&D Systems	MAB1358
	p-Chk2 (Thr68)	Rabbit	1:400 (0.5 µg/mL)	65 kDa	R&D Systems	AF1626
	p53	Mouse	1:1000 (0.2 µg/mL)	53 kDa	Santa Cruz Biotech	sc-126
	p-p53 (S15)	Rabbit	1:666 (0.13 µg/mL)	53 kDa	R&D Systems	AF1043
	CDK1	Mouse	1:1000 (0.2 µg/mL)	34 kDa	Santa Cruz Biotech	sc-54
	p-CDK1	Rabbit	1:666 (0.09 µg/mL)	34 kDa	Cell Signaling Technologies	#9114
	Cyclin B1	Mouse	1:1000 (0.2 µg/mL)	60 kDa	Santa Cruz Biotech	sc-245
	Caspase-9	Rabbit	1:1000 (0.2 µg/mL)	46 kDa	Santa Cruz Biotech	sc-8355
	Caspase-3	Rabbit	1:1000 (0.2 µg/mL)	32 kDa	Santa Cruz Biotech	sc-7148
	Cytochrome c	Goat	1:2000 (0.1 µg/mL)	15 kDa	Santa Cruz Biotech	sc-8385
	Keap1	Goat	1:1000 (0.2 µg/mL)	69 kDa	Santa Cruz Biotech	sc-15246
	PGAM5	Mouse	1:1000 (0.2 µg/mL)	32 kDa	Santa Cruz Biotech	sc-515880
	AIF	Rabbit	1:6500 (0.1 µg/mL)	66 kDa	R&D Systems	AF1457
	p-AIF (Ser116)	Rabbit	1:1000 (0.2 µg/mL)	66-57 kDa	ECM Biosciences	AP5501
	FAK	Mouse	1:200 (1 µg/mL)	125 kDa	Santa Cruz Biotech	sc-1688
	p-FAK (Tyr397)	Mouse	1:200 (1 µg/mL)	125 kDa	Santa Cruz Biotech	sc-81493

	Antigen	Host	Dilution	Molecular weight	Supplier	Catalogue number
Primary antibodies	STAT3	Rabbit	1:2000 (0.5 µg/mL)	79, 86 kDa	Upstate	06-596
	p-STAT3 (Tyr705)	Rabbit	1:2000	79, 86 kDa	Cell Signaling Technologies	#9145
	E-Cadherin	Goat	1:4000 (0.025 µg/mL)	135 kDa	R&D Systems	AF748
	N-Cadherin	Mouse	1:2000 (0.25 µg/mL)	130 kDa	R&D Systems	MAB13881
	β-Actin	Mouse	1:2000 (0.1 µg/mL)	43 kDa	Santa Cruz Biotech	sc-47778
	β-Actin	Rabbit	1:5000	43 kDa	Cell Signaling Technologies	#4970
Secondary antibodies	IRDye® 800CW Mouse	Donkey	1:10000 (1 µg/mL)	N/A	LI-COR	926-32212
	IRDye® 800CW Rabbit	Donkey	1:10000 (1 µg/mL)	N/A	LI-COR	926-32213
	IRDye® 800CW Goat	Donkey	1:10000 (1 µg/mL)	N/A	LI-COR	926-32214
	IRDye® 680LT Rabbit	Donkey	1:10000 (1 µg/mL)	N/A	LI-COR	926-68023
	IRDye® 680LT Mouse	Goat	1:10000 (1 µg/mL)	N/A	LI-COR	926-68020

2.10 Gene expression analysis RT-qPCR

The quantitative polymerase chain reaction (PCR) allows to amplify a specific gene of interest to a detectable level. RNA is first converted in cDNA through a reaction of reverse transcriptase and then it is subjected to the PCR. A mixture of nucleotides, enzyme, primers and cDNA go through a three-step cycling process with DNA denaturation, primers annealing, and primer extension, all repeated between 20-40 times [196]. The amplification result is usually visualised using a common agarose gel but without precise quantification. Quantification methods require a post-PCR manipulation that can lead to errors and increased labour time. For this reason, development of the real time quantitative PCR (RT-qPCR) was completed, which enabled the precise quantification of the gene copies that arise from the PCR. TaqMan qPCR is characterised by a dual-labeled fluorescent probe system constituted by a reporter FAM and a quencher TAMRA [197]. Once the probe is degraded by the 5' nuclease activity of the Taq polymerase the reporter FAM is

released and emits a fluorescent signal that is detected at 518 nm. The signal is strongly proportional to the product number and measured in real time.

2.10.1 RNA extraction and reverse transcription

Total RNA content was extracted from treated cells using the Mammalian Total RNA Miniprep Kit following manufacturer instructions. RNA samples were quantified using a Nanodrop 2000 and 500 ng where used for RT reaction using qScript cDNA SuperMix following manufacturer instructions using the Veriti 96 well thermal cycler.

2.10.2 Real-Time quantitative PCR

A TaqMan Real-Time PCR assay was run on a QuantStudio 5 (ThermoFisher Scientific UK Ltd, Loughborough, UK) using the standard Thermofisher protocol, with a 10 µL reaction composed of 20 ng of the sample cDNA mixed with Precision-LR qPCR Mastermix, 300 nM of forward and reverse primers, 150 nM of FAM-TAMRA probe. Primers and probes (**TABLE 2.8**) were obtained from Merck. Data were analysed for ΔΔCT analysis using β-Actin as housekeeping gene.

TABLE 2.5 | List of primer sequences

	Forward 5′ —> 3′	**Reverse 3′ —> 5′**	**Probe FAM/TAMRA**
VEGF	CTGCTGTCTTGGGTG	TCGTGATGATTCTGCC	CCTTGCCTTGCTGCTCTACCT
ANG	TGCGGACTTGTTCTG	GCACGAAGACCAACA	ATCACCATCTCTTCCAACACAGGC
PlGF	CAGTGCCTTCAACAAC	CCAAGAACAGGTAGCA	AGAGAAGCCAGCCACAGACC
β-Actin	CCTGGCACCCAGCACAAT	GCCGATCCACACGGAGTACT	ATCAAGATCATTGCTCCTCCTGAGCGC

2.11 Tumour growth *in vivo* - Murine syngeneic subcutaneous tumour model

The most used preclinical model to evaluate the efficacy of cancer treatments are currently the murine model systems. Indeed, mouse model systems are crucial to determine safety, validity and therapeutic window before moving forward to clinical studies [198]. In this study an ectopic syngeneic model with subcutaneous injection of hepatocellular carcinoma Hepa 1-6 cells have been used. This model is the most simple, with synchronous tumour growth, cost effective and most used for this type of tumour.

A subcutaneous syngeneic HCC murine model was generated injecting 5×10^6 Hepa 1-6 cells in 100 µL of MEM in the right flank of 9–10-week-old female C57BL6 mice. Animal were weighed and the tumour development was measured with a calliper twice per week (**FIGURE 20**). After 10 days, the tumour reached an average of 170 mm^3 and the mice were randomised into 4 groups with 10 mice per group. Each group was administered daily 5 days a week by oral gavage with 100 µL of corn oil using a 20 gauge x 30 mm feeding tube. Dasatinib was dissolved in DMSO at a concentration of 100 mg/mL while PEITC was added straight to the corn oil as readily lipophilic. Stocks were prepared fresh at the beginning of every week. The groups treatment were as follows: 2% (v/v) DMSO as vehicle control group, 40 mg/kg PEITC + 2% (v/v) DMSO, 10 mg/kg dasatinib (2% (v/v) DMSO), combination PEITC + dasatinib. Tumour volume was calculated using the following formula:

$$V_r = 0.52 \times (D \times d^2)$$

where D is the length or greater diameter of the tumour and d is the width or smallest diameter. After 3 weeks of treatment, the mice were euthanised and the excised tumours were measured and weighed.

All animal work was carried out in accordance with regulations established by the UK Home Office (London, United Kingdom) and the Animal Scientific Procedures Act of 1986 under the Home Office Project Licence PP5500397 (Nicole J. Horwood). Experiments were conducted in accordance with the locally animal handling protocol in the Disease Modelling Unit (DMU), School of Biological Sciences, University of East Anglia (Norwich, UK). Mice were housed under 12-12 light dark cycle and fed ad libitum with standard chow diet.

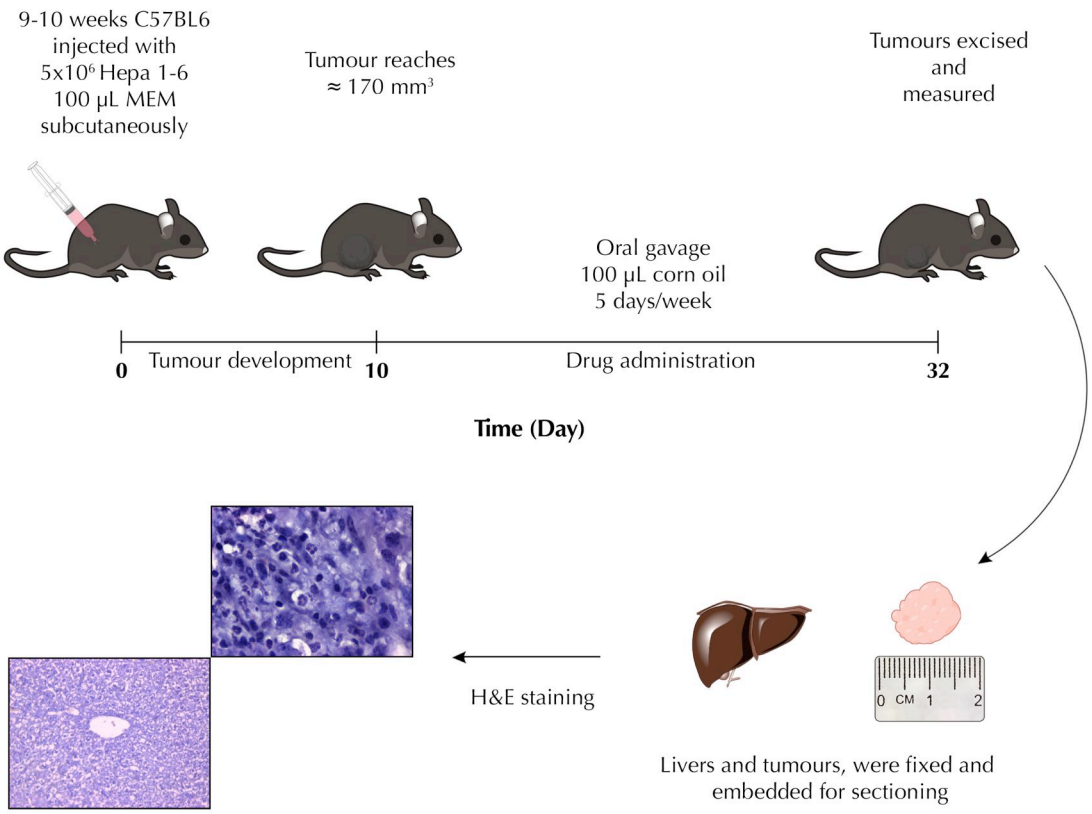

FIGURE 2.20 | Murine syngeneic tumour model

2.12 Histology - Hematoxylin and Eosin staining

Histology and histopathology, which are strictly correlated, are fundamental techniques to examine biological tissues to understand morphological changes associated with disease [199]. Tissue sections can be stained with different techniques depending on the structure of interest or can be subjected to immunohistochemistry to study specific proteins within the tissue. Haematoxylin and eosin have been used for decades to evaluate the morphological changes in numerous tissues samples playing an important role in cancer diagnosis [200]. Hematoxylin is a deep blue colour that stains nucleic acid while eosin stains proteins non specifically. In this study H&E staining has been used to evaluate tumour invasivity in CAM xenograft samples, tumour cell morphology changes and hepatotoxicity in the murine syngeneic tumour model. Furthermore, immunohistochemistry has been used to evaluate the expression of protein of interest in CAM xenograft samples.

Tissue samples (HepG2 tumour CAM xenograft, Hepa1-6 tumour murine syngeneic model and murine livers) were fixed overnight in 10% (v/v) formalin at 4 °C and then were cryopreserved through incubation with 15% (w/v) sucrose PBS overnight at 4 °C, and then

30% sucrose PBS overnight at 4 °. Fixed and sucrose infiltrated samples were placed in a plastic cryomold, covered with OCT compound, placed on top of dry ice for snap freezing and then stored at -80 °C until ready for sectioning. Samples were sectioned at 6 µm using a cryostat Leica CM1850 UV with MX35 Ultra low profile blades. Sections were placed on glass slides and let dry overnight at 37 °C.

Sections were stained with Haematoxylin and Eosin as follows: dH_2O 5 mins, Haematoxylin 1 min, running Tap water 4 mins, 0.5% (v/v) Eosin 5 mins, running Tap water 4 mins. Stained sections were then dehydrated and cleared as follows: 95% (v/v) Ethanol 1 min, 100% (v/v) Ethanol 1 min, 100% (v/v) Ethanol 1 min, Shandon Xylene substitute 2 mins, Shandon Xylene substitute 2 mins. Slides finally were mounted with a glass coverslip using DPX mountant. Mounted slides were observed using a Leica DMI3000 B.

2.13 Statistical analysis

Data presented are expressed as mean ± SEM unless otherwise. Statistical analyses were performed using the software Prism 9.1.1. Data sets were firstly tested for normality using the Shapiro-Wilk test. Normal distributed data sets were subjected to one-way ANOVA with Tukey's post hoc test for multiple comparison between 3 or more groups, or to the Student's t-test for 2 groups comparison. Non-normal distributed datasets were subjected to the non parametric test Kruscal-Wallis with Dunn's multiple comparison between 3 or more groups, or to the Mann-Whitney U test for 2 groups comparison. Sample size (n) represents number of independent experiments or biological replicates for *in vivo* studies. The degrees of significance are indicated as * $p \leq 0.05$, ** $p \leq 0.01$, *** $p \leq 0.001$, **** $p \leq 0.0001$.

Chapter 3
Preliminary screening: exploring the combination efficiency of isothiocyanates and chemotherapeutic drugs

3.1 Introduction

The average 5-year survival for metastatic cancers is still poor so new therapies are required [1]. Liver cancer is among the most aggressive tumours, and HCC is the most frequently occurring type [5]. HCC systemic treatment is not very effective, and for more than a decade, sorafenib was the only cytotoxic drug available. New single-agent therapies have been approved during the last ten years, but the response rate is still low, and the development of new compounds is time and cost-demanding [7]. Therefore, combination therapy has a cardinal role in cancer treatment, allowing the employment of molecules that were considered inefficient as a single treatment [201]. Combining one or more compounds can improve the efficacy of the single molecules, reducing cancer growth and progression more effectively because of an additive or synergistic effect, targeting multiple molecular mechanisms simultaneously. Indeed, the most recent systemic treatment approved by the FDA for the treatment of HCC consists of the combination of two drugs, tremelimumab and durvalumab, that shows superior efficacy compared to the single drug treatments or the canonical sorafenib administration [202].

Several TKIs showed positive effects on HCC treatment *in vitro*. For example, lapatinib, an inhibitor of epidermal growth factor receptors (EGFR) used for breast cancer, induces cell toxicity in several HCC cell lines through the induction of autophagy [35, 203]. Gefitinib, another EGFR inhibitor approved for non-small cell lung carcinoma, showed inhibition the growth of HCC cells with induction of apoptosis, cell cycle arrest and reduced secretion of pro-angiogenic factors [35, 204, 205]. Dasatinib, a potent steroid receptor coactivator (Src) inhibitor approved for the treatment of chronic myeloid leukaemia, was proved effective in HCC cell lines with inhibition of proliferation, migration and invasion through the Src/FAK and Akt pathways [34, 35]. It is also true that the mentioned TKIs have never reached the advanced phases in clinical trials because of an inferior efficacy compared to sorafenib or severe side effects. Lapatinib did not perform well in phase II study in HCC because it did not meet the predefined efficacy rate and was only useful in a restricted subset of patients [206, 207]. In the same way, gefitinib failed in phase II studies as it showed to be ineffective in

advanced HCC [208]. Finally, a phase II trial of dasatinib treatment of unresectable HCC patients was terminated early because of discouraging results [209].

ITCs, like other natural compounds, have a promising treatment efficacy in several cancer types due to their ability to inhibit the capacity of cancer cells to grow and interact with the ECM to develop a malignant tumour mass [210]. ITCs have been shown to be able to synergise with different chemotherapeutic agents in several types of cancer, improving the overall drug efficacy *in vitro*. For example, PEITC synergises with gefitinib inducing apoptosis in non-small cell lung cancer [211]. Lapatinib efficacy in breast cancer is improved by co-treatment with erucin or sulforaphane overcoming drug resistance [212], and sulforaphane and lapatinib combination induces cell cycle arrest and apoptosis in gastric cancer [213]. ITCs have a broad anticancer activity inhibiting several pathways; therefore they can support and potentiate the efficacy of other chemotherapeutic drugs [214]. In spite of that, more studies are required to assess the capability of ITCs to aid chemotherapy, with a better understanding of the molecular mechanisms behind the synergistic action with studies on the pharmacokinetics and pharmacodynamics [215].

The possibility of combining isothiocyanates and approved chemotherapeutic agents to treat hepatocellular carcinoma has not yet been investigated. Therefore, in this study, dasatinib, gefitinib, and lapatinib, which showed positive effects in HCC treatment *in vitro* [35], and the most extensively used approved treatment, sorafenib, have been combined with several ITCs to evaluate their effect on HepG2 cell line. Dasatinib has been introduced in the previous Chapter, while lapatinib is a selective tyrosine kinase inhibitor, approved for breast and other solid cancers, that targets the EGFR receptor and the human epidermal group factor receptor-2 (HER2). These receptors control several pathways involved in the unstoppable growth of cancerous cells and and their inhibition can reverse the progression of the tumour [28]. Gefitinib is a tyrosine kinase inhibitor approved for therapy of non-small cell lung cancer that selectively target EGFR to block the Ras signalling responsible for the uncontrolled tumour growth [28]. Sorafenib is a multi-kinase inhibitors approved for the treatment of HCC, renal cell and thyroid cancer that targets tumour angiogenesis through inhibition of VEGF receptor and PDGF receptor [28]. The effect on HepG2 cell viability was also investigated in immortalised human hepatocytes HHL-5 to test the *in vitro* toxicity in non-cancerous cells. The more efficient combination has been selected for further studies to characterise the effect on several cancer hallmarks and to investigate the involved molecular mechanisms.

Chapter 3 objectives

- Identify the most effective ITC-TKI combination using cell viability assay

3.2 Results

3.2.1 Toxicity of Isothiocyanates and chemotherapeutic agents in hepatocellular carcinoma and normal hepatocytes

The cytotoxicity of four TKIs (i.e. dasatinib, sorafenib, gefitinib, and lapatinib) and three isothiocyanates (i.e. PEITC, BITC, and SFN) was evaluated with the MTT assay. The cell viability was assessed on the cell lines HepG2 and HHL-5, which were cultured in 96-well plates. Once reached 80-90% of confluence, cells were treated with the selected compounds at different concentrations (1.25 to 80 µM) for 72 hours. The dose response curves are presented in FIGURE 3.1 and the IC_{50} values are shown in TABLE 3.1. As expected, sorafenib was the most cytotoxic compound in HepG2 cells with a IC_{50} of 9.3 µM, followed by PEITC 14 µM, while the less effective compound resulted gefitinib with a IC_{50} of 24.7 µM. On the other hand, sorafenib and BITC were the most cytotoxic in normal cells HHL-5 with a IC_{50} of 8.7 µM and 9.3 µM respectively, whereas SFN was the less toxic at 31.8 µM.

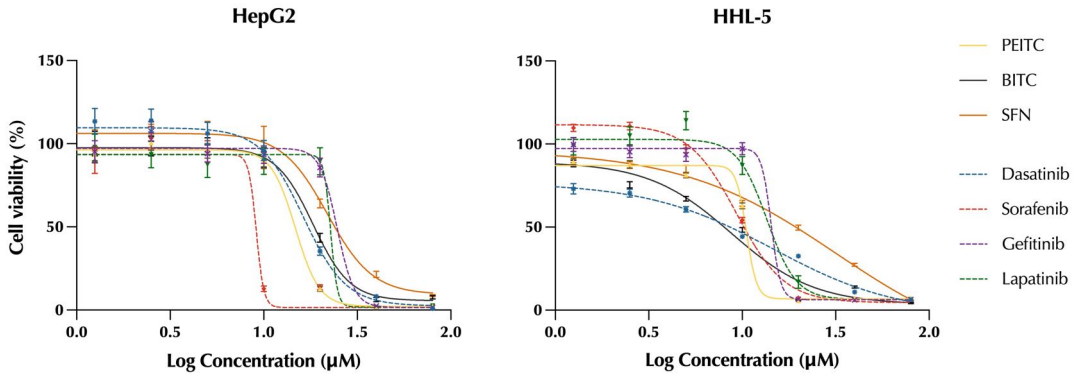

FIGURE 3.1 | Effect of ITCs and different TKIs on HepG2 and HHL-5 cell viability.
Cells were treated with different concentrations (1.25 to 80 µM) of the selected compounds for 72 h. The cell viability was determined with MTT assay (mean ± SD n=1).

TABLE 3.1 | IC_{50} concentrations of ITCs and TKIs on HepG2 and HHL-5 after 72h of treatment

		PEITC	BITC	SFN	Dasatinib	Sorafenib	Gefitinib	Lapatinib
IC_{50} (μM)	HepG2	14.8	18.3	21.9	16.3	9.1	24.7	22.8
	HHL-5	10.5	8.7	31.8	14.6	9.3	14.3	13.6

3.2.2 Efficiency of Isothiocyanates and chemotherapeutic agents combination in hepatocelluar carcinoma

In this study CompuSyn software was employed to determine the combination index (CI) values that is a quantitative indication of the ability of two compounds to synergise, following the Chou Talalay method [216]. First, to determine the best non-toxic synergistic concentration of ITCs, PEITC, BITC, and SFN were combined with dasatinib, which was shown to be the most predisposed TKI to synergise with other compounds in HCC [35]. One viable strategy to select a concentration for synergistic studies is to test non-toxic concentrations that gives 10-20% of the cell viability inhibition and select the most effective for further studies [217]. Consequently, the IC_{20}, IC_{10}, and IC_5 concentrations of ITCs on HepG2 were calculated using Prism 9 (**TABLE 3.2**).

TABLE 3.2 | Sub-toxic concentrations of ITCs on HepG2 and HHL-5 at 72 h

	HepG2			HHL-5
	IC_{20}	IC_{10}	IC_5	IC_{20}
PEITC (μM)	12	10.6	9.5	9.5
BITC (μM)	13.4	11.1	9.4	4.3
SFN (μM)	14.9	11.9	9.6	8.5

The sub-toxic concentrations selected of ITCs were combined with different concentrations of dasatinib (0.625-20 μM) as a baseline to determine the most effective concentration to be used for the TKIs preliminary screening. The CI plots (**FIGURE 3.2**) shows a group of dots that can be above or below the threshold line (CI = 1) that indicate an additive effect. All the dots above the threshold line (CI > 1) indicate an antagonistic effect while the dots below the threshold line (CI < 1) indicate a synergistic effect.

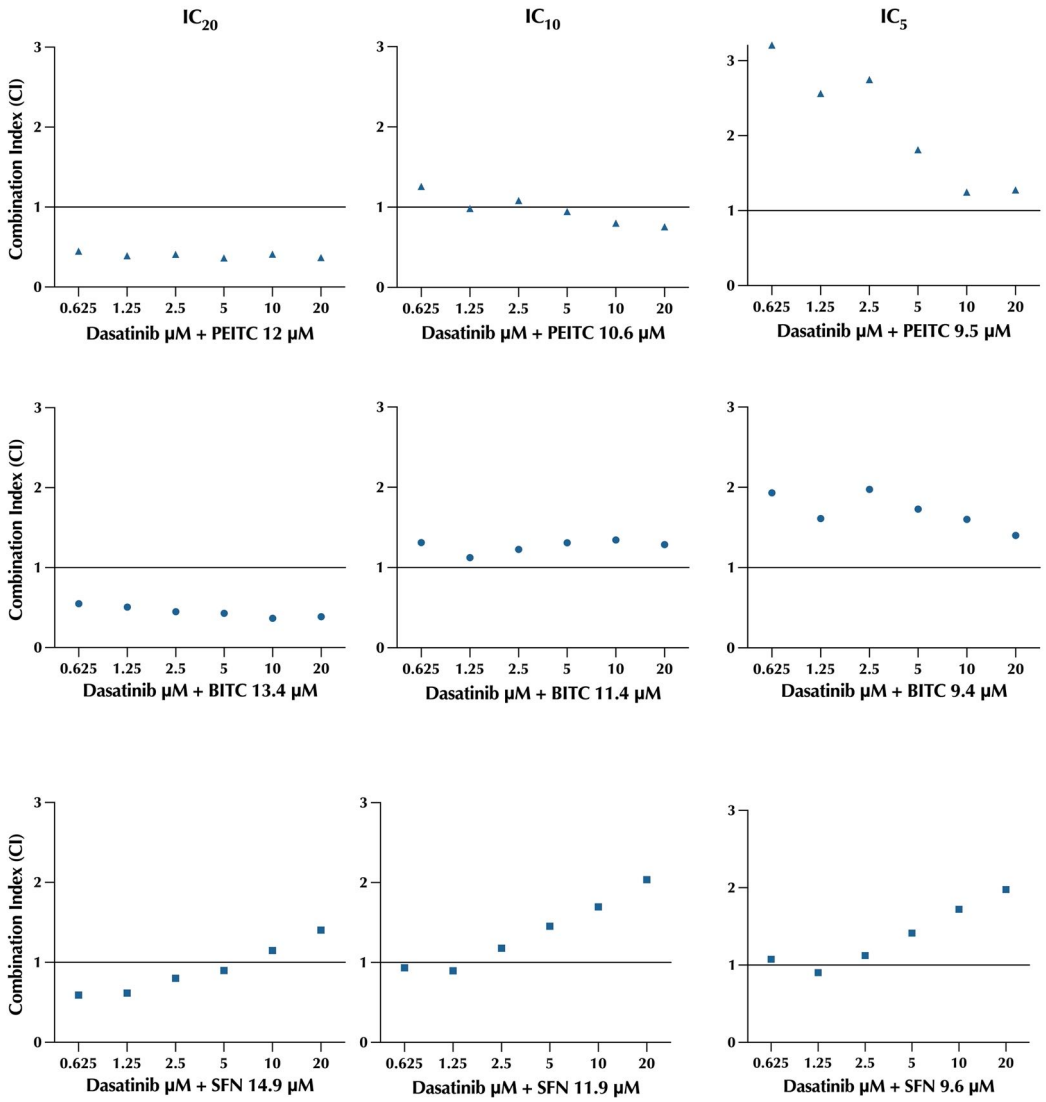

FIGURE 3.2 | Effect of sub-toxic concentrations of ITCs combined with dasatinib. HepG2 cells were treated with different increasing concentrations of dasatinib (0.625 to 20 µM) the $IC_{5\ 10}$ and $_{20}$ of ITCs and the cell proliferation was measured after 72 h of treatment. CI values were calculated with Compusyn software and presented in CI plots.

The results shows that the IC_{20} concentration is the most effective for all the ITCs selected with PEITC and BITC as the most prone potentially act synergistically with dasatinib over all of the concentrations tested. SFN may act synergistically only with dasatinib < 5 µM concentrations. Consequently, IC_{20} concentrations were selected for the preliminary screening also considering the effect of the selected concentrations in non-cancerous cells HHL-5.

In FIGURE 3.3 the CI plot shows the effect of the combination between IC_{20} ITCs concentrations and sorafenib (0.625-20 µM) on both HepG2 and HHL-5. PEITC was the

less effective in HepG2 and the most toxic for HHL-5 while both BITC and SFN showed a weak synergistic effect in the tumour cell line with the most effective combination with BITC at 20 µM that reached a CI of 0.422 (**TABLE 3.3**).

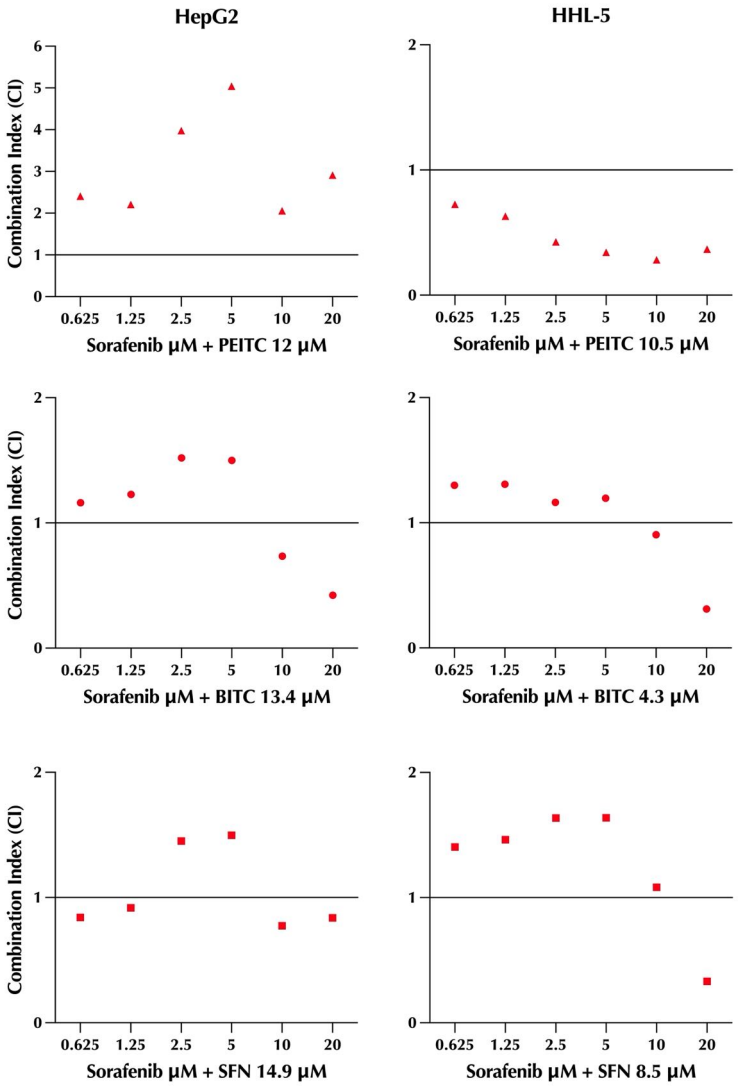

FIGURE 3.3 | CI plots of sorafenib combined with ITCs IC_{20} concentrations.
HepG2 and HHL-5 cells were treated with different increasing concentrations of sorafenib (0.625 to 20 µM) in combination with the IC_{20} of ITCs and the cell proliferation was measured after 72 h of treatment. CI values were calculated with Compusyn software and presented in CI plots.

TABLE 3.3 | CI values of sorafenib combined with fixed ITCs sub-toxic IC_{20} concentration on HepG2 and HHL-5 after 72h of treatment

		HepG2			HHL-5		
		PEITC	**BITC**	**SFN**	**PEITC**	**BITC**	**SFN**
Sorafenib (μM)	**0.625**	2.406	1.161	0.841	0.726	1.299	1.404
	1.25	2.205	1.228	0.917	0.631	1.308	1.462
	2.5	3.978	1.520	1.450	0.427	1.162	1.636
	5	5.041	1.500	1.498	0.342	1.195	1.637
	10	2.058	0.734	0.775	0.282	0.904	1.083
	20	2.915	0.422	0.838	0.367	0.310	0.331

FIGURE 3.4 shows the CI plots resultant by the addition of ITCs to gefitinib treatment (0.625-20 μM). SFN resulted the only ITC able to synergistically increase the efficiency of gefitinib in HepG2 cells but only at lower concentrations with values of weak synergy (**TABLE 3.4**).

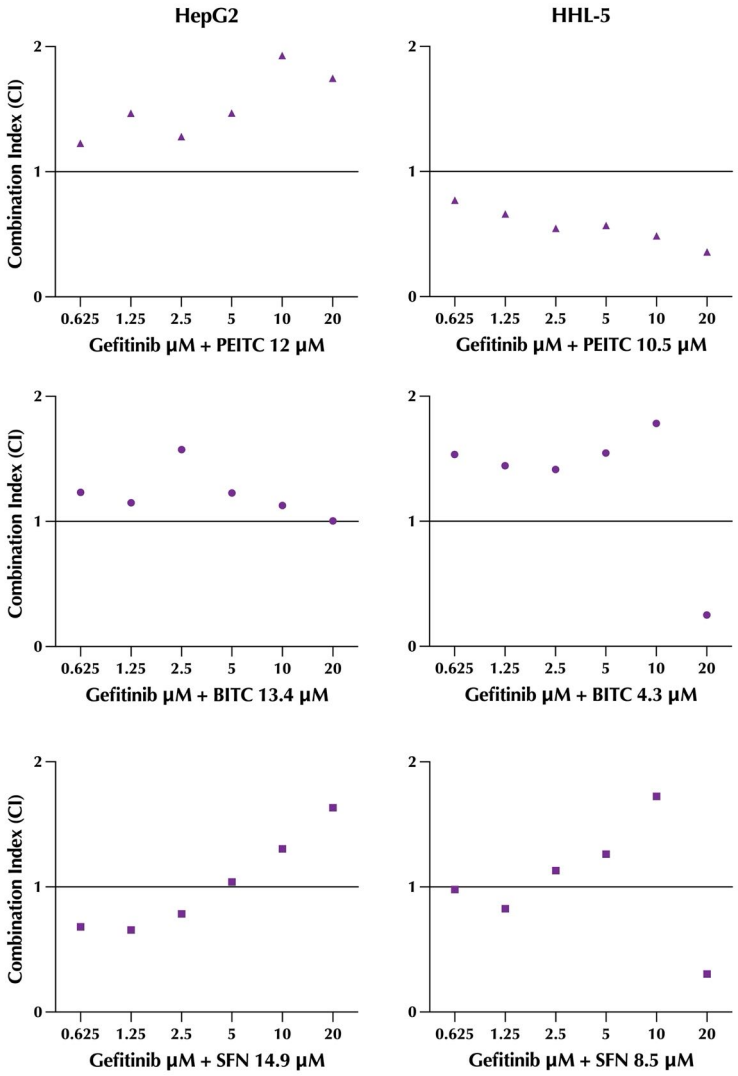

FIGURE 3.4 | CI plots of gefitinib combined with ITCs IC_{20} concentrations.
HepG2 and HHL-5 cells were treated with different increasing concentrations of gefitinib (0.625 to 20 µM) in combination with the IC_{20} of ITCs and the cell proliferation was measured after 72 h of treatment. CI values were calculated with Compusyn software and presented in CI plots.

TABLE 3.4 | CI values of gefitinib combined with fixed ITCs sub-toxic IC_{20} concentration on HepG2 and HHL-5 after 72h of treatment

		HepG2			HHL-5		
		PEITC	**BITC**	**SFN**	**PEITC**	**BITC**	**SFN**
Gefitinib (μM)	**0.625**	1.228	1.232	0.681	0.771	1.534	0.979
	1.25	1.467	1.149	0.656	0.661	1.445	0.825
	2.5	1.281	1.574	0.785	0.546	1.414	1.130
	5	1.469	1.228	1.039	0.569	1.545	1.263
	10	1.929	1.127	1.304	0.485	1.783	1.724
	20	1.747	1.004	1.632	0.358	0.251	0.305

The effects of PEITC and BITC appeared to be counterproductive as their effect was antagonistic in cancer cells and synergistic in non-cancer cells. Lapatinib CI plots showed in **FIGURE 3.5** indicated that lapatinib was weakly potentiated by BITC and SNF while PEITC was antagonistic in HepG2 and synergistic in HHL-5. The CI values in **TABLE 3.5** show only a weak synergy between 0.7 and 0.9 for the two lowest concentrations of SFN and BITC.

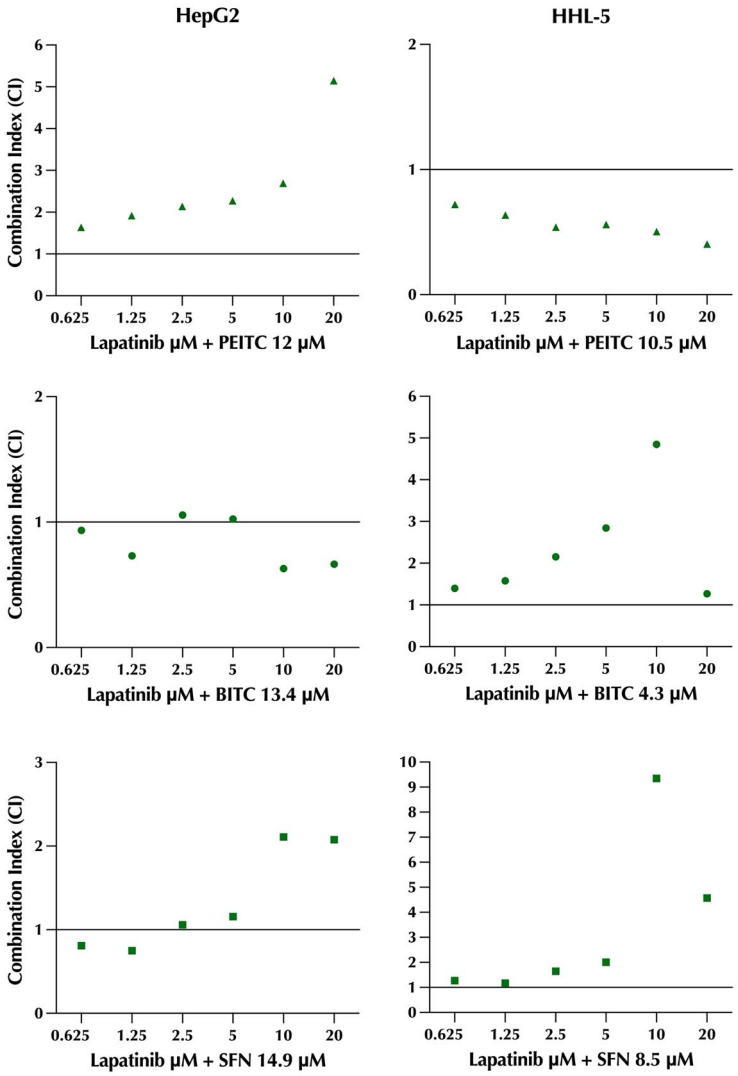

FIGURE 3.5 | CI plots of lapatinib combined with ITCs IC_{20} concentrations.
HepG2 and HHL-5 cells were treated with different increasing concentrations of lapatinib (0.625 to 20 µM) in combination with the IC_{20} of ITCs and the cell proliferation was measured after 72 h of treatment. CI values were calculated with Compusyn software and presented in CI plots

TABLE 3.5 | CI values of lapatinib combined with fixed ITCs sub-toxic IC_{20} concentration on HepG2 and HHL-5 after 72h of treatment

		HepG2			HHL-5		
		PEITC	**BITC**	**SFN**	**PEITC**	**BITC**	**SFN**
Lapatinib (μM)	**0.625**	1.640	0.933	0.808	0.720	1.399	1.267
	1.25	1.917	0.730	0.748	0.636	1.578	1.168
	2.5	2.136	1.055	1.058	0.540	2.151	1.648
	5	2.271	1.024	1.155	0.560	2.841	2.001
	10	2.692	0.629	2.108	0.504	4.848	9.346
	20	5.147	0.664	2.076	0.404	1.270	4.573

Finally, the dasatinib CI plot for both HepG2 (same as **FIGURE 3.2**) and HHL-5 are presented in **FIGURE 3.6** after 72 hours incubation and in **FIGURE 3.7** after 24 hours incubation. BITC and PEITC appeared to increase the toxicity of dasatinib in non-cancer cells HHL-5 while SFN was less toxic towards non-cancer cells. The addition of PEITC and BITC resulted in the most potent synergy at all the dasatinib concentrations at both 24 and 72 hours, whereas SFN was effective at < 5 μM only at 72 hours, as the synergistic effect was not observed at the shorter incubation time of 24 h (**TABLE 3.6**, **TABLE 3.7**).

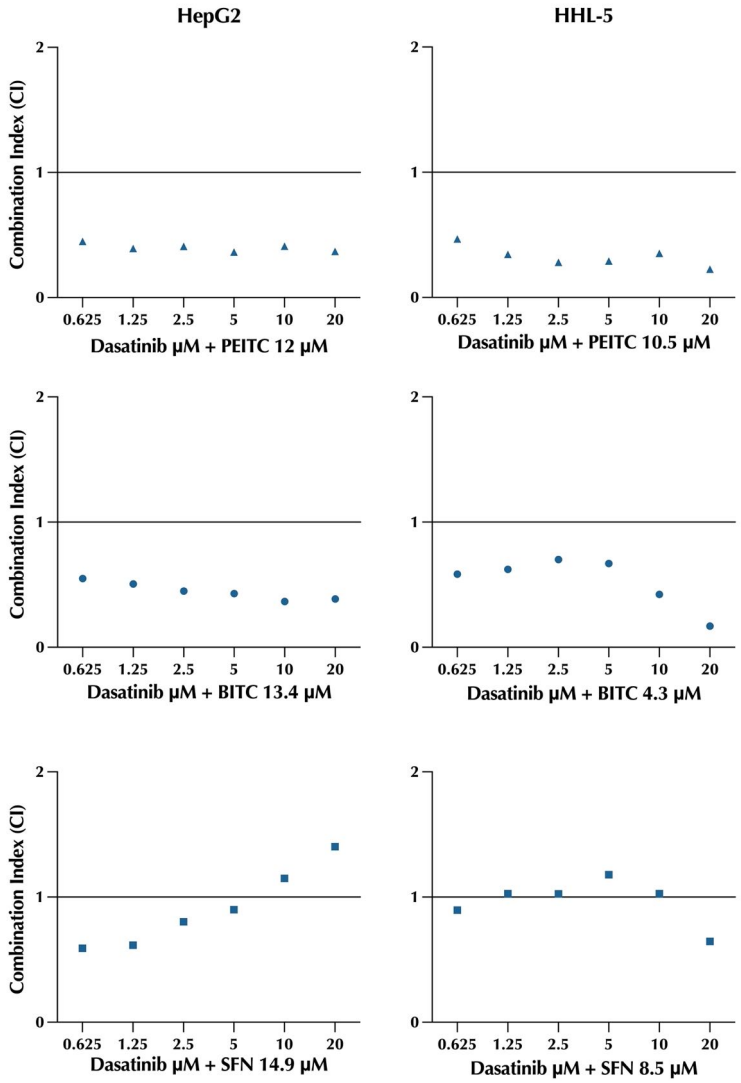

FIGURE 3.6 | CI plots of dasatinib combined with ITCs IC_{20} concentrations.
HepG2 and HHL-5 cells were treated with different increasing concentrations of dasatinib (0.625 to 20 µM) in combination with the IC_{20} of ITCs and the cell proliferation was measured after 72 h of treatment. CI values were calculated with Compusyn software and presented in CI plots

TABLE 3.6 | CI values of dasatinib combined with fixed ITCs sub-toxic IC_{20} concentration on HepG2 and HHL-5 after 72 h of treatment

		HepG2			HHL-5		
		PEITC	**BITC**	**SFN**	**PEITC**	**BITC**	**SFN**
Dasatinib (μM)	**0.625**	0.449	0.550	0.590	0.468	0.585	0.895
	1.25	0.392	0.550	0.615	0.345	0.623	1.027
	2.5	0.410	0.506	0.802	0.280	0.701	1.026
	5	0.365	0.449	0.899	0.292	0.670	1.180
	10	0.411	0.429	1.150	0.352	0.423	1.028
	20	0.370	0.366	1.403	0.225	0.169	0.646

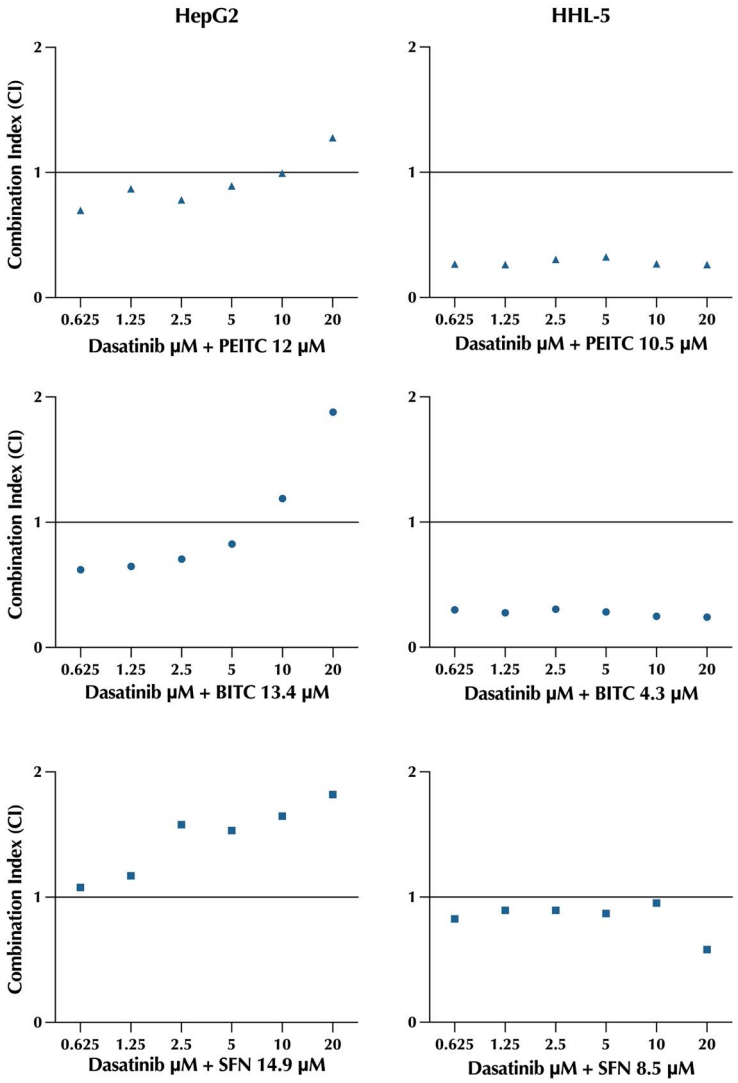

FIGURE 3.7 | CI plots of dasatinib combined with ITCs IC_{20} concentrations.

HepG2 and HHL-5 cells were treated with different increasing concentrations of dasatinib (0.625 to 20 µM) in combination with the IC_{20} of ITCs and the cell proliferation was measured after 24 h of treatment. CI values were calculated with Compusyn software and presented in CI plots

TABLE 3.7 | CI values of dasatinib combined with fixed ITCs sub-toxic IC_{20} concentration on HepG2 and HHL-5 after 24h of treatment

		HepG2			HHL-5		
		PEITC	**BITC**	**SFN**	**PEITC**	**BITC**	**SFN**
Dasatinib (μM)	**0.625**	0.697	0.622	1.078	0.267	0.299	0.826
	1.25	0.869	0.648	1.170	0.263	0.275	0.895
	2.5	0.781	0.705	1.580	0.305	0.304	0.894
	5	0.893	0.826	1.532	0.324	0.282	0.869
	10	0.994	1.189	1.648	0.269	0.248	0.952
	20	1.278	1.879	1.819	0.263	0.241	0.582

3.3 Discussion

The results presented in this chapter highlight the possibility of using ITCs to increase the toxicity of chemotherapeutic agents towards cancerous cells. Addition of BITC or PEITC to dasatinib administration can lead to potential benefit from an increased cytotoxicity towards cancer cells, leading to the reduction of tumour volume that can be resected with an improved outcome for the affected patients. As previously shown in the literature, ITCs can enhance the anticancer activity of different drugs. ITCs can support the action of chemotherapeutic agents in the treatment of different types of cancer because of their broad anticancer activity. The superiority of combination treatment lies in simultaneously targeting multiple pathways potentiating downstream effects, targeting multiple cellular processes usually exploited by tumour cells to proliferate and spread into the organism.

Mutations of tumour suppressor genes can lead to the inactivation of cellular control mechanisms responsible for repairing of corrupted DNA and the abortion of replication in damaged cells. As mentioned before ITCs can target different proteins involved in DNA repair and organisation, leading to cell death due to the induction of apoptosis. For example, PEITC can enhance the activity of cisplatin, blocking the phosphorylation of the H2A histone family member X (H2AX) with a consequent increase of apoptosis [218]. ITCs also regulate the cell cycle reducing the control cancer cells have on the cell cycle checkpoints, inducing cell death. ITCs can bind to several structural proteins, such as tubulin, making them perfect candidates for combination with platinum anticancer agents [219]. The binding to tubulin leads to microtubule depolymerisation preventing the formation of spindle fibres and inducing cell cycle arrest at mitosis stage [220]. ITCs can also directly

induce apoptosis through caspase and non-caspase dependent pathways, and this has been exploited to increase the efficacy of gefitinib in non-small cell lung cancer cells using PEITC and in breast cancer associating erucin and lapatinib [211, 221].

Cancer cell proliferation is linked to different genetic aberrations and misregulated signalling pathways with a high level of ROS, which are often involved in cell signalling processes [222]. Indeed, antioxidant genes are often up-regulated in cancerous cells to control the high production of ROS. This abnormal redox homeostasis is frequently exploited with the induction of oxidative stress combined with chemotherapy to achieve enhanced cytotoxicity. ITCs are directly involved in redox processes as they enhance the expression of detoxifying enzymes such as glutathione transferases and are directly conjugated with GSH influencing the cell redox state [223]. PEITC can be combined with cisplatin to increase the production of ROS in malignant pleural mesothelioma to induce enhanced DNA damage [218]. Different mechanisms can be responsible for the increased ROS production, such as depletion of GSH due to the direct linkage between the ITCs thiol groups and GSH [223]. The latter mechanism has been exploited by sulforaphane co-treatment to increase the cytotoxicity of arsenic trioxide in leukaemia and to restore the cisplatin chemosensitivity in breast cancer in an *in vivo* model [105, 224].

Cancerous cells can also control gene expression to activate mechanisms to induce differentiation towards more aggressive cells that can invade surrounding tissues, propagating to various tissues and increasing the metastatic potential [2, 225]. Cancer cells adhesion, migration, and invasion are fundamental processes in this context [226]. Therefore, drugs that target genes and proteins involved in these processes have a crucial role in combating metastatic cancers. ITCs are known to inhibit cell migration and invasion, targeting several molecules responsible for the cancer cells' invasive capabilities [144, 145]. For example, in a positive HER2 breast cancer model with developed drug resistance, the isothiocyanate erucin downregulated the Akt-mTOR pathway, which is the main target of lapatinib treatment, together with MEK-ERK signalling [212]. The result was the inhibition of the motility and invasion of cancer cells.

Another fundamental aspect of cancer development is the tumour induction of angiogenesis [2, 225]. Tumours, like other tissues, require nutrients, oxygen, and the need to remove waste deposits and CO_2. Cancer cells have the increased ability to up-regulate growth factors to chronically activate angiogenesis, forming an aberrant neovasculature. Allyl isothiocyanate combined improved the anticancer activity of celecoxib in urinary

bladder cancer *in vivo*, with reduction of the tumour microvasculature, probably caused by the diminished VEGF secretion [227]. Furthermore, a co-treatment of erucin and lapatinib reduced the secretion of VEGF in lapatinib-resistant cells, highlighting the role that ITCs can have in treating of drug-resistant tumours [212].

The co-treatment with ITCs may allow a reduction of the treatment dose with a consequent reduction of the associated side effects. On the other hand, it is also essential to consider the possible disadvantages of the simultaneous administration of two or more compounds. The results in the present study showed that the two most successful combinations of PEITC or BITC with dasatinib are also responsible for a pronounced cytotoxic effect in normal cells. Therefore, the therapeutic benefits can be accompanied by severe toxicity, impacting the quality and expectancy of patients' life [201]. Drugs can have toxic effects on non-cancerous cells, or their metabolites can build up with unexpected reactions that further exacerbate side effects. Thus, it is crucial to consider the feasibility of the combination treatment with *in vivo* pre-clinical models, evaluating not only the efficacy of tumour growth inhibition but also the possible toxicity.

Targeting multiple pathways to inhibit strategically different malignant mechanisms simultaneously seems to be an effective way to control the tumour growth, spreading, and development of its aberrant microenvironment. The addition of ITCs at a non-toxic concentration to some TKIs treatment showed an increased cytotoxic effect in HCC HepG2 cells. In particular, BITC and PEITC showed a marked synergy with lowest CI values that indicates a strong synergy. In the following chapters, dasatinib and PEITC combination (PDc) (**FIGURE 3.8**) has been selected for further analysis to evaluate more extensively the effect of this drug combination on the main cancer hallmarks that characterise cancer development and progression. Particular attention was paid to the ability of PDc to suppress tumour growth, tumour metastatic potential, and tumour-induced angiogenesis.

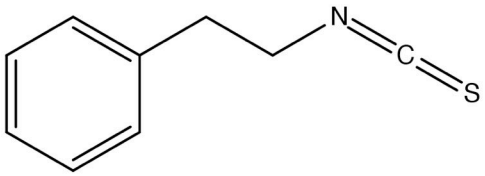

Phenethyl isothiocyanate
PEITC

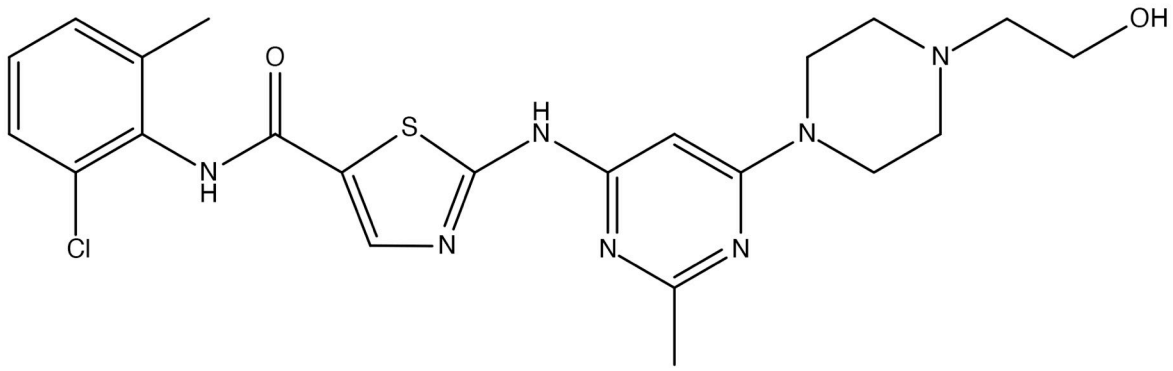

Dasatinib

FIGURE 3.8 | Structures of phenethyl isothiocyanate and dasatinib.

Chapter 4
PEITC and Dasatinib combination effect on tumour cell growth

4.1 Introduction

Tumorigenesis is a multistep process that starts with genetic alterations, and production of oncogenes responsible for functional gain and suppressor genes responsible for functional loss [228]. Both gain and loss of functionality are exploited by tumour cells to drive the cancer progression with the transformation of normal cells into malignant ones. Therefore, cancer cells acquire new functional capabilities, which have been identified as hallmarks of cancer [228]. Six fundamental cancer hallmarks were identified, i.e. sustaining proliferative signalling, evading growth suppressors, resisting cell death, enabling replicative immortality, inducing angiogenesis, and activating invasion and metastasis. With the constant growth of the knowledge and understanding of tumour development and progression, there is now closer attention to the tumour microenvironment. A tumour mass can not be merely considered as a single cell type but more like a group of different cell types recruited to form a tumour-associated stroma [2]. The six hallmarks of cancer increased in the last 20 years, reaching four so-called enabling characteristics that allow the activation of ten functional capabilities [2, 225]. Cancer therapeutic research works to develop drugs targeting these specific tumour-acquired capabilities to inhibits tumour development and progression.

Cancer genomic instability is often associated with an increased accumulation of DNA damage that can be exploited by conventional chemotherapy or radiotherapy [114]. The main issue is that DNA damage induction leads to side effects due to concomitant damage to healthy cells and tissues. Consequently, a more targeted therapy is required to selectively kill cancerous cells, which can be achieved with the simultaneous inhibition of DNA damage response [229]. Over-activated tumour repair mechanisms can be selectively targeted to achieve a more specific action, hence reducing healthy tissue's damage. An example of this approach is the inhibition of poly(ADP-ribose) polymerase (PARP) by olaparib, a drug approved for the treatment of advanced ovarian cancer. Dasatinib was also shown to induce DNA damage in solid tumours and to inhibit DNA repair processes [230, 231], whereas PEITC triggered DNA damage through the activation of ATM-Chk2-p53 pathway [91], and enhanced the activity of PARP inhibitors [232]. DNA damage activates a cascade of signals

that leads to the repair or cell death through cell cycle arrest and apoptosis [229]. For example, the kinase ATM is responsible for the DNA damage with phosphorylation of numerous substrates, such as Chks that downregulate cyclin-dependent kinases CDKs to induce cell cycle arrest [229]. Therefore, DNA damage is an important marker that can lead to other mechanisms useful to overcome uncontrolled cancer growth.

Strictly related to DNA damage and cell cycle arrest is the induction of programmed cell death (PCD) (i.e. apoptosis, autophagy, necroptosis, ferroptosis). The ability of cancer cells to avoid PCD leads to the accumulation of damaged cells, expanding the number of tumour cells not only by the increased rate of proliferation but also by the decreased rate of recycling of damaged cells [228]. Induction of PCD can be exploited to induce cancer cell death reducing the growth of a malignant tumour mass. An example of this approach is the molecule ABT-737, an inhibitor of Bcl-2 family, a group of apoptosis inhibitors upregulated in B-cell malignancies [233]. Apoptosis is the most known form of PCD that relies on releasing the cellular contents in the extracellular environment. Both PEITC and dasatinib showed to induce apoptosis in different solid tumours. While PEITC induces apoptosis in different ways, such as activation of caspases -3, -9 [234] and JNK activation [235], the mechanism by which dasatinib induces apoptosis is not yet clarified [236-238]. A more profound understanding of PCD can lead to the formulation of new therapies to effectively induce cell death in tumours.

DNA damage, cell cycle arrest, and PCD can be all triggered by the induction of oxidative stress in cancer cells, exploiting the imbalanced redox state that characterises malignant cells [239]. Indeed, DNA damage induced by oxidative stress can lead to the activation of p53, which in turn induces caspase-dependent apoptosis through activation of the Bax/Bak porous complex that leads to cytochrome c release and cell cycle arrest with p21 transcription [239]. PEITC is well known to induce the accumulation of ROS selectively in cancerous cells while sparing normal cells [240]. The ability of PEITC to increase ROS accumulation may be linked to the depletion of GSH and inhibition of glutathione peroxidase (GPX1) [240, 241]. While the role of dasatinib in ROS production is unclear, it is known that dasatinib can sensitise gastric cancer cells to cisplatin, which mainly relies on an increased ROS accumulation [242].

In this chapter, the ability of PDc to reduce HepG2 cells proliferation was investigated, looking at understanding the different mechanisms responsible for the reduced cancer growth. The effect of PDc on DNA damage, cell cycle arrest and programmed cell death

was evaluated, as well as the possible involvement of the cell redox disturbance as one of the causes of the cytotoxic effect.

Chapter 4 objectives

- Evaluate PDc effect on cell proliferation
- Evaluate PDc effect on DNA damage
- Evaluate PDc effect on cell cycle
- Evaluate PDc effect on apoptosis
- Elucidate PDc mechanism of action

4.2 Results

4.2.1 PDc synergistically reduces HepG2 cell viability

The efficacy of PDc at different concentrations has been evaluated on HepG2 cells using MTT assay at 24 h (FIGURE 4.1), and CI values (TABLE 4.1) were calculated by means of CompuSyn software. The synergistic effect was achieved by adding a PEITC concentration of 12 μM to a concentration of dasatinib below 10 μM. The addition of lower concentrations (1.5 - 6 μM) of PEITC did not elicit a synergistic effect, with a similar dose-response curve of dasatinib alone. Therefore, 12 μM PEITC was used for most of the experiments on HepG2 with some exceptions (i.e. adhesion assay and colony assay).

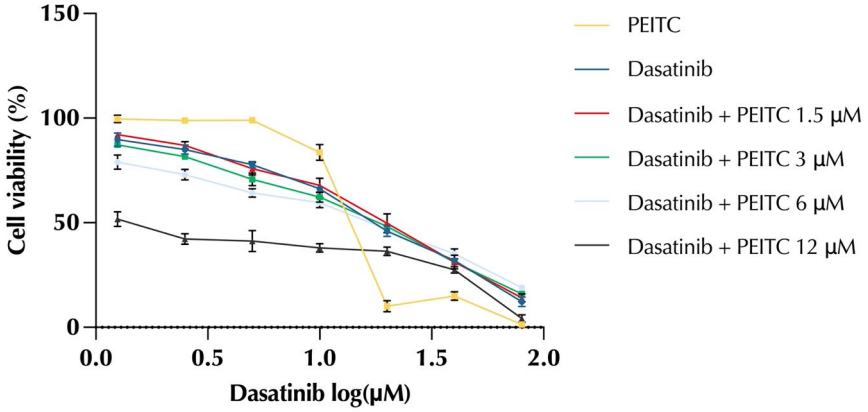

FIGURE 4.1 | Dose-response curve of PEITC and dasatinib combination (PDc).
HepG2 cells were treated with different concentrations of PEITC and dasatinib (1.25 to 80 μM) or with dasatinib plus fixed concentrations of PEITC (1.5, 3, 6, 12 μM) for 24 h. The data presented were normalised to control proliferation (mean ± SEM, n=3).

TABLE 4.1 | CI values of PDc on HepG2 at 24 h

		Dasatinib (μM)			
		1.25	**2.5**	**5**	**10**
PEITC (μM)	**1.5**	1.770	1.735	1.427	1.715
	3	1.258	1.329	1.177	1.399
	6	1.118	1.144	1.161	1.515
	12	0.869	0.781	0.893	0.994

The effect of PDc on HepG2 cell viability was also consistent on a time course of 72 h with a constant decrease of cell viability at the four tested dasatinib concentrations (1.25 - 10 μM) (FIGURE 4.2A). The effect on HepG2 cell viability is also evident in FIGURE 4.2B where, contrast phase images of the formazan crystals formed by the tetrazolium reduction are presented.

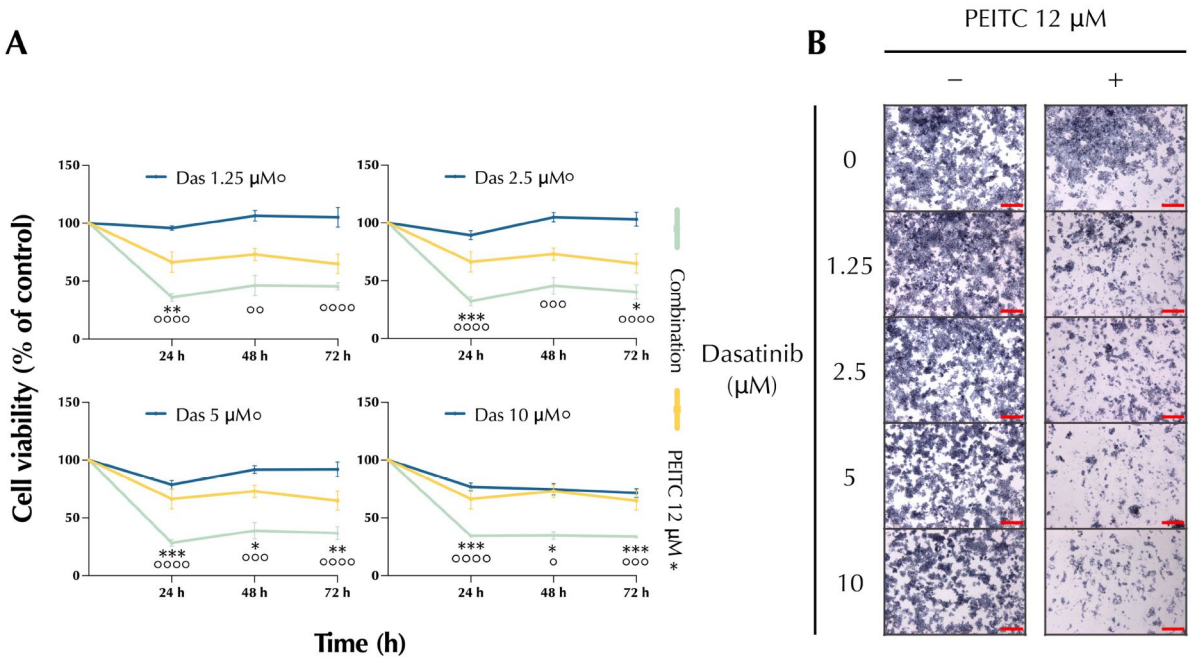

FIGURE 4.2 | Effect of PDc on HepG2 cell viability over time.
(A) Cells were treated for 24, 48, and 72 h with different concentrations of dasatinib (1.25 to 10 μM) plus a fixed concentration of PEITC (12 μM). Data presented was normalised to control proliferation (mean ± SEM, n=3). **(B)** Representative images of MTT crystals 24 h (10x, scale bar 200 μm). The cell able to metabolise MTT were massively reduced in PDc treated cells.

4.2.2 PDc reduces the growth of 3D HepG2 spheroids

The canonical 2D plastic culture does not represent the tumour complexity, thereby 3D models are employed to test the effect of different stimuli on tumour cell behaviour. PDc has been tested on HepG2 spheroids formed using an ECM gel through short centrifugation (ECM concentration optimisation in FIGURE A1 of the appendices). The size of the spheroids was measured before and after treatment with PDc showing a decrease of spheroid area (FIGURE 4.3A) at the combination with dasatinib 5 and 10 µM. However, only the latter concentration resulted statistically significant compared to both single drug treatments (FIGURE 4.3B). The PDc cytotoxic effect was also evaluated with dual cell viability staining using Calcein AM to stain viable cells and ethidium homodimer to stain dead cells (FIGURE 4.4). Spheroids treated with PDc dasatinib 10 µM showed an increase of dead cells in the core of the spheroid, indicating that the drug combination can reduce the size of the spheroids, slowing down the cell replication and increasing the percentage of dead cells.

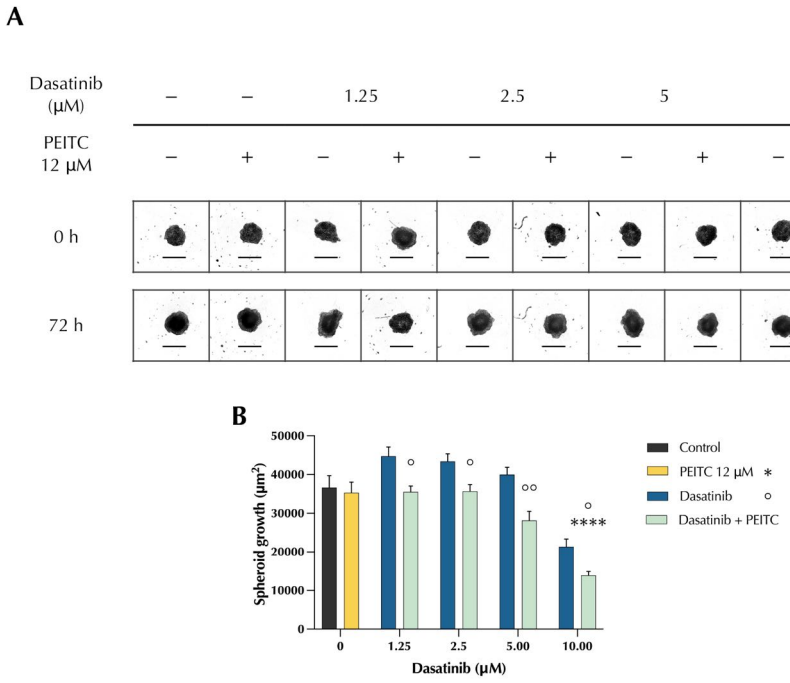

FIGURE 4.3 | Effect of PDc on HepG2 spheroids growth.
Spheroids were treated for 3 days with different concentrations of dasatinib (1.25 to 10 µM) plus a fixed concentration of PEITC (12 µM). **(A)** Effect on spheroids growth (4x, scale bar 500 µm). PDc treated spheroids appear smaller compared to single drug treatments. **(B)** Spheroids area quantification on ED 6 (mean ± SEM, n=4). PDc significantly reduced the spheroids growth. The degrees of significance were calculated with non-parametric Kruskal-Wallis test with Dunn's multiple comparisons test and are indicated as °/* $p < 0.05$, °°/** $p < 0.01$, °°°°/**** $p < 0.0001$ (* PEITC vs combination, ° dasatinib vs combination).

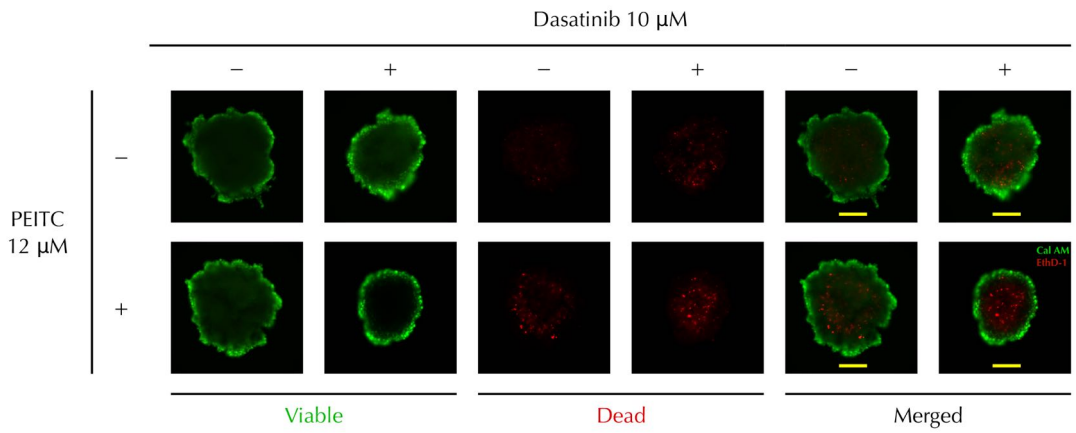

FIGURE 4.4 | Effect of PDc on spheroids viability.
Cells were treated for 3 days with dasatinib 10 µM with or without PEITC at 12 µM. Dead cells and viable cells were stained with EthD-1 (red) and Calcein AM (Green), respectively (10x, scale bar 200 µm). The images show an increase of dead cells into the core of PDc treated spheroids

4.2.4 PDc induces DNA damage and cell cycle G2/M phase arrest

As discussed before, the induction of DNA damage can be exploited together with the inhibition of tumour DNA repair mechanisms to target cancerous cells. Here the effect of PDc on DNA damage has been investigated, looking at the presence of DNA fragmentation using an agarose gel, the presence of chromatin condensation using a DAPI stain, and with Western blot to evaluate the expression of proteins involved in DNA damage and repair. The agarose gel (FIGURE 4.5A) showed a slight increase in DNA fragmentation in cells treated with PDc, while DAPI staining showed a consistent increase in cells presenting chromatin condensation and apoptotic bodies (FIGURE 4.5B). Protein expression analysis showed that PDc decreased the expression of PARP-1, which is a factor mainly involved in the process of DNA repair (FIGURE 4.6C-D). Furthermore, PDc significantly increased the phosphorylation of Chk2 and p53 phosphorylation, which are markers for DNA damage (FIGURE 4.5C-D).

DNA damage leads to a cascade of signals responsible for the cell fate, which can activate repair mechanisms or, if the insult is unbearable, the cell goes to programmed cell death through cell cycle arrest. Therefore, cell cycle phases were analysed using propidium iodide staining and flow cytometry, as shown by the plots in FIGURE 4.6A. Gating strategy is presented in appendices in FIGURE A3. PDc treatment showed that the drug combination was able to induce an arrest of the cell cycle at the G2/M phase with a reduction of cells in the

G1 phase (FIGURE 4.6B), explaining the ability of the drug combination to decrease the cell proliferation observed in the previous experiments.

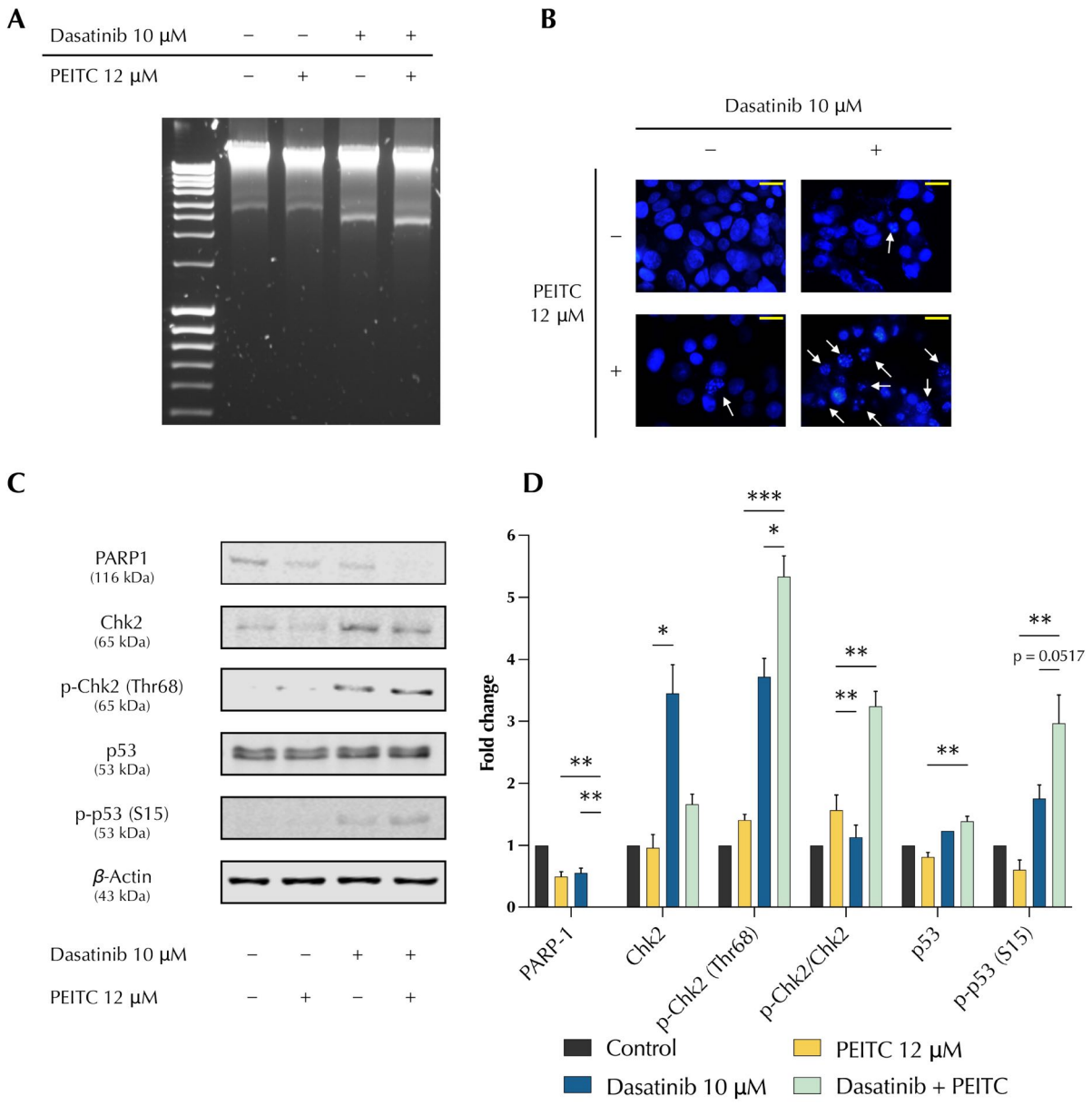

FIGURE 4.5 | Effect of PDc on DNA damage.

(A) DNA laddering indicates DNA fragmentation. PDc lane shows a longer smear compared to single drug treatments after 24 h of treatment. **(B)** DAPI staining showed signs of apoptosis with chromatin condensation and cell blebbing, **(C-D)** HepG2 cells were treated for 24 h, and the proteins extracted were analysed with Western blot. Effect of PDc on PAR1, Chk2, and p53 expression (Full blots are presented in FIGURE A5-7), the results presented are representative of independent protein extractions (mean ± SEM, n=3). The degrees of significance were calculated with one-way ANOVA test with Tukey's multiple comparisons test and are indicated as * $p < 0.05$, ** $p < 0.01$, *** $p < 0.001$.

The protein expression analysis using Western blot highlighted a change in the phosphorylation of CDK1 and expression of Cyclin B1. Indeed, CDK1 and Cyclin B1 form a complex to allow the progression from the G2 phase into the mitosis. The limitation of the sole propidium iodide staining is that it is not possible to discern between cells in G2 and M phases.

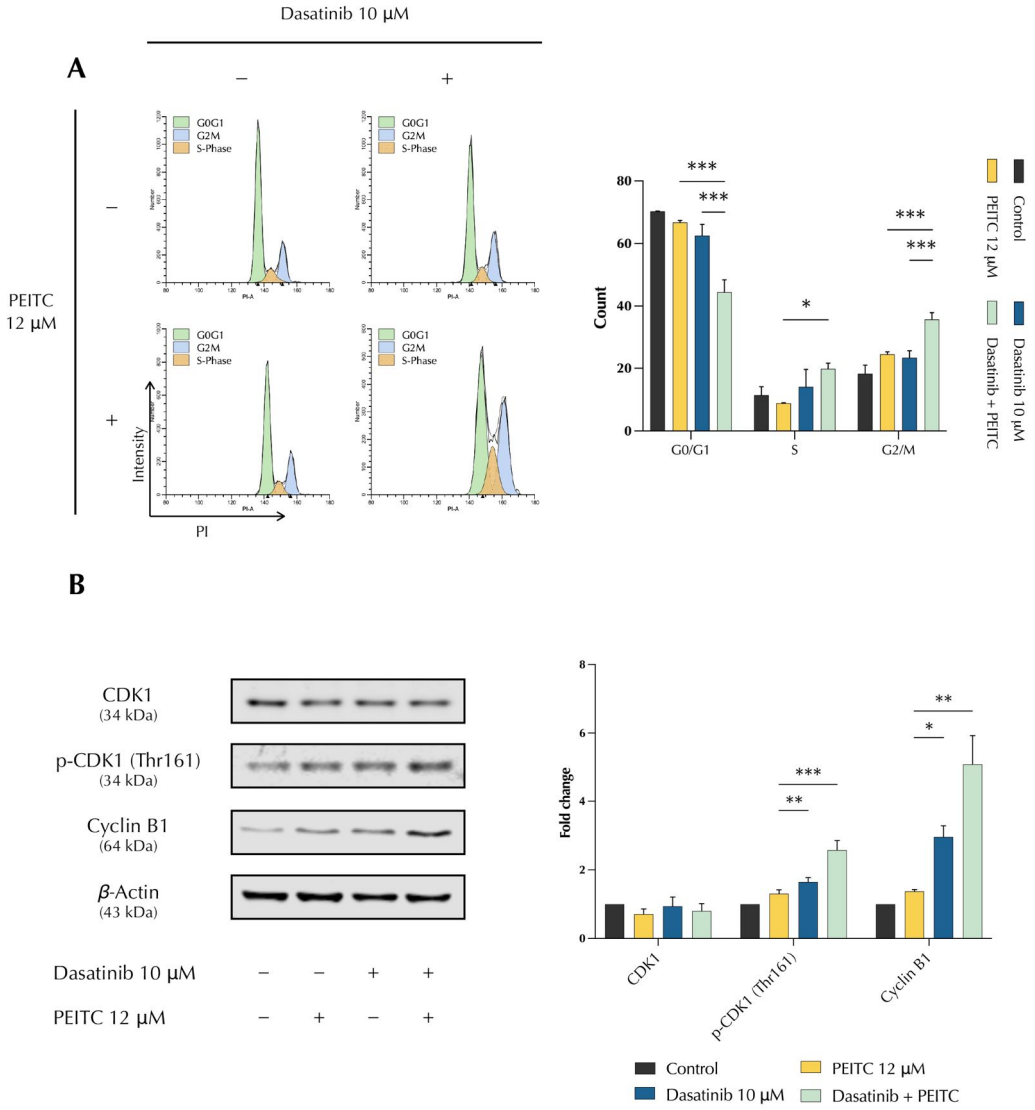

FIGURE 4.6 | PDc induces cell cycle arrest at the G2/M phase.

(A) PI staining for cell cycle analysis through flow cytometry. PDc induces an arrest at the G2/M phase. The degrees of significance are indicated as * $p < 0.05$, *** $p < 0.001$. **(B)** HepG2 cells were treated for 24 h, and the proteins extracted were analysed with Western blot. Effect of PDc on the expression of CDK1 and Cyclin B1 (Full blots are presented in **FIGURE A8-10**), the results presented are representative of independent protein extractions (mean ± SEM, CDK1 n=3, pCDK1 n=6, Cyclin B1 n=4). The degrees of significance were calculated with one-way ANOVA test with Tukey's multiple comparisons test and are indicated as * $p < 0.05$, ** $p < 0.01$, *** $p < 0.001$.

Immunostaining of α-Tubulin was employed to clarify the status of microtubule polymerisation, considering that PEITC is known to bind tubulin to destabilise microtubule formation, which involved in the formation of mitosis spindle fibres. Surprisingly, the overall intensity of α-Tubulin did not change between PDc and single drug treatments, highlighting that the cell cycle arrest was not related to tubulin degradation. Interestingly, the PDc-treated cells showed a consistent increased number of cells presenting mitotic spindle fibres (FIGURE 4.7A), often in a jumbled state (FIGURE 4.7B).

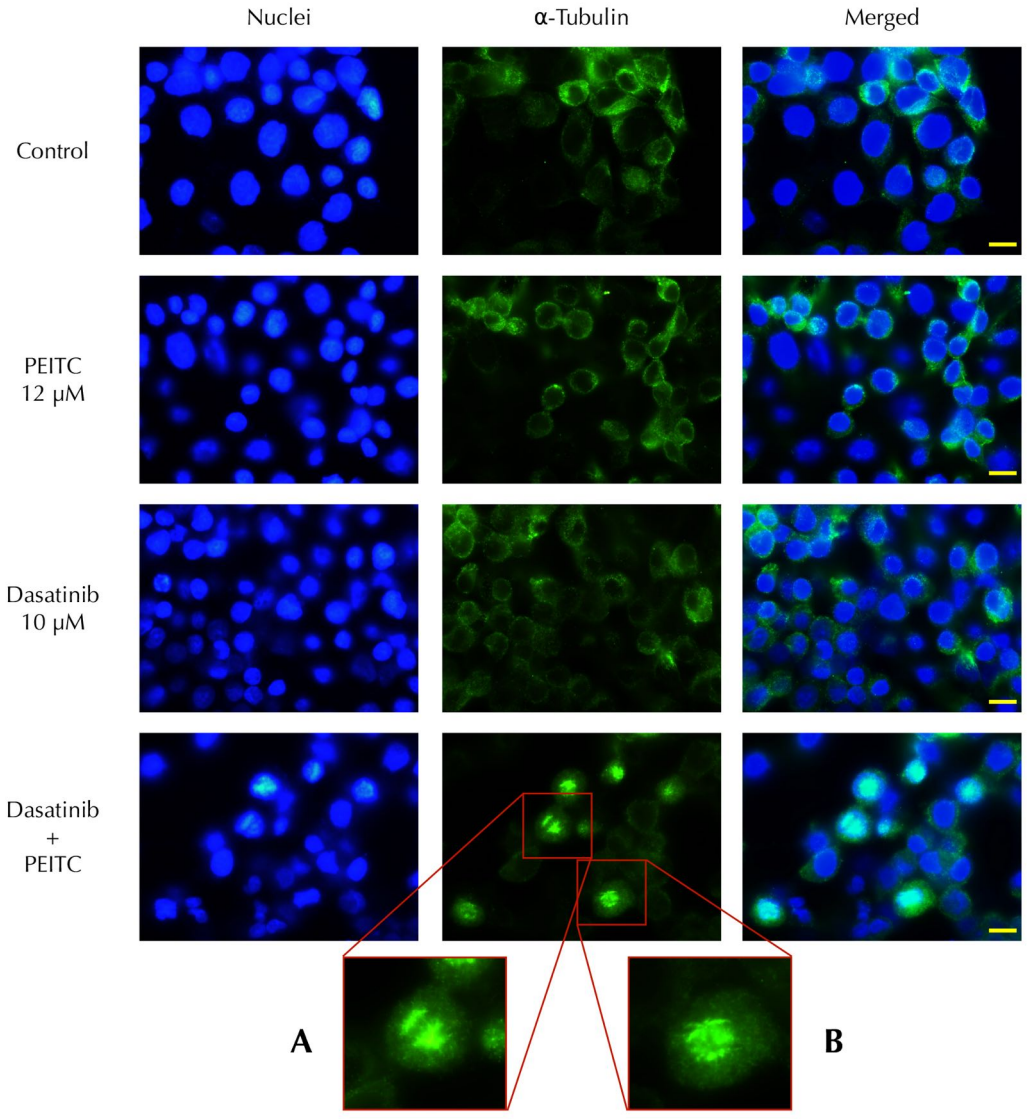

FIGURE 4.7 | Effect of PDc on α-Tubulin in formation of mitosis spindle fibres.
(A) α-Tubulin immunocytochemistry shows that PDc-treated cells present a higher number of cells with in an early stage of mitosis (63x, scale bar 20 μm). **(B)** The spindle fibres often appears in a disorganised state which it is a phenomenon observed in mitotic catastrophe.

4.2.5 PDc induces apoptosis in HepG2 cells

Since cell cycle arrest and apoptosis are strictly related, the effect of PDc on apoptosis induction was assessed using flow cytometry and dual staining with Annexin V FITC conjugated and propidium iodide. Compensation controls and positive controls are presented in appendices in FIGURE A4. The addition of PEITC 12 µM to different dasatinib concentrations consistently increased the number of cells presenting apoptotic staining (FIGURE 4.8A). In particular, the combination with dasatinib 10 µM led to a higher number of apoptotic cells (FIGURE 4.8B-C).

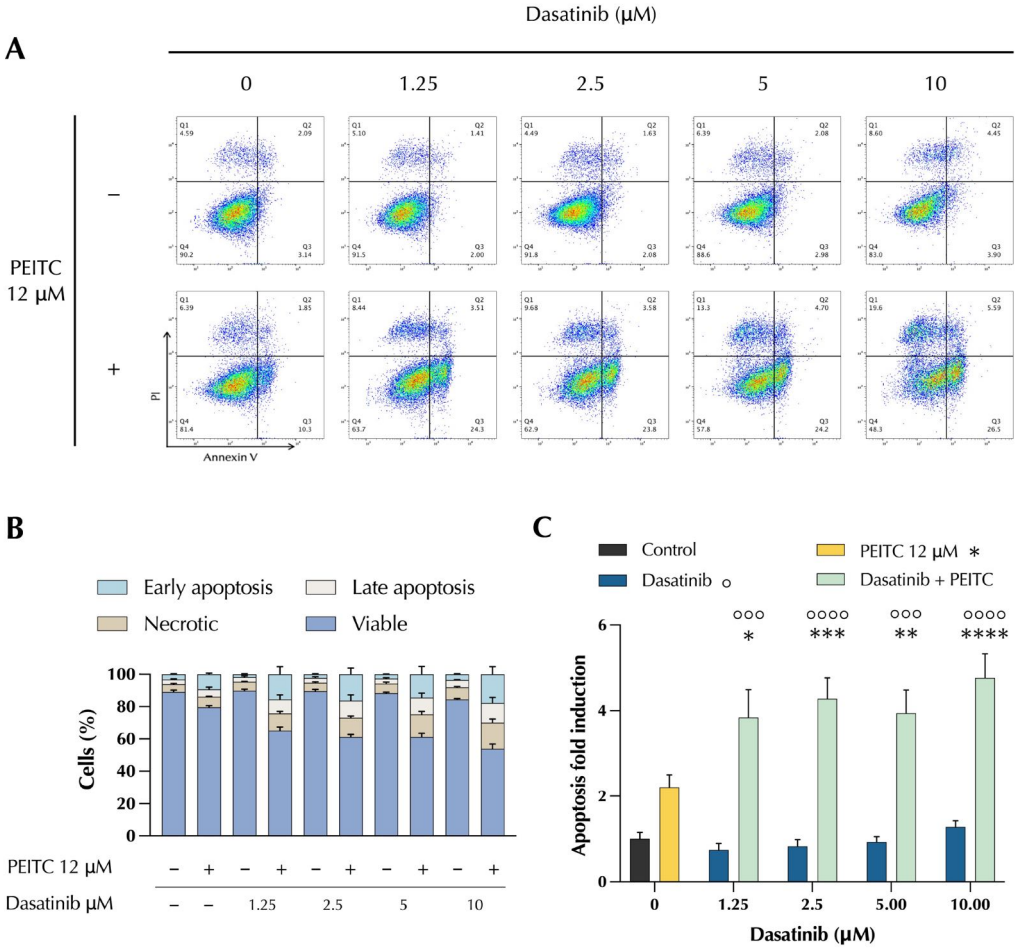

FIGURE 4.8 | Effect of PDc on apoptosis induction.
HepG2 cells have been treated with increasing concentrations (1.25 - 10 µM) of dasatinib with or without PEITC 12 µM for 24 h and then subjected to Annexin V (AV) and PI staining. **(A)** Apoptosis assay representative images from FlowJo. **(B)** Apoptotic cell percentages (mean ± SEM, n=3). **(C)** Apoptosis (early + late) fold induction (mean ± SEM, n=3). The degrees of significance were calculated with one-way ANOVA test with Tukey's multiple comparisons test and are indicated as °°°/*** $p < 0.001$, °°°°/**** $p < 0.0001$. (* combination vs PEITC, ° combination vs dasatinib).

4.2.6 PDc apoptosis induction is not related to canonical apoptosis pathways

To investigate the mechanism of increased apoptosis induced by PDc, a proteome profiler was employed to screen for significant changes in the expression of several apoptosis markers (**FIGURE 4.9**). Even if the proteome profiler confirmed a slight increase in phosphorylation of p53 (S15), the other pro-apoptosis factors (right-hand side of the graph) did not show significant changes. In the same way, no changes in the expression of anti-apoptosis factors were observed (left-hand side of the graph). These findings were confirmed with Western blot analysis of the expression of caspase -3, -9, and cytochrome c (**FIGURE 4.10**).

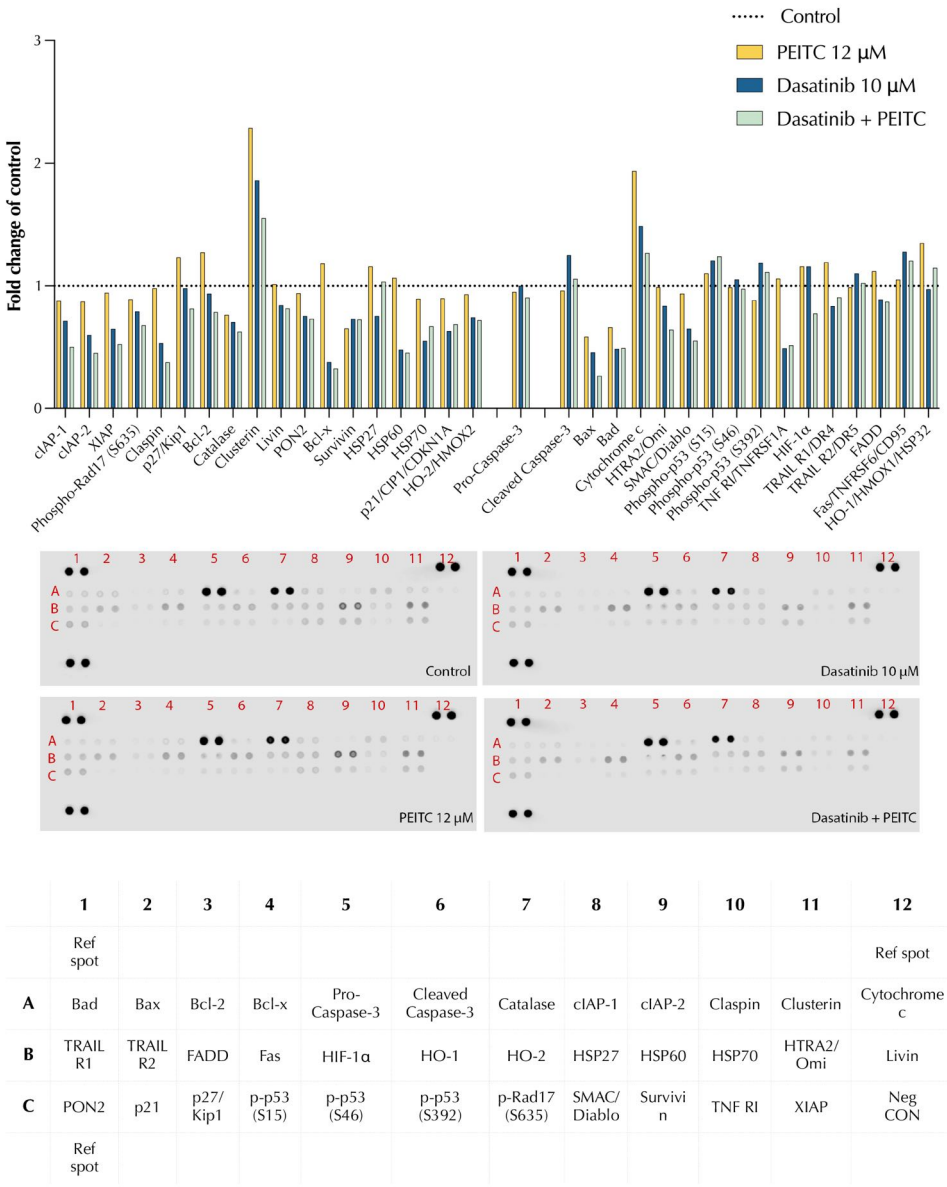

	1	2	3	4	5	6	7	8	9	10	11	12
	Ref spot											Ref spot
A	Bad	Bax	Bcl-2	Bcl-x	Pro-Caspase-3	Cleaved Caspase-3	Catalase	cIAP-1	cIAP-2	Claspin	Clusterin	Cytochrome c
B	TRAIL R1	TRAIL R2	FADD	Fas	HIF-1α	HO-1	HO-2	HSP27	HSP60	HSP70	HTRA2/ Omi	Livin
C	PON2	p21	p27/ Kip1	p-p53 (S15)	p-p53 (S46)	p-p53 (S392)	p-Rad17 (S635)	SMAC/ Diablo	Survivi n	TNF RI	XIAP	Neg CON
	Ref spot											

FIGURE 4.9 | Effect of PDc on apoptosis markers.

On top of the image, quantitative results of proteome profiler are presented with anti apoptotic and pro-apoptotic targets on left and right of the graph respectively. No significant changes (fold change higher than 1) have been identified and could be linked to the observed increased apoptosis induction in PDc treated cells. Below images of single blots indicate the coordinates that refer to the following legend of targets location.

No changes in pro-caspases as well as cleaved caspases were observed, while only a slight non-significant increase in cytochrome c expression was observed in PDc-treated cells. These results confirmed the absence of caspases activation in apoptosis induction observed in PDc treatment.

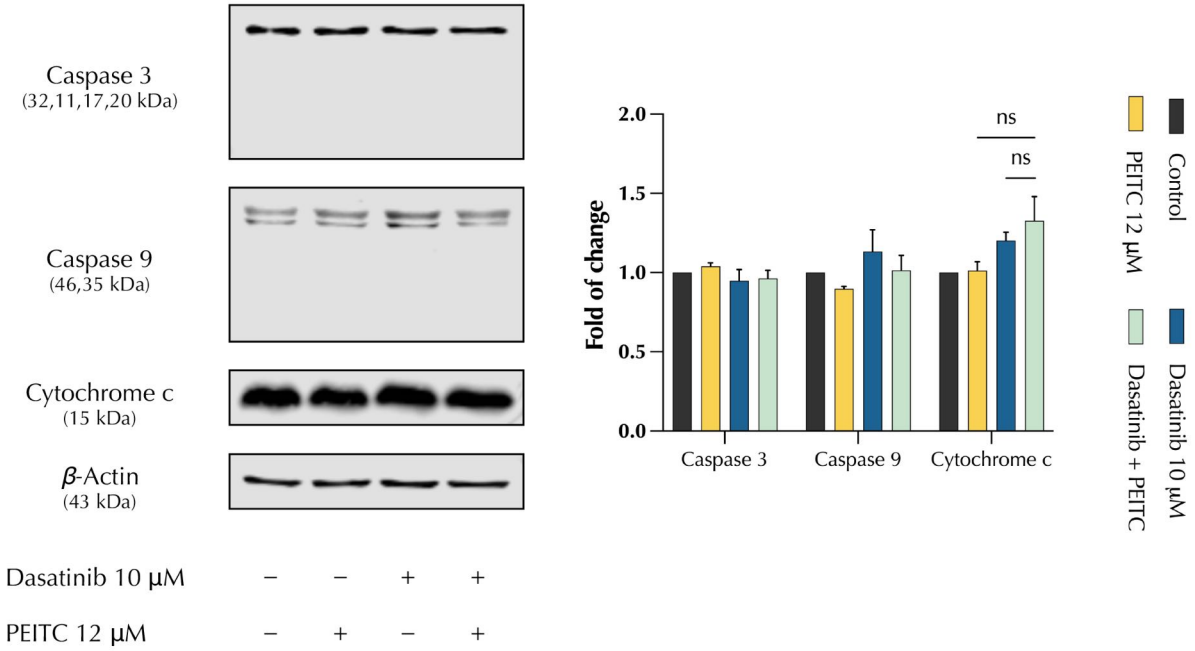

FIGURE 4.10 | Effect of PDc on Caspases and Cytochrome expression
HepG2 cells were treated for 24 h, and the proteins extracted were analysed with Western blot. (Full blots are presented in FIGURE A10-12). The results presented are representative of independent protein extractions (mean ± SEM, n=3). The degrees of significance were calculated with non-parametric Kruskal-Wallis test with Dunn's multiple comparisons test and are indicated as ns = non significant.

4.2.7 PDc induces ROS production

A staining of 2',7'-dichlorodihydrofluorescein diacetate (DCFDA) was employed to assess the role of PDc in the cell redox state. Cell esterases deacetylate DCFDA, and the product obtained is oxidised by ROS, producing DCF. DCF is a fluorescent compound that can be observed with fluorescence microscopy and quantitatively measured with a plate reader. HepG2 cells were stained with DCFDA for 45 minutes and then treated with PDc and single drugs at two dasatinib concentrations (1.25 and 10 µM). After 4 hours of treatment, visualisation of HepG2 cells with a fluorescence microscope showed the increased production of ROS in PDc-treated cells (FIGURE 4.11A). The quantitative analysis showed that the addition of PEITC to dasatinib 10 µM increases the production of ROS starting from 1 hour to 4 hours of treatment with a significant difference between PDc and single drug treatments (FIGURE 4.11B-C). The assay reliability was confirmed by treatments with tert-Butyl hydroperoxide (t-BHP) (50, 100, 250 µM) (FIGURE 4.11D), which leads to a concentration-dependent increase in ROS production. PDc with the lower dasatinib concentration (1.25

μM) did not show a detectable increase in ROS production; therefore for the subsequent ROS experiments, only dasatinib 10 μM was used.

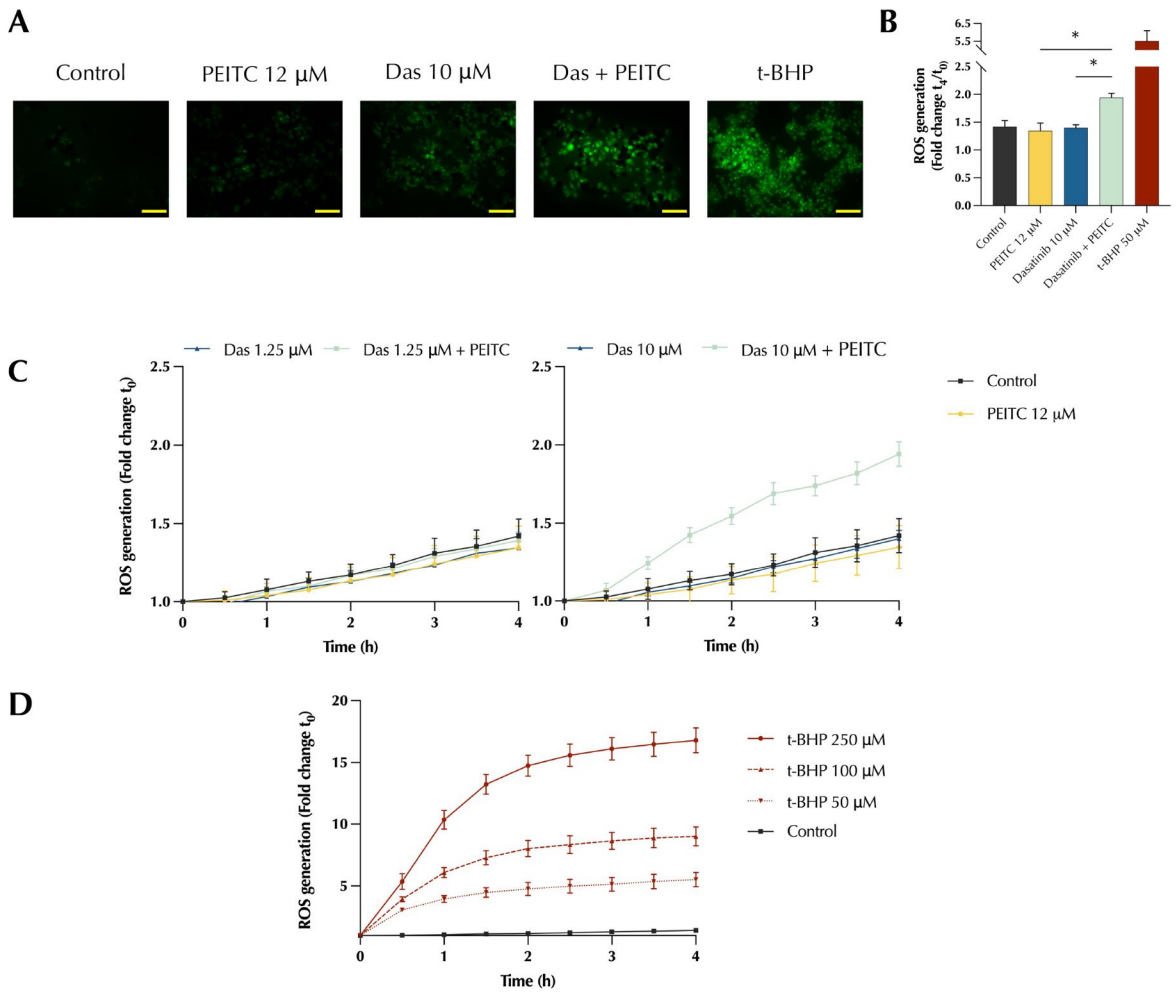

FIGURE 4.11 | Effect of PDc on ROS production.
(A) DCFDA staining after 4 h of treatment. The intensity result higher in PDc treated cells compared to single drug treatments, with a strong signal from the positive control t-BHP 50 μM (20x, scale bar 100 μm). **(B)** ROS production at t_4 (mean ± SEM, n=3). The degrees of significance were calculated with one-way ANOVA test with Tukey's multiple comparisons test and are indicated as * $p < 0.05$. **(C)** ROS quantification with DCDFA fluorescence over a time course of 4 h, **(D)** effect of different increasing concentrations of t-BHP on ROS production (50, 100, 250 μM).

4.2.8 Effect of PDc on glutathione balance

Considering that PEITC is known to deplete cellular glutathione (GSH), HPLC was employed to quantify the levels of glutathione disulphide (GSSG) and reduced GSH using monobromobimane (mBBr) as a fluorescent label. The levels of GSH and GSSG were

assessed in HepG2 treated with PDc and single drugs at 1, 3, 6, 16, and 24 hours (FIGURE 4.12A). The results showed that PEITC, compared to dasatinib and control, increased both GSH and GSSG production between 3-6 hours and sustained the production till 16 hours, when it started to decline. PDc presented a similar trend but with a marked depression of GSH at 6 hours. Therefore, PDc at 6 hours showed a significant increase in the GSSG/GSH ratio compared to the other treatments, while at 16 and 24 hours there was no significant difference between all the treatments (FIGURE 4.12B).

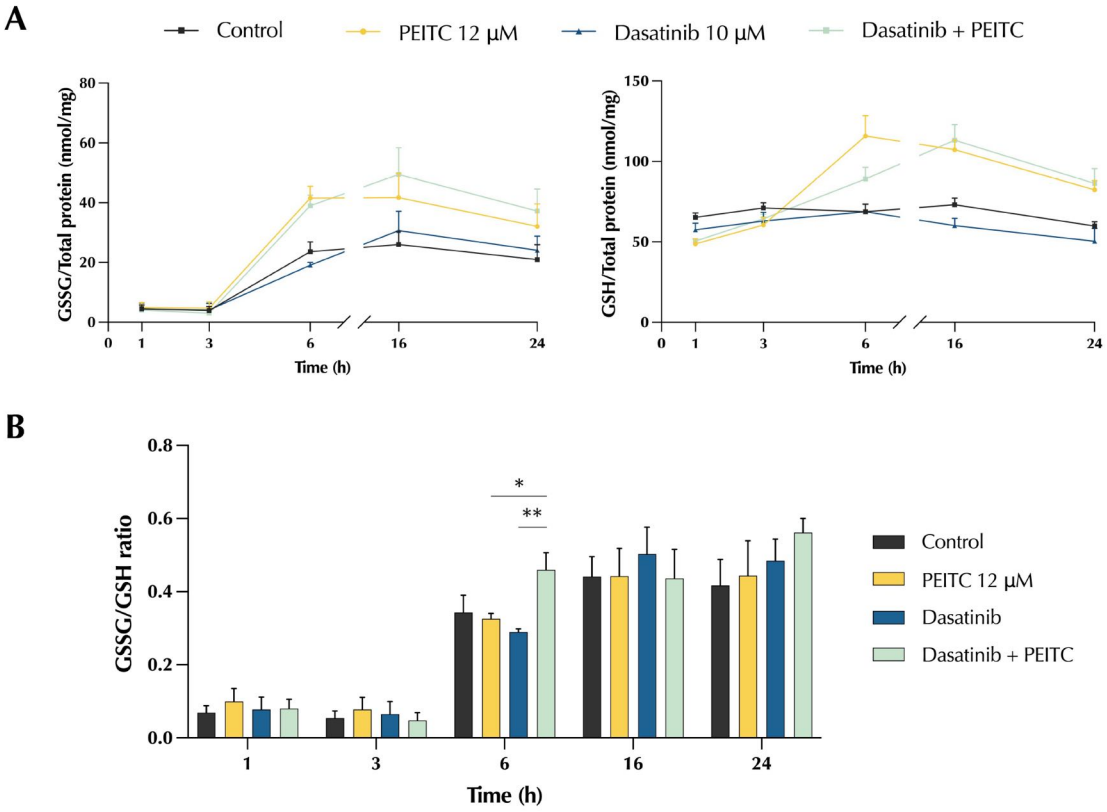

FIGURE 4.12 | Effect of PDc on GSSG/GSH balance.
HepG2 cells were treated for 1, 3, 6, 16, 24 h and protein were extracted. GSH and GSSG were extracted and conjugated with mBBr and subjected to HPLC **(A)** Time course of GSH and GSSG levels. **(B)** Time course of GSSG/GSH ratio (mean ± SEM, n=3). The degrees of significance were calculated with one-way ANOVA test with Tukey's multiple comparisons test and are indicated as * $p < 0.05$, ** $p < 0.01$.

4.2.9 PDc induces apoptosis and cell cycle arrest through oxidative stress

Considering that PDc leads to an imbalance of the cell redox state, the role of the increased ROS production was investigated using NAC in different cell assays. NAC is a

GSH precursor that neutralises ROS and is often used in mechanistic studies to determine the effective involvement of ROS. HepG2 cells were pre-treated with NAC (1, 5, 10, 20 mM) for 2 hours and then treated with PDc or control media for 24 hours. The MTT assay data showed that NAC pre-treatment abolished PDc cytotoxicity in a concentration-dependent manner (**FIGURE 4.13A**). In particular, NAC 20 mM pre-treatment was able to abolish the PDc cytotoxic effect on HepG2 almost completely; thus, NAC 20 mM pre-treatment was selected for subsequent experiments (**FIGURE 4.13B**). Annexin V and PI staining and flow cytometry analysis showed that the NAC pre-treatment significantly suppressed the PDc induction of apoptosis (**FIGURE 4.13C-D**). The NAC antioxidant pre-treatment reduced the activation of Chk2 and p-53 but the cytoprotective effect did not re-establish normal levels in terms of phosphorylated proteins (**FIGURE 4.13E-F**).

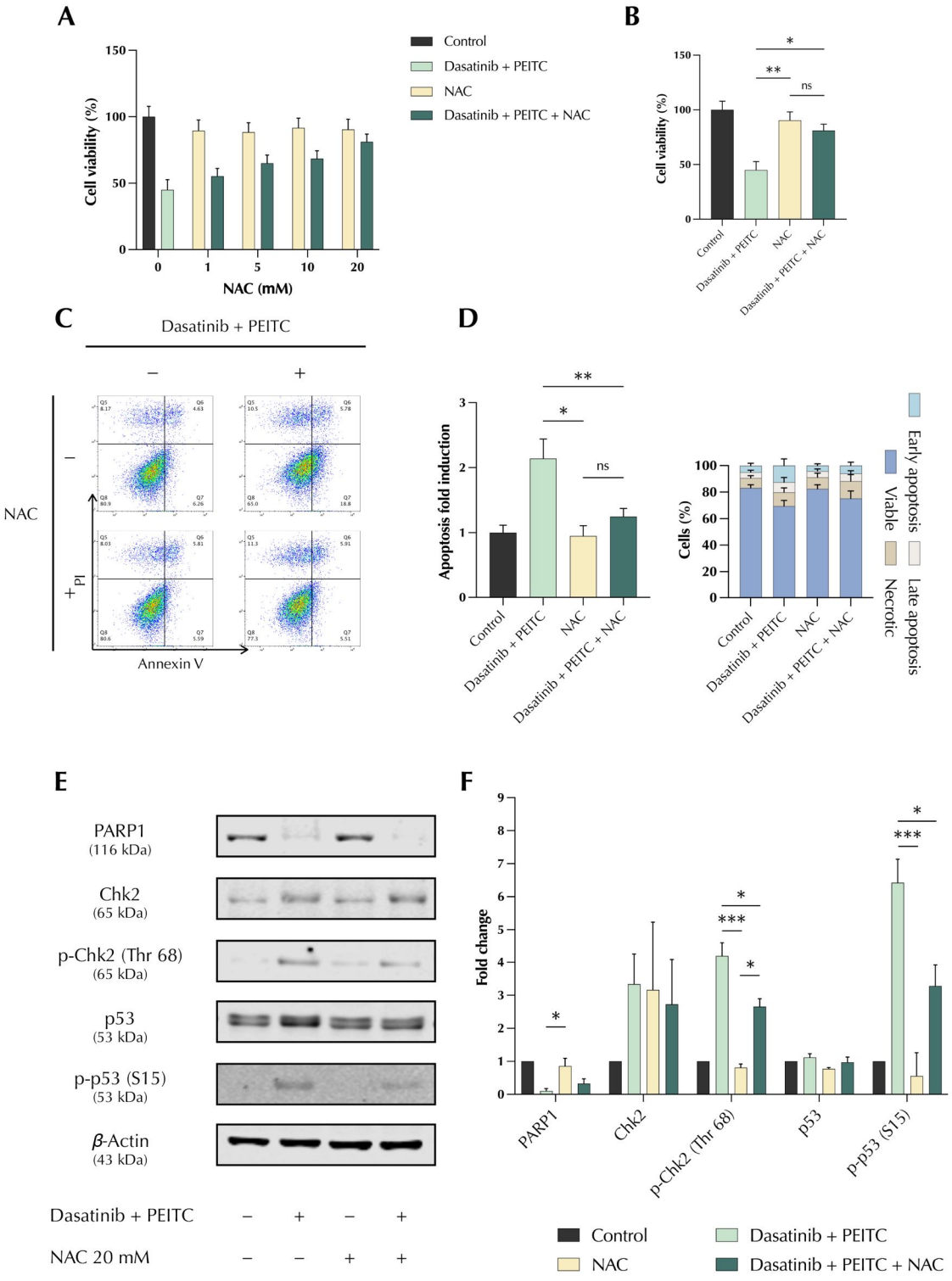

FIGURE 4.13 | PDc induction of apoptosis is abolished with NAC pre-treatment. **(A)** Dose-dependent effect of NAC (1, 5, 10, 20 mM) on PDc treated cells (mean ± SEM, n=3). **(B)** NAC 20 mM abolishes PDc toxicity. **(C)** Representative images of Flow Jo Annexin V/PI staining. **(D)** PDc apoptosis induction is abolished by NAC pre-treatment (mean ± SEM, n=3). The degrees of significance were calculated with one-way ANOVA test with Tukey's multiple comparisons test and are indicated as * $p < 0.05$, ** $p < 0.01$, ns = not significant. **(E)** HepG2

cells were treated for 24 h, and the proteins extracted were analysed with Western blot. Effect of PDc on PARP1, Chk2, and p53 expression (Full blots are presented in FIGURE A5-7), the results presented are representative of independent protein extractions (mean ± SEM, n=3). The degrees of significance are indicated as * $p < 0.05$, ** $p < 0.01$, ns = not significant.

Furthermore, the NAC pre-treatment abolished the cell cycle arrest induced by PDc, restoring the number of cells in the G0/G1 phase (FIGURE 4.14A). As expected, the neutralisation of ROS also reduced the phosphorylation of CDK1 but not the expression of Cyclin B1 (FIGURE 4.14B).

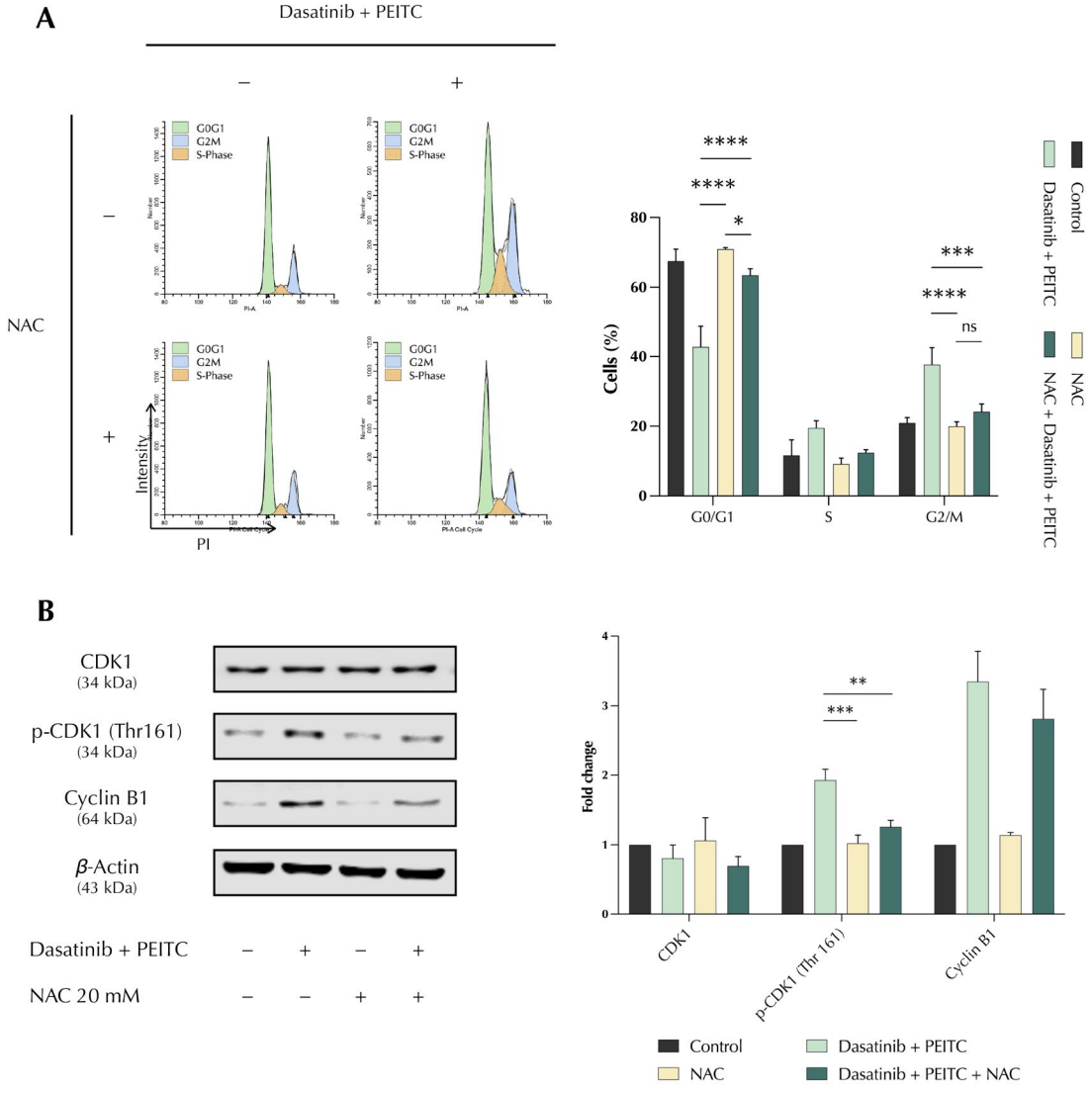

FIGURE 4.14 | PDc-induced cell cycle arrest is abolished with NAC pre-treatment.
(A) PI staining for cell cycle analysis through flow cytometry. The degrees of significance are indicated as * p < 0.05, ** p < 0.01, *** p < 0.001, **** p < 0.0001, ns = not significant. **(B)** HepG2 cells were treated for 24 h, and the proteins extracted were analysed with Western blot.

Effect of PDc on the expression of CDK1 and Cyclin B1 (Full blots are presented in **FIGURE A8-10**), the results presented are representative of independent protein extractions (mean ± SEM, CDK1 n=3, pCDK1 n=6, Cyclin B1 n=4)). The degrees of significance were calculated with one-way ANOVA test with Tukey's multiple comparisons test and are indicated as ** $p < 0.01$, *** $p < 0.001$.

4.2.10 PDc oxidative stress induction leads to oxeiptosis

Among the different known types of PCD oxeiptosis stands out as an apoptosis-like cell death induced by increased production of ROS. Considering that PDc significantly induces ROS production, leading to a redox imbalance, the expression of oxeiptosis markers was investigated using Western blot. Interestingly, PDc treatment reduced the accumulation of Keap1, induced PGAM5 cleavage, and reduced the de-phosphorylation of AIFM1 (**FIGURE 4.15A**). The pre-treatment with NAC confirmed the involvement of ROS production as a consequence of PDc action. Indeed, the antioxidant pre-treatment abolished all the effects of PDc on oxeiptosis markers aforementioned (**FIGURE 4.15B**).

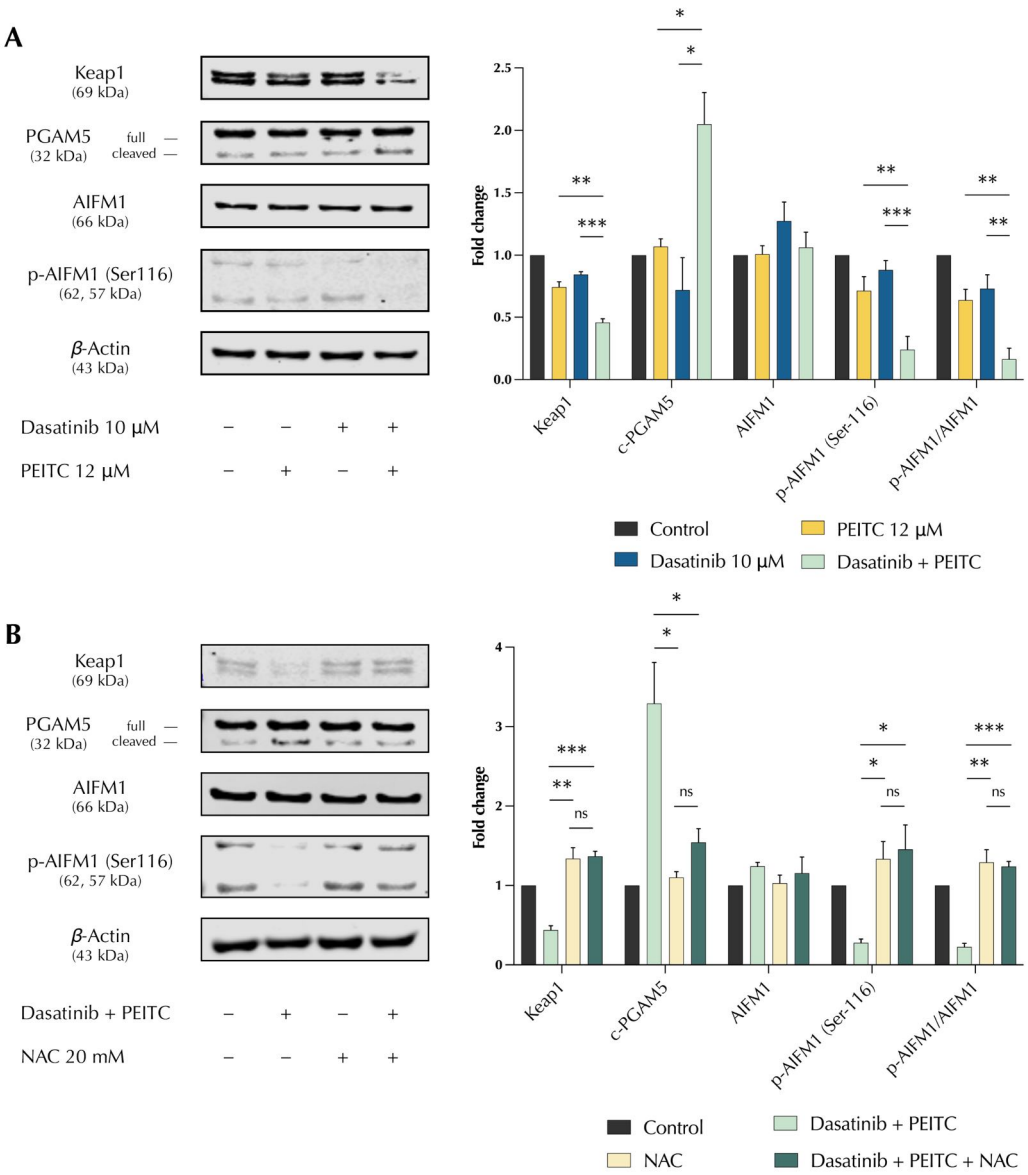

FIGURE 4.15 | PDc induces oxeiptosis through the Keap1-PGAM5-AIFM1 axis.
HepG2 cells were treated for 24 h, and the proteins extracted were analysed with Western blot. **(A)** Effect of PDc on the expression of oxeiptosis markers (mean ± SEM, Keap1, and PGAM5, n=3 AIFM1 and p-AIFM n=6) The degrees of significance were calculated with one-way ANOVA test with Tukey's multiple comparisons test and are indicated as * $p < 0.05$, ** $p < 0.01$, *** $p < 0.001$. **(B)** Pre-treatment with NAC 20 mM abolishes PDc induction of oxeiptosis (mean ± SEM, n=3). (Full blots are presented in FIGURE A1-15). The degrees of significance were calculated with one-way ANOVA test with Tukey's multiple comparisons test and are indicated as * $p < 0.05$, ** $p < 0.01$, ns = not significant.

4.3 Discussion

As widely described in the literature, ITCs can enhance the anticancer activity of other drugs, targeting different pathways [218, 227, 232]. On the other hand, dasatinib showed anticancer activity towards several HCC cells but did not appear to produce effective results in the clinical setting. This chapter investigated the effect of the addition of PEITC to dasatinib treatment on HCC cells HepG2. The addition of PEITC at a concentration equal to its IC_{20} led to increased toxicity with a synergistic loss of cell viability, as shown by the Chow-Talalay method. Moreover, PDc reduced the ability of HepG2 to grow within a 3D structure, reducing the volume of the spheroid, which is a model that better resembles the spatial organisation of tumour masses. Numerous cell interactions happen in this context, leading to cell signalling and deposition of the ECM. Different gradients in the spheroid can lead to oxidative stress that causes cell death at the core of the spheroid [243]. Indeed, PDc increased ROS production, leading to an imbalance of the cellular redox state.

The results underlined that ROS production plays a fundamental role in the PDc increased anticancer activity. It is known that ITCs can inhibit both phase I and II enzymes, and PEITC is known to induce ROS production through the depletion of GSH and inhibition of GPX [241]. On the other hand, dasatinib may have a potential role in combination with other drugs that relies on oxidative stress as an anticancer mechanism [242]. *In vitro* data showed that dasatinib is metabolised by CYP3A4 [244]. However, in Li *et al*. work dasatinib was shown to inactivate CYP3A4 through an oxidative mechanism, and that dasatinib metabolites react with GSH [245]. Interestingly, it has been reported that also PEITC can alter the pharmacokinetics of different drugs and in particular, can inhibit CYP3A4 activity [246]. Therefore, the combination of the two molecules may have a synergistic effect that involves CYP3A4, leading to an increased oxidative imbalance. In the present work, PDc-induced an increase of GSSG/GSH ratio in the first 6 hours of treatment, representing the crucial event that explains the PDc's improved ability to perturb the cellular redox status through increased production of ROS. The involvement of oxidative stress consequential of PDc synergistic activity was confirmed with the antioxidant NAC pre-treatment, which abolished PDc cytotoxic effect in a concentration-dependent manner.

The generated imbalance of the redox state can lead to different mechanisms, including DNA damage and cell cycle arrest. The increased ROS production can induce double-

strand breaks, leading to chromosomal rearrangements and impaired DNA repair [247]. The triggering of DNA damage response can activate cell cycle checkpoints to allow time for DNA repair. Once the damage is fixed, the cell can progress through the cell cycle and continue to divide and proliferate. In the present work, DNA damage analysis indicated that PDc induces DNA chromatin condensation and the formation of apoptotic bodies. The DNA laddering assay needs improvement as the gel did not properly resolved. The use of a positive control, such as staurosporine, may also improve the assay reliability to confirm the results and clarify the presence of DNA fragmentation in the control. Western blot analysis confirmed the activation of Chk2 and p53. Phosphorylation of Chk2 is associated with a cellular response to DNA damage [248]. Indeed, Chk2 has a role as a transducer and tumour suppressor in the ATM-Chk2-p53 pathway, where ATM phosphorylate both p53 Ser-15 and Chk2 Thr-68 to play a role in cell cycle arrest and apoptosis [116]. The pre-treatment with the antioxidant NAC showed only partial protection of PDc-induced DNA damage as the activation of Chk2 and p53 was reduced but not completely abolished. Therefore, the PDc effect on DNA damage is not entirely relatable to the induction of oxidative stress. Indeed, PEITC induced DNA damage in a ROS-independent way [88] and through the direct inhibition DNA repair through the control of HDAC expression [45]. On the other hand, dasatinib showed the ability to direct binding to DNA molecules [249] and to induce DNA damage through the c-Raf pathway [231].

Another essential factor in DNA damage response is PARP1, a member of the poly(ADP-ribose) polymerases protein family [250]. PARP1 is activated by proteolytic cleavage to induce DNA repair and it is highly expressed in liver cancer tissue. PEITC has been previously correlated with PARP degradation due to DNA damage induced by p53 activation [251]. In the present work, the Western blot analysis showed that both PEITC and dasatinib reduced the expression of PARP1, while PDc abolished it entirely. Conversely, the pre-treatment with NAC did not rescue from PDc-induced PARP1 inhibition, confirming the independence of DNA damage from oxidative stress induced by PDc. Recently, the combination of Src and PARP1 inhibition has been identified as a novel synthetic lethal strategy for HCC growth inhibition [252]. Indeed, the Src inhibitor dasatinib combined with the PARP1 inhibitor olaparib showed a potent synergistic effect in inhibiting HCC *in vitro* and *in vivo* with phosphorylation of Chk2 and inactivation of STAT3 pathway [252]. Ergo, the PDc-induced DNA damage could also be related to the co-inhibition of PARP1.

DNA damage and cell cycle arrest are two strictly related processes. Cancerous cells present an imbalanced expression of the proteins involved in the regulation of the cell cycle. Consequently, cancerous cells can proliferate with uncontrolled cell growth, allowing tumour expansion. Cancer therapy targets the dysregulated protein to induce cell cycle arrest and death [253]. Both PEITC and dasatinib were previously shown to influence different cell cycle regulators to induce cell cycle arrest. A drug combination containing dasatinib has been reported to induce cell cycle arrest at the G1 phase in lung cancer cells [254] laryngeal squamous cell carcinoma [255]. It has been demonstrated that PEITC is able to target several cell cycle regulators inducing cell cycle arrest in different cancerous cell types, also through ROS generation [256, 257].

In this work, cell cycle analysis showed that PDc induces cell cycle arrest at the G2/M phase in a ROS-dependent manner, as pre-treatment with NAC abolished the accumulation of cells in the G2/M phase and reduction of cells in the G1 phase. PEITC has already been associated with G2/M phase cell cycle arrest. In particular, PEITC induces cell cycle arrest with covalent binding [258], and degradation through ROS production [220] of α- and β- tubulins, which are the fundamental bricks of microtubules. Microtubules play a crucial role in different cellular processes, particularly cell division, with the formation of the mitotic spindle for chromosome segregation. Therefore, the effect of PDc on α-tubulin was investigated using immunofluorescence to examine the expression and organisation of α-tubulin. Surprisingly, α-tubulin expression did not appear to be affected by PDc treatment or PEITC alone, but a higher number of cells possessing irregular mitotic spindle fibres occurred in PDc-treated cells. CDK1 usually regulates cell cycle arrest at the G2/M phase; specifically, the complex CDK1/Cyclin B1 has a role in the progression towards mitosis [259]. PEITC has already been associated with the regulation of CDK1 and Cyclin B1 expression through ROS induction [91]. Here, Western blot analysis highlighted an increased activation of CDK1 (Thr-161) and accumulation of Cyclin B1. The over-expression of CDK1 and Cyclin B1 has been reported as responsible for the formation of a premature CDK1/Cyclin B1 complex [260, 261]. The formed complex is associated with mitotic catastrophe, leading to cell death due to aberrant mitosis [260]. Interestingly, mitotic catastrophe is generally induced by anti-microtubular drugs [260] and partially by Chk2 activation after DNA damage [262]. Considering that the cell cycle arrest induced by PDc is reversed by the NAC pre-treatment, this indicates that oxidative stress is the main mechanism of PDc-induced cell cycle arrest (**FIGURE 4.16**). To further confirm the mitotic catastrophe event,

Western blot analysis and immunostaining of α-tubulin could be repeated using Nocodazole as positive control. Nocodazole is a compound that inhibit the polymerisation of microtubules, arresting the cell cycle at the mitosis phase [263].

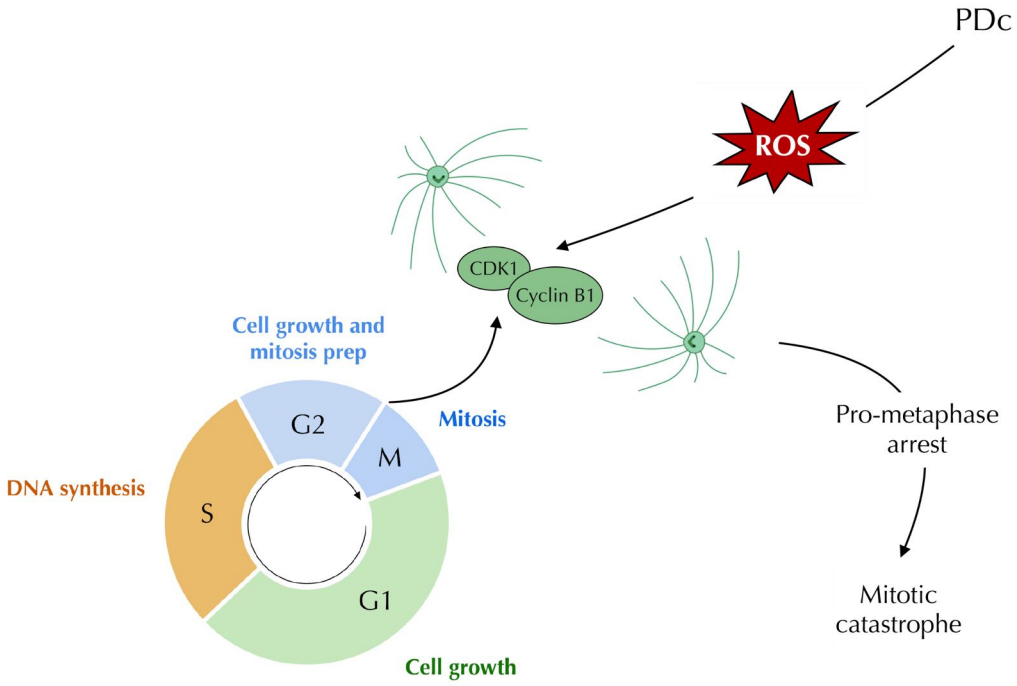

FIGURE 4.16 | Diagram of PDc induction of G2/M phase arrest and mitotic catastrophe. PDc induce increased ROS production that lead to formation of a premature CDK1/Cyclin B1 complex that induces mitotic catastrophe with a pro-metaphase arrest.

Mitotic catastrophe is usually followed by programmed cell death. Once the cell leave the cell cycle cycle and the DNA damage cannot be repaired its destiny leans towards the programmed cell death. Programmed cell death allow the organism to control the cells number, avoiding the duplication of cells that contain errors that can threat the cell homeostasis [127]. The most studied form of programmed cell death is apoptosis, characterised by different pathways triggered by different factors that finally lead the cell to auto-destruction [264]. Within the tumour's uncontrolled growth, cancerous cells tend to inhibit the process of apoptosis, increasing the expression of apoptotic suppressors and reducing the expression of pro-apoptotic factors. Therefore, targeting apoptosis is an important anticancer strategy. In the present work, PEITC and dasatinib have been demonstrated to induce apoptosis in cancerous cells; hence, the effect of PDc on apoptosis induction has been investigated. PDc induces apoptosis to a greater extent compared to the single drug treatments, as showed by the staining of phosphatidylserine using Annexin

V. Surprisingly, the analysis of the protein expression of the most significant factors involved in apoptosis was inconclusive. Neither changes in the accumulation of most important apoptosis indicators such as cytochrome c and caspases, nor reduction in expression of apoptosis inhibitors have been observed. For a long time, it was thought that the exposure of phosphatidylserine on the outer cell membrane layer, the so-called "eat me" signal, was a specific way for apoptotic cells to signal the need for phagocytosis [265]. Recently, the phosphatidylserine dogma has been challenged with the association of outer membrane phosphatidylserine exposure in different types of cell death other than apoptosis [265].

Considering the role of ROS production in PDc anticancer activity, particular attention was drawn to a type of cell death triggered by a high production of ROS. Oxeiptosis is a novel form of apoptosis-like programmed cell death identified in 2018 by Holze *et al*. [266]. The activation of this mechanism of cell death relies on the Nrf2-Keap1-PGAM5 complex that works as an oxidative stress sensor [126]. At a low levels of ROS, only Nrf2 is released, which leads to the expression of antioxidant genes to counterbalance oxidative stress. At higher levels of ROS, the action of the expressed antioxidant genes is not enough to contrast the oxidative stress; thus, Keap1 is released to activate the oxeiptosis [125]. PGAM5 is translocated into the mitochondria where de-phosphorylates AIFM1, the main effector of ROS-induced cell death [266].

PDc was associated with a marked de-phosphorylation of AIFM1, but Keap1 and PGAM5 expression was not as expected. First, Keap1 accumulation decreased after PDc treatment, while it was reported as up-regulated in conditions of oxidative stress induced in melanocytes [267]. This difference could be explained by the results of previous work that studied the role of the Keap1-PGAM5 complex in the context of mitophagy [268]. The inactivation of Keap1 by menadione treatment inhibited PGAM5 degradation, allowing its accumulation. Furthermore, recent work that investigated the role of oxeiptosis in colon cancer observed an increase of Keap1 expression only in the first 2 hours of the treatment with a drastic reduction after 8 hours [269]. Second, PGAM5 was previously described as up-regulated in oxidative stress-induced oxeiptosis [266, 267]. PDc did not change the accumulation of total PGAM5 but increased its cleavage. It has been shown that PGAM5 cleavage increases in conditions of stress and that it plays a role in mitochondria dynamics, triggering different types of programmed cell death [270]. The localisation of PGAM5 is controversial as it can be located on the outer mitochondrial membrane, considering its

interactions with factors found in the cytosol. Nonetheless, increased evidence shows that PGAM5 may be located in the internal mitochondrial membrane [270, 271]. It has been proposed that PGAM5 can shuttle between outer and inner membranes, according to the cell state and the mitochondrial membrane potential [270], and that the cleavage of PGAM5 can happen only when it is located in the inner membrane [272]. The central hypothesis is that PDc induces high levels of ROS that lead to the PGAM5 release by Keap1. After translocation to the inner mitochondrial membrane, where it is proteolytically cleaved, PGAM5 de-phosphorylate AIFM1 to trigger oxeiptosis (FIGURE 4.17).

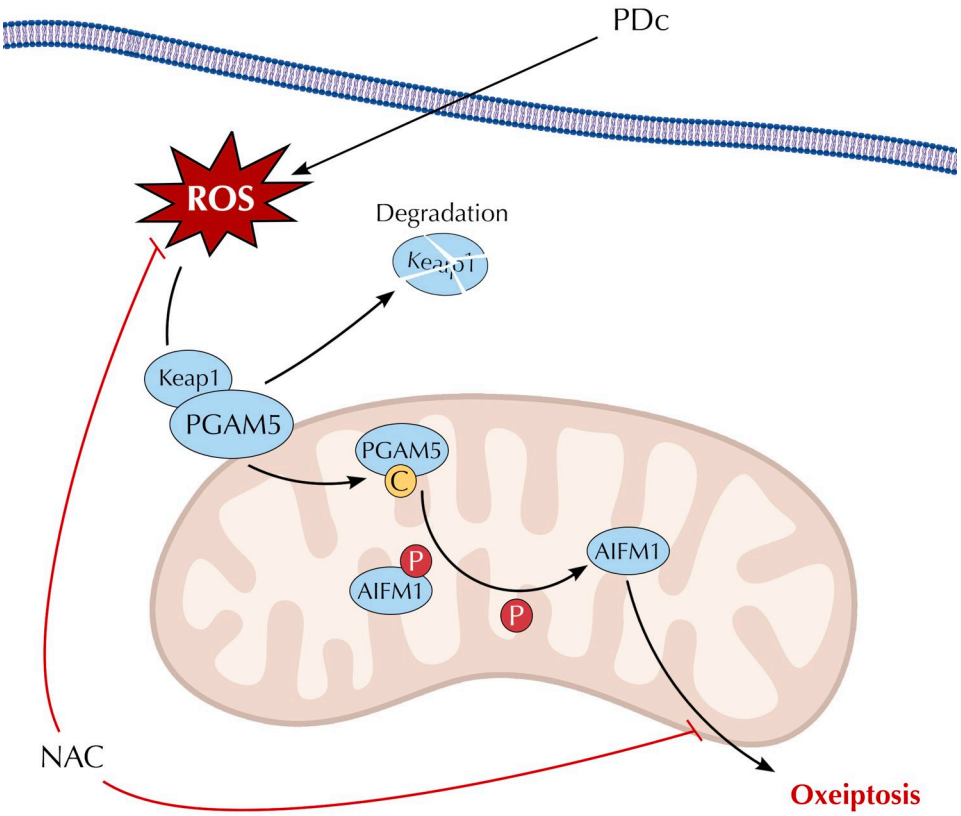

FIGURE 4.17 | Diagram of PDc induction of oxeiptosis.
PDc induction of ROS production lead to the dissociation of Keap1/PGAM5 complex with consequent Keap1 degradation and PGAM5 translocation to internal mitochondrial membrane where it is cleaved. On the internal mitochondrial membrane PGAM5 is cleaved (Yellow circle) determinint AIFM1 de-phosphorylation, which activates the oxeiptosis programmed cell death.

Chapter 5
PEITC and Dasatinib combination effect on metastatic potential

5.1 Introduction

As discussed before, tumours metastatic capabilities are acquired through hijacking the epithelial-mesenchymal transition (EMT), a developmental program employed by normal cells during embryogenesis [273]. In contrast with canonical EMT, carcinoma cells acquire increased motility and invasiveness and may reach new tissues in a collective migration, maintaining cell-cell interactions [129]. Indeed, carcinoma cells with activated EMT acquire new mesenchymal traits, retaining epithelial traits. It has been defined "partial EMT" state, which allows cancerous cells to progress and metastasise [274], while a full mesenchymal state would reduce the tumour-initiating ability [129]. It is consequently vital to target both traits of cancerous cells, reducing cell-cell adhesion and migratory and invasive capabilities.

A protein that plays a pivotal role in several cellular processes (i.e. cell attachment, migration, invasion, and proliferation) is FAK [275]. FAK has been associated with an uncontrolled proliferation and migration of cancerous cells, with activation of several receptor tyrosine kinases (RTK) involved in tumour development and progression. FAK is a potential target in cancer therapy as it was over-expressed in different types of tumours [275]. Interestingly, the dasatinib effect on HCC *in vitro* and *in vivo* was found to be limited by the activation of FAK and enhanced by association with FAK inhibitors [276]. The association of dasatinib with rosuvastatin showed a synergistic effect in HCC *in vivo* with inhibition of the Src/FAK pathway as the crucial pathway for the enhanced anticancer activity associated with decreased activation of other signalling pathways (i.e. Ras-Rac, STAT3, caspase 3-dependent apoptosis, reduced levels of VEGF, MMP-9) [277]. This result is not entirely unexpected considering that one of the primary targets of dasatinib is the c-Src kinase, which is strictly related to FAK. The formation of the FAK and c-Src complex has several effects, starting with forming new focal adhesion complexes and activating downstream signalling pathways that promote cell survival, proliferation and migration [278, 279]. As a result, the association of dasatinib with FAK inhibitors is a promising strategy for tackling HCC.

Isothiocyanates are known to reduce the metastatic potential of various cancer cell lines. PEITC-induced FAK inhibition decreased the migration and invasion of human gastric cancer cells through suppression of MAPK pathway [280] and in glioma cells through JNK signalling [144]. Furthermore, PEITC resulted in the more potent isothiocyanate to inhibit the metastatic potential of several cancer cell lines and adenocarcinoma *in vivo* with a marked reduction of FAK activation [145]. The effect of dasatinib and PEITC (PDc) on the metastatic potential of HepG2 cells has been explored by looking at the effect on cell migration, invasion, adhesion, and colony formation and in *in vivo* with the HepG2 xenograft model of the chorioallantoic membrane (CAM) assay.

Chapter 5 objectives

- Evaluate PDc effect on migration, invasion, adhesion, and colony formation
- Evaluate PDc effect on tumour metastatic potential *in vivo*
- Elucidate PDc mechanism of action

5.2 Results

5.2.1 Effect of PDc on HepG2 cell migration and invasion

The effect of PDc on inhibition of cancer cell migration was investigated first with a scratch wound healing assay. Fully confluent HepG2 cells were scratched with a p200 tip and then treated with PDc and single drugs for 72 hours. Pictures were taken at 0, 24, 48, and 72 hours and the wound area of the different time points were compared with the initial wound area to determine a migration rate. The addition of PEITC 1.5 and 3 μM did not improve the ability of dasatinib to reduce the migration of HepG2, while PEITC 6 μM and dasatinib induced a reduction only at 24 hours. On the other hand, PEITC 12 μM consistently reduced HepG2 migration at all time points and dasatinib concentrations (**FIGURE 5.1A-B**).

A Boyden chamber assay was employed to confirm the effect of PDc on the reduction of HepG2 migration and test its effect on HepG2 invasion. The Boyden chamber is a plastic insert with a lower porous membrane, which is added on top of a cell culture well. Therefore, cells can be seeded in the top chamber while the bottom chamber is filled with a chemoattractant to induce cell migration. In this way, the effect of drugs on cell migration can be tested. The addition of Matrigel® on the top chamber allows to study the cells'

invasive capability. The results from the Boyden chamber assay confirmed the capability of PDc to reduce the number of migrated HepG2 cells if compared with the single treatments and reduce the number of invasive cells to a minor extent (FIGURE 5.2).

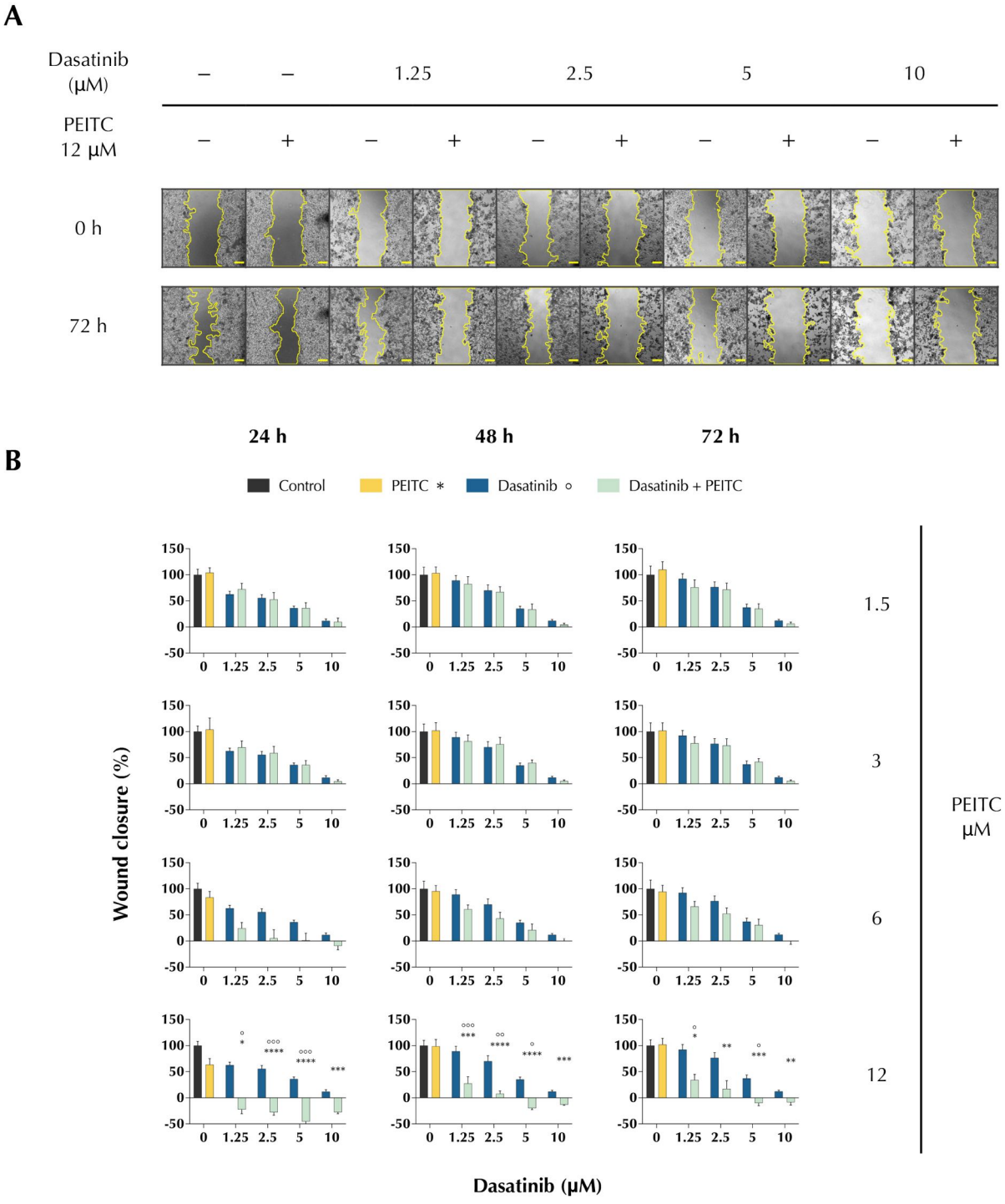

FIGURE 5.1 | Effect of PDc on cell migration, scratch wound healing assay.
HepG2 cells were treated with increasing concentrations (1.25 - 10 μM) of dasatinib with or without PEITC 1.5, 3, 6, 12 μM. **(A)** Representative images at 0 h and 72 h of 12 μM PEITC combinations. **(B)** The quantitative data presented were normalised to control migration rate

(mean ± SEM, n=3). Negative values indicate shrinking of cells that made the wound larger. The values become positive once the cells react to the stress and start to migrate. The degrees of significance were calculated with one-way ANOVA test with Tukey's multiple comparisons test and are indicated as °/* $p < 0.05$, °°/** $p < 0.01$, °°°/*** $p < 0.001$, °°°°/**** $p < 0.0001$. (* combination vs PEITC, ° combination vs dasatinib).

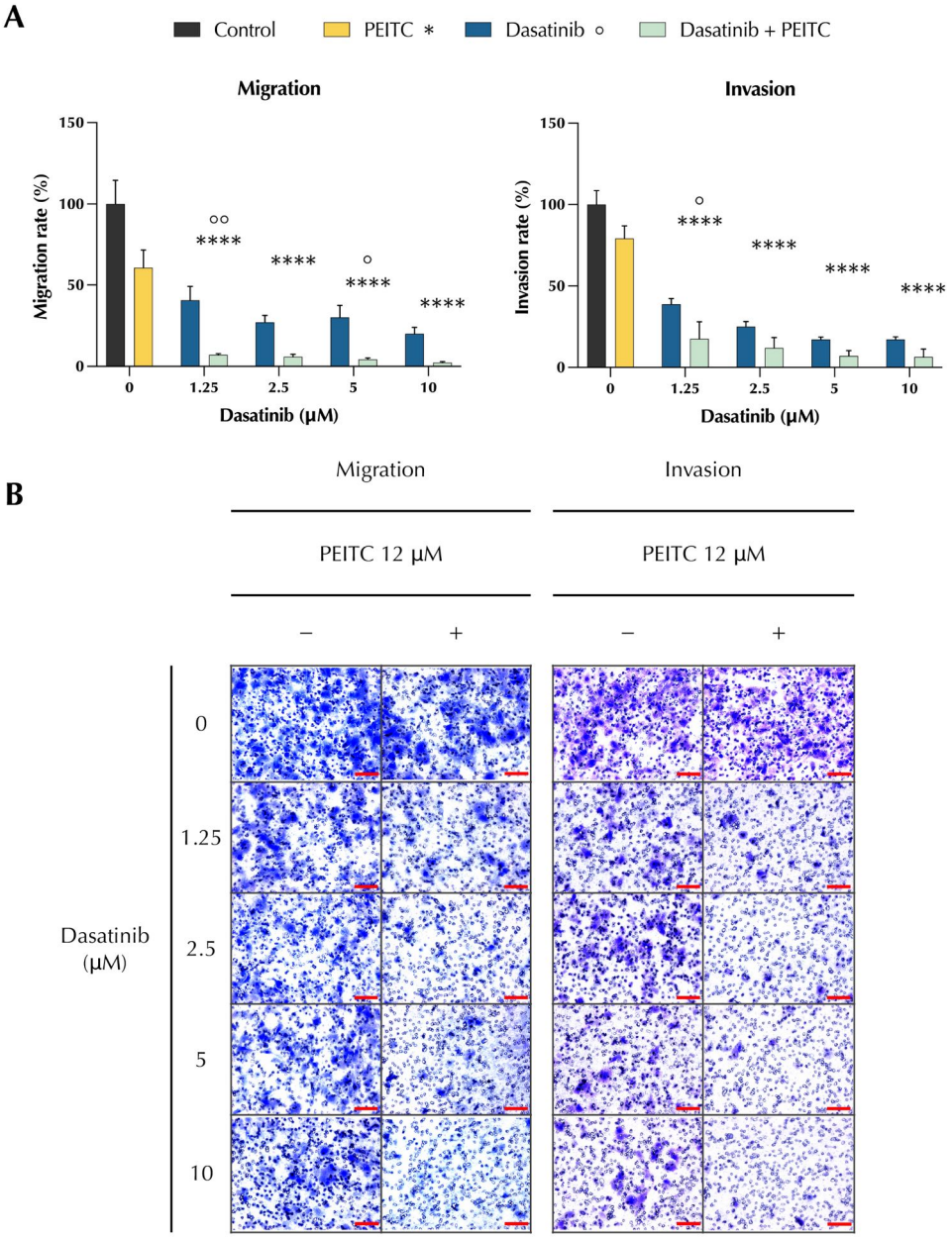

FIGURE 5.2 | Effect of PDc on cell migration and invasion, Boyden chamber assay.
HepG2 cells were treated with increasing concentrations (1.25 - 10 μM) of dasatinib with or without PEITC 12 μM and seeded on the top chamber in FBS-free DMEM. The bottom chamber was filled with 10% FBS DMEM as a chemoattractant. The number of cells migrated/invaded and attached to the bottom side of the membrane was counted after 48 h and normalised to the control. In the invasion assay, the top chamber was coated with 100 μg/mL Matrigel and the

bottom chamber was filled with 30% FBS DMEM. **(a)** Quantitative data normalised to control migration/invasion rate (mean ± SEM, n=3). The degrees of significance were calculated with one-way ANOVA test with Tukey's multiple comparisons test and are indicated as °/* $p < 0.05$, ° °/** $p < 0.01$, °°°/*** $p < 0.001$, °°°°/**** $p < 0.0001$. (* combination vs PEITC, ° combination vs dasatinib). **(b)** Representative images from 5 pictures/experiment (20x, scale bar 100 µm).

5.2.2 Effect of PDc on HepG2 cell adhesion

Cancerous cells often enhance adhesion capability to facilitate migration and adhesion to a new site. The ability of PDc to reduce cell adhesion was investigated using a Matrigel® plate-based assay. HepG2 cells were seeded in a Matrigel® coated plate to facilitate adhesion and treated with PDc and single drugs (PEITC 1.5, 3, 6, 12 µM, dasatinib 1.25, 2,5, 5, 10 µM) and the percentage of adhered cells was evaluated after 3 hours with a crystal violet staining. PDc showed the ability to inhibit the adhesion of HepG2 cells starting from at PEITC 3 µM, with a potent inhibition at 6-12 µM (**FIGURE 5.3A-B**).

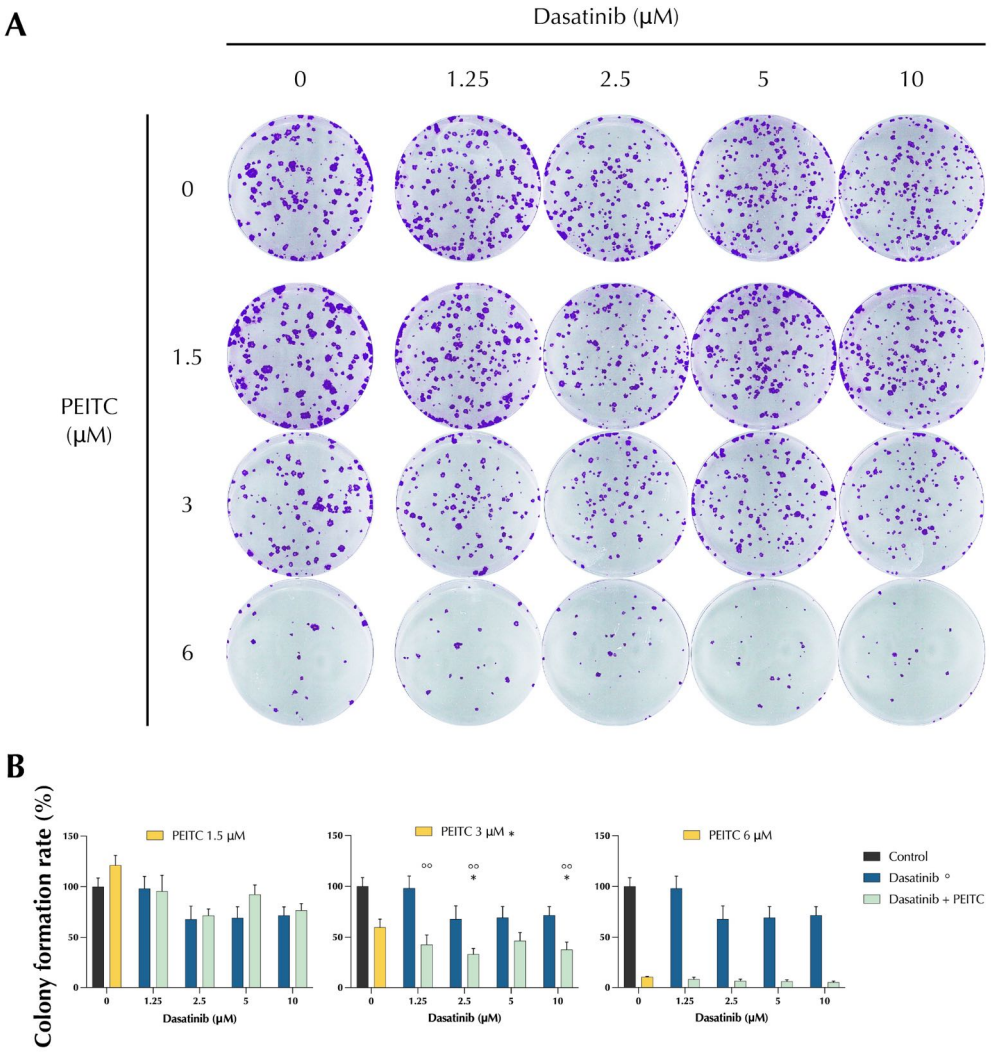

FIGURE 5.3 | Effect of PDc on cell adhesion.

HepG2 cells were seeded on a 200 µg/mL Matrigel-coated plate and treated with increasing concentrations (1.25 - 10 µM) of dasatinib with or without PEITC 1.5, 3, 6, and 12 µM. The adhesion was evaluated after 3 h. **(a)** Cells were stained with crystal violet and imaged with an inverted microscope. Representative images from 3 independent experiments (20x, scale bar 100 µm). **(b)** Quantitative data normalised to control (mean ± SEM, n=3). The degrees of significance were calculated with one-way ANOVA test with Tukey's multiple comparisons test and are indicated as °/* $p < 0.05$, °°/** $p < 0.01$, °°°/*** $p < 0.001$, °°°°/**** $p < 0.0001$. (* combination vs PEITC, ° combination vs dasatinib).

5.2.3 PDc inhibits HepG2 cells clonogenic capacity

A colony formation assay was employed to test the capacity of PDc to inhibit the clonogenic potential of cancer cells. HepG2 cells were treated with PDc with different concentrations of PEITC as the selected concentration of 12 µM and 6 µM were too toxic

for such a low seeding density (FIGURE 5.4A). The combination of PEITC 3 µM to dasatinib resulted in the most efficient in reducing the number of colonies formed by HepG2 single cells after a culture of 18 days. In particular, PDc with dasatinib 2.5 and 10 µM showed a statistically significant reduction of the HepG2 clonogenic potential (FIGURE 5.4B).

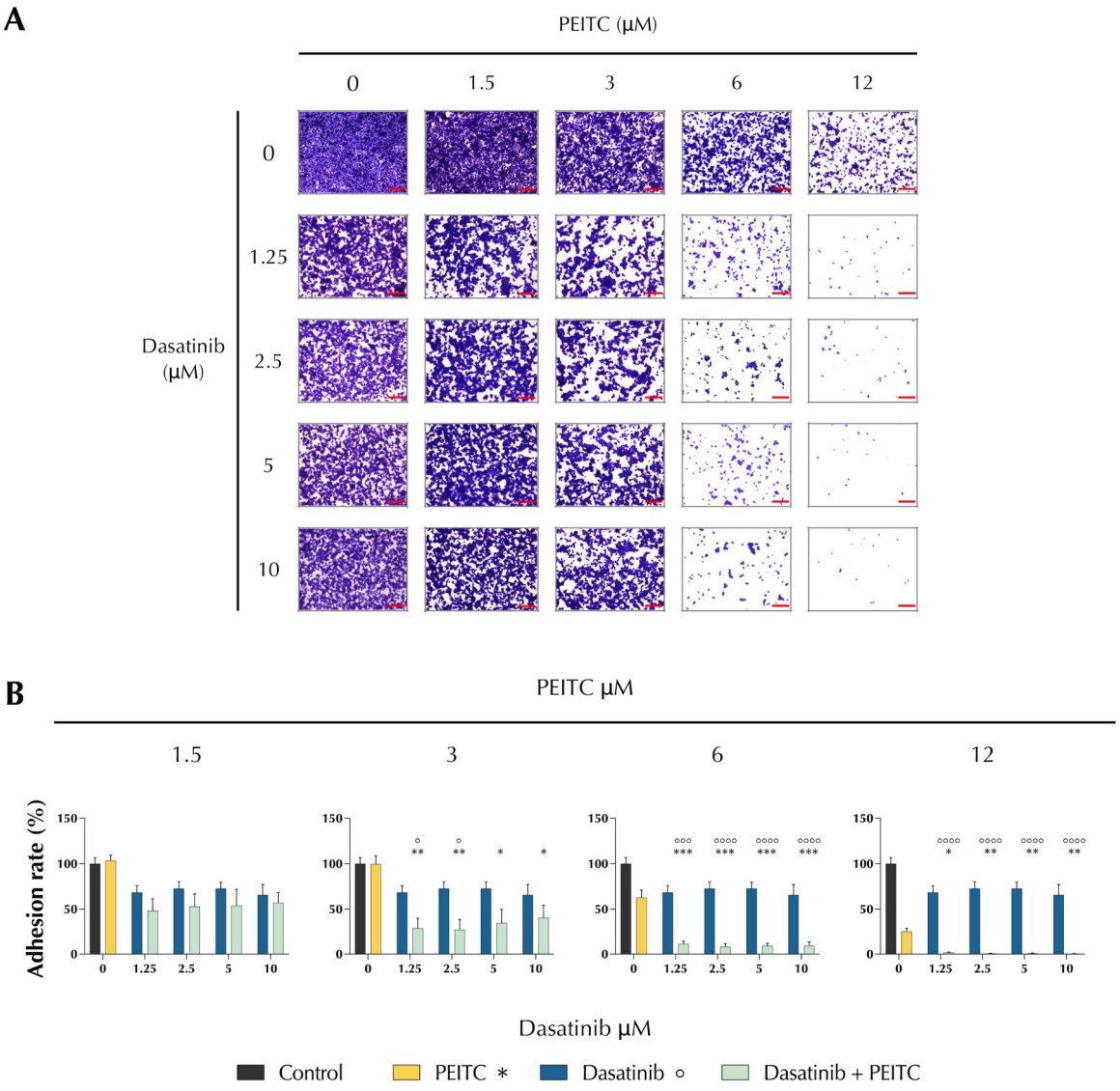

FIGURE 5.4 | Effect of PDc on clonogenic capability.

HepG2 cells were treated with increasing concentrations (1.25 - 10 µM) of dasatinib with or without PEITC 6, 3, 1.5 µM for 24 h. The medium was changed after 24 h of treatment and then every 5 days until day 18. **(a)** Representative images from 3 of 6-well plates scanned at 600 dpi. **(b)** The quantitative data presented were normalised to control colony formation rate (mean ± SEM, n=3). The degrees of significance were calculated with one-way ANOVA test with Tukey's multiple comparisons test and are indicated as °/* $p < 0.05$, °°/** $p < 0.01$ (* PEITC vs combination, ° dasatinib vs combination).

5.2.4 Effect of PDc on HepG2 morphology

Actin cytoskeleton is crucially involved in adhesion to the extracellular environment as it is physically linked to focal adhesion complexes. Moreover, adhesion serves as a starting point for different types of signalling, activating downstream pathways [281]. The effect of PDc on cytoskeleton organisation shortly after the start of the treatment (1 h) was evaluated using fluorescence microscopy with a phalloidin staining that binds selectively to F-actin. The observation of cell morphology highlighted a significant change in the cytoskeletal organisation in PDc-treated cells. Cells usually form structures to interact with the extracellular environment called lamellipodia, spreading to maximise the adhesion to the plastic surface. After 1 hour of treatment, PDc-treated cells appeared to have shrunk with less spreading on the cell culture surface and a morphology significantly different from control and single treatment. A quantification by manual count underlined that PDc treatment increased the number of cells presenting filopodia, which differs from the lamellipodia observed in the control and single-drug treatment (**FIGURE 5.5**).

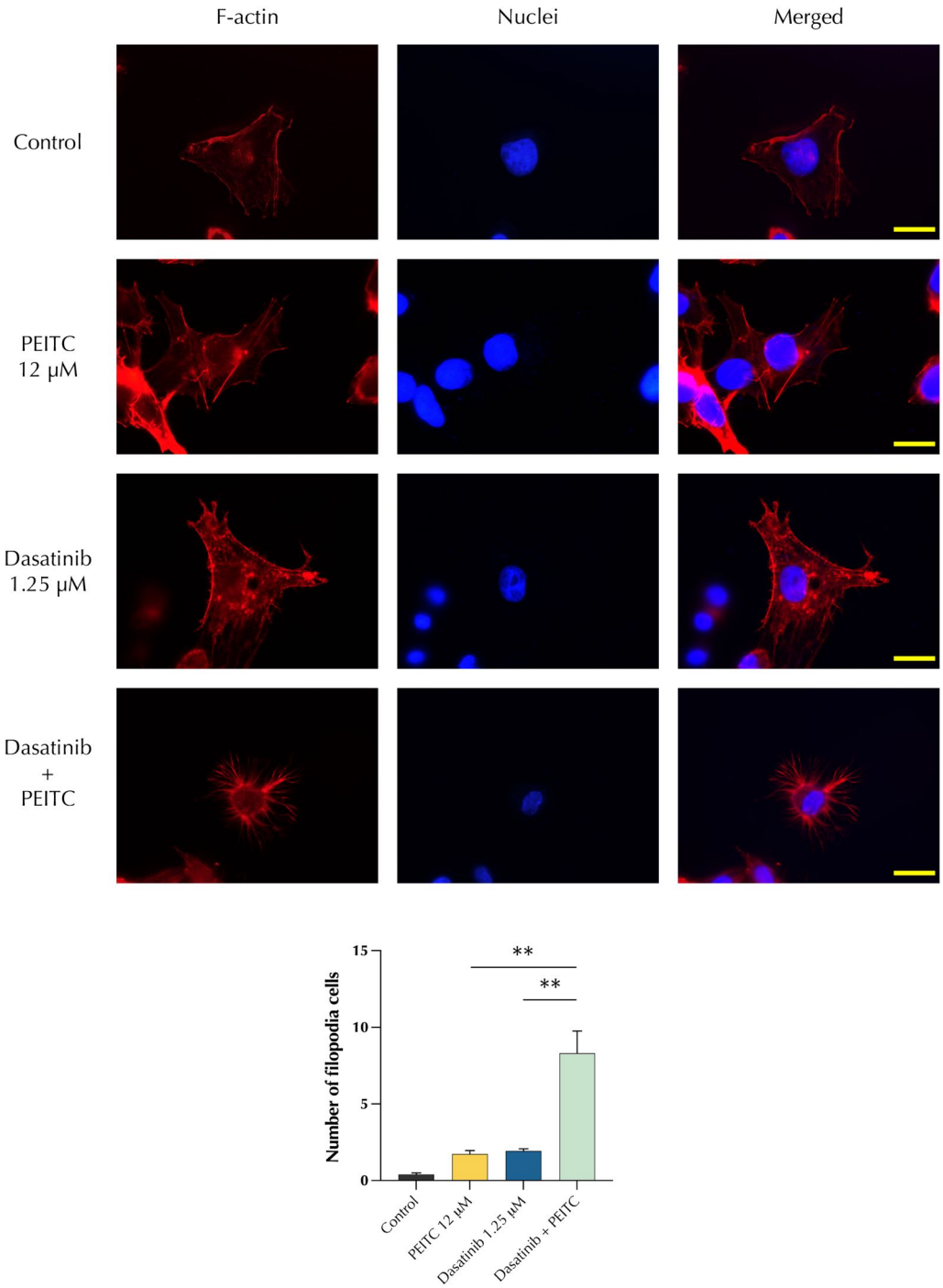

FIGURE 5.5 | Effect of PDc on HepG2 actin filaments after 1 h of treatment.

The combination treatment led to an increased number of cells that presented a shrunken morphology with filopodia-like cytoskeleton protrusion. Single drug treatments showed a morphology similar to the control (100x, scale bar 20 μm). Cells presenting altered morphology have been counted from 10 different random fields 100x (mean ± SEM, n=3). The degrees of significance were calculated with one-way ANOVA test with Tukey's multiple comparisons test and are indicated as ** $p < 0.01$.

5.2.5 PDc inhibits tumour cell motility through FAK/STAT3 pathways

Focal adhesions (FA) link the cytoskeleton with the ECM to migrate and receive external stimuli. Indeed, FA contains multiple components with structural and signalling proteins, such as FAK, which communicate with structural proteins such as cadherins. FAK is known to have a role in numerous cellular processes such as proliferation, survival and migration and invasion. Protein expression analysis using Western blot was investigated to evaluate the effect of PDc on proteins involved in the formation of adhesion complexes and downstream signalling. The results showed that PDc deactivates FAK and STAT3 pathways (FIGURE 5.6 TOP), and increases the expression of E-cadherin while reducing the expression of N-cadherin (FIGURE 5.6 BOTTOM).

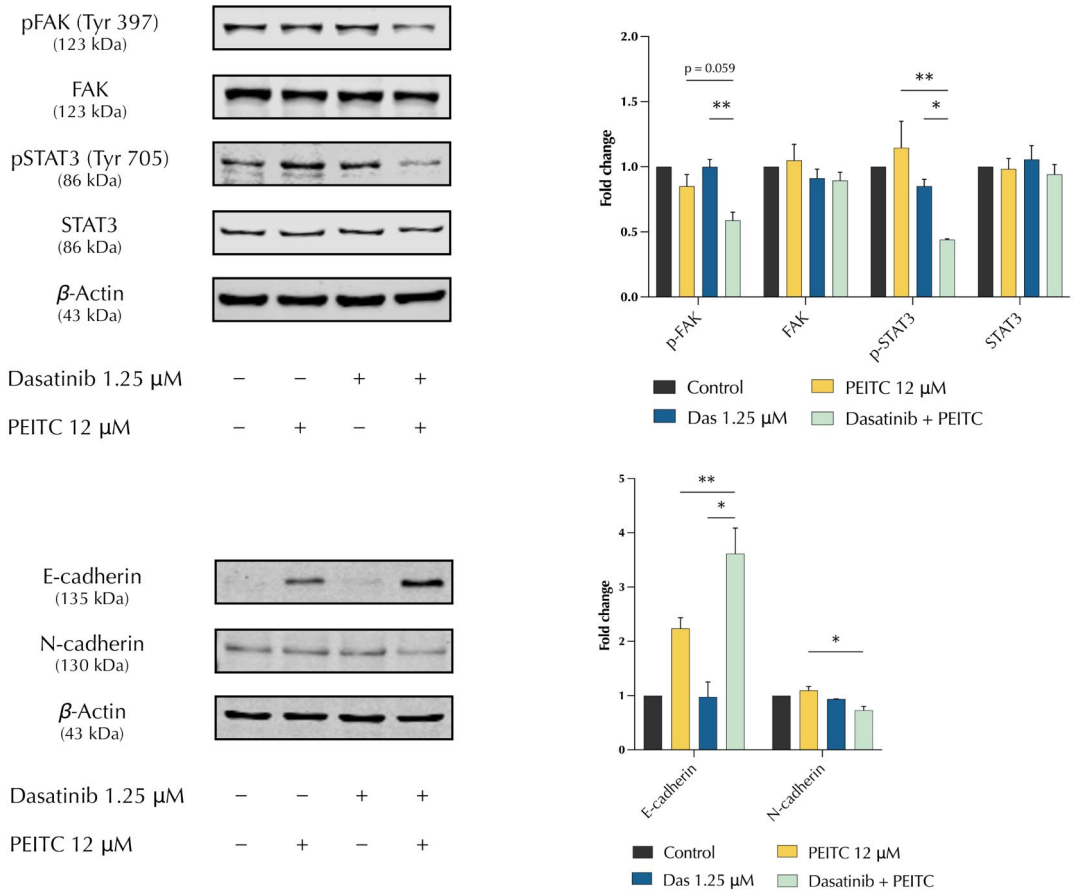

FIGURE 5.6 | PDc inhibiting FAK and STAT3 signalling.
HepG2 cells were treated for 24 h, and the proteins extracted were analysed with Western blot. Top, effect of PDc on the expression of FAK and STAT3. Bottom, effect of PDc on the expression of E-cadherin and N-cadherin. (Full blots are presented in FIGURE A16-19), the results presented are representative of independent protein extractions (mean ± SEM, n=3). The degrees of significance were calculated with one-way ANOVA test with Tukey's multiple comparisons test and are indicated as * $p < 0.05$, ** $p < 0.01$.

5.2.6 Effect of PDc on tumour invasion in CAM HepG2 xenograft model

The effect of PDc on the relationship between cancer cells and the extracellular environment was investigated using a chorioallantoic membrane assay (CAM) with a xenograft of HepG2 cells. A 3D culture of HepG2 was prepared with an ECM gel and the PDc or the single drugs and then implanted on top of the CAM. The results showed that PDc significantly reduced the growth of the tumour mass compared to control and single-drug treatments (**FIGURE 5.7 TOP**). Tumour sections stained with H&E showed a difference in tumour embedding into the CAM. It appeared that PDc-treated HepG2 xenografts were not integrated into the CAM as they could not invade the vascularised chick membrane and were therefore precluded from nutrients retrieval, explaining the reduced growth (**FIGURE 5.7 BOTTOM**).

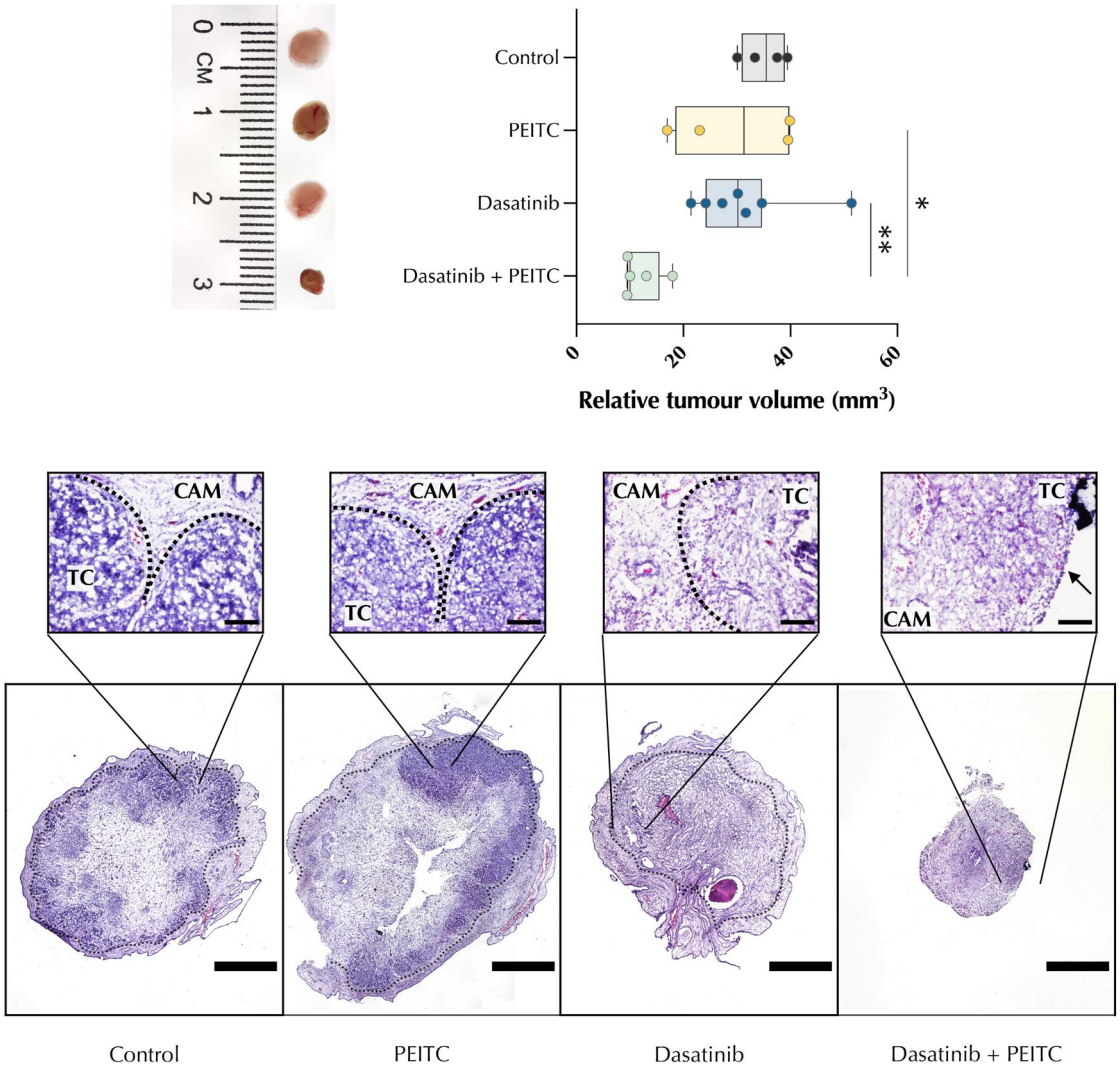

FIGURE 5.7 | Chorioallantoic membrane (CAM) xenograft assay.

Top left, representative images of the xenograft tumour samples captured with a stereomicroscope. Top right, relative quantitative data of the tumour volume after 7 days of incubation (Control n=4, PEITC 12 µM n=4, dasatinib 1.25 µM n=6, dasatinib + PEITC n=5) from 3 independent experiments. The degrees of significance were calculated with one-way ANOVA test with Tukey's multiple comparisons test and are indicated as * $p < 0.05$, ** $p < 0.01$. Bottom, H&E staining of xenograft tumour samples 10x images were stitched together to form a picture of the complete section (10x, scale bar 1 mm). Detailed pictures highlighted the difference in tumour embedding into the CAM. The dotted line indicates the boundaries between CAM and tumour cells (TC). PDc do not present a clear boundary between TC and CAM as the tumour cells were not embedded into the membrane (20x, scale bar 100 µm).

5.3 Discussion

The ability of PDc to inhibit the processes enabled by cancerous cells to spread and grow into other tissues has been explored in this chapter. Dasatinib could be better exploited in HCC when combined with other agents [282], with particular potential in sorafenib resistant cells [34]. Notably, the association with FAK inhibitors such as PEITC could be a solution to exploit its full potential. Indeed, PDc reduced the ability of HepG2 cells to migrate and invade an ECM and adhere to the extracellular environment. The fact that PDc can affect both adhesion and migration simultaneously could be crucial for its anticancer potential. Tumour cells need to form transient attachments to other cells and the ECM to metastasise, but at the same time, they need to detach to allow migration from the primary tumour [283]. PDc anticancer activity may be tailored to target the "partial EMT", characterised by adhesion capability, belonging to the epithelial traits that the cancer cells maintain to form cancerous clusters, and migration capability, which allow them to reach different regions of the body [274]. Finally, PDc influences the ability of HepG2 cells to form new colonies starting from small cell agglomerates. The growth of new colonies is the final phase in the tumour progression and represents the less understood due to the complex interactions of the highly diverse cell population that composes the metastatic microenvironment. All these effects elicited by PDc on HepG2 *in vitro* were congruent with the effect *in vivo* with the xenograft CAM assay. The results from the CAM assay experiments are supported by several works that observed the reduced tumour growth and invasion of the CAM, as presented in this study [284-286]. Future experiments using immunocytochemistry of cytoskeleton proteins in CAM sections could confirm the reduced tumour cell invasion capability.

As discussed above, the dasatinib effect can benefit from the combination with a FAK inhibitor, and the findings of this study are in agreement with this. As aforementioned, PEITC showed to suppress FAK signalling activation [145]. Therefore, it is probable that the anticancer activity of PDc pivots on the role of FAK and c-Src interaction, as protein expression analysis confirmed that PDc reduces the activation of the FAK Tyr-397 phosphorylation site. The cell interaction with the ECM triggers the auto-phosphorylation of Tyr-397, situated on the FAK N-terminus, allowing the binding of Src and leading to its enzymatical activation to propagate the downstream signal [275, 287]. FAK and c-Src have a fundamental role in the focal adhesion complex rich in actin-binding proteins responsible for stabilising actin filaments [287]. The actin filaments of the cytoskeleton have a primary

role in generating forces employed for cell migration and adhesion to the extracellular environment [142]. Actin filaments organise in large bundles to form lamellipodia, structures responsible for cell motility.

The effect of PDc on the actin filaments was investigated with immunofluorescence with phalloidin as an f-actin stain. The results highlighted that the drug combination leads HepG2 cells to form numerous filopodia compared to single-drug treatments. Filopodia are thin and extended structures which mainly possess a sensory function rather than a motility or adhesive role. Filopodia rapidly reorganise to form lamellipodia, allowing the cell to migrate. The induction of filopodia formation has been previously described in human breast cancer cells treated with polyphenol resveratrol [288]. The increased number of filopodia observed in response to resveratrol was accompanied by a reduction of cancer cell migration, a marked depression of phosphorylation of Tyr-397 FAK and reduced formation of focal adhesions. The study concluded that resveratrol inhibited cell migration by inhibiting focal adhesion formation. A previous study showed that FAK is differentially activated in adherent and non-adherent cells and FAK inactivation leads to loss of adhesion followed by apoptosis in colon cancer cells [281]. It can be hypothesised that PDc treatment inhibits the formation of focal adhesion complexes through FAK inhibition, leading to loss of adhesion and cell death. Further experiments of actin staining with induced over-expression of FAK could confirm that the effect of PDc treatment on filopodia formation is due to the altered formation of focal adhesion complexes.

FAK also play a role in JAK2/STAT3 pathway in promoting EMT [289]. Indeed, JAK and STAT3 bind to the FAK-Src complex to promote glioblastoma cell motility and cellular signalling [289], while the inhibition of STAT3 results in reduction of the invasive capabilities of astrocytoma cells [290]. Moreover, FAK regulates the expression of E-cadherin through the activation of Src and STAT3 signalling pathways, controlling the migration capability of melanoma cells [291]. PDc was consistently shown to inhibit STAT3 and increase the expression of E-cadherin while reducing N-cadherin. During EMT, a marked loss of E-cadherin and gain of N-cadherin expression is described as a “cadherin switch” linked with breast cancer progression [292]. This switch increases the cancerous cells' capability to migrate and invade, potentiating their metastatic potential. A lower expression of E-cadherin is often associated with more invasive tumours, and thus E-cadherin is generally considered a tumour suppressor. The results suggest that, at least in part, PDc reduces the metastatic potential of HepG2 cells by inhibiting EMT via STAT3 upregulation of E-

cadherin (FIGURE 5.8). Protein expression analysis of JAK could reveal the linkage between FAK and STAT3 signalling. Moreover, gene manipulation could help in confirming the correlation between FAK/STAT3 signalling and Cadherin expression. Silencing of E-cadherin expression followed by the experiment of adhesion, migration, and adhesion analysis could further demonstrate the linkage of Cadherin switch and reduced metastatic potential of HepG2 cells.

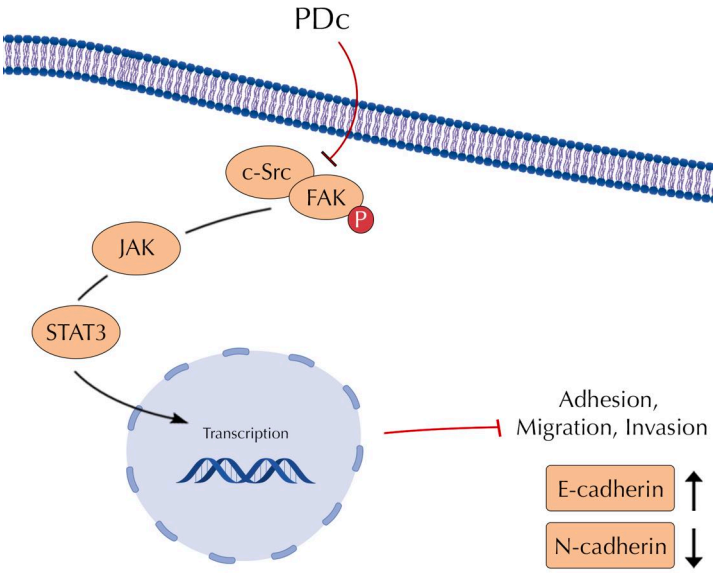

FIGURE 5.8 | Diagram of PDc effect on HepG2 metastatic potential
PDc modulates adhesion, migration, and invasion through the regulation of E-cadherin and N-cadherin expression. The hypothesis is that PDc target c-Src and FAK simultaneously reduce the downstreatm signalling of JAK2/STAT3 pathway.

Chapter 6

PEITC and Dasatinib combination effect on tumour-induced angiogenesis

6.1 Introduction

In normal conditions, the process of angiogenesis is related to embryogenesis before being turned on transiently during specific processes of the human body's life [2]. During tumour progression, an “angiogenic switch” allows the development of new vessels to sustain the growth of the tumour mass. Cancerous cells are able to control the expression of angiogenic factors to drive the sprouting of new vessels [2]. Angiogenesis also plays a crucial role in tumour metastasis as the cancerous cell ability expands to extravasate into the bloodstream to escape from the tumour's primary site and reach other body regions [293]. Moreover, once cancerous cells reach a different tissue in the body, they have to proliferate and re-induce angiogenesis to promote metastasis growth.

In early 2000, several anti-angiogenic drugs were developed to tackle different types of cancer, but their effect was only transitory, with the re-establishment of tumour growth after a period of apparent stop [294]. The transitory effect could be related to a tumour adaptation that finds alternative pathways to re-establish the induction of angiogenesis. The concept of metronomic chemotherapy has been introduced to contrast the drug resistance phenomenon [295]. Instead of high doses of chemotherapy with extended periods of pause between treatment cycles, low doses of chemotherapeutic agent with frequent administration could improve the outcomes and reduces events of acute toxicity [295]. Therefore, switching from a strategy of total eradication of the tumour to a maintenance therapy of chronic disease has been proposed, reducing toxicity and preventing drug resistance [296]. Furthermore, the association of low doses of chemotherapeutics and angiogenesis inhibitors could improve anticancer activity, making the metronomic therapy strategy more plausible [296].

Dasatinib has shown positive results *in vitro* associated with angiogenesis inhibitors in breast cancer and hepatocellular carcinoma [37, 297]. As discussed previously, ITCs can inhibit angiogenesis in several tumour models. PEITC showed to suppress the expression of VEGF through inhibition of HIF1α and VEGFR-2’s down-regulation [130, 298, 299]. Therefore, the effect of PDc on the ability of tumour cells to induce angiogenesis has been investigated in this chapter. As presented in **Figure 5.1**, the effect of PDc on tumour-induced

angiogenesis was tested by employing a dual cell line model. HepG2 cells were treated with PDc, and after 24 hours, the conditioned medium (CM) was concentrated with a 3 kDa protein concentrator to collect the HepG2-secreted factors and to discard drug metabolites and non-metabolised drugs. CM was used in different assays using HUVECs and the yolk sac membrane (YSM) assay to define the inhibitory effect of PDc on angiogenesis *in vitro* and *in vivo*.

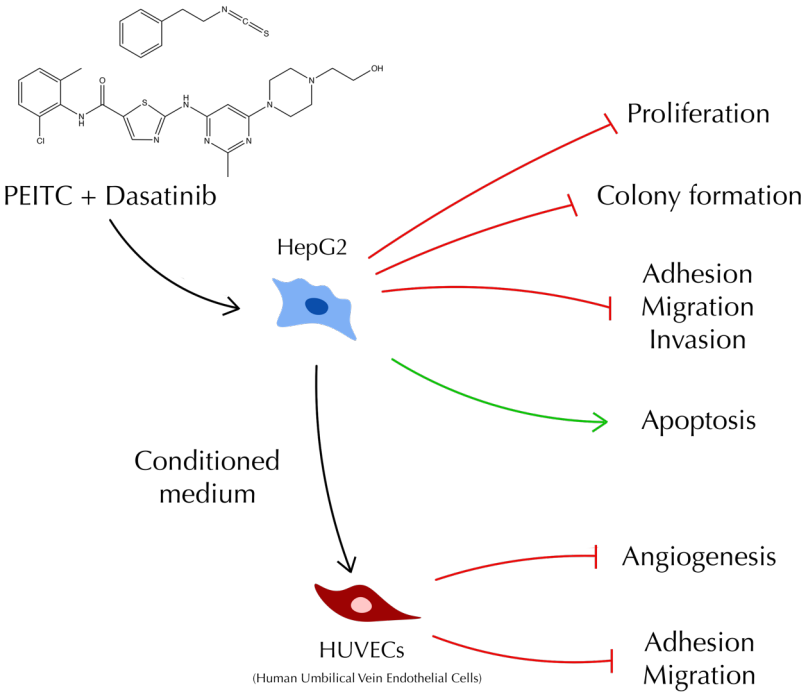

FIGURE 6.1 | Diagram of CM preparation from HepG2 PDc-treated cells.
HepG2 cells were treated with PDc and single drugs for 24 h. After that, CM was collected and concentrated with protein concentrators. CM was subsequently applied in different assays using endothelial human cells to test the effects of PDc on tumour-induced angiogenesis and the related processes.

Chapter 6 objectives

- Evaluate PDc effect on tumour induced angiogenesis *in vitro*
- Evaluate PDc effect on tumour induced angiogenesis *in vivo*
- Elucidate PDc mechanism of action

6.2 Results

6.2.1 HepG2 CM stimulates HUVECs adhesion and migration

CM concentrated from HepG2 cells was added to cultivated HUVECs to to assess whether the tumour cells were able to influence the behaviour of endothelial cells. Cell viability, adhesion, and migration were evaluated by MTT assay, ECM coated plate-based assay, and Boyden's chamber assay respectively. The results showed that HepG2 cells were able to slightly induce (16%) HUVECs proliferation even if not significantly (**FIGURE 6.2**). On the other hand, CM had a significant impact on the adhesion and migration of HUVECs cells, indicating that the concentration of conditioned medium can be employed to study the tumour influence on endothelial cells (**FIGURE 6.2**).

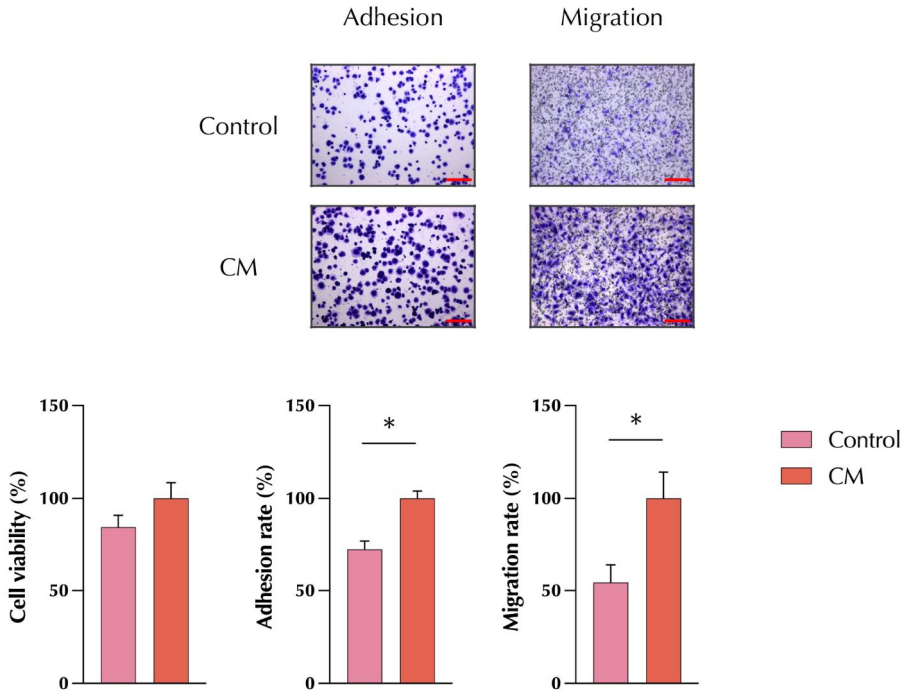

FIGURE 6.2 | Effect of HepG2 CM on HUVECs viability, adhesion and migration.
Control = HUVECs complete medium, CM = HUVECs complete medium with 0.1 mg/mL HepG2 CM. Top, representative images of HUVECs adhesion and migration assay (10x, scale bar 200 µm). Bottom, quantitative data of viability (mean ± SEM, n=3) adhesion (mean ± SEM, n=3) and migration (mean ± SEM, n=4). The degrees of significance were calculated with one-way ANOVA test with Tukey's multiple comparisons test and are indicated as * $p < 0.05$.

6.2.2 PDc CM affects HUVECs adhesion and migration, but not their viability

To assess if PDc can influence tumour-induced angiogenesis, HepG2 cells were treated with PDc and single drugs, and the medium was concentrated to obtain the CM. The MTT assay was initially employed to exclude that the observed effects were not a result of the drug toxicity itself but the effect of the cancer cells' secretome. Indeed, CM did not show a toxic effect on HUVECs, while the free drugs greatly affected HUVECs viability (FIGURE 6.3A-B). To avoid any possible toxic effects induced by the higher dasatinib concentrations, CM was produced using the lowest concentration of dasatinib (i.e. 1.25 µM) combined with PEITC 12 µM. As the highest CM concentration reduced the HUVECs viability compared to control, the lowest concentration of CM (0.1 mg/mL) was selected for the subsequent experiments.

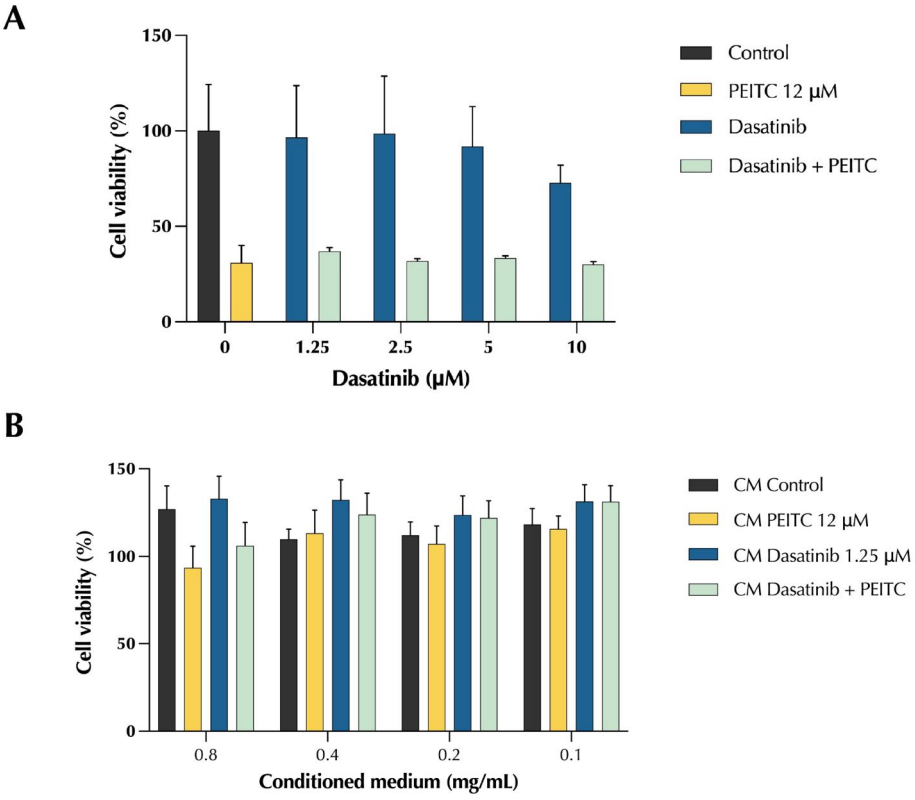

FIGURE 6.3 | Effect of drug direct treatment and CM treatment on HUVECs.
The validity of CM concentration as method to assess the effect of PDc on HepG2 secretome was tested comparing the effect of PDc and CM on HUVECs with MTT assay after 24 h treatment. **(A)** HUVECs viability assessed after PEITC and dasatinib treatment (mean ± SEM, n=2), and **(B)** condition media treatment (mean ± SEM, n=3).

The effect of CM was then tested on HUVECs adhesion and migration, and the results showed that PDc treatment reduced the tumour-induced effect on the ability of the

endothelial cells to adhere and migrate (FIGURE 6.4). Indeed, just 24.8 ± 3.56% of CM PDc treated cells adhered to the plate, while just 39.9 ± 6.18% migrate within the Boyden chamber if compared to control.

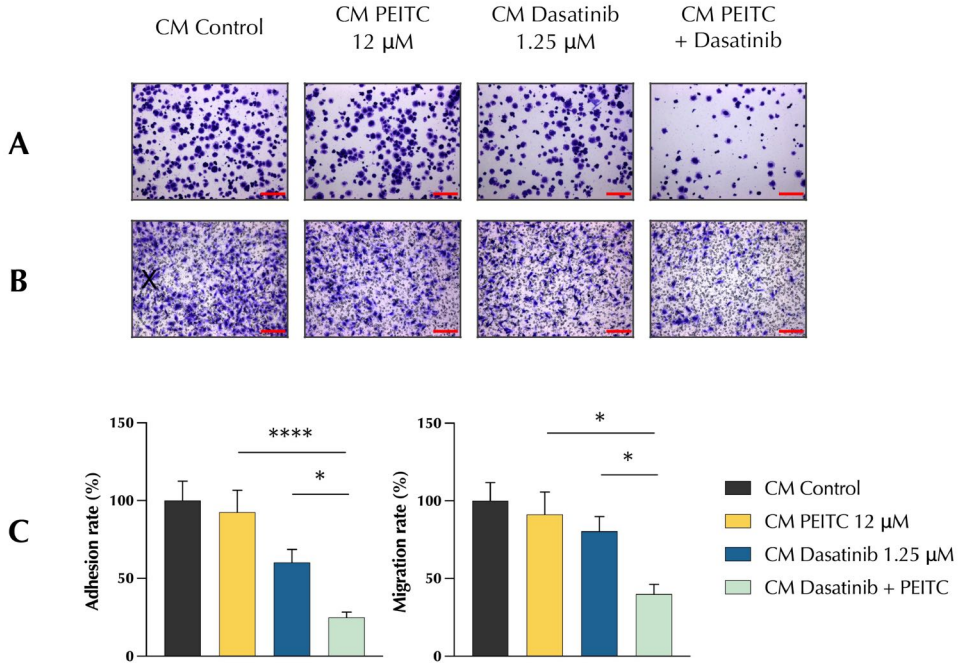

FIGURE 6.4 | Effect of CM from HepG2 treated with PDc on HUVECs adhesion and migration. **(A)** Representative images of HUVECs adhesion assay (10x, scale bar 200 µm). **(B)** Representative images of HUVECs migration assay (10x, scale bar 200 µm). **(C)** Quantitative data of HUVECs adhesion (mean ± SEM, n=6) and migration normalised to HUVECs medium (mean ± SEM, n=5) after treatment with CM. The degrees of significance were calculated with one-way ANOVA test with Tukey's multiple comparisons test and are indicated as * $p < 0.05$, **** $p < 0.0001$.

6.2.3 PDc CM inhibits tumour-induced angiogenesis *in vitro*

The effect of CM on angiogenesis *in vitro* was investigated by seeding the HUVECs on top of a layer of Matrigel®, which gives the extracellular support to allow the endothelial cells to form tubular structures spontaneously. The results showed that the CM derived from PDc-treated cancer cells inhibited the reorganisation of HUVECs to form tubular structures in a concentration-dependent manner. Indeed, 0.1 mg/mL of CM reduced the complexity of the tubular network significantly, while at 0.2 mg/mL, the HUVECs reorganisation was wholly inhibited by PDc CM and also by CM dasatinib (FIGURE 6.5). Therefore, 0.1 mg/mL of CM was employed to repeat the experiment.

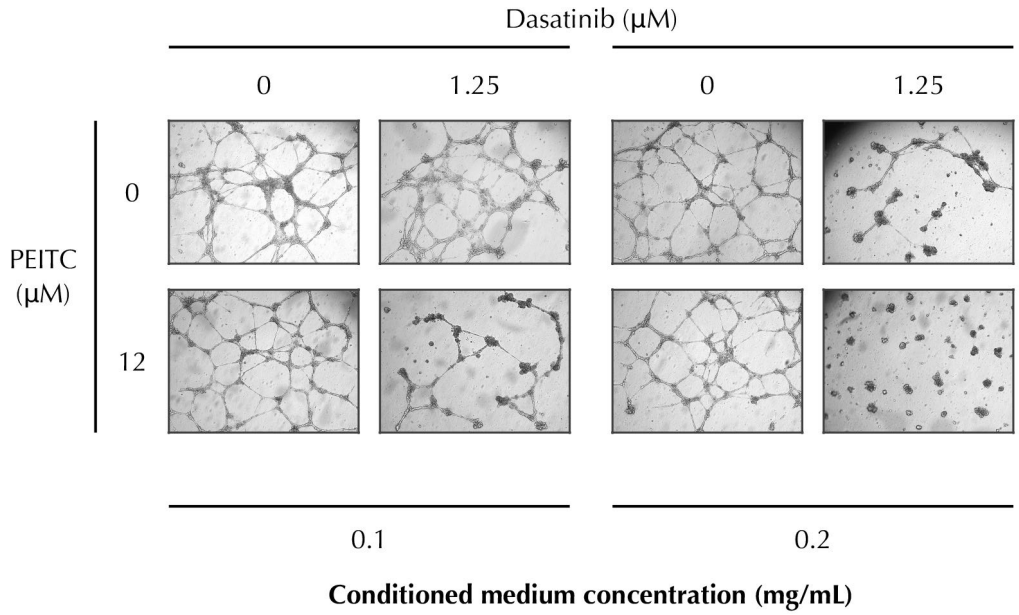

FIGURE 6.5 | Concentration dependent effect of CM on tube formation assay.
HUVECs cells were seeded on top of a thick layer of Matrigel and treated with different concentrations of CM (0.1 and 0.2 mg/mL). PDc derived CM inhibited the formation of tubular structures if compared to single drug treatments derived CM.

In figure **FIGURE 6.6 TOP**, staining with Calcein AM was used to show the tubular structure formed by the endothelial cells. The tubular network was analysed with an ImageJ macro to quantify different parameters that describe the complexity of the formed network (**FIGURE 6.6 BOTTOM**). CM from PDc-treated cells reduced most of the network complexity parameters compared to the CM derived from the single drug treatments, while dasatinib alone reduced only the area meshes formed.

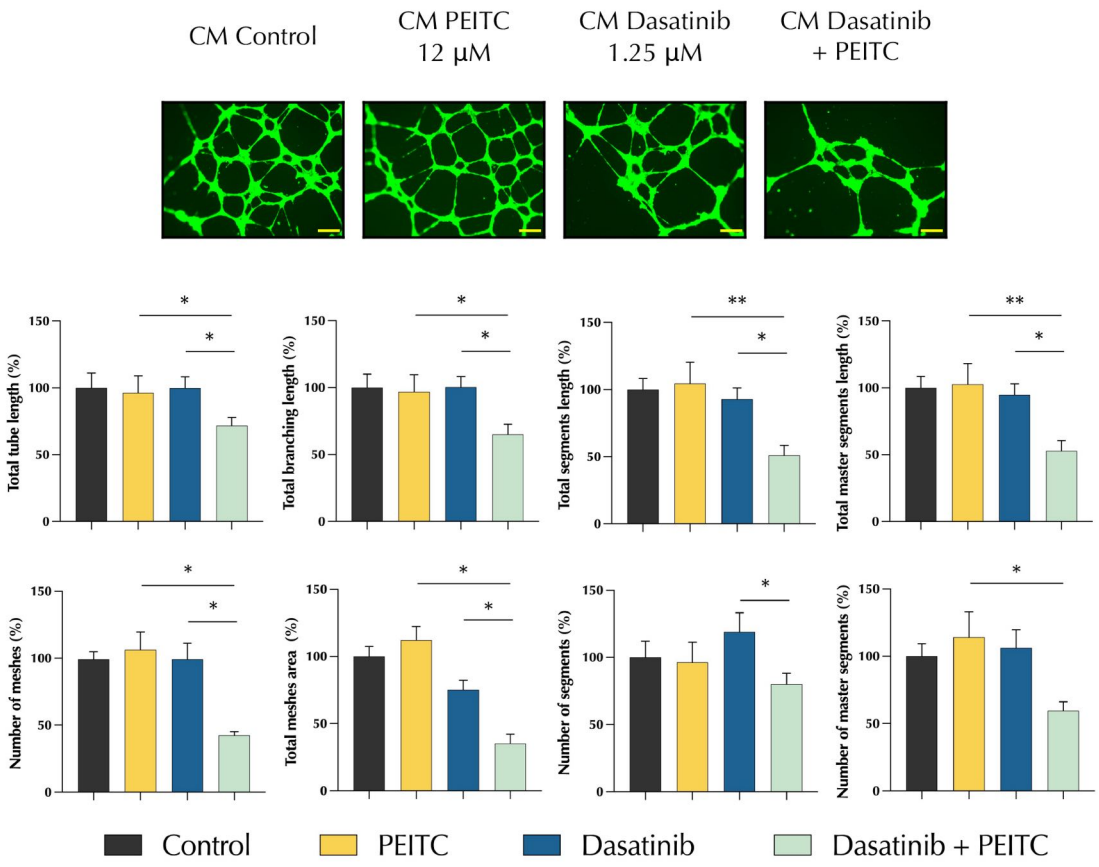

FIGURE 6.6 | Effect of CM from HepG2 treated with PDc on tube formation assay.
Tubular structure were stained with Calcein AM and the network complexity was calculated with ImageJ referring to different parameters. **(A)** Representative images of HUVECs tube formation assay stained with Calcein AM (4x, scale bar 200 µm). **(B)** Quantitative data of tube formations from 8 different parameters (mean ± SEM, n=5). The degrees of significance were calculated with one-way ANOVA test with Tukey's multiple comparisons test and are indicated as * $p < 0.05$, ** $p < 0.01$. Only the paramter Number of meshes showed a non-normal distribution, therefore degrees of significance were calculated with non-parametric Kruskal-Wallis test with Dunn's multiple comparisons test.

6.2.4 PDc CM does not affect angiogenesis *in vivo*

The effect of PDc on tumour-induced angiogenesis was further studied using a chick yolk sac membrane (YSM) ex ovo assay. The yolk sac is highly vascularised, and the addition of materials and compounds can give insight into their ability to influence the process of angiogenesis *in vivo*. CM (2.5 mg/mL) was applied inside a plastic ring on top of the YSM, and pictures were taken every 12 hours. At 36 hours, the vessels formed reached a complexity to the extent of quaternary vessels, which are smaller vessels that arise from branches that, in turn, arise from branches originating from a principal vessel. The manual

counting of the vessels showed only a slight trend in quaternary vessels, with fewer vessels in CM derived from the treatment of cancer cells with PDc (FIGURE 6.7).

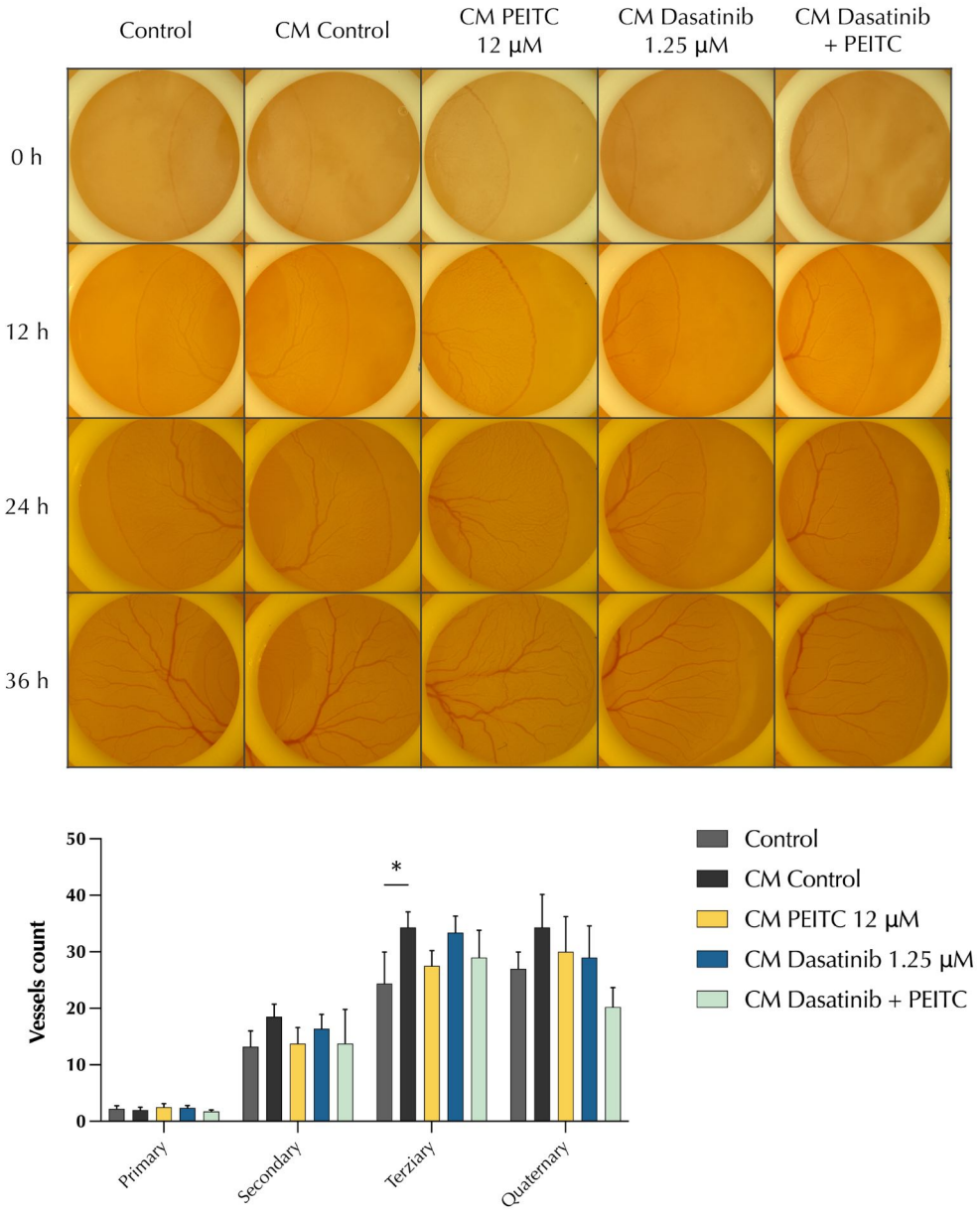

FIGURE 6.7 | Effect of CM from HepG2 treated with PDc on YSM assay.

Top, representative images of the vessels on the yolk sac membrane captured with a stereomicroscope. Bottom, manual count quantification of vessels observed on the YSM (Control n=4, CM Control n=6, CM PEITC 12 µM n=4, CM dasatinib 1.25 µM n=5, CM dasatinib + PEITC n=4) from 3 independent experiments. Only Control and CM Control showed a significant difference calculated with an unpaired two-tailed Student's t-test, the degree of significance is indicated as * $p < 0.05$.

6.2.5 PDc treatment reduces HepG2 secretion of pro-angiogenic factors

Angiogenesis can be induced by pro-angiogenic factors or inhibited by antiangiogenic ones. Therefore, the CM concentrated from the medium of HepG2 cells treated with PDc and single drugs was subjected to an angiogenesis proteome profiler. A profile of the factors up or downregulated present in the CM could give insights on the effect of PDc on tumour-induced angiogenesis. The heatmap showed a summary of the blot results, underlying a difference in terms of Angiogenin and VEGF concentration, which resulted lower in PDc conditioned medium (**FIGURE 6.8**). Also, CXCL16 and placental growth factor (PlGF) secretion resulted slightly lower in PDc-treated cells but the signal from these targets was quite low. The results of the proteome profiler were confirmed with an ELISA assay, which showed a lower VEGF level in CM PDc compared with the CM from the single drug-treated cells (**FIGURE 6.9**).

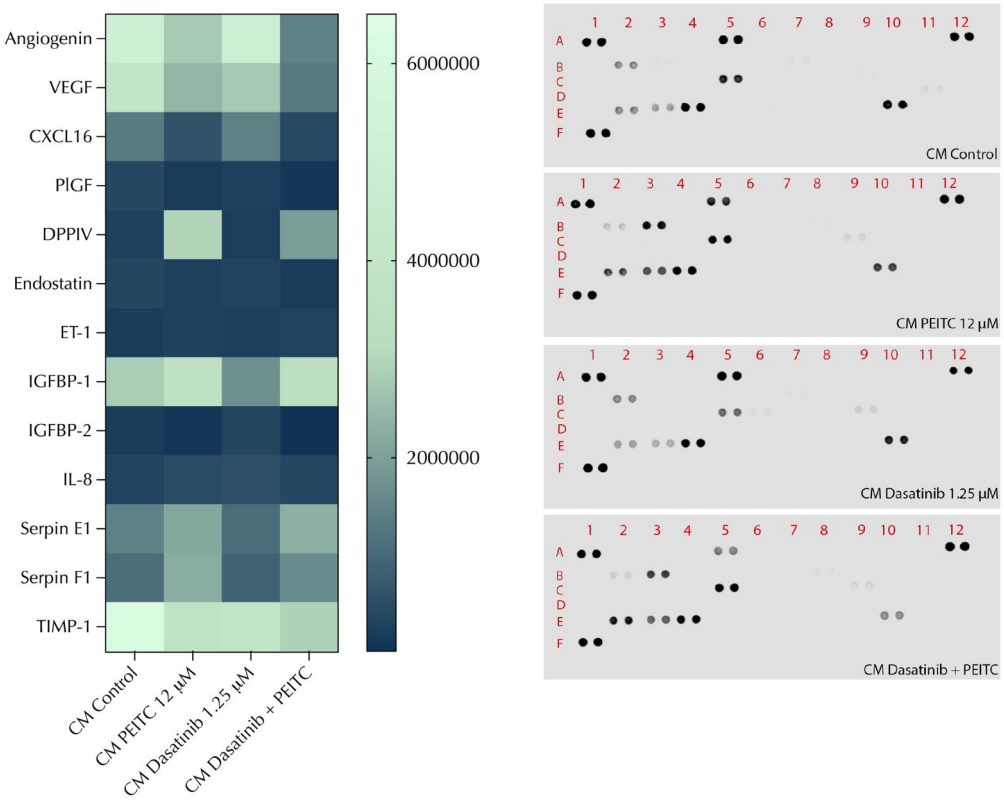

	1	2	3	4	5	6	7	8	9	10	11	12
A	Ref spot		Ativin A	ADAMTS-1	Angiogenin	Ang-1	Ang-2	Angiostatin	AR	Artemin		Ref spot
B	TF	CXCL16	DPPIV	EGF	EG-VEGF	Endoglin	Endostatin	ET-1	FGF 1	FGF 2	FGF-4	FGF-7
C	GDNF	GM-CSF	HB-EGF	HGF	IGFBP-1	IGFBP-2	IGFBP-3	IL-1β	IL-8	TGF-β	Leptin	MCP-1
D	MIP-1α	MMP-8	MMP-9	NRG1-β1	PTX3	PD-ECGF	PDGF-AA	PDGF-AB/BB	Persephin	PF4	PlGF	Prolactin
E	Serpin B5	Serpin E1	Serpin F1	TIMP-1	TIMP-4	TSP-1	TSP-2	uPA	Vasohibin	VEGF	VEGF-C	
F	Ref spot											Neg CON

FIGURE 6.8 | Analysis of CM from HepG2 treated with PDc.

The angiogenesis proteome profiler was employed for the detection of angiogenesis involved factors. Top left, heatmap of targets that shows a significant change. Top right, images of blots of proteome profiler. Bottom, the legend of targets location.

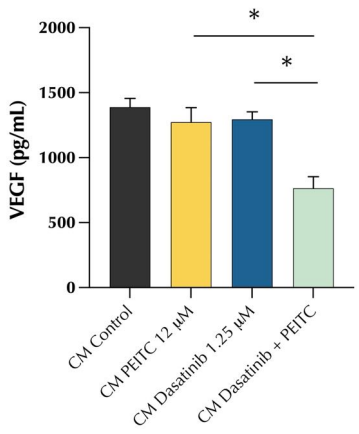

FIGURE 6.9 | CM ELISA assay for VEGF detection.
ELISA assay results for the detection of VEGF in CM (mean ± SEM, n=3). The degrees of significance were calculated with one-way ANOVA test with Tukey's multiple comparisons test and are indicated as * $p < 0.05$.

6.2.6 PDc affects HepG2 PlGF, but not ANG and VEGF gene expression

To further assess the effect of PDc on the expression of pro-angiogenic factors, RT-qPCR was employed to analyse the expression of the three most interesting factors identified with the angiogenesis proteome profiler (i.e. angiogenin, VEGF, PlGF). As depicted in **FIGURE 6.10**, ANG, VEGF, and PlGF expression levels were assessed at three different time points. ANG did not show any significant difference in expression between the treatments at any experimental time. VEGF analysis showed an increase in expression at 6 and 12 hours in PEITC and PDc-treated cells, while at 24 hours the expression went down below the control level. Interestingly, PlGF analysis showed a significant increase in PDc-treated cells at 6 hours, returning to the control level at 24 hours.

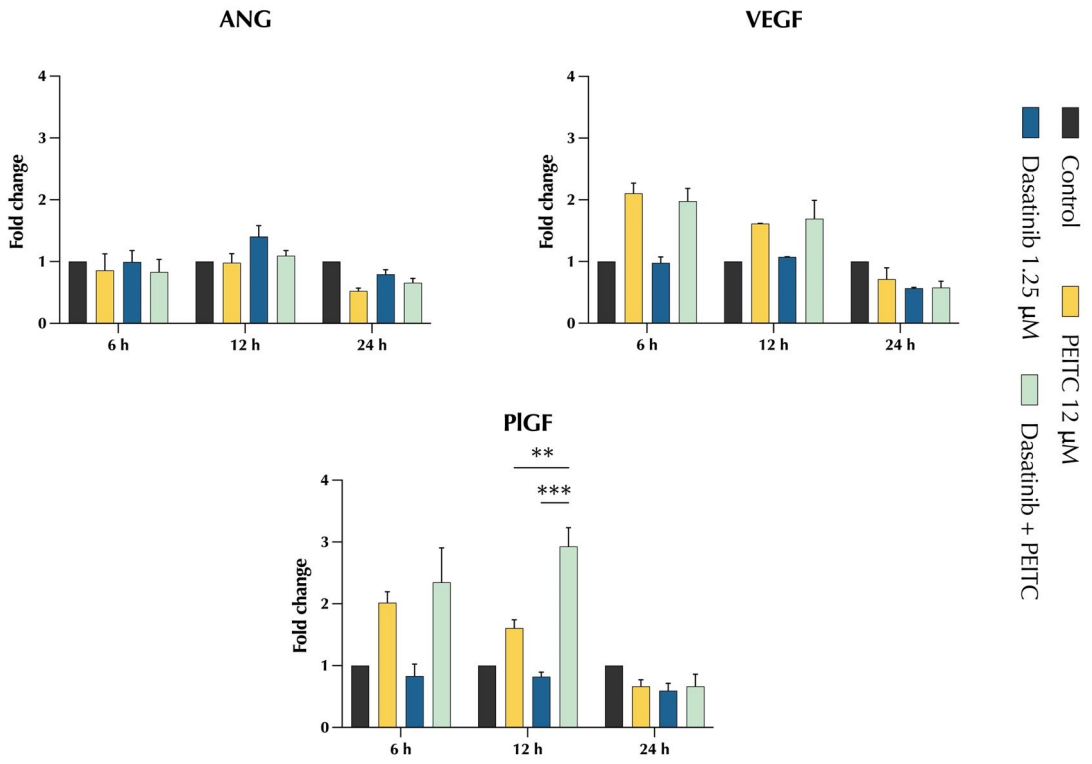

FIGURE 6.10 | Gene expression analysis for angiogenesis factors.
Expression of ANG, VEGF, and PlGF was analysed by RT-qPCR after 6, 12, and 24 h (mean ± SEM, n=3). Data were normalised to β-Actin expression before being subjected to $2^{-\Delta\Delta CT}$ method. The degrees of significance were calculated with one-way ANOVA test with Tukey's multiple comparisons test and are indicated as ** $p < 0.01$, *** $p < 0.001$.

6.2.7 Effect of PDc on PlGF/VEGF heterodimers formation in HepG2

The study of the literature highlighted the potential of PlGF to form a heterodimer with VEGF that has anti-angiogenic properties. Therefore, the presence of PlGF/VEGF heterodimers in CM was assessed by ELISA assay. Non-concentrated and concentrated medium resulted in a lower presence of PlGF/VEGF heterodimers in PEITC and PDc compared to the control, while dasatinib treated cells did not significantly change their secretion in CM (FIGURE 6.11).

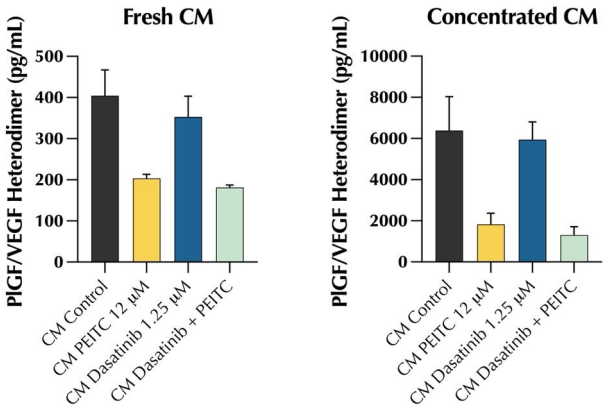

FIGURE 6.11 | Presence of PlGF/VEGF heterodimer in CM.
CM from HepG2 treated with PDc and single drugs was subjected to ELISA assay for the presence of PlGF/VEGF heterodimers (mean ± SEM, n=3) No difference was observed between the non concentrated CM collect straight from the plate (left) and the CM collected and concentrated for HUVECs and YSM assays (right).

6.3 Discussion

Chemotherapy coupled with angiogenesis inhibition could be an advantageous strategy in cancer treatment. PDc showed a promising effect on HUVECs *in vitro*. The concentrated CM from HepG2 treated with PDc was able to reduce HUVECs adhesion and migration capability as well as the ability to form tubular structures *in vitro*. The effect *in vivo* was not marked as expected due to the high intrinsic variability of the YSM assay, which lacked standardisation capability [300]. The analysis of the CM using an angiogenesis proteome profiler highlighted that PDc treatment significantly reduced two pro-angiogenic factors, angiogenin and VEGF while changing the expression of CXCL16 and PlGF to a smaller extent.

Angiogenin serum levels have been associated with a poor prognosis in different tumours [301] particularly in HCC, indicating more tumour vascularity and patient mortality [302, 303]. Angiogenin is secreted by hepatocytes and is internalised by endothelial cells to promote the transcription of pro-angiogenic factors [304]. The analysis of the secretome in hepatoma cells showed that angiogenin is also responsible for promoting liver cancer through the activation of hepatic stellate cells [301]. Previous publications have indicated that prostate cancer cells highly express angiogenin that can be responsible for STAT3 signalling activation [305], and hypoxia-inducible factor 1α (HIF-1α) may up-regulate angiogenin in oral cancer [306].

CXCL16 has been identified as a potent mediator of angiogenesis, particularly influencing endothelial cells' chemotaxis for de novo vessel development [307]. Zhuge *et al*. demonstrated that CXCL16 stimulates HUVECs proliferation and migration and formation of a tubular network *in vivo* through activation of ERK pathway [308]. Moreover, CXCL16 has been associated with increased secretion of VEGF in prostate cancer cells [309]. Indeed, solid tumours secrete CXCL16 to attract endothelial cells and to induce angiogenesis [310]. Finally, the mRNA expression of CXCL16 was associated with hypoxic conditions and, therefore, with transcription induced by HIF-1α [310].

VEGF is the critical mediator in angiogenesis, typically expressed during embryogenic development or wound healing in adult life [311]. During the before mentioned "angiogenic switch", VEGF becomes highly expressed in cancer together with other pro-angiogenic factors to allow the development of de novo vasculature, favouring the exponential tumour growth [311]. The condition of hypoxia generally induces VEGF expression. Indeed, overexpression of STAT3 regulates VEGF expression [312] and, in particular, activation of HIF-1α mediates the expression of VEGF [313]. As the literature shows, inhibition of this signalling axis led to reduced angiogenesis in HepG2 treated with sulforaphane [286]. Recently, STAT3 angiogenesis mediation has also been associated with the c-Src/FAK complex [314]. As discussed before, PDc synergistic efficiency could also be associated with the simultaneous targeting of c-Src and FAK to reduce the metastatic tumour potential. C-Src induces angiogenesis through VEGF expression [315], while FAK plays an important role in the proliferation and migration of endothelial cells [316]. It may be hypothesised that the observed effect of PDc on the inhibition of angiogenesis is linked to the inhibition of c-Src/FAK/STAT3 signalling, which results in the reduced expression of pro-angiogenic factors (**FIGURE 6.12**).

Further experiments could be helpful to support the above conclusions. The supplementation of the CM with the pro-angiogenic factors (i.e. PlGF, CXCL16, VEGF) that resulted reduced after treatment of PDc could highlight the involvement of these factors in the reduced tumour induced angiogenesis. Even if the correlation between STAT3 and reduced expression of VEGF has been reported in the literature [286], further experiments to study the expression of HIF-1α could confirm the linkage between FAK/STAT3 signalling and the reduced expression of pro-angiogenic factors. Indeed, nuclear HIF-1α could be isolated to analyse its nuclear translocation, which is responsible for the expression of pro-angiogenic factors.

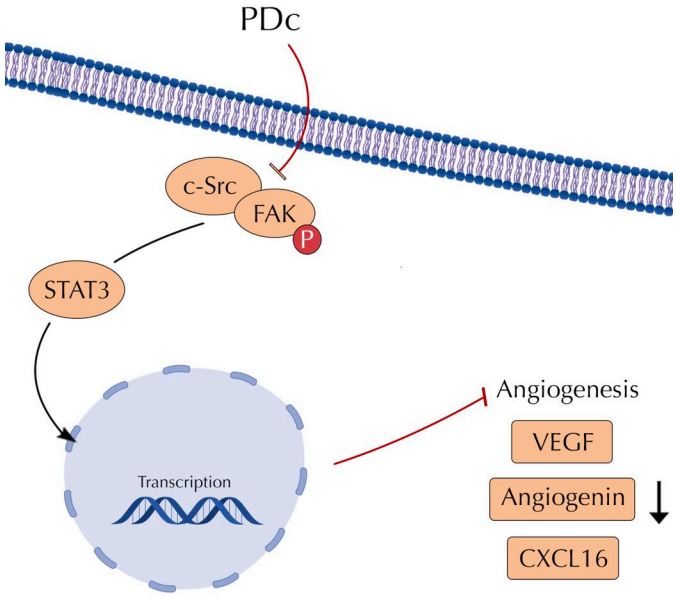

FIGURE 6.12 | Schematic diagram of PDC in inhibition of angiogenesis.
The concomitant inhibition of c-Src and FAK lead to the inactivation of STAT3, which is involved in the transcription of different pro-angiogenic factors. In particular, PDc reduced the accumulation of VEGF, angiogenin, and CXCL16 in CM.

The analysis of the mRNA expression of the main pro-angiogenic factors identified by the proteome profiler highlighted something unexpected. PDc treatment induced an over-expression of PlGF at 6 hours with a peak at 12 hours. The placental growth factor (PlGF) is a protein that belongs to the VEGF family, and VEGFR-1 was identified as its primary receptor [317]. The role of PlGF is controversial, some reports this protein involved in pathological angiogenesis with a potential role in cancer treatment of PlGF inhibition [317]. On the contrary, other studies highlighted the potential of PlGF as an inhibitor of tumour growth and metastasis [318-320]. It has been shown that the over-expression of PlGF inhibits angiogenesis by forming a PlGF/VEGF heterodimer, reducing tumour growth *in vivo*. The role of VEGF and PlGF in angiogenesis is strictly related to the presence of specific receptors on endothelial cells. VEGF usually forms homodimers that bind VEGFR-2 to promote angiogenesis [321]. Once VEGF binds to VEGFR-2, an intracellular calcium reserve is mobilised to activate downstream signalling to promote angiogenesis, while PlGF homodimers bind to VEGFR-1, leading only to weak angiogenesis [322].

On the other hand, PlGF/VEGF heterodimers bind to VEGFR1/2, the heterodimer receptor, and inhibit the signals responsible for the calcium release, delaying the activation of the downstream signalling, thus inducing a negative regulation of angiogenesis [322].

Therefore, PlGF/VEGF heterodimers inhibit angiogenesis in relation to VEGF receptors found on endothelial cells. The inhibition can be direct through activation of the VEGFR-1/2 negative regulation and indirect via blocking the formation of angiogenic active VEGF homodimers (**FIGURE 6.13**). The data from the ELISA assay for PlGF/VEGF heterodimers showed that PDc does not lead to increased secretion of PlGF/VEGF heterodimers. Therefore, PDc reduction of angiogenesis is unrelated to PlGF/VEGF heterodimer formation. PlGF increased expression may not lead to the production of PlGF protein to a sufficient extent to sequester VEGF from homodimer formation and to bind VEGFR-1/2 in an effective manner.

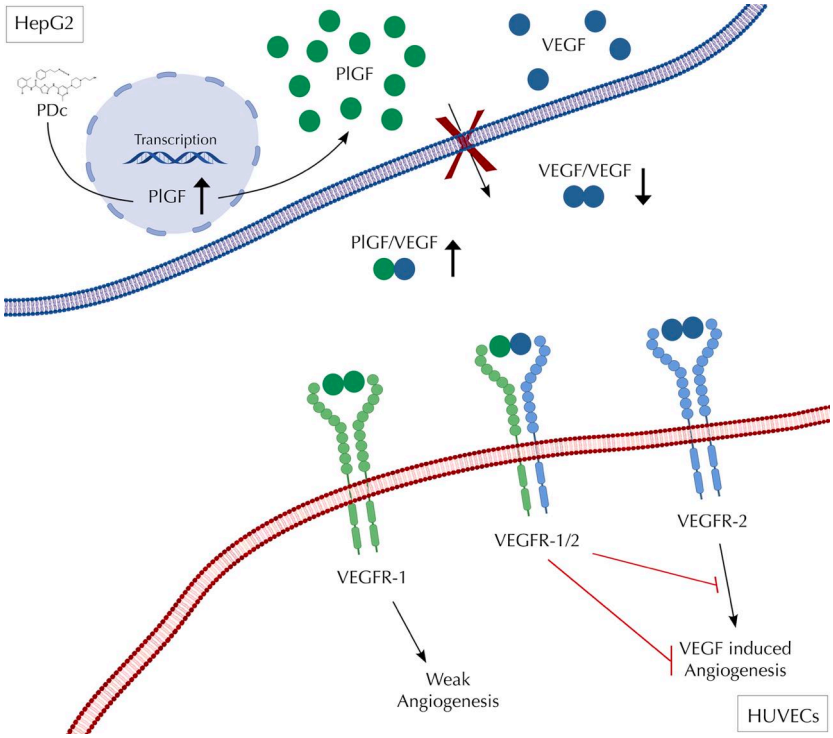

FIGURE 6.13 | Hypothesis of angiogenesis inhibition by PlGF/VEGF heterodimers.
PDc increases the expression of PlGF but this is not enough to affect the formation of PlGF/VEGF heterodimers, which are known to inhibit angiogenesis directly and indirectly. PlGF/VEGF heterodimers bind to the VEGFR-1/2 receptor which delays the VEGFR-2 downstream signalling activation. Furthermore, PlGF/VEGF heterodimers formation reduces the formation of active VEGF homodimers.

Chapter 7
PEITC and Dasatinib combination and murine syngeneic model: *in vivo* preliminary data

7.1 Introduction

Pre-clinical *in vivo* models are crucial for the development of new drug candidates and their advancement to clinical studies [323]. The likelihood of approval of new oncology drugs is extremely low compared to drugs for other types of disease. 80% of the drugs that showed positive results in murine models fail at the clinical stage, resulting in poor translatability [324]. This lack of translational power between *in vivo* and clinical settings and the rise of ethical concern is pushing the research towards different models that are more acceptable under the ethical profile (i.e. 3D cultures, organoids, organs on a chip) [198]. However, the high failure rate at the clinical stage of drugs that showed promising results in mouse models can be attributed to a weak pre-clinical study design [324]. Therefore, it is crucial to refine the pre-clinical study design to improve the reliability of the results. Nonetheless, *in vivo* pre-clinical models, particularly mouse models, are and will be relevant for drug development for years to come [323].

Different mouse models are employed to evaluate the effect of different stimuli on the growth and progression of a tumour *in vivo* [198]. The formation of a tumour can be induced genetically, environmentally (i.e. radiation, chemicals, pathogens) or physically implanting a human-derived xenograft or inoculating a tumour cell line. Cell line-based mouse tumour models are the most used, accounting for 82% of all employed models [198]. Cell lines models can count on lower costs, easy technical manipulability and consistent tumour growth [198]. Human-derived tumour cell lines can be injected in immunocompromised mice to generate a xenograft; on the other hand, mouse cell lines are injected in immunocompetent mice to generate an allograft. The cell line inoculation can be performed on the organ of its origin (orthotopic) or subcutaneously (ectopic). In this work, a cell line derived from the same host strain was inoculated in C57BL6 mice to generate a subcutaneous syngeneic model to determine PDc efficacy and safety.

Chapter 7 objectives

- Evaluate PDc effect on tumour growth *in vivo*

7.2 Results

7.2.1 Murine syngeneic model parameters

The literature was scanned to study the most reliable model to study PDc' effect on HCC in vivo. Mice strains, sex, gender, cell lines, and cell number injected were considered and listed in **TABLE 7.1**. Hepa 1-6 is among the most used syngeneic models for the study of HCC *in vivo,* and it is considered a suitable cell line to inject in C57BL6 mice due to the reliable tumour growth [325]. Furthermore, the literature was scanned to determine the safest treatment time and dose for dasatinib and PEITC, considering that the time remaining for the project's completion did not allow to carry out a pilot study (**TABLE 7.2**). The mice chosen for the *in vivo* study to evaluate PDc effect were 8-9 weeks old females, as the average between the selected articles is 8.7 weeks, and no intersex difference was observed. Female mice offer an advantage over male mice as they are easier to manage in a colony because of the absence of territoriality. The number of cells chosen was $5x10^6$, which was the most used. For what concern the drug treatment, three weeks of daily oral gavage were selected together with the lowest concentrations of the two drugs to ensure a consistent gap in tumour size between single drugs and combination treatments (dasatinib 10 mg/kg and PEITC 40 mg/kg). Corn oil was the selected vehicle as PEITC do not dissolve in citric acid (the usual dasatinib vehicle), while DMSO dissolved dasatinib resulted miscible in corn oil if prepared right before the administration.

TABLE 7.1 | Most used parameters for Hepa 1-6 murine syngeneic model.

Model	Mice	Cell number and vehicle	Treatment start	Treatment end
Allograft Subcutaneous [164]	8-10 weeks C57L/J	$4×10^6$	Tumour at 100 mm^3	Day 22
Allograf Subcutaneous [164]	8-10 weeks CAnN.Cg-Foxn1nu/ CrlCrlj	$4×10^6$	Tumour at 100 mm^3	Day 15
Allograft Subcutaneous [326]	5-6 weeks Male (no gender difference observed) C57L/6J	$5×10^6$ 100 µL PBS	Tumour at 200 mm^3	Day 15
Allograft Subcutaneous [325]	10-25 weeks C57L/J	$1×10^7$ 0.1 mL FBS free MEM	Tumour visible (6 days)	Day 18 (2000 mm^3)

Model	Mice	Cell number and vehicle	Treatment start	Treatment end
Allograft Subcutaneous [327]	8-12 weeks Female C57BL/6	2×10^7/mL 0.1 mL PBS	Tumour at 1 cm (9-10 days)	After 2 weeks of treatment
Allograft Subcutaneous [328]	C57L/J	5×10^6 0.1 mL FBS free MEM	Tumour visible (15 days)	Day 40 (4000 mm^3)

TABLE 7.2 | Most used parameters for dasatinib and PEITC *in vivo*.

Drug	Route of administration	Dose, vehicle and frequency	Tumour	Treatment start	Treatment end
Dasatinib [329]	Oral gavage	30/60 mg/kg x day 80 nM citric acid Daily	Neuroblastoma	7 days after tumour cell injection	40 days
Dasatinib [330]	Oral gavage	10 mg/kg x day DMSO 5 days a week	Colon cancer	2 weeks	4 weeks
Dasatinib [331]	Oral gavage	30 mg/kg x day Citrate buffer	Melanoma	Tumour at 50–100 mg	
Dasatinib [331]	Oral gavage	30 mg/kg x day Citrate buffer	Melanoma	Tumour at 50–100 mg	
Dasatinib [332]	Oral gavage	1, 5, 15, 50 mg/kg PG in water (50:50) Twice x day	Prostate cancer	Tumour at 150–250 mg	Tumour at 1g
Dasatinib [297]	Oral gavage	15 mg/kg 50 µl Labrasol Daily	Breast cancer	10 days after tumour cell injection	Day 34
Dasatinib [333]	Intraperitoneal	10 mg/kg x day DMSO 5 days a week	Ovarian cancer	Tumour at 0.3 mm^3 (4 days)	2 ½ weeks
Dasatinib [334]	Oral gavage	10 mg/kg x day 80 mM citrate buffer	Breast cancer		Tumour at 1.7 cm
Dasatinib [36]	Topical	100 mg/kg CMC-Na Every 2 days	HCC	Tumour at 50–100 mm^3	30 days
Dasatinib [335]	Oral gavage	30 mg/kg x day 80 nM citric acid	Ovarian cancer	Tumour at 75 mm^3	16 days
Dasatinib [335]	Oral gavage	30 mg/kg x day 80 nM citric acid	Ovarian cancer	Tumour at 75 mm^3	19 days
Dasatinib [336]	Oral gavage	70 mg/kg/day dH_2O 5 days a week	Colon cancer	Tumour at 50 mm^3	

Drug	Route of administration	Dose, vehicle and frequency	Tumour	Treatment start	Treatment end
PEITC [337]	Oral gavage	60 mg/kg 0.1 mL PBS 5 days a week	Prostate cancer	Day of injection	Day 38
PEITC [337]	Oral gavage	40 mg/kg 0.1 mL PBS 5 days a week	Prostate cancer	Tumour at 50 mm^3 (15 days)	Day 38
PEITC [338]	Oral gavage	81 mg/kg x day PBS	Breast cancer	Tumour at 150 mm^3	Day 35
PEITC [339]	Oral gavage	81 mg/kg/day PBS	Breast cancer	Tumour at 80 mm^3	Day 35
PEITC [340]	Oral gavage	60 mg/kg x day 0.1 mL oil 21 days	Breast cancer	Tumour at 50-100 mm^3 (5 days)	Day 22
PEITC [341]	Oral gavage	67.5/135 mg/kg x day 0.1 mL + 0.01 mL DMSO	Glioblastoma	Tumour at 100-120 mm^3	Day 21

7.2.2 PDc reduces Hepa 1-6 cells viability and induces apoptosis

To assess the validity of the Hepa 1-6 cell line as a model for testing PDc *in vivo*, an MTT assay was employed to evaluate the efficiency of PEITC addition to dasatinib treatment on Hepa 1-6 cells. Hepa 1-6 cells were treated with PEITC or dasatinib alone and in combination using concentrations of PEITC below the IC20 (i.e. 6, 9, 12 μM) (**FIGURE 7.1A**). The results showed that PDc significantly reduced cell viability compared to single treatments. In particular, the addition of PEITC 9 and 12 μM led to a strong synergy with CI values lower than 0.5 (**TABLE 7.3**). Moreover, the combination of PEITC 12 μM and dasatinib 0.625 μM lead to a statistically significant increase in apoptotic cells (**FIGURE 7.1B-D**).

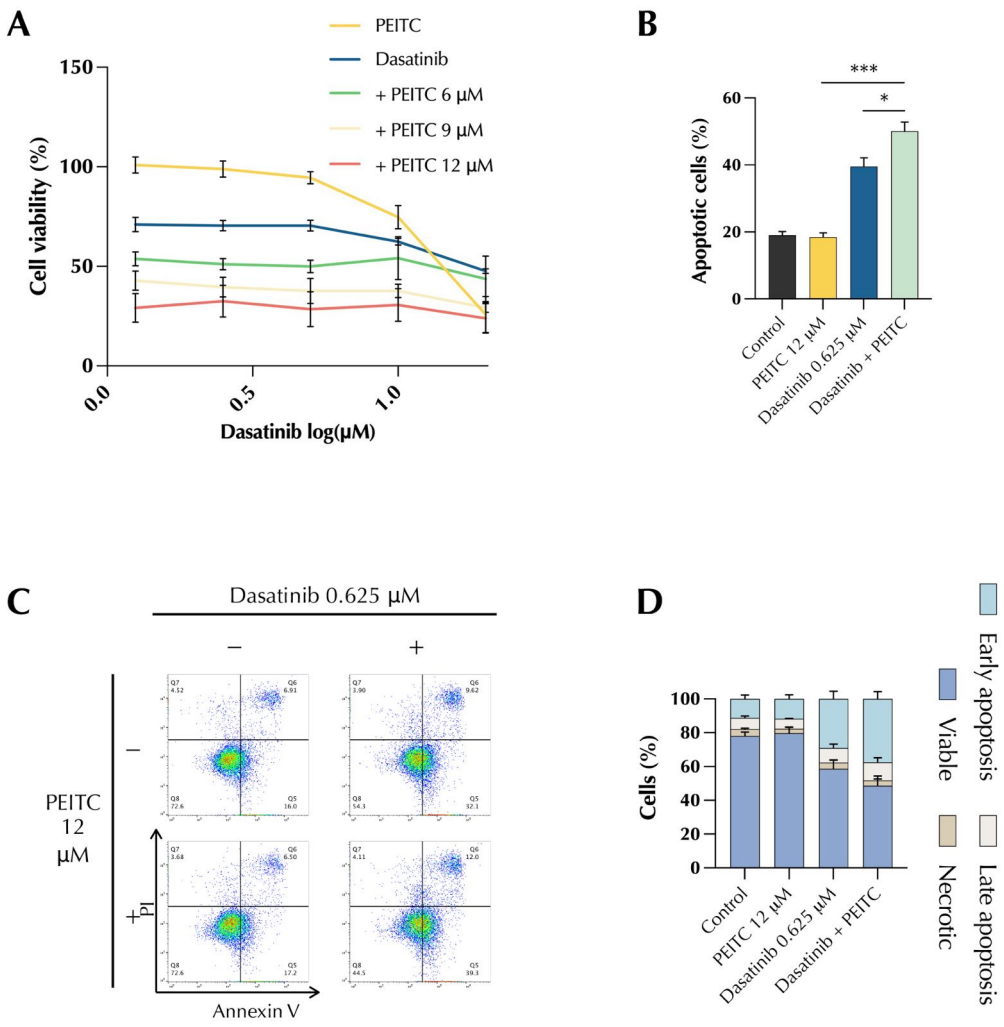

FIGURE 7.1 | PDc induces cell death and increases apoptosis in Hepa 1-6 cells.

(A) Hepa 1-6 cells were treated with different concentrations of PEITC and dasatinib (0.625 to 10 µM) or with dasatinib plus fixed concentrations of PEITC (6, 9, 12 µM) for 24 h. The data presented were normalised to control's proliferation (mean ± SEM, n=3). **(B)** Hepa 1-6 cells were treated with dasatinib 0.625 µM with or without PEITC 12 µM for 24 h and then subjected to Annexin V (AV) and PI staining (mean ± SEM, n=3). The degrees of significance were calculated with a one-way ANOVA test with Tukey's multiple comparisons test and are indicated as * $p < 0.05$, *** $p < 0.001$. **(C)** Apoptosis assay representative images from FlowJo software. **(D)** Apoptotic cell percentages (mean ± SEM, n=3).

TABLE 7.3 | CI values of PDc calculated after 24 h of treatment.

		Dasatinib (μM)				
		0.625	**1.25**	**2.5**	**5**	**10**
PEITC (μM)	**6**	0.541	0.599	0.685	0.949	2.043
	9	0.497	0.498	0.499	0.560	0.770
	12	0.411	0.363	0.444	0.484	0.676

7.2.3 PDc affects Hepa 1-6 spheroids' viability and growth

PDc efficiency was tested using a 3D spheroid model. The effect on spheroids viability was tested by employing Calcein AM (viable cells) and ethidium homodimer (dead cells) stains. The combination-treated spheroids (dasatinib 0.625 μM + PEITC 9 μM) showed an increase of dead cells in the core of the spheroid (FIGURE 7.2A). The analysis of the spheroids area highlighted a decreased size of dasatinib and PDc-treated spheroids but the difference was not significant (FIGURE 7.2B).

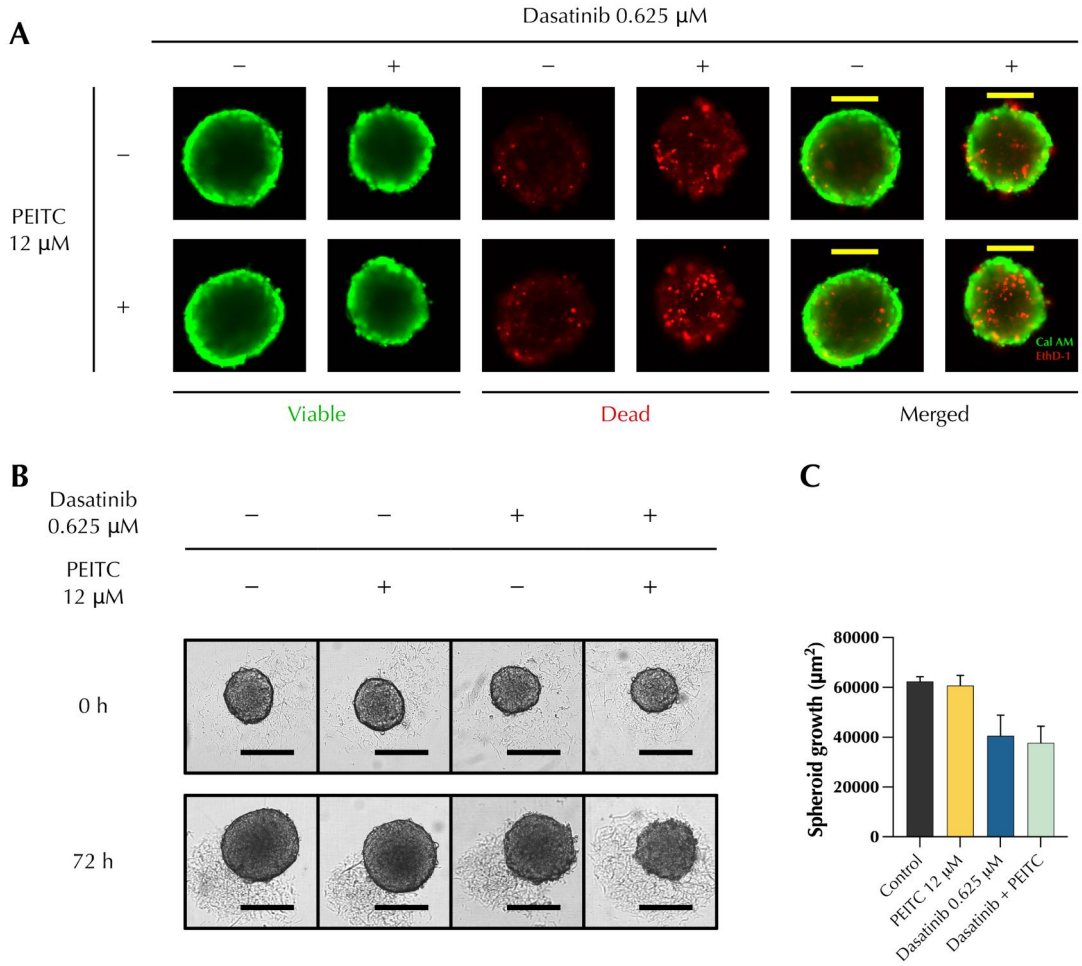

FIGURE 7.2 | PDc affects Hepa 1-6 spheroids' viability and size growth.
Spheroids were treated for three days with dasatinib 0.625 µM with or without PEITC 12 µM. **(A)** Dead cells and viable cells are stained with EthD-1 (red) and Calcein AM (Green) respectively (10x, scale bar 200 µm). **(B)** Effect of drugs on spheroids growth based on the surface area (4x, scale bar 500 µm). **(C)** Spheroids area quantification on ED 6 (mean ± SEM, n=3).

7.2.4 PDc inhibits Hepa 1-6 adhesion and migration

The ability of PDc to influence cell adhesion and migration was investigated in Hepa 1-6 cells. Cells were seeded on an ECM-coated plate to facilitate adhesion and treated with PDc and single drugs; the number of adherent cells was evaluated after 3 hours. The results showed potent inhibition of adhesion in PDc-treated cells, while PEITC led to a reduction of just 20% and dasatinib reduced to <50% the adhesion potential of Hepa 1-6 cells (FIGURE 7.3A-B). The scratch wound healing assay highlighted the ability of PEITC to enhance the migration inhibition of dasatinib, with the combination cell treatment further reducing the migration rate to less than 20% when compared with the control cells (FIGURE 7.3C-D).

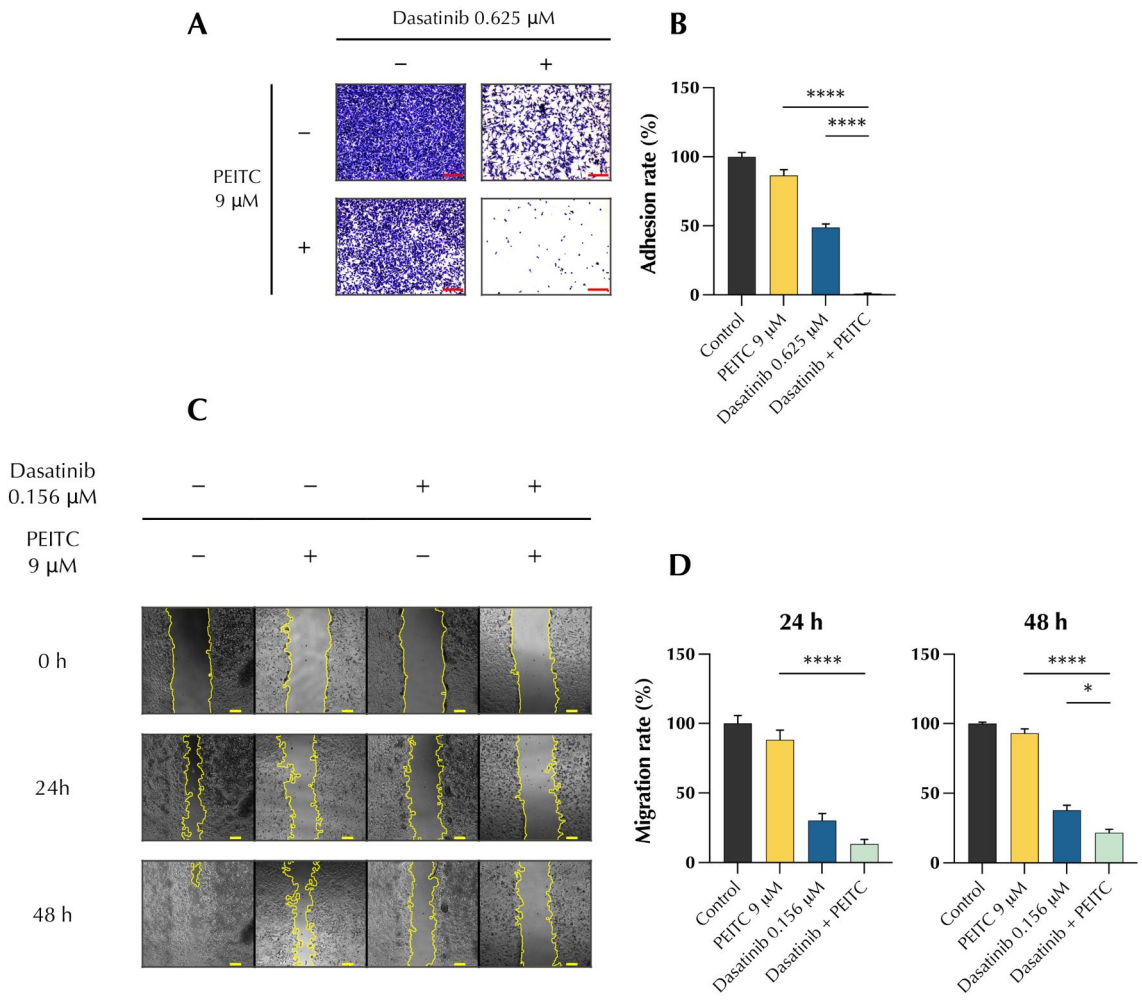

FIGURE 7.3 | PDc suppresses Hepa 1-6 adhesion and impairs cell migration.
Hepa 1-6 cells were seeded on a 200 µg/mL Matrigel-coated plate and treated with dasatinib 0.625 µM with or without PEITC 9 µM. **(A)** Cells were stained with crystal violet and imaged with an inverted microscope. Representative images from 3 independent experiments (20x, scale bar 100 µm). **(B)** Adhesion assay's quantitative data were normalised to control (mean ± SEM, n=3). Hepa 1-6 cells were treated with dasatinib 0.156 µM with or without PEITC 9 µM, and pictures were taken at 0, 24 and 48 h. **(C)** Representative images at 0 h and 72 h. **(D)** Quantitative data presented were normalised to control's migration rate (mean ± SEM, n=3).

7.2.5 PDc inhibits tumour growth *in vivo*

PDc efficacy was further tested *in vivo* with a syngeneic subcutaneous murine model. Hepa 1-6 were injected subcutaneously (on the right flank); once the tumour mass developed, mice were treated with PDc, single drugs, or vehicle control by oral gavage for three weeks, five days a week (FIGURE 7.4A). Animals were culled after 22 days from the start of the treatment. The treatment regimen did not negatively influence the animal's growth,

which gained weight throughout the experiment (FIGURE 7.4B). Tumour controls steadily developed, reaching 966.8 ± 329.9 mm^3 at the end of the experiment, while PEITC reached 967.7 ± 453.8 mm^3 and dasatinib 773.6 ± 292.8 mm^3 (FIGURE 7.4C). PDc proved to synergistically reduce tumour growth 343.7 ± 134.0 mm^3 with a CI value of 2.064, which was calculated with the fractional tumour volume method (TABLE 7.4). The final tumour volume was normalised to its initial volume; the results are presented in FIGURE 7.4D.

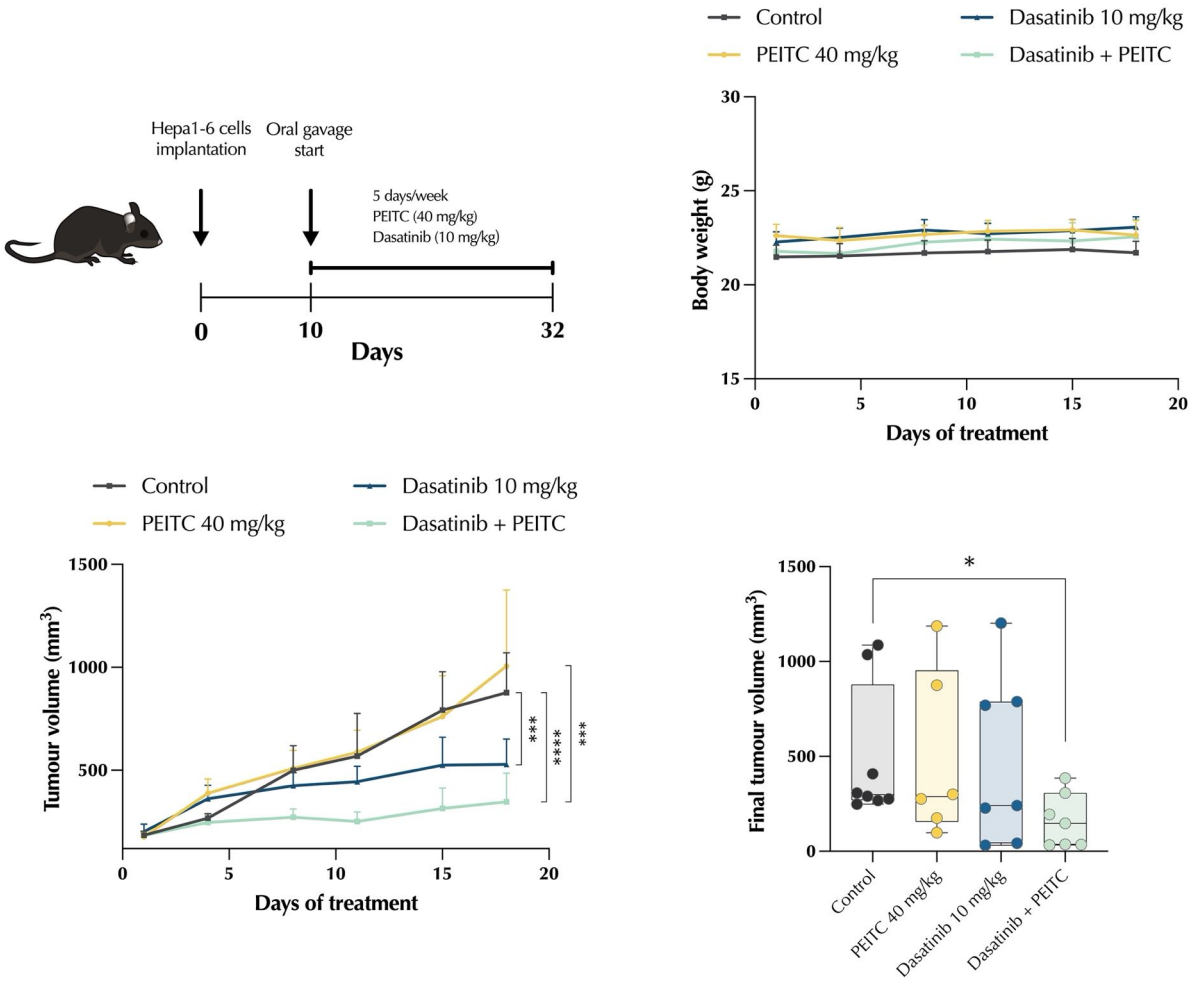

FIGURE 7.4 | PDc reduces tumour growth in *in vivo* murine model.

Diagram of experimental conditions. Mice were injected subcutaneously with Hepa 1-6 cells and treated by oral gavage after 10 days, 5 days a week for 3 weeks **(B)** Body weight was closely monitored over the treatment time. **(C)** Tumour volume over the treatment time (mean ± SEM, Control n=9, PEITC n=6, dasatinib n=8, P+D n=8); The degrees of significance are indicated as *** $p < 0.001$, **** $p < 0.0001$ calculated with linear regression. **(D)** Tumour final volume normalised to the volume measured on the day of the first treatment. The degree of significance is indicated as * $p < 0.05$ calculated with non parametric Kruskal-Wallis test with uncorrected Dunn's test.

TABLE 7.4 | Drug combination synergistic effect calculated with CI values related to fractional tumour volume

	Fractional tumour volume (FTV) relative to control [1]				
			Dasatinib + PEITC		
Day of treatment	**PEITC 40 mg/kg**	**Dasatinib 10 mg/kg**	**Expected [2]**	**Observed [1]**	**Combination index [3]**
8	1.019	0.849	0.866	0.610	1.418
11	0.884	0.782	0.691	0.494	1.400
15	0.961	0.663	0.638	0.418	1.524
18	1.146	0.602	0.690	0.426	1.619
End	1.001	0.800	0.801	0.388	2.064

[1] FTV = (mean tumour volume) ÷ (mean tumour volume control)
[2] Expected FTV = (FTV of PEITC) × (FTV of dasatinib)
[3] Combination index = (FTV Expected) ÷ (FTV Observed)
>1 Synergy, =1 Addition, <1 Antagonism

The tumours were also stained to evaluate the appearance and cell morphology. H&E staining of tumour sections is presented in FIGURE 7.5 and FIGURE 7.6. PDc-treated tumours were less prone to form multilobular masses. The higher magnification images showed no significant difference in cell morphology or tissue organisation between the treatments. The PDc treatments resulted in significant reduction in the size of the tumour but also the heterogeneity and the formation of multilobular masses.

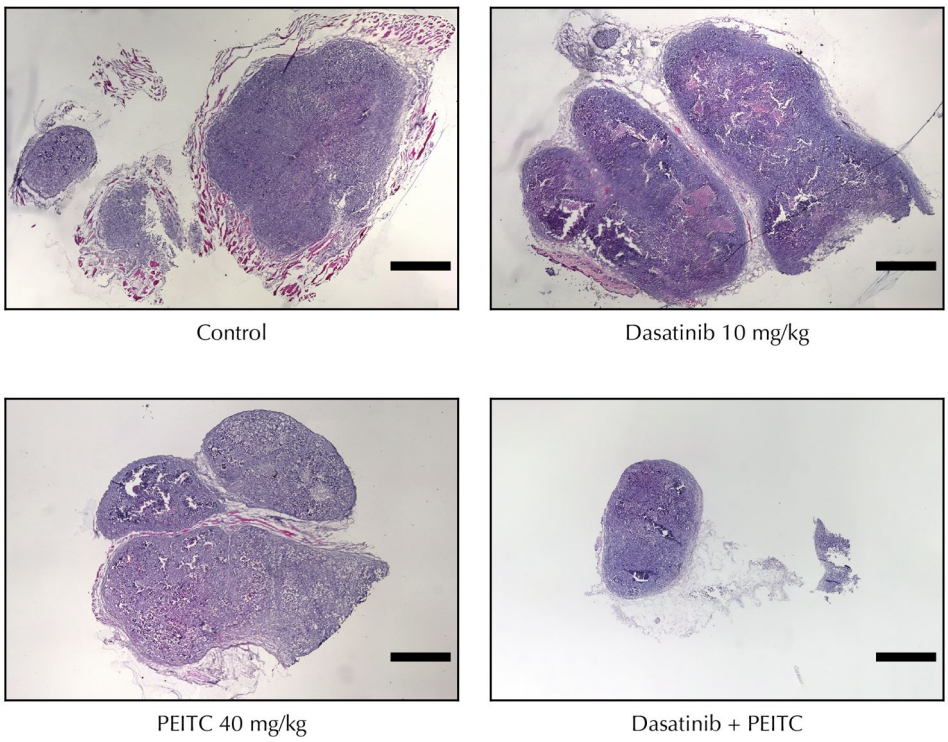

FIGURE 7.5 | Tumour tissue morphology is not affected by the drug treatment.
Mice tumour samples were cryo-embedded, sectioned, and stained with H&E. The 10x images were stitched together to form a picture of the complete section (10x, scale bar 1 mm).

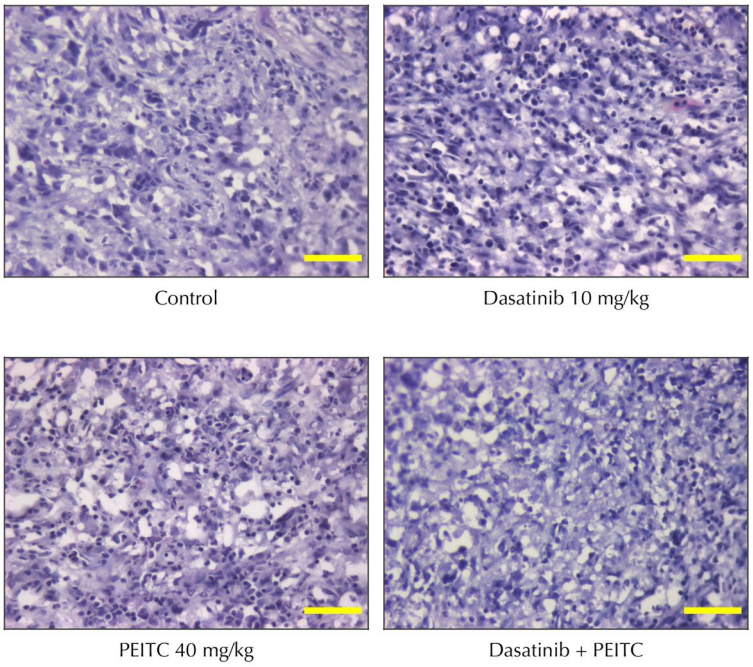

FIGURE 7.6 | Tumour cells' morphology is not affected by drugs' treatment
Mice tumour samples were cryo-embedded, sectioned, and stained with H&E. (40x, scale bar 50 μm).

7.2.6 PDc does not affect liver microstructure

PDc effect on the liver was assessed with microscopical analysis of livers sectioned and stained with H&E. The observation of the liver section did not highlight the presence of any sign of hepatocyte vacuolation, focal necrotic cell death, diffuse fatty changes, microvesicular steatosis, inflammatory infiltrations, necrosis, or fibrosis (FIGURE 7.6).

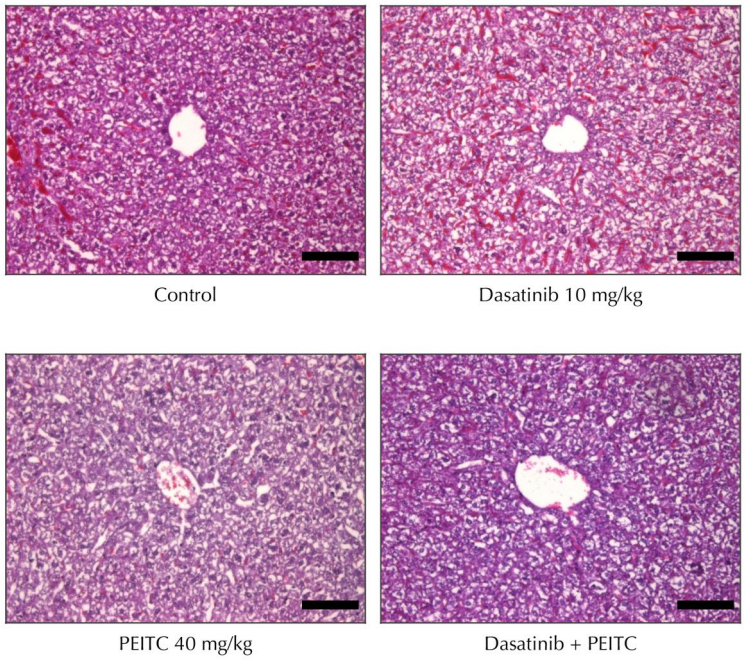

FIGURE 7.6 | Liver gross morphology does not change in response of drugs' treatment
Mouse liver samples were cryo-embedded, sectioned, and stained with H&E. The liver microstructure was observed to assess the effect of the drug treatments on liver damage (20x, scale bar 100 µm).

7.3 Discussion

The use of murine models is a critical step to assess the safety and efficacy of test compounds in the pre-clinical setting. Mouse models have numerous positive aspects such as low costs, high tumour growth rate, easy manipulation of bred strains, and fast reproductive cycle [342]. On the other hand, ethical implications are pushing the research to the development of alternative models (3D cultures, organoids, organs on a chip) [343, 344]. Nonetheless, cancer drug discovery and development field still relies on mouse models to assess the validity of a candidate drug in tumour development and progression and to establish the correct therapeutic window, avoiding dangerous side effects [323]. The high

failure rate at the clinical stage of drugs that showed promising results in mouse models can be attributed to a poor pre-clinical study design [324].

The liver is the main organ responsible for the metabolisation of most substances introduced into the body. Therefore, the disposition of therapeutic drugs also goes through the liver detoxification process. Indeed, hepatic injury induced by medication is a potentially dangerous complication that could shut down the body's detoxification system [345]. The only treatment of drug-induced liver damage is the withdrawal of the therapy responsible for the hepatic injury. Liver damage can be a limiting factor in repurposing chemotherapeutic drugs for different tumour types due to the need for higher doses that lead to unbearable side effects [346]. For example, dasatinib is often associated with hepatotoxicity due to off-target effects that damage normal cells other than cancerous ones [347]. Indeed, dasatinib showed damage to hepatocytes *in vivo*, leading to a significant reduction in the rat body weight [348].

Conversely, ITCs showed to protect normal cells from drug-induced toxicity. For example, PEITC has been shown to protect from acetaminophen-induced hepatotoxicity *in vivo* through the inactivation of P450 enzymes, thus reducing the production of toxic metabolites [349] or to protect from streptozotocin-induced liver disease via Nrf2/SIRT1 pathway [350]. On the other hand, the combination of multiple drugs can have a synergistic anticancer activity but with no specificity, damaging normal cells, as shown in the first chapter of this thesis. Therefore, it is essential to take into consideration that the PDc could positively reduce tumour growth but with severe toxic effects that make the drug combination unsuitable for clinical use. The preliminary results of the murine syngeneic model experiment revealed that PDc did not have a negative impact on the mice's body weight and did not induce any visible liver damage in the liver sections stained with H&E. Indeed, no ballooning degeneration, focal necrotic cell death, focal hepatocellular degeneration, or vacuolisation were observed as outlined in other studies [350, 351].

PDc showed promising results in reducing the growth of HCC *in vivo* without affecting the health status of the animals tested, as demonstrated by their increasing body weight and no detectable damaged liver microstructure. The exact mechanism of PDc action *in vivo* has not been confirmed. PDc showed similar results *in vitro* in the murine HCC cell line Hepa 1-6 and in the human cell line HepG2. PDc inhibited the growth of both cell lines tested, induced apoptosis, and reduced adhesion and migration. It has to be confirmed whether the cell cycle arrest and oxeiptosis induced by ROS production, as well

as inhibition of angiogenesis and tumour metastatic potential through c-Src/FAK/STAT3 signalling can also be relatable to the effect of PDc *in vivo*. Indeed, it is of fundamental importance to optimise the experimental model to increase its predictive power to translate the results to the humans, considering that a model system will always be an approximation of the effects predicted in a clinical setting [323].

Chapter 8
Conclusion

8.1 Summary

ITCs are compounds derived from naturally occurring glucosinolates found in cruciferous vegetables. Evidence from more than 30 years of research showed that these compounds exert a role in chemoprevention and in cancer therapy. Their anticancer activity is broad as it involves numerous different pathways. Therefore, it is likely that these compounds can work in synergy when combined with other molecules that possess anticancer properties. In particular, numerous reports showed the potential of ITCs to improve the efficacy of classic chemotherapeutic agents. Combination therapy is an effective strategy to exploit compounds approved for clinical use; this strategy allows the repurposing of clinically safe drugs for different tumour types. Adding a second compound indeed broadens the spectrum of anticancer activity, even towards tumours where the drug was initially not efficacious.

HCC is among the most lethal malignant tumours, with a constant increase in incidence. Systemic treatment is not very effective, and sorafenib has been the only approved treatment for ten years. In the last six years, several drugs have been approved and in particular, just recently, a drug combination has become one of the four approved first-line treatments of HCC. Dasatinib is a multi-targeted inhibitor clinically approved for use in leukaemia. Currently, there are numerous clinical trials to evaluate dasatinib efficacy in different types of solid tumours alone or in combination with other compounds, but none in HCC. Different pre-clinical studies evaluated the efficacy of dasatinib in HCC, showing promising effects *in vivo* and *in vitro* with limitations due to the activation of not-targeted pathways that reduced the overall efficacy [34, 35, 276, 282].

So far, there are no clinical trials to evaluate the efficacy of ITCs in HCC because of a lack of pre-clinical evidences. ITCs and combination therapy with chemotherapy drugs may represent as a valuable advance for the treatment of HCC. Therefore, dasatinib efficacy in HCC may be improved with the addition of the broad ITCs anticancer activity, improving the overall treatment efficacy in HCC. This thesis investigated the possibility of combining ITCs and chemotherapeutic agents to treat HCC, focusing on PDc that showed a promising synergistic activity.

8.2 Key findings

8.2.1 ITCs improve anticancer activity of TKIs

The results presented in Chapter 3 support the hypothesis that ITCs can improve the anticancer activity of chemotherapeutic agents. Furthermore, the first objective of thesis was achieved, identifying PEITC as the most efficient ITC in synergistically improving the anticancer activity of dasatinib in the hepatoma cell line HepG2. Also, the BITC and dasatinib combination may be interesting for further studies. ITCs may support the action of chemotherapeutic agents by simultaneously targeting multiple pathways, which are exploited by cancerous cells in their uncontrolled growth. On the other hand, the improved cytotoxic effect of the drug combinations was also observed in the immortalised hepatocytes cell line HHL-5. This result underlines the fact that multiple drugs can also target normal cells. Therefore it is essential to carefully study the pharmacokinetics of these drug combinations to modulate the drug concentrations to exploit the anticancer potential while also reducing potential toxic effects on non-targeted tissues.

8.2.2 PDc reduces tumour growth through DNA damage, cell cycle arrest, and oxeiptosis

In Chapter 4, the effect of PDc on DNA damage, cell cycle arrest, and oxeiptosis was investigated. The results highlighted the ability of PDc to reduce the growth of the HepG2 cell line. The main effect can be attributed to the increase of ROS that perturbs the already imbalanced redox status of the cancerous cells. The presence of increased ROS is also confirmed by the increased oxidation of GSH, which reduces the ability of the cell to detoxify from H_2O_2 production, which negatively impact on tumour cell health. ROS are partially responsible for DNA damage, also playing a crucial role in the induction of cell cycle arrest followed by mitotic catastrophe and induction of oxeiptosis. It is known that DNA damage is strictly related to the induction of both cell cycle arrest and programmed cell death. At the same time, cell cycle arrest, in particular the mitotic catastrophe, culminates with programmed cell death. The antioxidant pre-treatment showed that ROS represent the cause of mitotic catastrophe and oxeiptosis, but not of DNA damage through Chk2 and p53 activation. Therefore, it is not clear what is the role of DNA damage in these phenomena. It could be hypothesised that the antioxidant treatment reduced the PDc-induced DNA damage only to a certain extent that results in a reversible effect.

8.2.3 PDc reduces metastatic potential

In Chapter 5, the effect of PDc on the metastatic potential of HepG2 cells was investigated. PDc was shown to target the Src/FAK complex, leading to inhibition of STAT3 signalling with a consequent increased expression of E-cadherin and diminished expression of N-cadherin. As discussed, the cadherin switch is an important event in the EMT mechanism that potentiates the metastatic potential of solid tumours. Indeed, the ability of HepG2 cells to migrate, invade, adhere, and colonise was strongly impaired in the presence of PDc. Moreover, the growth of HepG2 xenograft in the in-ovo CAM assay was reduced with a diminished ability to invade the surrounding membrane. FAK has a fundamental role in the formation of focal adhesions to provide cells with migratory capabilities [352]. FAK activation has also been correlated with the downregulation of p53, increasing the survival of cancerous cells that avoid apoptosis [275, 287]. STAT3 modulates DNA damage response and is correlated with cytoprotection; its downregulation makes cells sensitive to oxidative stress, leading to DNA damage evidenced by increased activation of Chk2 [353]. Therefore, the effect of PDc on c-Src/FAK/STAT3 signalling can also be linked to increased p53 and Chk2 activation related to DNA damage, which increases with concomitant induction of oxidative stress. This finding further confirms the ability of PDc to target multiple pathways to result in increased anticancer activity.

8.2.4 PDc decreases tumour-induced angiogenesis

The efficacy of PDc on angiogenesis inhibition was investigated in Chapter 5 by studying the effects of conditioned medium (CM). CM was concentrated from PDc treated HepG2 cells to evaluate the effect on secreted angiogenic factors and to evaluate the effect on HUVECs cells' behaviour *in vitro* and on angiogenesis *in vivo*, using the yolk sac membrane (YSM) model. The effects of CM indicated that PDc reduced the tumour cells' secretion of pro-angiogenic factors. The reduced secretion may be associated with the c-Src/FAK pathway that plays a role in the transcription of angiogenin, VEGF and CXCL16 through the STAT3 activation of HIF-1α. Moreover, angiogenin has been previously associated with focal adhesion dynamics, playing a role in forming stress fibres involved in cell motility [354]. Angiogenin can be internalised by receptor-mediated endocytosis and, in the cytoplasm, it interacts with actin fibres for the formation of focal adhesion complexes. Furthermore, angiogenin has been associated with the regulation of cell migration in breast cancer cells, interacting on the cell surface to regulate plasmin formation [355]. Therefore, the

reduction of angiogenin secretion induced by PDc can also have a detrimental effect on cell migration through a negative feedback loop on the formation of adhesion complexes.

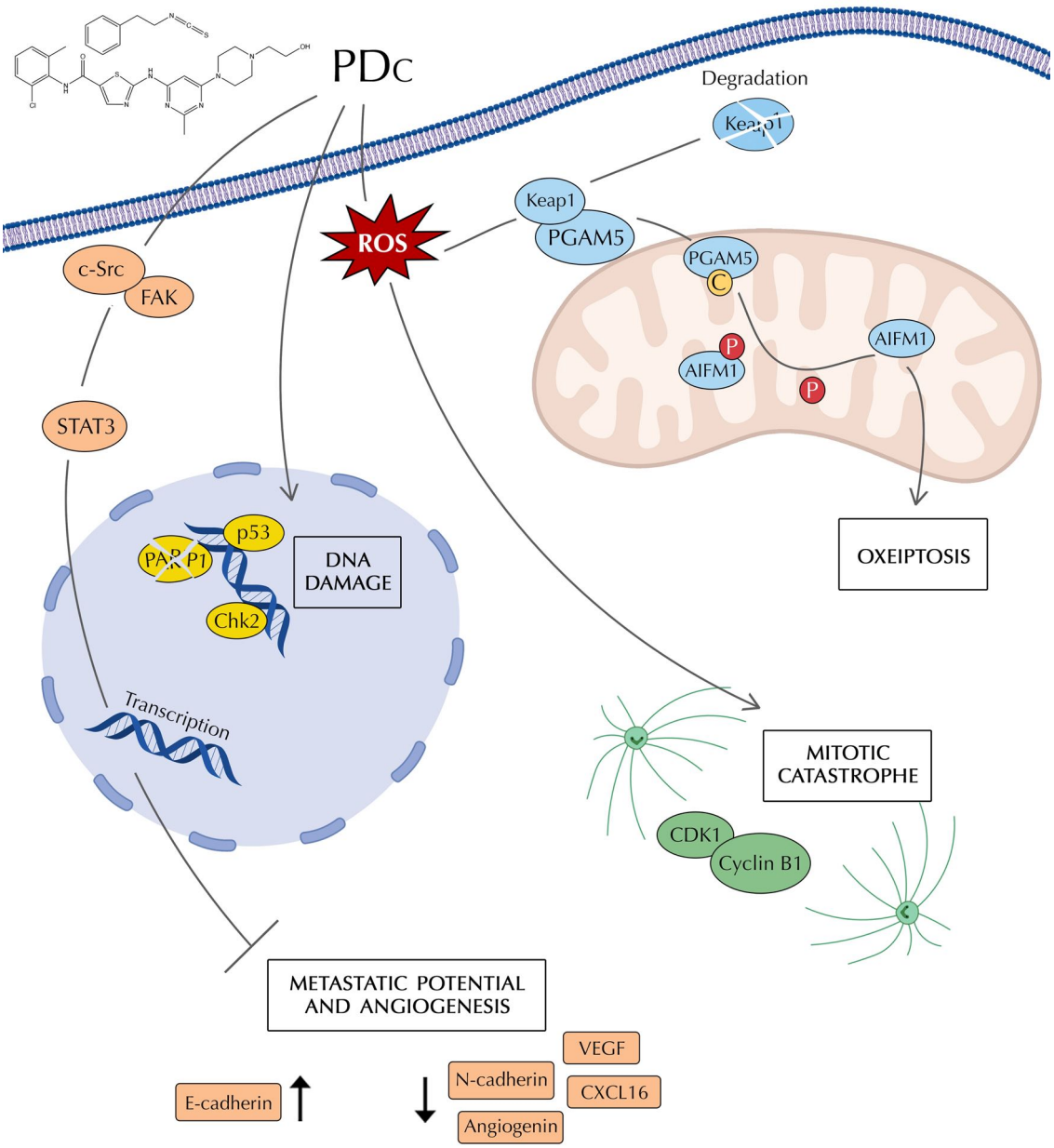

FIGURE 8.1 | Putative mechanism of PDc in cancer therapeutics.
PDc targets c-Src/FAK pathway to reduce the metastatic potential and tumour induced angiogenesis; PDc directly induces DNA damage; PDc induces ROS production that lead to oxeiptosis and mitotic catastrophe.

8.2.5 PDc reduces tumour volume *in vivo*

The fifth and last objective was to evaluate PDc in an *in vivo* setting, evaluating the efficacy and safety of the drug combination. Chapter 7 presented the preliminary results of a

murine syngeneic model. *In vivo* work is often carried out using mouse models. This step is fundamental in pre-clinical studies to evaluate the efficacy and safety of a drug before reaching human studies. The results showed that PDc can effectively inhibit the growth of a tumour mass composed of HCC cells *in vivo* without eliciting detrimental effects on the weight of the mouse or inducing apparent liver tissue damage. These preliminary results confirmed that ITCs might exert a promising role in enhancing the chemotherapeutic drugs' anticancer activity.

8.3 Limitations

Although the results of this study highlight the possibility of using ITCs to improve the efficacy of chemotherapeutic agents, there are several limitations. Most of the experiments were carried out on a single cell line, and in particular, the molecular mechanism of PDc action was observed only in HepG2 cells. A cell line is derived from a tumour originating in a patient with a specific age, sex, grade of cancer, and pathology. Therefore, a single cell line cannot fully represent all the phenotypes characterising a cancerous disease's complexity. HepG2 is the most used cell line, and according to a recent review it accounts for 76% of the manuscripts that use hepatic tumour cell lines found in the PubMed database [356]. The American Type Culture Collection (ATCC) describes HepG2 as a "cell line derived from the HCC of a 15 year old caucasian male" [357]. Surprisingly, there is a controversy regarding the origin of HepG2 cells; a report from 2009 describes this cell line as derived from hepatoblastoma (HB) instead of HCC [358]. Nevertheless, recent studies published in reputable journals use the HepG2 cell line as an HCC model [36, 359-364].

The use of RNA silencing techniques could benefit further mechanistic investigation into the anticancer activity of PDc. RNA interference is a valuable technique that allows the knockdown of the expression of specific genes post-transcriptionally, elucidating the role of the protein in mechanistic studies [365]. RNA silencing techniques may have contributed to further insights into the role of key targets involved in the molecular mechanism of mitotic catastrophe, oxeiptosis, and Src/FAK/STAT3 signalling described in the previous chapters.

The *in vivo* work was limited in the first instance because of the absence of an extensive pilot study to select the optimal parameters (i.e. PDc concentration, cell number, treatment time) to achieve a significant result. Furthermore, the murine syngeneic model work was limited to a single experiment, leading to high variability. More experiments could yield

more robust statistical evidence of PDc synergistic action compared to the single drug treatment.

8.4 Future research

Interesting insights for future research are included below.

8.4.1 Oxeiptosis and hormetic effect

As discussed, the Nrf2-Keap1 complex is a crucial target in the ITCs' antioxidant activity; indeed Nrf2 ubiquitination is inhibited, and consequently it translocates to the nucleus to activate the transcription of antioxidant genes. On the other hand, high doses of ITCs activate an alternative pathway where the complex Keap1-PGAM5 plays a fundamental role in the activation of oxeiptosis. The complex Nrf2-Keap1-PGAM5 may have a role in the observed hormetic effect, which characterises the ITCs' dual activity in cancer prevention and therapy. Therefore, the complex Nrf2-Keap1-PGAM5 may be an exciting topic for further research to understand the relevance of ITCs in clinical applications.

8.4.2 Mitotic catastrophe and oxeiptosis

It is unclear whether a link exists between mitotic catastrophe and oxeiptosis. Mitotic catastrophe and oxeiptosis may be separate events with ROS as a communal trigger, or the latter could be the consequence of the other one. Oxeiptosis has been recently identified, and only a few reports describe the Keap1-PGAM5-AIFM1 pathway. Oxeiptosis role in the ensemble of all programmed cell death mechanisms is not clarified. On the other hand, the link between mitotic catastrophe and programmed cell death is also unclear. Some reports consider mitotic catastrophe as a modality of cell death on its own; others assert that it is a process that leads to apoptosis or necrosis [366]. In some cases, mitotic catastrophe is not concomitant with caspase activation and cytochrome c release. Indeed, mitotic catastrophe can lead to a caspase-independent programmed cell death [367]. Therefore, it is likely that oxeiptosis could be the consequence of mitotic catastrophe, representing an appealing topic for further investigations.

8.4.3 PDc effect on cancerous EMT

As discussed in Chapter 5, PDc targets the cadherin switch through c-Src/FAK/STAT3 signalling to inhibit the cancerous EMT. In previous works, the JAK/STAT3 pathway has

been found to be required for the TGF-β/Smad signalling [368]. It has been determined that STAT3 inhibition lead to reduced TGF-β1-induced p-Smad3, Snail, and MMP2 expression. Indeed, PEITC has been previously associated with the inhibition of EMT through suppression of Smad pathway [138]. The effect of STAT3 effect on the cadherin switch has been linked with Twist activation in HCC cells [369]. PDc could exert its anti-metastatic action through Smad, Snail, and Twist to reduce the potential of cancerous cells to activate the EMT program to invade new tissues. Therefore, the above mentioned targets may open new prospects for PDc anticancer activity.

8.4.4 Omics and single-cell analysis approaches

Omics and single-cell analysis could be a useful approaches that could help to investigate the mechanisms aforementioned and also to investigate potential new mechanisms of action. The omics approach in medical research is a useful strategy that allows the analysis of pools of biological molecules and their interactions [370]. Omics analysis can be applied to understand the effect of PDc, identifying new targets that the drug combination may affect, thus deepening the understanding mechanism of action of the combination therapy. The omics approaches are able to generate enormous amount of data (e.g. next generation sequencing (NGS) technologies for genomics and transcriptomics, mass spectrometry for proteomics) [371]; genome (WGS), exome sequencing (WES) and complete transcriptome sequencing (RNA-seq) are useful to determine the interactions between cell molecular components [372]. NGS technologies can be employed to study the effect of PDc on cell culture or pre-clinical *in vivo* models to highlight specific genes targeted by the drug combination. Understanding the relationship between cancer mutations and PDc action could give insights on the most susceptible tumours to this type of treatment. Proteomics analysis using mass spectrometry can identify peptide sequence, protein abundance, post-translational modifications, and protein interactions [373]. In this instance, proteomics analysis can be employed to obtain more detailed information regarding the changes in the activity and kinetics of proteins secreted in the conditioned medium after PDc treatment. Moreover, the emergent single-cell analysis can reveal additional information regarding the nature of the cells present in a complex tissue [374]. For example, tumour samples derived from pre-clinical studies in mice can be dissected and the cell populations analysed, understanding how the drug combination affect the tumour heterogeneity and the cell origin in metastasis models.

8.5 Conclusion

In conclusion, ITCs have shown to be a promising potential addition to the treatment of HCC when combined with chemotherapeutic agents. In particular, PEITC was demonstrated to enhance the activity of dasatinib. The novel combination inhibited the growth and proliferation of HepG2 cells and reduced the volume of an HCC *in vivo*. PDc induced DNA damage, and the increased production of ROS led to cell cycle arrest with a consequent mitotic catastrophe. Moreover, ROS production induced cell death through the novel form of programmed cell death, oxeiptosis. PDc reduced the HCC metastatic potential targeting the processes that are crucial for the metastasis development (i.e. migration, invasion, adhesion, and colony formation). PDc reduced the c-Src/FAK/STAT3 signalling to contrast the process of cadherin switch, which is a process that plays a crucial role in the malignant EMT to confer cancerous cells the ability to form a metastatic disease. Finally, PDc was associated with a decrease of the ability of cancerous cells to induce the formation of new vessels, a crucial step in tumour progression and metastasis.

Future work is needed to better understand the complex molecular mechanism of the synergistic anticancer activity and the drug behaviour in *in vivo* pre-clinical models. Determining the pharmacokinetics and pharmacodynamics is crucial to pursue the clinical application of ITCs. ITCs may represent a breakthrough in cancer therapy, enhancing the efficacy of clinically approved chemotherapeutic agents.

Appendices

A 1 Comparison of drug vehicle concentrations

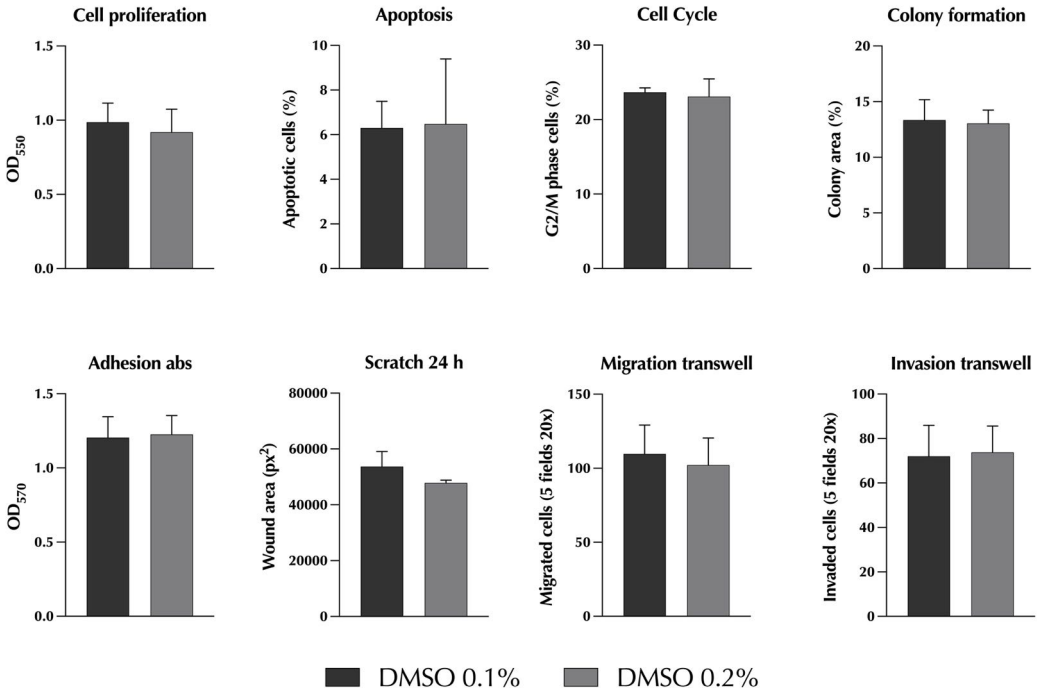

FIGURE A1 | Effect of DMSO concentrations on HepG2 cell line.

There is no significant difference between the DMSO concentration used in single drugs and combination treatments.

A 2 Optimisation of HepG2 spheroids formation

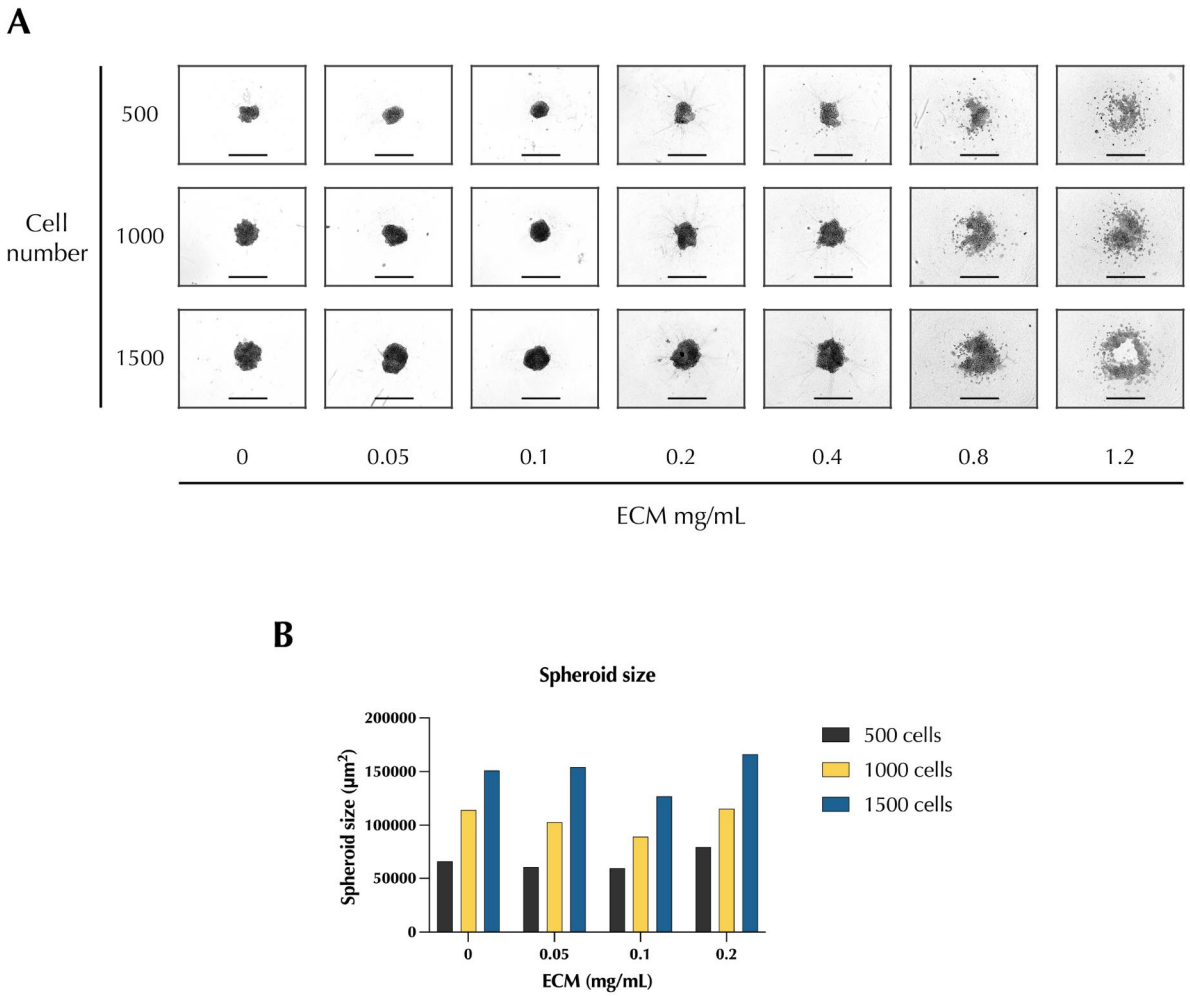

FIGURE A2 | Optimisation of HepG2 spheroids formation.

A 3 Gating strategy for PI staining for flow cytometry cell cycle analysis

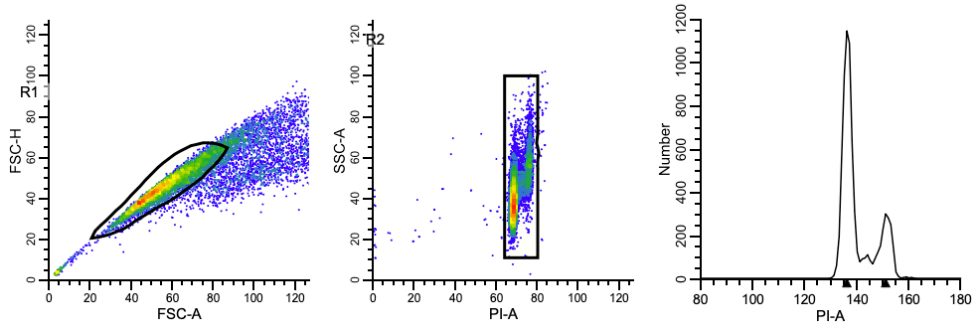

FIGURE A3 | Gating strategy for Propidium Iodide staining for detection of cell cycle phases in HepG2.

A 4 Compensation and controls for Annexin V and PI staining for flow cytometry apoptosis analysis

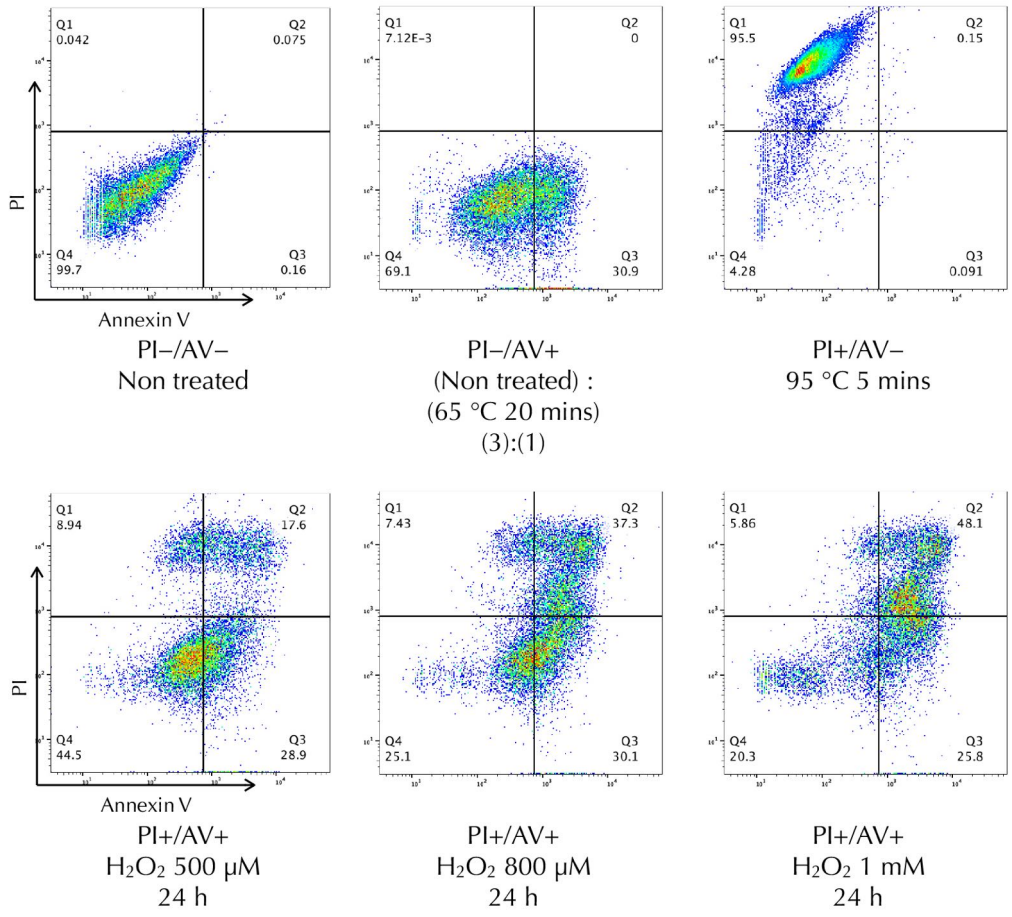

FIGURE A4 | Representative compensation data and positive control for Annexin V and Propidium Iodide apoptosis assay in HepG2.

A 5 Full blots images of Western Blot

A 5.1 PARP1

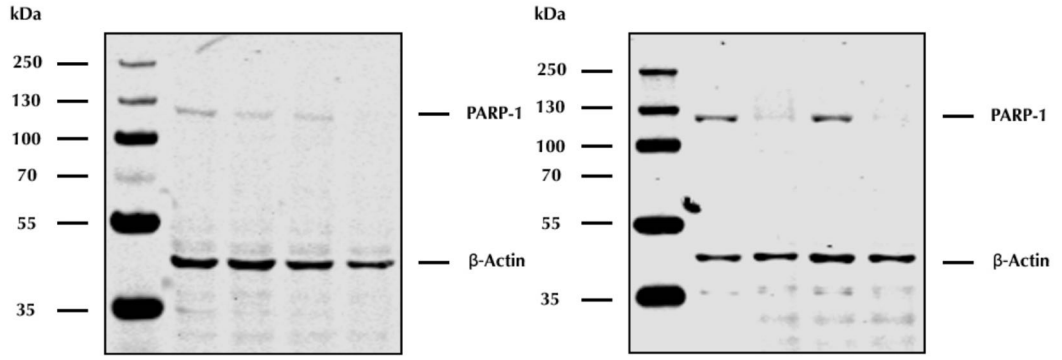

FIGURE A5 | Representative full blots of PARP1.

Samples order **Left**: Control, PEITC 12 μM, dasatinib 10 μM, PEITC + dasatinib. Samples order **right** Control, PEITC + dasatinib, NAC 20 mM, NAC + PEITC + dasatinib.

A 5.2 Chk2

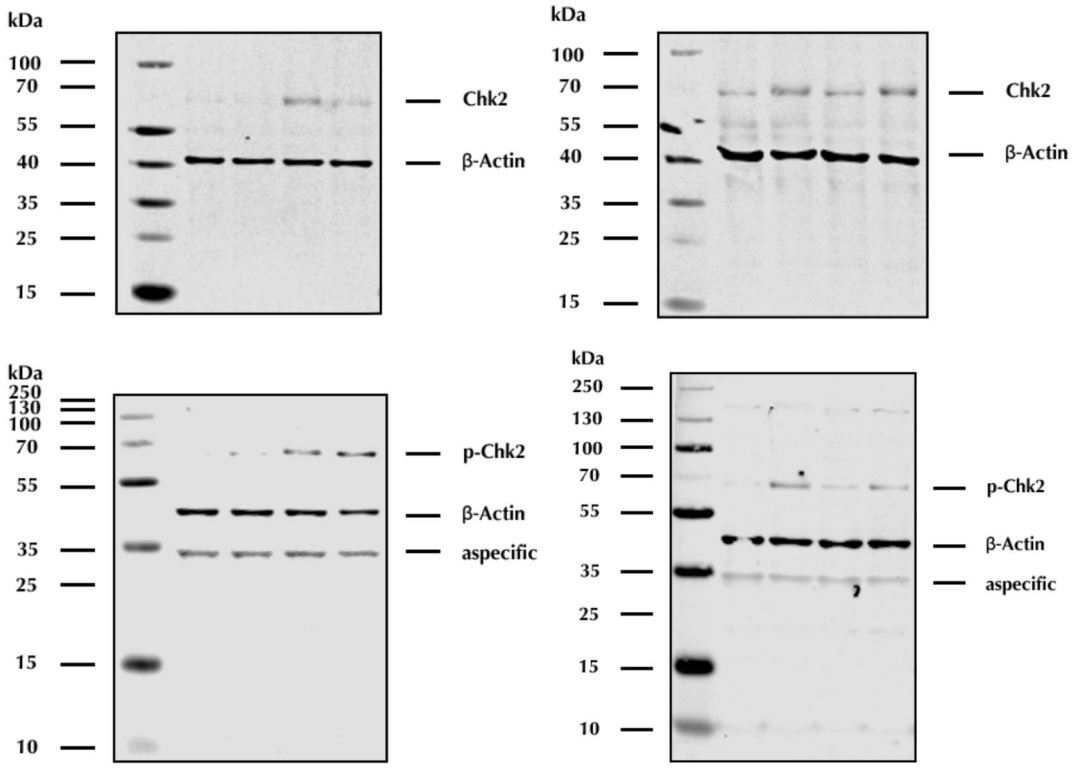

FIGURE A6 | Representative full blots of Chk2 and p-Chk2 (Thr-68).

Samples order **Left**: Control, PEITC 12 μM, dasatinib 10 μM, PEITC + dasatinib. Samples order **right:** Control, PEITC + dasatinib, NAC 20 mM, NAC + PEITC + dasatinib.

A 5.3 p53

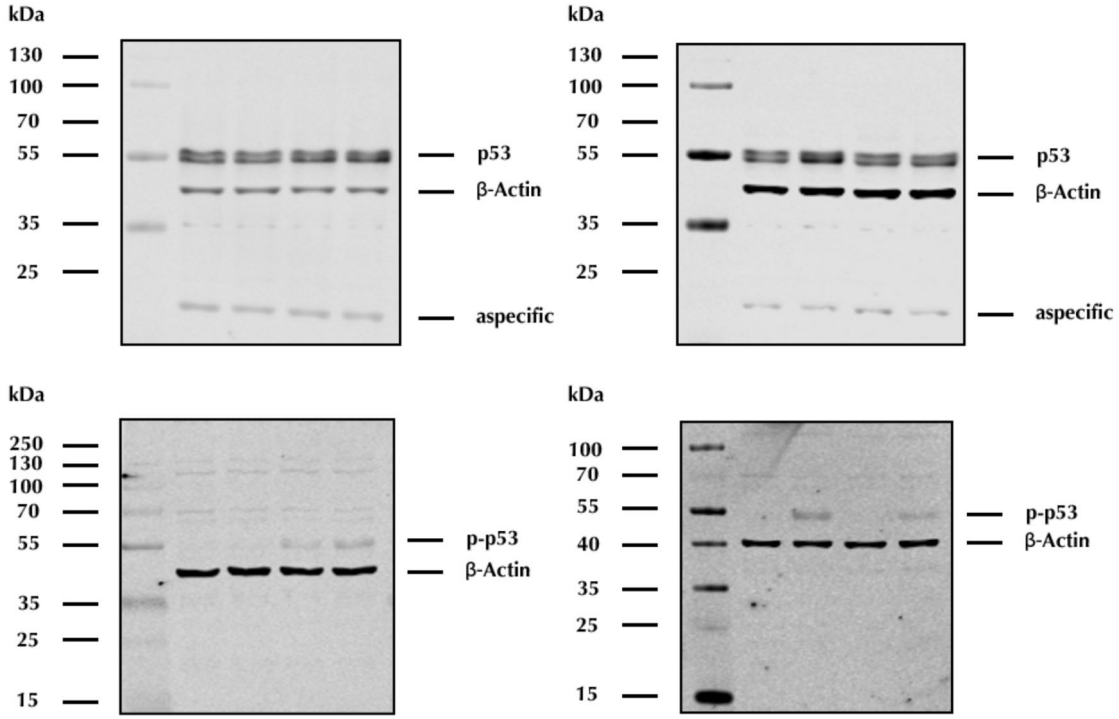

FIGURE A7 | Representative full blots of p53 and p-p53 (Ser-15)

Samples order **left**: Control, PEITC 12 µM, dasatinib 10 µM, PEITC + dasatinib. Samples order **right:** Control, PEITC + dasatinib, NAC 20 mM, NAC + PEITC + dasatinib.

A 5.4 CDK1

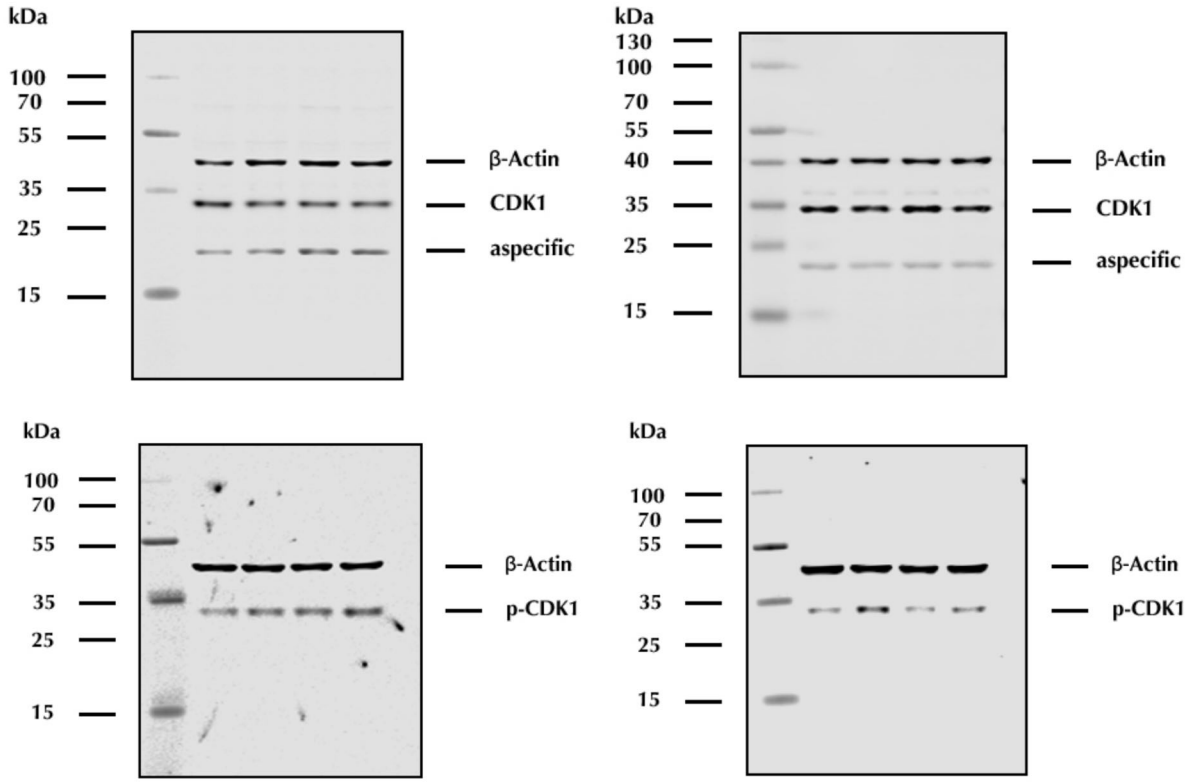

FIGURE A8 | Representative full blots of CDK1 and p-CDK1 (Thr-161).
Samples order **left**: Control, PEITC 12 μM, dasatinib 10 μM, PEITC + dasatinib. Samples order **right:** Control, PEITC + dasatinib, NAC 20 mM, NAC + PEITC + dasatinib.

A 5.5 Cyclin B1

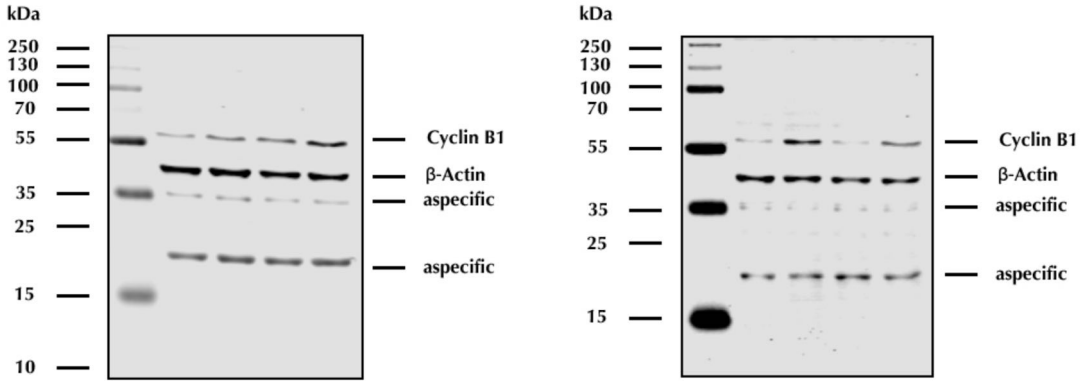

FIGURE A9 | Representative full blots of Cyclin B1.
Samples order **left**: Control, PEITC 12 μM, dasatinib 10 μM, PEITC + dasatinib. Samples order **right:** Control, PEITC + dasatinib, NAC 20 mM, NAC + PEITC + dasatinib.

A 5.6 Caspase 3

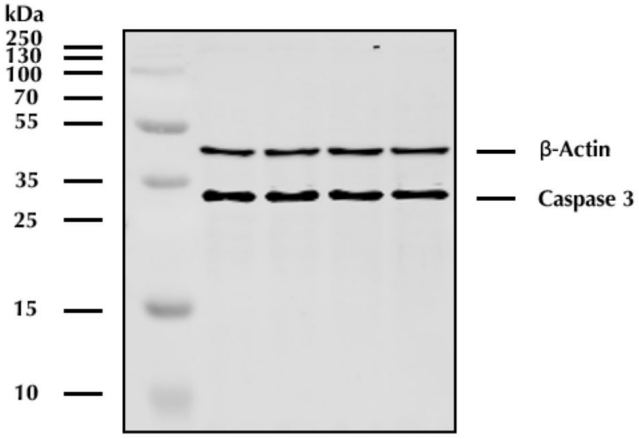

FIGURE A10 | Representative full blot of Caspase 3.
Samples order: Control, PEITC 12 μM, dasatinib 10 μM, PEITC + dasatinib.

A 5.7 Caspase 9

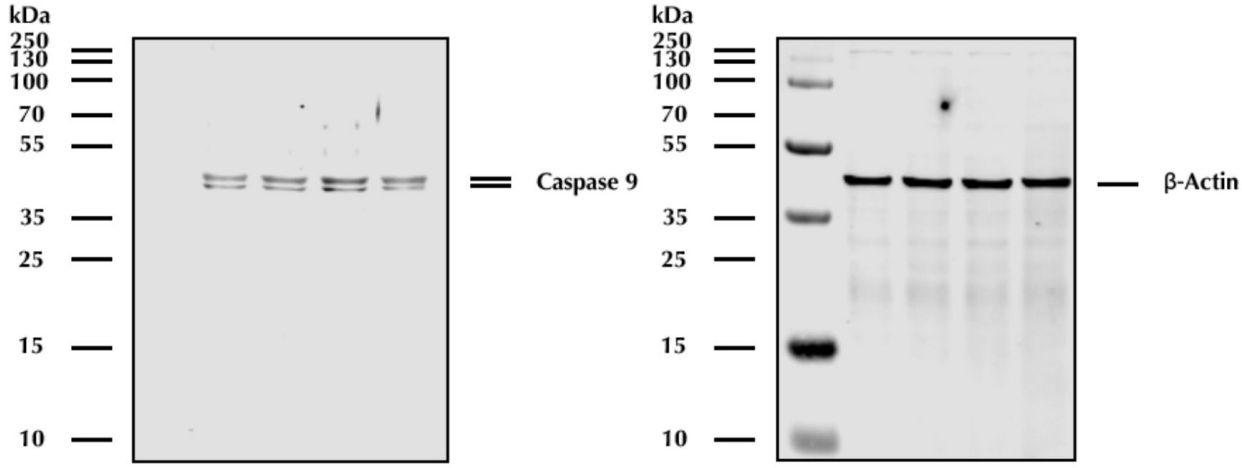

FIGURE A11 | Representative full blots of Caspase 9.
Samples order: Control, PEITC 12 μM, dasatinib 10 μM, PEITC + dasatinib. Caspase-9 and β-actin bands are on the same blot on different near infrared channels, but as they have similar molecular weight they cannot be on the same black and white image.

A 5.8 Cytochrome C

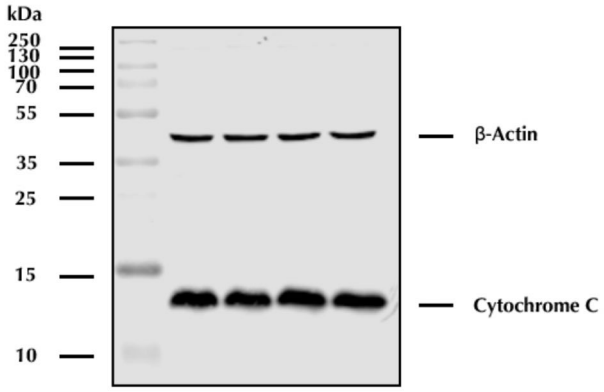

FIGURE A12 | Representative full blot of Cytochrome C.
Samples order: Control, PEITC 12 μM, dasatinib 10 μM, PEITC + dasatinib.

A 5.9 Keap1

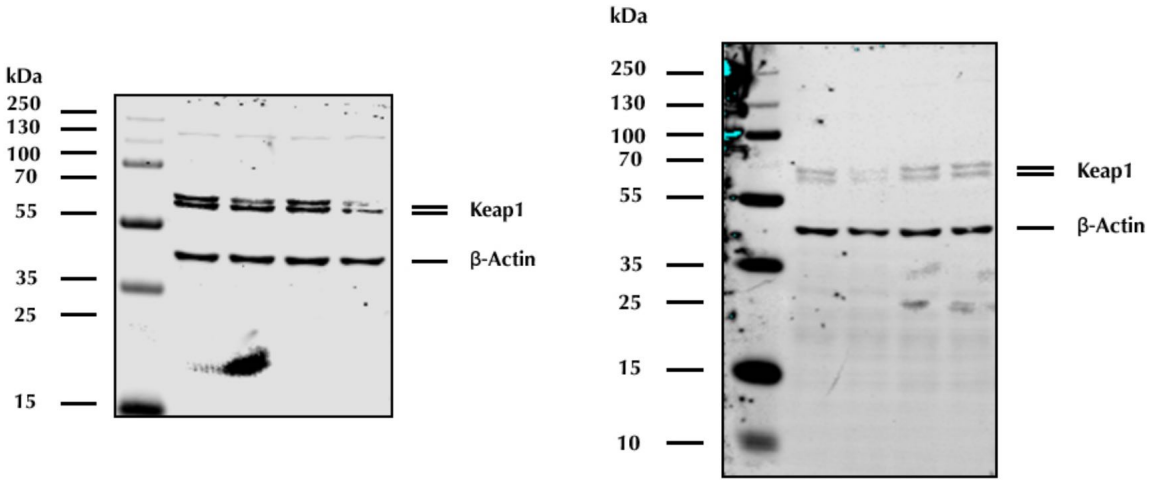

FIGURE A13 | Representative full blots of Keap1.
Samples order **left**: Control, PEITC 12 μM, dasatinib 10 μM, PEITC + dasatinib. Samples order **right:** Control, PEITC + dasatinib, NAC 20 mM, NAC + PEITC + dasatinib.

A 5.10 PGAM5

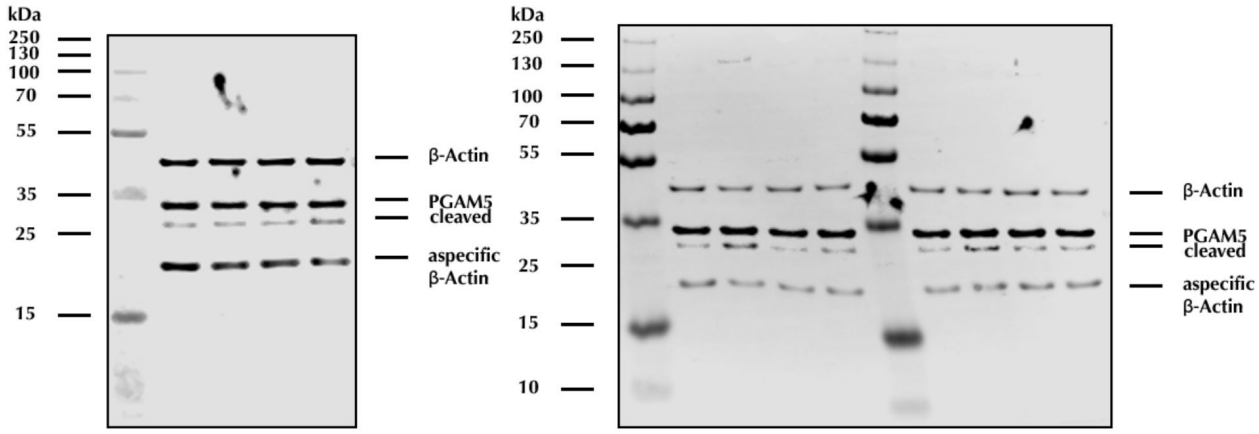

FIGURE A14 | Representative full blots of PGAM5.

Samples order **left**: Control, PEITC 12 µM, dasatinib 10 µM, PEITC + dasatinib. Samples order **right:** Control, PEITC + dasatinib, NAC 20 mM, NAC + PEITC + dasatinib.

A 5.11 AIFM

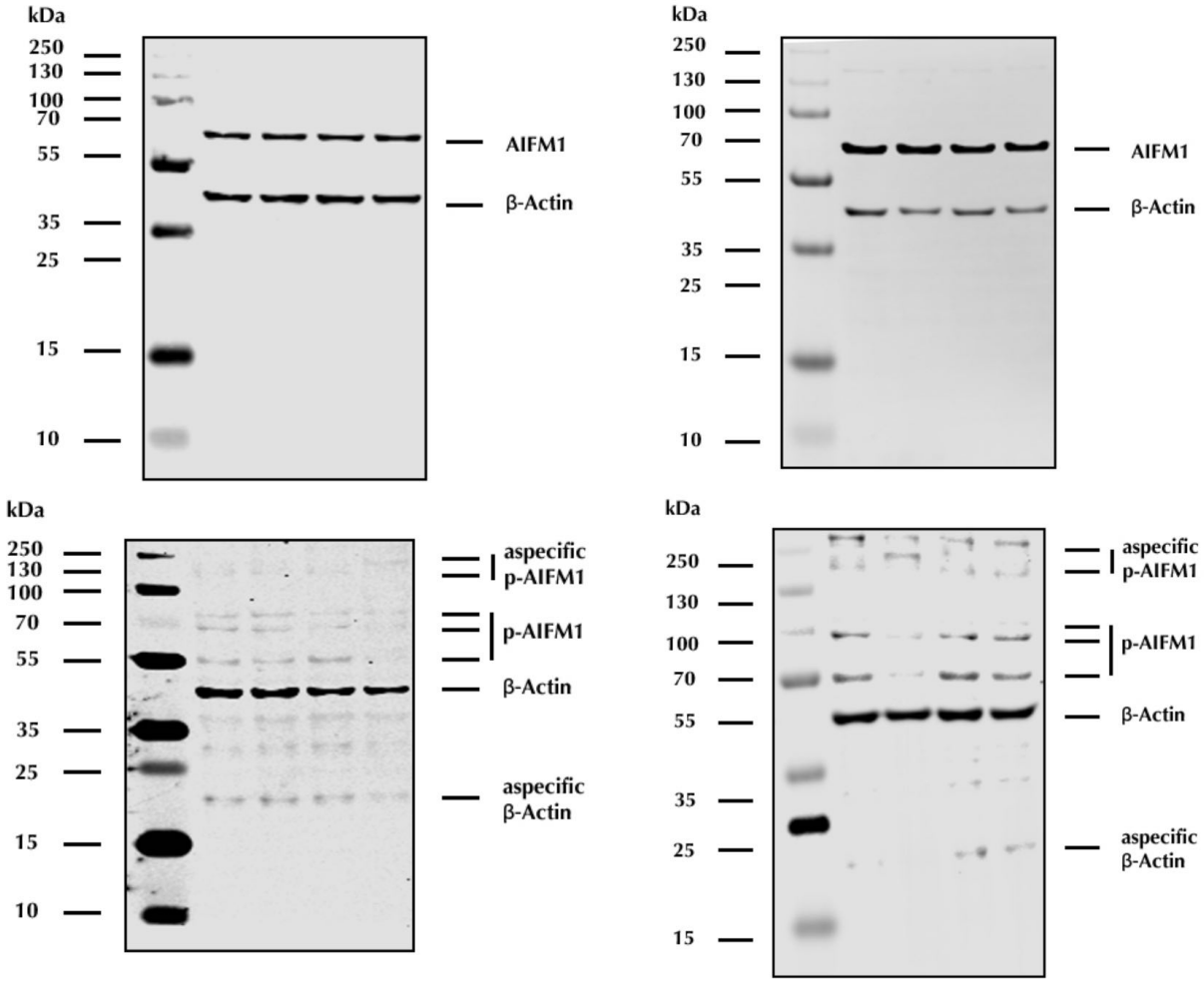

FIGURE A15 | Representative full blots of AIFM1 and p-AIFM1 (Ser-116).
Samples order **left**: Control, PEITC 12 μM, dasatinib 10 μM, PEITC + dasatinib. Samples order **right:** Control, PEITC + dasatinib, NAC 20 mM, NAC + PEITC + dasatinib.

A 5.12 FAK

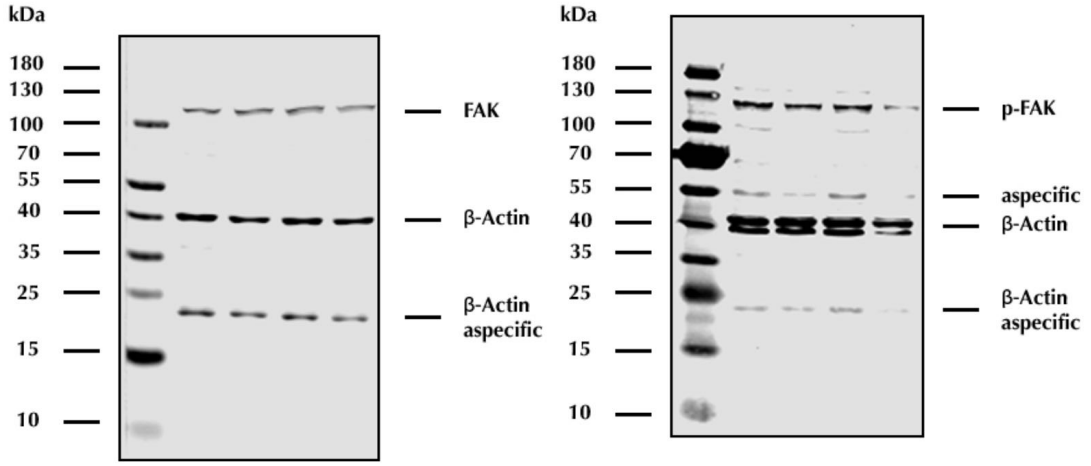

FIGURE A16 | Representative full blots of FAK and p-FAK (Tyr-397).
Samples order: Control, PEITC 12 μM, dasatinib 10 μM, PEITC + dasatinib.

A 5.13 STAT3

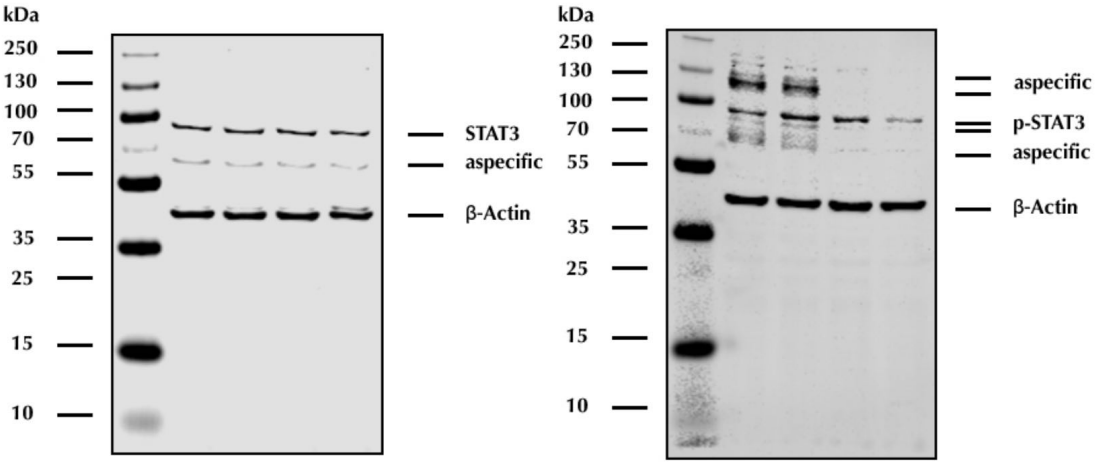

FIGURE A17 | Representative full blots of STAT3 and p-STAT3 (Tyr-705).
Samples order: Control, PEITC 12 μM, dasatinib 10 μM, PEITC + dasatinib.

A 5.14 E-Cadherin

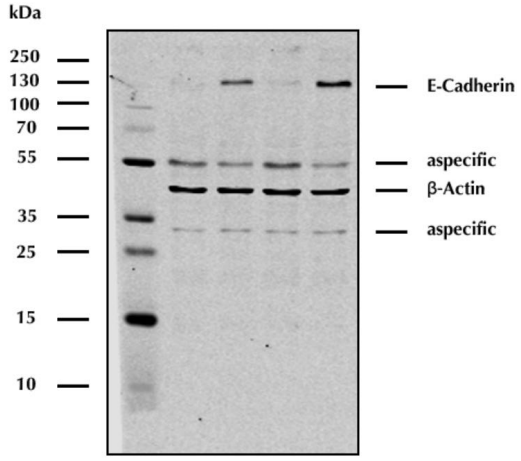

FIGURE A18 | Representative full blot of E-cadherin.
Samples order: Control, PEITC 12 µM, dasatinib 10 µM, PEITC + dasatinib.

A 5.15 N-Cadherin

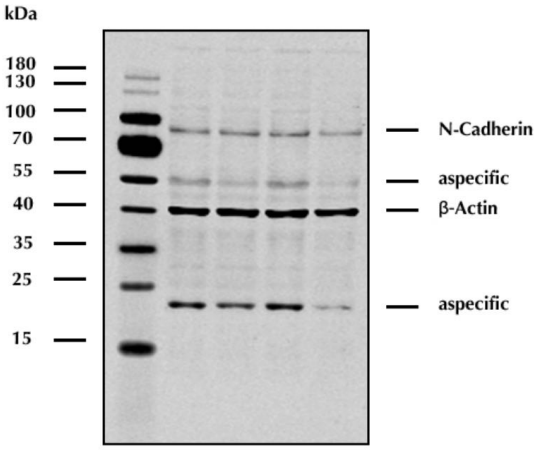

FIGURE A19 | Representative full blot of N-cadherin.
Samples order: Control, PEITC 12 µM, dasatinib 10 µM, PEITC + dasatinib.

References

1. World Health Organisation, Cancer fact sheet. Accessed June 2023; Available from: https://www.who.int/news-room/fact-sheets/detail/cancer.
2. Hanahan, Douglas and Robert A Weinberg, Hallmarks of Cancer: The Next Generation. Cell, 2011. 144(5): p. 646-674.
3. Surh, Y. J., Cancer chemoprevention with dietary phytochemicals. Nat Rev Cancer, 2003. 3(10): p. 768-80.
4. Keum, Young-Sam, Woo-Sik Jeong, and A. N. Tony Kong, Chemoprevention by isothiocyanates and their underlying molecular signaling mechanisms. Mutation Research/Fundamental and Molecular Mechanisms of Mutagenesis, 2004. 555(1): p. 191-202.
5. El-Serag, Hashem B., Epidemiology of Hepatocellular Carcinoma. The Liver, 2020: p. 758-772.
6. Cancer Research UK, Liver cancer incidence statistics. Accessed June 2023; Available from: https://www.cancerresearchuk.org/health-professional/cancer-statistics/statistics-by-cancer-type/liver-cancer/incidence#heading-Two.
7. Zhang, Huajun, Wuyang Zhang, Longying Jiang, and Yongheng Chen, Recent advances in systemic therapy for hepatocellular carcinoma. Biomarker Research, 2022. 10: p. 1-21.
8. McGlynn, Katherine A, Jessica L Petrick, and W Thomas London, Global epidemiology of hepatocellular carcinoma: an emphasis on demographic and regional variability. Clinics in liver disease, 2015. 19(2): p. 223-238.
9. Cancer, International Agency for Research on, *Review of human carcinogens*. Vol. 100. 2012: IARC Monographs on the Evaluat.
10. George, E. S., S. Sood, A. Broughton, G. Cogan, M. Hickey*, et al.*, The Association between Diet and Hepatocellular Carcinoma: A Systematic Review. Nutrients, 2021. 13(1).
11. Balogh, Julius, David Victor, Emad H. Asham, Sherilyn Gordon Burroughs, Maha Boktour*, et al.*, Hepatocellular carcinoma: a review. Journal of Hepatocellular Carcinoma, 2016. 3(null): p. 41-53.
12. Ding, X. X., Q. G. Zhu, S. M. Zhang, L. Guan, T. Li*, et al.*, Precision medicine for hepatocellular carcinoma: driver mutations and targeted therapy. Oncotarget, 2017. 8(33): p. 55715-55730.

13. Tummala, K. S., M. Brandt, A. Teijeiro, O. Graña, R. F. Schwabe*, et al.*, Hepatocellular Carcinomas Originate Predominantly from Hepatocytes and Benign Lesions from Hepatic Progenitor Cells. Cell Rep, 2017. 19(3): p. 584-600.
14. Schneller, Doris and Peter Angel, Cellular origin of hepatocellular carcinoma. Exon Publications, 2019: p. 1-28.
15. Zender, L., M. S. Spector, W. Xue, P. Flemming, C. Cordon-Cardo*, et al.*, Identification and validation of oncogenes in liver cancer using an integrative oncogenomic approach. Cell, 2006. 125(7): p. 1253-67.
16. Tang, Y., K. Kitisin, W. Jogunoori, C. Li, C. X. Deng*, et al.*, Progenitor/stem cells give rise to liver cancer due to aberrant TGF-beta and IL-6 signaling. Proc Natl Acad Sci U S A, 2008. 105(7): p. 2445-50.
17. Nikolaou, K. C., P. Moulos, G. Chalepakis, P. Hatzis, H. Oda*, et al.*, Spontaneous development of hepatocellular carcinoma with cancer stem cell properties in PR-SET7-deficient livers. Embo j, 2015. 34(4): p. 430-47.
18. Sia, D., A. Villanueva, S. L. Friedman, and J. M. Llovet, Liver Cancer Cell of Origin, Molecular Class, and Effects on Patient Prognosis. Gastroenterology, 2017. 152(4): p. 745-761.
19. Huang, Ao, Xin-Rong Yang, Wen-Yuan Chung, Ashley R. Dennison, and Jian Zhou, Targeted therapy for hepatocellular carcinoma. Signal Transduction and Targeted Therapy, 2020. 5(1): p. 146.
20. Zhu, Andrew X, Olivier Rosmorduc, TR Evans, Paul J Ross, Armando Santoro*, et al.*, SEARCH: a phase III, randomized, double-blind, placebo-controlled trial of sorafenib plus erlotinib in patients with advanced hepatocellular carcinoma. Journal of Clinical Oncology, 2014, vol. 33, num. 6, p. 559-566, 2014.
21. Johnson, Philip J, Shukui Qin, Joong-Won Park, RT Poon, Jean-Luc Raoul*, et al.*, Brivanib versus sorafenib as first-line therapy in patients with unresectable, advanced hepatocellular carcinoma: results from the randomized phase III BRISK-FL study. J Clin Oncol, 2013. 31(28): p. 3517-3524.
22. Cheng, Ann-Lii, Yoon-Koo Kang, Deng-Yn Lin, Joong-Won Park, Masatoshi Kudo*, et al.*, Sunitinib versus sorafenib in advanced hepatocellular cancer: results of a randomized phase III trial. Journal of clinical oncology, 2013. 31(32): p. 4067-4075.
23. Cainap, Calin, Shukui Qin, Wen-Tsung Huang, Ik Joo Chung, Hongming Pan*, et al.*, Linifanib versus Sorafenib in patients with advanced hepatocellular carcinoma:

results of a randomized phase III trial. Journal of Clinical Oncology, 2015. 33(2): p. 172.

24. Zhu, Andrew X, Masatoshi Kudo, Eric Assenat, Stéphane Cattan, Yoon-Koo Kang*, et al.*, Effect of everolimus on survival in advanced hepatocellular carcinoma after failure of sorafenib: the EVOLVE-1 randomized clinical trial. Jama, 2014. 312(1): p. 57-67.
25. Rimassa, Lorenza, Eric Assenat, Markus Peck-Radosavljevic, Marc Pracht, Vittorina Zagonel*, et al.*, Tivantinib for second-line treatment of MET-high, advanced hepatocellular carcinoma (METIV-HCC): a final analysis of a phase 3, randomised, placebo-controlled study. The Lancet Oncology, 2018. 19(5): p. 682-693.
26. El-Khoueiry, Anthony B, Thomas Yau, Yoon-Koo Kang, Tae-You Kim, Armando Santoro*, et al.*, Nivolumab (NIVO) plus ipilimumab (IPI) combination therapy in patients (Pts) with advanced hepatocellular carcinoma (aHCC): Long-term results from CheckMate 040. 2021, American Society of Clinical Oncology.
27. Scott, Emma C., Andrea C. Baines, Yutao Gong, Rodney Moore, Gulsum E. Pamuk*, et al.*, Trends in the approval of cancer therapies by the FDA in the twenty-first century. Nature Reviews Drug Discovery, 2023. 22(8): p. 625-640.
28. Diabetes, National Institute of, Digestive, and Kidney Diseases, LiverTox: clinical and research information on drug-induced liver injury. Protein Kinase Inhibitors. 2012: National Institute of Diabetes and Digestive and Kidney Diseases.
29. Ferguson, Fleur M. and Nathanael S. Gray, Kinase inhibitors: the road ahead. Nature Reviews Drug Discovery, 2018. 17(5): p. 353-377.
30. Zhang, Jianming, Priscilla L. Yang, and Nathanael S. Gray, Targeting cancer with small molecule kinase inhibitors. Nature Reviews Cancer, 2009. 9(1): p. 28-39.
31. Huang, Liling, Shiyu Jiang, and Yuankai Shi, Tyrosine kinase inhibitors for solid tumors in the past 20 years (2001–2020). Journal of Hematology & Oncology, 2020. 13(1): p. 143.
32. Chen, Ruyin, Qiong Li, Shuaishuai Xu, Chanqi Ye, Tian Tian*, et al.*, Modulation of the tumour microenvironment in hepatocellular carcinoma by tyrosine kinase inhibitors: from modulation to combination therapy targeting the microenvironment. Cancer Cell International, 2022. 22(1): p. 73.
33. Levêque, Dominique, Guillaume Becker, Karin Bilger, and Shanti Natarajan-Amé, Clinical Pharmacokinetics and Pharmacodynamics of Dasatinib. Clinical Pharmacokinetics, 2020. 59(7): p. 849-856.

34. Chang, Alex Y and Miao Wang, Molecular mechanisms of action and potential biomarkers of growth inhibition of dasatinib (BMS-354825) on hepatocellular carcinoma cells. BMC cancer, 2013. 13: p. 1-12.
35. Chang, A. Y. and M. Wang, In-vitro growth inhibition of chemotherapy and molecular targeted agents in hepatocellular carcinoma. Anticancer Drugs, 2013. 24(3): p. 251-9.
36. Xu, L., Y. Zhu, J. Shao, M. Chen, H. Yan*, et al.*, Dasatinib synergises with irinotecan to suppress hepatocellular carcinoma via inhibiting the protein synthesis of PLK1. Br J Cancer, 2017. 116(8): p. 1027-1036.
37. Cheng, C. C., W. T. Chao, J. H. Shih, Y. S. Lai, Y. H. Hsu*, et al.*, Sorafenib combined with dasatinib therapy inhibits cell viability, migration, and angiogenesis synergistically in hepatocellular carcinoma. Cancer Chemother Pharmacol, 2021.
38. Sporn, M. B., N. M. Dunlop, D. L. Newton, and J. M. Smith, Prevention of chemical carcinogenesis by vitamin A and its synthetic analogs (retinoids). Federation proceedings, 1976. 35(6): p. 1332-1338.
39. Wattenberg, Lee W., Chemoprevention of Cancer. Cancer Research, 1985. 45(1): p. 1.
40. Miller, P. E. and D. C. Snyder, Phytochemicals and cancer risk: a review of the epidemiological evidence. Nutr Clin Pract, 2012. 27(5): p. 599-612.
41. Broccoli In Osteoarthritis (Clinicaltrials.gov Identifier NCT03878368).
42. Hosseini, Azar and Ahmad Ghorbani, Cancer therapy with phytochemicals: evidence from clinical studies. Avicenna journal of phytomedicine, 2015. 5(2): p. 84-97.
43. Kumar, Shashank, Deepak Kumar, Audesh Bhat, and Ajay Kumar, Phytochemicals in Clinical Studies: Current Perspective, in Functional Food and Human Health, V. Rani and U.C.S. Yadav, Editors. 2018, Springer Singapore: Singapore. p. 471-511.
44. Harborne, Jeffrey B., *Classes and functions of secondary products from plants*. Chemicals from Plants. 1999: World Scientific / Imperial College Press. 1-25.
45. Mitsiogianni, Melina, Georgios Koutsidis, Nikos Mavroudis, Dimitrios T. Trafalis, Sotiris Botaitis*, et al.*, The Role of Isothiocyanates as Cancer Chemo-Preventive, Chemo-Therapeutic and Anti-Melanoma Agents. Antioxidants (Basel, Switzerland), 2019. 8(4): p. 106.
46. Zhang, Z., R. Bergan, J. Shannon, C. G. Slatore, G. Bobe*, et al.*, The Role of Cruciferous Vegetables and Isothiocyanates for Lung Cancer Prevention: Current

Status, Challenges, and Future Research Directions. Mol Nutr Food Res, 2018. 62(18): p. e1700936.

47. Johnson, I. T., Cruciferous Vegetables and Risk of Cancers of the Gastrointestinal Tract. Mol Nutr Food Res, 2018. 62(18): p. e1701000.
48. Fowke, J. H., F. L. Chung, F. Jin, D. Qi, Q. Cai*, et al.*, Urinary isothiocyanate levels, brassica, and human breast cancer. Cancer Res, 2003. 63(14): p. 3980-6.
49. Abbaoui, B., C. R. Lucas, K. M. Riedl, S. K. Clinton, and A. Mortazavi, Cruciferous Vegetables, Isothiocyanates, and Bladder Cancer Prevention. Mol Nutr Food Res, 2018. 62(18): p. e1800079.
50. Giovannucci, E., E. B. Rimm, Y. Liu, M. J. Stampfer, and W. C. Willett, A prospective study of cruciferous vegetables and prostate cancer. Cancer Epidemiol Biomarkers Prev, 2003. 12(12): p. 1403-9.
51. Li, Y. Z., Z. Y. Yang, T. T. Gong, Y. S. Liu, F. H. Liu*, et al.*, Cruciferous vegetable consumption and multiple health outcomes: an umbrella review of 41 systematic reviews and meta-analyses of 303 observational studies. Food Funct, 2022. 13(8): p. 4247-4259.
52. Crowley, E., N. J. Rowan, D. Faller, and A. M. Friel, Natural and Synthetic Isothiocyanates Possess Anticancer Potential Against Liver and Prostate Cancer In Vitro. Anticancer Res, 2019. 39(7): p. 3469-3485.
53. Vaughn, Steven F. and Mark A. Berhow, Glucosinolate hydrolysis products from various plant sources: pH effects, isolation, and purification. Industrial Crops and Products, 2005. 21(2): p. 193-202.
54. Traka, Maria and Richard Mithen, Glucosinolates, isothiocyanates and human health. Phytochemistry Reviews, 2009. 8: p. 269-282.
55. Hecht, Stephen S., Chemoprevention of Cancer by Isothiocyanates, Modifiers of Carcinogen Metabolism. The Journal of Nutrition, 1999. 129(3): p. 768S-774S.
56. Bayat Mokhtari, R., N. Baluch, T. S. Homayouni, E. Morgatskaya, S. Kumar*, et al.*, The role of Sulforaphane in cancer chemoprevention and health benefits: a mini-review. J Cell Commun Signal, 2018. 12(1): p. 91-101.
57. Halkier, Barbara Ann and Liangcheng Du, The biosynthesis of glucosinolates. Trends in Plant Science, 1997. 2(11): p. 425-431.
58. Kissen, Ralph, John T. Rossiter, and Atle M. Bones, The 'mustard oil bomb': not so easy to assemble?! Localization, expression and distribution of the components of the myrosinase enzyme system. Phytochemistry Reviews, 2009. 8(1): p. 69-86.

59. Barba, Francisco J., Nooshin Nikmaram, Shahin Roohinejad, Anissa Khelfa, Zhenzhou Zhu*, et al.*, Bioavailability of Glucosinolates and Their Breakdown Products: Impact of Processing. Frontiers in nutrition, 2016. 3: p. 24-24.
60. Liou, Catherine S., Shannon J. Sirk, Camil A. C. Diaz, Andrew P. Klein, Curt R. Fischer*, et al.*, A Metabolic Pathway for Activation of Dietary Glucosinolates by a Human Gut Symbiont. Cell, 2020. 180(4): p. 717-728.e19.
61. Zhang, Yuesheng and Eileen C. Callaway, High cellular accumulation of sulphoraphane, a dietary anticarcinogen, is followed by rapid transporter-mediated export as a glutathione conjugate. The Biochemical journal, 2002. 364(Pt 1): p. 301-307.
62. Gasper, A. V., A. Al-Janobi, J. A. Smith, J. R. Bacon, P. Fortun*, et al.*, Glutathione S-transferase M1 polymorphism and metabolism of sulforaphane from standard and high-glucosinolate broccoli. Am J Clin Nutr, 2005. 82(6): p. 1283-91.
63. Lamy, E., C. Scholtes, C. Herz, and V. Mersch-Sundermann, Pharmacokinetics and pharmacodynamics of isothiocyanates. Drug Metab Rev, 2011. 43(3): p. 387-407.
64. Bao, Yongping, Wei Wang, Zhigang Zhou, and Changhao Sun, Benefits and risks of the hormetic effects of dietary isothiocyanates on cancer prevention. PloS one, 2014. 9(12): p. e114764-e114764.
65. Calabrese, E. J., I. Iavicoli, and V. Calabrese, Hormesis: Its impact on medicine and health. Human & Experimental Toxicology, 2012. 32(2): p. 120-152.
66. Son, Tae Gen, Simonetta Camandola, and Mark P. Mattson, Hormetic dietary phytochemicals. Neuromolecular medicine, 2008. 10(4): p. 236-246.
67. Calabrese, Edward J., Cancer biology and hormesis: human tumor cell lines commonly display hormetic (biphasic) dose responses. Critical reviews in toxicology, 2005. 35(6): p. 463-582.
68. Calabrese, E. J. and W. J. Kozumbo, The phytoprotective agent sulforaphane prevents inflammatory degenerative diseases and age-related pathologies via Nrf2-mediated hormesis. Pharmacol Res, 2021. 163: p. 105283.
69. Liu, Peng, Mehrnaz Behray, Qi Wang, Wei Wang, Zhigang Zhou*, et al.*, Anti-cancer activities of allyl isothiocyanate and its conjugated silicon quantum dots. Scientific Reports, 2018. 8(1): p. 1084.
70. Mennicke, W. H., K. Gorler, G. Krumbiegel, D. Lorenz, and N. Rittmann, Studies on the metabolism and excretion of benzyl isothiocyanate in man. Xenobiotica, 1988. 18(4): p. 441-7.

71. Vermeulen, M., H. J. van Rooijen, and W. H. Vaes, Analysis of isothiocyanate mercapturic acids in urine: a biomarker for cruciferous vegetable intake. J Agric Food Chem, 2003. 51(12): p. 3554-9.
72. Platz, Stefanie, Carla Kühn, Sonja Schiess, Monika Schreiner, Margrit Kemper*, et al.*, Bioavailability and metabolism of benzyl glucosinolate in humans consuming Indian cress (Tropaeolum majus L.). Molecular Nutrition & Food Research, 2016. 60(3): p. 652-660.
73. Liebes, L., C. C. Conaway, H. Hochster, S. Mendoza, S. S. Hecht*, et al.*, High-performance liquid chromatography-based determination of total isothiocyanate levels in human plasma: application to studies with 2-phenethyl isothiocyanate. Anal Biochem, 2001. 291(2): p. 279-89.
74. Ji, Y. and M. E. Morris, Determination of phenethyl isothiocyanate in human plasma and urine by ammonia derivatization and liquid chromatography-tandem mass spectrometry. Anal Biochem, 2003. 323(1): p. 39-47.
75. Ye, L., A. T. Dinkova-Kostova, K. L. Wade, Y. Zhang, T. A. Shapiro*, et al.*, Quantitative determination of dithiocarbamates in human plasma, serum, erythrocytes and urine: pharmacokinetics of broccoli sprout isothiocyanates in humans. Clin Chim Acta, 2002. 316(1-2): p. 43-53.
76. Song, L., J. J. Morrison, N. P. Botting, and P. J. Thornalley, Analysis of glucosinolates, isothiocyanates, and amine degradation products in vegetable extracts and blood plasma by LC-MS/MS. Anal Biochem, 2005. 347(2): p. 234-43.
77. Yuan, Jian-Min, Irina Stepanov, Sharon E. Murphy, Renwei Wang, Sharon Allen*, et al.*, Clinical Trial of 2-Phenethyl Isothiocyanate as an Inhibitor of Metabolic Activation of a Tobacco-Specific Lung Carcinogen in Cigarette Smokers. Cancer prevention research (Philadelphia, Pa.), 2016. 9(5): p. 396-405.
78. Alumkal, Joshi J., Rachel Slottke, Jacob Schwartzman, Ganesh Cherala, Myrna Munar*, et al.*, A phase II study of sulforaphane-rich broccoli sprout extracts in men with recurrent prostate cancer. Investigational new drugs, 2015. 33(2): p. 480-489.
79. Study to Evaluate the Effect of Sulforaphane in Broccoli Sprout Extract on Breast Tissue (ClinicalTrials.gov Identifier NCT00982319).
80. Zhang, Z., M. Garzotto, E. W. Davis, 2nd, M. Mori, W. A. Stoller*, et al.*, Sulforaphane Bioavailability and Chemopreventive Activity in Men Presenting for Biopsy of the Prostate Gland: A Randomized Controlled Trial. Nutr Cancer, 2020. 72(1): p. 74-87.

81. Atwell, Lauren L., Zhenzhen Zhang, Motomi Mori, Paige Farris, John T. Vetto*, et al.*, Sulforaphane Bioavailability and Chemopreventive Activity in Women Scheduled for Breast Biopsy. Cancer prevention research (Philadelphia, Pa.), 2015. 8(12): p. 1184-1191.
82. Bauman, Julie E, Chiu-Hsieh Hsu, Sara Centuori, Jose Guillen-Rodriguez, Linda L Garland*, et al.*, Randomized crossover trial evaluating detoxification of tobacco carcinogens by broccoli seed and sprout extract in current smokers. Cancers, 2022. 14(9): p. 2129.
83. Egner, Patricia A., Jian-Guo Chen, Adam T. Zarth, Derek K. Ng, Jin-Bing Wang*, et al.*, Rapid and sustainable detoxication of airborne pollutants by broccoli sprout beverage: results of a randomized clinical trial in China. Cancer prevention research (Philadelphia, Pa.), 2014. 7(8): p. 813-823.
84. Verhoeven, D. T., R. A. Goldbohm, G. van Poppel, H. Verhagen, and P. A. van den Brandt, Epidemiological studies on brassica vegetables and cancer risk. Cancer Epidemiol Biomarkers Prev, 1996. 5(9): p. 733-48.
85. Lenzi, M., C. Fimognari, and P. Hrelia, Sulforaphane as a promising molecule for fighting cancer. Cancer Treat Res, 2014. 159: p. 207-23.
86. Zhang, Yuting, Huiting Huang, Libo Jin, and Sue Lin, Anticarcinogenic Effects of Isothiocyanates on Hepatocellular Carcinoma. International Journal of Molecular Sciences, 2022. 23(22): p. 13834.
87. Nian, H., B. Delage, E. Ho, and R. H. Dashwood, Modulation of histone deacetylase activity by dietary isothiocyanates and allyl sulfides: studies with sulforaphane and garlic organosulfur compounds. Environ Mol Mutagen, 2009. 50(3): p. 213-21.
88. Hac, A., J. Brokowska, E. Rintz, M. Bartkowski, G. Wegrzyn*, et al.*, Mechanism of selective anticancer activity of isothiocyanates relies on differences in DNA damage repair between cancer and healthy cells. Eur J Nutr, 2019.
89. Singh, Shivendra V, Anna Herman-Antosiewicz, Ajita V Singh, Karen L Lew, Sanjay K Srivastava*, et al.*, Sulforaphane-induced G2/M phase cell cycle arrest involves checkpoint kinase 2-mediated phosphorylation of cell division cycle 25C. Journal of Biological Chemistry, 2004. 279(24): p. 25813-25822.
90. Visanji, James M., Susan J. Duthie, Lynn Pirie, David G. Thompson, and Philip J. Padfield, Dietary Isothiocyanates Inhibit Caco-2 Cell Proliferation and Induce G2/M Phase Cell Cycle Arrest, DNA Damage, and G2/M Checkpoint Activation. The Journal of Nutrition, 2004. 134(11): p. 3121-3126.

91. Yeh, Yao-Tsung, Hua Yeh, Shu-Hui Su, Jian-Sheng Lin, Kuo-Jui Lee*, et al.*, Phenethyl isothiocyanate induces DNA damage-associated G2/M arrest and subsequent apoptosis in oral cancer cells with varying p53 mutations. Free Radical Biology and Medicine, 2014. 74: p. 1-13.
92. Cheung, Ka Lung, Tin Oo Khor, Siwang Yu, and Ah-Ng Tony Kong, PEITC induces G1 cell cycle arrest on HT-29 cells through the activation of p38 MAPK signaling pathway. The AAPS journal, 2008. 10(2): p. 277.
93. Wu, Xiang, Qing-hua Zhou, and Ke Xu, Are isothiocyanates potential anti-cancer drugs? Acta Pharmacologica Sinica, 2009. 30(5): p. 501-512.
94. Cavell, B. E., S. S. Syed Alwi, A. Donlevy, and G. Packham, Anti-angiogenic effects of dietary isothiocyanates: mechanisms of action and implications for human health. Biochem Pharmacol, 2011. 81(3): p. 327-36.
95. Chen, C. H., Activation and detoxification enzymes: Functions and implications. Activation and Detoxification Enzymes: Functions and Implications, 2013. 9781461410492: p. 1-177.
96. Talalay, P., Chemoprotection against cancer by induction of phase 2 enzymes. Biofactors, 2000. 12(1-4): p. 5-11.
97. Navarro, S. L., F. Li, and J. W. Lampe, Mechanisms of action of isothiocyanates in cancer chemoprevention: an update. Food Funct, 2011. 2(10): p. 579-87.
98. Cheung, K. L. and A. N. Kong, Molecular targets of dietary phenethyl isothiocyanate and sulforaphane for cancer chemoprevention. Aaps j, 2010. 12(1): p. 87-97.
99. Das, B. N., Y. W. Kim, and Y. S. Keum, Mechanisms of Nrf2/Keap1-dependent phase II cytoprotective and detoxifying gene expression and potential cellular targets of chemopreventive isothiocyanates. Oxid Med Cell Longev, 2013. 2013: p. 839409.
100. Dinkova-Kostova, Albena T, W David Holtzclaw, Robert N Cole, Ken Itoh, Nobunao Wakabayashi*, et al.*, Direct evidence that sulfhydryl groups of Keap1 are the sensors regulating induction of phase 2 enzymes that protect against carcinogens and oxidants. Proceedings of the National Academy of Sciences, 2002. 99(18): p. 11908-11913.
101. Myzak, M. C. and R. H. Dashwood, Chemoprotection by sulforaphane: keep one eye beyond Keap1. Cancer Lett, 2006. 233(2): p. 208-18.
102. Sies, H., Oxidative stress: oxidants and antioxidants. Experimental Physiology, 1997. 82(2): p. 291-295.

103. Jacob, Robert A, The integrated antioxidant system. Nutrition research, 1995. 15(5): p. 755-766.
104. Clarke, J. D., R. H. Dashwood, and E. Ho, Multi-targeted prevention of cancer by sulforaphane. Cancer Lett, 2008. 269(2): p. 291-304.
105. Xu, Ying, Xuexiang Han, Yiye Li, Huan Min, Xiao Zhao*, et al.*, Sulforaphane Mediates Glutathione Depletion via Polymeric Nanoparticles to Restore Cisplatin Chemosensitivity. ACS Nano, 2019. 13(11): p. 13445-13455.
106. Fuentes, Francisco, Ximena Paredes-Gonzalez, and Ah-Ng Tony Kong, Dietary Glucosinolates Sulforaphane, Phenethyl Isothiocyanate, Indole-3-Carbinol/3,3′-Diindolylmethane: Antioxidative Stress/Inflammation, Nrf2, Epigenetics/Epigenomics and In Vivo Cancer Chemopreventive Efficacy. Current Pharmacology Reports, 2015. 1(3): p. 179-196.
107. Marks, P. A. and X. Jiang, Histone deacetylase inhibitors in programmed cell death and cancer therapy. Cell Cycle, 2005. 4(4): p. 549-51.
108. Dashwood, Roderick H. and Emily Ho, Dietary agents as histone deacetylase inhibitors: sulforaphane and structurally related isothiocyanates. Nutrition Reviews, 2008. 66(suppl_1): p. S36-S38.
109. Chik, Flora and Moshe Szyf, Effects of specific DNMT gene depletion on cancer cell transformation and breast cancer cell invasion; toward selective DNMT inhibitors. Carcinogenesis, 2010. 32(2): p. 224-232.
110. Saito, Yoshimasa, Yae Kanai, Tohru Nakagawa, Michiie Sakamoto, Hidetsugu Saito*, et al.*, Increased protein expression of DNA methyltransferase (DNMT) 1 is significantly correlated with the malignant potential and poor prognosis of human hepatocellular carcinomas. International Journal of Cancer, 2003. 105(4): p. 527-532.
111. Belinsky, Steven A., Donna M. Klinge, Christine A. Stidley, Jean-Pierre Issa, James G. Herman*, et al.*, Inhibition of DNA Methylation and Histone Deacetylation Prevents Murine Lung Cancer. Cancer Research, 2003. 63(21): p. 7089.
112. Pathania, R., S. Ramachandran, G. Mariappan, P. Thakur, H. Shi*, et al.*, Combined Inhibition of DNMT and HDAC Blocks the Tumorigenicity of Cancer Stem-like Cells and Attenuates Mammary Tumor Growth. Cancer Res, 2016. 76(11): p. 3224-35.
113. Steele, N., P. Finn, R. Brown, and J. A. Plumb, Combined inhibition of DNA methylation and histone acetylation enhances gene re-expression and drug sensitivity in vivo. British Journal of Cancer, 2009. 100(5): p. 758-763.

114. O'Connor, Mark J, Targeting the DNA Damage Response in Cancer. Molecular Cell, 2015. 60(4): p. 547-560.
115. Smith, Joanne, Lye Mun Tho, Naihan Xu, and David A. Gillespie, Chapter 3 - The ATM–Chk2 and ATR–Chk1 Pathways in DNA Damage Signaling and Cancer, in Advances in Cancer Research, G.F. Vande Woude and G. Klein, Editors. 2010, Academic Press. p. 73-112.
116. Cao, Liu, Sangsoo Kim, Cuiying Xiao, Rui-Hong Wang, Xavier Coumoul*, et al.*, ATM–Chk2–p53 activation prevents tumorigenesis at an expense of organ homeostasis upon Brca1 deficiency. The EMBO Journal, 2006. 25(10): p. 2167-2177.
117. Pietenpol, J. A. and Z. A. Stewart, Cell cycle checkpoint signaling:: Cell cycle arrest versus apoptosis. Toxicology, 2002. 181-182: p. 475-481.
118. Malumbres, Marcos and Mariano Barbacid, Cell cycle, CDKs and cancer: a changing paradigm. Nature reviews cancer, 2009. 9(3): p. 153-166.
119. Xiao, Dong, Candace S Johnson, Donald L Trump, and Shivendra V Singh, Proteasome-mediated degradation of cell division cycle 25C and cyclin-dependent kinase 1 in phenethyl isothiocyanate-induced G2-M-phase cell cycle arrest in PC-3 human prostate cancer cells. Molecular cancer therapeutics, 2004. 3(5): p. 567-576.
120. Pasquier, Eddy and Maria Kavallaris, Microtubules: A dynamic target in cancer therapy. IUBMB Life, 2008. 60(3): p. 165-170.
121. Øverby, Anders, Mette S. Bævre, Ole P. Thangstad, and Atle M. Bones, Disintegration of microtubules in Arabidopsis thaliana and bladder cancer cells by isothiocyanates. Frontiers in Plant Science, 2015. 6.
122. Grzywa, Renata, Mateusz Psurski, Anna Gajda, Tadeusz Gajda, and Łukasz Janczewski, Isothiocyanates as Tubulin Polymerization Inhibitors—Synthesis and Structure–Activity Relationship Studies. International Journal of Molecular Sciences, 2023. 24(18): p. 13674.
123. Galluzzi, Lorenzo, Ilio Vitale, Stuart A. Aaronson, John M. Abrams, Dieter Adam*, et al.*, Molecular mechanisms of cell death: recommendations of the Nomenclature Committee on Cell Death 2018. Cell Death & Differentiation, 2018. 25(3): p. 486-541.
124. Tang, Daolin, Rui Kang, Tom Vanden Berghe, Peter Vandenabeele, and Guido Kroemer, The molecular machinery of regulated cell death. Cell Research, 2019. 29(5): p. 347-364.

125. Scaturro, P. and A. Pichlmair, Oxeiptosis: a discreet way to respond to radicals. Curr Opin Immunol, 2019. 56: p. 37-43.
126. Scaturro, Pietro and Andreas Pichlmair, Oxeiptosis—a cell death pathway to mitigate damage caused by radicals. Cell Death & Differentiation, 2018. 25(7): p. 1191-1193.
127. Hengartner, Michael O, The biochemistry of apoptosis. Nature, 2000. 407(6805): p. 770-776.
128. Xu, C., G. Shen, X. Yuan, J. H. Kim, A. Gopalkrishnan*, et al.*, ERK and JNK signaling pathways are involved in the regulation of activator protein 1 and cell death elicited by three isothiocyanates in human prostate cancer PC-3 cells. Carcinogenesis, 2006. 27(3): p. 437-45.
129. Lambert, Arthur W., Diwakar R. Pattabiraman, and Robert A. Weinberg, Emerging Biological Principles of Metastasis. Cell, 2017. 168(4): p. 670-691.
130. Xiao, D. and S. V. Singh, Phenethyl isothiocyanate inhibits angiogenesis in vitro and ex vivo. Cancer Res, 2007. 67(5): p. 2239-46.
131. Zhu, Mingyue, Wei Li, Xu Dong, Yi Chen, Yan Lu*, et al.*, Benzyl-isothiocyanate Induces Apoptosis and Inhibits Migration and Invasion of Hepatocellular Carcinoma Cells in vitro. Journal of Cancer, 2017. 8(2): p. 240-248.
132. S, Sato, Kei Moriya, Furukawa M, Saikawa S, Tadashi Namisaki*, et al.*, Sulforaphane Inhibits Liver Cancer Cell Growth and Angiogenesis. Annals of Behavioural Science, 2018. 04.
133. Gheldof, Alexander and Geert Berx, Chapter Fourteen - Cadherins and Epithelial-to-Mesenchymal Transition, in Progress in Molecular Biology and Translational Science, F. van Roy, Editor. 2013, Academic Press. p. 317-336.
134. Singh, Shivendra V and Kamayani Singh, Cancer chemoprevention with dietary isothiocyanates mature for clinical translational research. Carcinogenesis, 2012. 33(10): p. 1833-1842.
135. Sehrawat, Anuradha and Shivendra V Singh, Benzyl Isothiocyanate Inhibits Epithelial-Mesenchymal Transition in Cultured and Xenografted Human Breast Cancer CellsBITC Inhibits EMT. Cancer Prevention Research, 2011. 4(7): p. 1107-1117.
136. Sehrawat, Anuradha, Su-Hyeong Kim, Andreas Vogt, and Shivendra V Singh, Suppression of FOXQ1 in benzyl isothiocyanate-mediated inhibition of epithelial–mesenchymal transition in human breast cancer cells. Carcinogenesis, 2013. 34(4): p. 864-873.

137. Wu, Wen-jing, Yan Zhang, Zhao-lei Zeng, Xiao-bing Li, Kai-shun Hu*, et al.*, β-phenylethyl isothiocyanate reverses platinum resistance by a GSH-dependent mechanism in cancer cells with epithelial-mesenchymal transition phenotype. Biochemical pharmacology, 2013. 85(4): p. 486-496.
138. Xiao, Jian, Ningning Zhou, Yin Li, Yunyun Xiao, Wei Chen*, et al.*, PEITC inhibits the invasion and migration of colorectal cancer cells by blocking TGF-β-induced EMT. Biomedicine & Pharmacotherapy, 2020. 130: p. 110743.
139. Sulzmaier, Florian J., Christine Jean, and David D. Schlaepfer, FAK in cancer: mechanistic findings and clinical applications. Nature Reviews Cancer, 2014. 14(9): p. 598-610.
140. Chen, Jing-Song, Xiao-Hui Huang, Qian Wang, Xi-Lin Chen, Xin-Hui Fu*, et al.*, FAK is involved in invasion and metastasis of hepatocellular carcinoma. Clinical & Experimental Metastasis, 2010. 27(2): p. 71-82.
141. Westhoff, M. A., B. Serrels, V. J. Fincham, M. C. Frame, and N. O. Carragher, Src-Mediated Phosphorylation of Focal Adhesion Kinase Couples Actin and Adhesion Dynamics to Survival Signaling. Molecular and Cellular Biology, 2004. 24(18): p. 8113-8133.
142. Svitkina, T., The Actin Cytoskeleton and Actin-Based Motility. Cold Spring Harb Perspect Biol, 2018. 10(1).
143. Bayless, K. J., K. J. Bayless, and G. A. Johnson, Role of the Cytoskeleton in Formation and Maintenance of Angiogenic Sprouts. Journal of Vascular Research, 2011. 48(5): p. 369-385.
144. Lee, C. S., H. J. Cho, Y. J. Jeong, J. M. Shin, K. K. Park*, et al.*, Isothiocyanates inhibit the invasion and migration of C6 glioma cells by blocking FAK/JNK-mediated MMP-9 expression. Oncol Rep, 2015. 34(6): p. 2901-8.
145. Jeong, Y. J., H. J. Cho, F. L. Chung, X. Wang, H. S. Hoe*, et al.*, Isothiocyanates suppress the invasion and metastasis of tumors by targeting FAK/MMP-9 activity. Oncotarget, 2017. 8(38): p. 63949-63962.
146. Li, Guo-bing, Qi Cheng, Lei Liu, Ting Zhou, Chang-yu Shan*, et al.*, Mitochondrial translocation of cofilin is required for allyl isothiocyanate-mediated cell death via ROCK1/PTEN/PI3K signaling pathway. Cell Communication and Signaling, 2013. 11(1): p. 50.
147. Pawlik, Andrzej, Mariusz Andrzej Szczepanski, Anna Klimaszewska, Lidia Gackowska, Agnieszka Zuryn*, et al.*, Phenethyl isothiocyanate-induced cytoskeletal

changes and cell death in lung cancer cells. Food and Chemical Toxicology, 2012. 50(10): p. 3577-3594.

148. Folkman, Judah, Angiogenesis: an organizing principle for drug discovery? Nature Reviews Drug Discovery, 2007. 6(4): p. 273-286.
149. Rak, J., Y. Mitsuhashi, C. Sheehan, A. Tamir, A. Viloria-Petit*, et al.*, Oncogenes and tumor angiogenesis: differential modes of vascular endothelial growth factor up-regulation in ras-transformed epithelial cells and fibroblasts. Cancer Res, 2000. 60(2): p. 490-8.
150. Rak, J., J. L. Yu, G. Klement, and R. S. Kerbel, Oncogenes and angiogenesis: signaling three-dimensional tumor growth. J Investig Dermatol Symp Proc, 2000. 5(1): p. 24-33.
151. Giuriato, S., S. Ryeom, A. C. Fan, P. Bachireddy, R. C. Lynch*, et al.*, Sustained regression of tumors upon MYC inactivation requires p53 or thrombospondin-1 to reverse the angiogenic switch. Proc Natl Acad Sci U S A, 2006. 103(44): p. 16266-71.
152. van Hinsbergh, Victor W. M. and Pieter Koolwijk, Endothelial sprouting and angiogenesis: matrix metalloproteinases in the lead. Cardiovascular Research, 2007. 78(2): p. 203-212.
153. Shibuya, M. and L. Claesson-Welsh, Signal transduction by VEGF receptors in regulation of angiogenesis and lymphangiogenesis. Exp Cell Res, 2006. 312(5): p. 549-60.
154. Kerbel, Robert S., Tumor angiogenesis. The New England journal of medicine, 2008. 358(19): p. 2039-2049.
155. Lee, T. H., S. Seng, M. Sekine, C. Hinton, Y. Fu*, et al.*, Vascular endothelial growth factor mediates intracrine survival in human breast carcinoma cells through internally expressed VEGFR1/FLT1. PLoS Med, 2007. 4(6): p. e186.
156. Semenza, G. L., Targeting HIF-1 for cancer therapy. Nat Rev Cancer, 2003. 3(10): p. 721-32.
157. Boreddy, S. R., R. P. Sahu, and S. K. Srivastava, Benzyl isothiocyanate suppresses pancreatic tumor angiogenesis and invasion by inhibiting HIF-alpha/VEGF/Rho-GTPases: pivotal role of STAT-3. PLoS One, 2011. 6(10): p. e25799.
158. Ziello, Jennifer E., Ion S. Jovin, and Yan Huang, Hypoxia-Inducible Factor (HIF)-1 regulatory pathway and its potential for therapeutic intervention in malignancy and ischemia. The Yale journal of biology and medicine, 2007. 80(2): p. 51-60.

159. Clayton, R. F., A. Rinaldi, E. E. Kandyba, M. Edward, C. Willberg*, et al.*, Liver cell lines for the study of hepatocyte functions and immunological response. Liver Int, 2005. 25(2): p. 389-402.
160. Guzmán, C., M. Bagga, A. Kaur, J. Westermarck, and D. Abankwa, ColonyArea: an ImageJ plugin to automatically quantify colony formation in clonogenic assays. PLoS One, 2014. 9(3): p. e92444.
161. Cormier, Nicholas, Alexander Yeo, Elizabeth Fiorentino, and Julia Paxson, Optimization of the Wound Scratch Assay to Detect Changes in Murine Mesenchymal Stromal Cell Migration After Damage by Soluble Cigarette Smoke Extract. Journal of visualized experiments : JoVE, 2015(106): p. e53414-e53414.
162. O'Brien, J., H. Hayder, and C. Peng, Automated Quantification and Analysis of Cell Counting Procedures Using ImageJ Plugins. J Vis Exp, 2016(117).
163. Carpentier, Gilles, Sarah Berndt, Ségolène Ferratge, Wayne Rasband, Muriel Cuendet*, et al.*, Angiogenesis Analyzer for ImageJ — A comparative morphometric analysis of "Endothelial Tube Formation Assay" and "Fibrin Bead Assay". Scientific Reports, 2020. 10(1): p. 11568.
164. Kimura, T., Y. Kato, Y. Ozawa, K. Kodama, J. Ito*, et al.*, Immunomodulatory activity of lenvatinib contributes to antitumor activity in the Hepa1-6 hepatocellular carcinoma model. Cancer Sci, 2018. 109(12): p. 3993-4002.
165. Riss, T. L., R. A. Moravec, A. L. Niles, S. Duellman, H. A. Benink*, et al.*, Cell Viability Assays, in Assay Guidance Manual, G.S. Sittampalam, et al., Editors. 2004: Bethesda (MD).
166. Franken, Nicolaas A. P., Hans M. Rodermond, Jan Stap, Jaap Haveman, and Chris van Bree, Clonogenic assay of cells in vitro. Nature Protocols, 2006. 1(5): p. 2315-2319.
167. Costa, Elisabete C., André F. Moreira, Duarte de Melo-Diogo, Vítor M. Gaspar, Marco P. Carvalho*, et al.*, 3D tumor spheroids: an overview on the tools and techniques used for their analysis. Biotechnology Advances, 2016. 34(8): p. 1427-1441.
168. Bortner, Carl D., Nicklas B. E. Oldenburg, and John A. Cidlowski, The role of DNA fragmentation in apoptosis. Trends in Cell Biology, 1995. 5(1): p. 21-26.
169. Matassov, Demetrius, Terri Kagan, Julie Leblanc, Marianna Sikorska, and Zahra Zakeri, Measurement of Apoptosis by DNA Fragmentation, in Apoptosis Methods and Protocols, H.J.M. Brady, Editor. 2004, Humana Press: Totowa, NJ. p. 1-17.

170. Pozarowski, Piotr and Zbigniew Darzynkiewicz, Analysis of Cell Cycle by Flow Cytometry, in Checkpoint Controls and Cancer: Volume 2: Activation and Regulation Protocols, A.H. Schönthal, Editor. 2004, Humana Press: Totowa, NJ. p. 301-311.
171. Wlodkowic, Donald, Joanna Skommer, and Zbigniew Darzynkiewicz, Flow cytometry-based apoptosis detection. Methods in molecular biology (Clifton, N.J.), 2009. 559: p. 19-32.
172. Morikawa, Kosuke and Mitsushiro Yanagida, Visualization of Individual DNA Molecules in Solution by Light Microscopy: DAPI Staining Method 1. The Journal of Biochemistry, 1981. 89(2): p. 693-696.
173. Doonan, Francesca and Thomas G. Cotter, Morphological assessment of apoptosis. Methods, 2008. 44(3): p. 200-204.
174. Haab, Brian B., Applications of antibody array platforms. Current Opinion in Biotechnology, 2006. 17(4): p. 415-421.
175. Murphy, Michael P., Hülya Bayir, Vsevolod Belousov, Christopher J. Chang, Kelvin J. A. Davies*, et al.*, Guidelines for measuring reactive oxygen species and oxidative damage in cells and in vivo. Nature Metabolism, 2022. 4(6): p. 651-662.
176. Wang, Jie and Jing Yi, Cancer cell killing via ROS: To increase or decrease, that is the question. Cancer Biology & Therapy, 2008. 7(12): p. 1875-1884.
177. Brandolini, Laura, Andrea Antonosante, Cristina Giorgio, Michela Bagnasco, Michele d'Angelo*, et al.*, NSAIDs-dependent adaption of the mitochondria-proteasome system in immortalized human cardiomyocytes. Scientific Reports, 2020. 10(1): p. 18337.
178. Reiniers, M. J., L. R. de Haan, L. F. Reeskamp, M. Broekgaarden, R. F. van Golen*, et al.*, Analysis and Optimization of Conditions for the Use of 2',7'-Dichlorofluorescein Diacetate in Cultured Hepatocytes. Antioxidants (Basel), 2021. 10(5).
179. Meister, A., Glutathione deficiency produced by inhibition of its synthesis, and its reversal; applications in research and therapy. Pharmacol Ther, 1991. 51(2): p. 155-94.
180. Zitka, O., S. Skalickova, J. Gumulec, M. Masarik, V. Adam*, et al.*, Redox status expressed as GSH:GSSG ratio as a marker for oxidative stress in paediatric tumour patients. Oncol Lett, 2012. 4(6): p. 1247-1253.
181. Newton, G. L. and R. C. Fahey, Determination of biothiols by bromobimane labeling and high-performance liquid chromatography. Methods Enzymol, 1995. 251: p. 148-66.

182. Quievryn, George and Anatoly Zhitkovich, Loss of DNA–protein crosslinks from formaldehyde-exposed cells occurs through spontaneous hydrolysis and an active repair process linked to proteosome function. Carcinogenesis, 2000. 21(8): p. 1573-1580.
183. Khalili, Amelia Ahmad and Mohd Ridzuan Ahmad, A Review of Cell Adhesion Studies for Biomedical and Biological Applications. International journal of molecular sciences, 2015. 16(8): p. 18149-18184.
184. Liang, Chun-Chi, Ann Y. Park, and Jun-Lin Guan, In vitro scratch assay: a convenient and inexpensive method for analysis of cell migration in vitro. Nature Protocols, 2007. 2(2): p. 329-333.
185. Chen, Hong-Chen, Boyden Chamber Assay, in Cell Migration: Developmental Methods and Protocols, J.-L. Guan, Editor. 2005, Humana Press: Totowa, NJ. p. 15-22.
186. Kunz, Pierre, Astrid Schenker, Heiner Sähr, Burkhard Lehner, and Jörg Fellenberg, Optimization of the chicken chorioallantoic membrane assay as reliable in vivo model for the analysis of osteosarcoma. PloS one, 2019. 14(4): p. e0215312-e0215312.
187. De Palma, M., D. Biziato, and T. V. Petrova, Microenvironmental regulation of tumour angiogenesis. Nat Rev Cancer, 2017. 17(8): p. 457-474.
188. Labelle, M. and R. O. Hynes, The initial hours of metastasis: the importance of cooperative host-tumor cell interactions during hematogenous dissemination. Cancer Discov, 2012. 2(12): p. 1091-9.
189. Reen, Denis J., Enzyme-Linked Immunosorbent Assay (ELISA), in Basic Protein and Peptide Protocols, J.M. Walker, Editor. 1994, Humana Press: Totowa, NJ. p. 461-466.
190. Lazarovici, Philip, Adi Lahiani, Galit Gincberg, Dikla Haham, Arnon Fluksman*, et al.*, Nerve growth factor-induced angiogenesis: 1. Endothelial cell tube formation assay, in Neurotrophic Factors. 2018, Springer. p. 239-250.
191. Yadgary, L., R. Yair, and Z. Uni, The chick embryo yolk sac membrane expresses nutrient transporter and digestive enzyme genes. Poultry Science, 2011. 90(2): p. 410-416.
192. Wang, Guang, Jia-hui Nie, Yongping Bao, and Xuesong Yang, Sulforaphane Rescues Ethanol-Suppressed Angiogenesis through Oxidative and Endoplasmic Reticulum Stress in Chick Embryos. Journal of Agricultural and Food Chemistry, 2018. 66(36): p. 9522-9533.

193. As, M. N., R. Deshpande, V. P. Kale, R. R. Bhonde, and S. P. Datar, Establishment of an in ovo chick embryo yolk sac membrane (YSM) assay for pilot screening of potential angiogenic and anti-angiogenic agents. Cell Biol Int, 2018. 42(11): p. 1474-1483.
194. Odell, Ian D and Deborah Cook, Immunofluorescence techniques. The Journal of investigative dermatology, 2013. 133(1): p. e4.
195. Mahmood, Tahrin and Ping-Chang Yang, Western blot: technique, theory, and trouble shooting. North American journal of medical sciences, 2012. 4(9): p. 429-434.
196. Schochetman, Gerald, Chin-Yih Ou, and Wanda K. Jones, Polymerase Chain Reaction. The Journal of Infectious Diseases, 1988. 158(6): p. 1154-1157.
197. Heid, C. A., J. Stevens, K. J. Livak, and P. M. Williams, Real time quantitative PCR. Genome Res, 1996. 6(10): p. 986-94.
198. Gengenbacher, Nicolas, Mahak Singhal, and Hellmut G. Augustin, Preclinical mouse solid tumour models: status quo, challenges and perspectives. Nature Reviews Cancer, 2017. 17(12): p. 751-765.
199. Musumeci, Giuseppe, Past, present and future: overview on histology and histopathology. J Histol Histopathol, 2014. 1(5): p. 1-3.
200. Fischer, Andrew H, Kenneth A Jacobson, Jack Rose, and Rolf Zeller, Hematoxylin and eosin staining of tissue and cell sections. Cold spring harbor protocols, 2008. 2008(5): p. pdb. prot4986.
201. Mokhtari, Reza Bayat, Tina S Homayouni, Narges Baluch, Evgeniya Morgatskaya, Sushil Kumar*, et al.*, Combination therapy in combating cancer. Oncotarget, 2017. 8(23): p. 38022.
202. Abou-Alfa, Ghassan K., George Lau, Masatoshi Kudo, Stephen L. Chan, Robin Kate Kelley*, et al.*, Tremelimumab plus Durvalumab in Unresectable Hepatocellular Carcinoma. NEJM Evidence, 2022. 1(8): p. EVIDoa2100070.
203. Chen, Y. J., C. W. Chi, W. C. Su, and H. L. Huang, Lapatinib induces autophagic cell death and inhibits growth of human hepatocellular carcinoma. Oncotarget, 2014. 5(13): p. 4845-54.
204. Höpfner, Michael, Andreas P. Sutter, Alexander Huether, Detlef Schuppan, Martin Zeitz*, et al.*, Targeting the epidermal growth factor receptor by gefitinib for treatment of hepatocellular carcinoma. Journal of Hepatology, 2004. 41(6): p. 1008-1016.
205. Ueda, Shu-ichi, Yuji Basaki, Masumi Yoshie, Katsuhiro Ogawa, Shotaro Sakisaka*, et al.*, PTEN/Akt Signaling through Epidermal Growth Factor Receptor Is Prerequisite for

Angiogenesis by Hepatocellular Carcinoma Cells That Is Susceptible to Inhibition by Gefitinib. Cancer Research, 2006. 66(10): p. 5346-5353.

206. Bekaii-Saab, Tanios, Joseph Markowitz, Nichole Prescott, Wolfgang Sadee, Nyla Heerema*, et al.*, A Multi-Institutional Phase II Study of the Efficacy and Tolerability of Lapatinib in Patients with Advanced Hepatocellular Carcinomas. Clinical Cancer Research, 2009. 15(18): p. 5895-5901.
207. Ramanathan, Ramesh K., Chandra P. Belani, Deepti A. Singh, Michael Tanaka, Heinz-Josef Lenz*, et al.*, A phase II study of lapatinib in patients with advanced biliary tree and hepatocellular cancer. Cancer Chemotherapy and Pharmacology, 2009. 64(4): p. 777-783.
208. O'Dwyer, P. J., B. J. Giantonio, D. E. Levy, J. S. Kauh, D. B. Fitzgerald*, et al.*, Gefitinib in advanced unresectable hepatocellular carcinoma: Results from the Eastern Cooperative Oncology Group's Study E1203. Journal of Clinical Oncology, 2006. 24(18_suppl): p. 4143-4143.
209. Dasatinib in Treating Patients With Advanced Liver Cancer That Cannot Be Removed by Surgery (ClinicalTrials.gov Identifier NCT00459108). 2015.
210. Sundaram, Madhumitha Kedhari, Preetha R, Shafiul Haque, Naseem Akhter, Saif Khan*, et al.*, Dietary isothiocyanates inhibit cancer progression by modulation of epigenome. Seminars in Cancer Biology, 2022. 83: p. 353-376.
211. Zhang, Q., M. Chen, L. Cao, Y. Ren, X. Guo*, et al.*, Phenethyl isothiocyanate synergistically induces apoptosis with Gefitinib in non-small cell lung cancer cells via endoplasmic reticulum stress-mediated degradation of Mcl-1. Mol Carcinog, 2020. 59(6): p. 590-603.
212. Kaczyńska, A. and A. Herman-Antosiewicz, Combination of lapatinib with isothiocyanates overcomes drug resistance and inhibits migration of HER2 positive breast cancer cells. Breast Cancer, 2017. 24(2): p. 271-280.
213. Yi, Huixing, Zheming Li, Xiaoxi Liu, Shijie Dai, and Shouye Li, Therapeutic mechanism of lapatinib combined with sulforaphane on gastric cancer. Evidence-based Complementary and Alternative Medicine: eCAM, 2021. 2021.
214. Mielczarek, L., Z. Chilmonczyk, P. Suchocki, P. WroczzDski, and Katarzyna Wiktorska. Combination of isothiocyanates with drugs: a chance or threat to chemoprevention and cancer treatment? 2018.

215. Minarini, Anna, Andrea Milelli, Carmela Fimognari, Elena Simoni, Eleonora Turrini*, et al.*, Exploring the effects of isothiocyanates on chemotherapeutic drugs. Expert Opinion on Drug Metabolism & Toxicology, 2014. 10(1): p. 25-38.
216. Chou, Ting-Chao, Drug combination studies and their synergy quantification using the Chou-Talalay methodsynergy quantification method. Cancer research, 2010. 70(2): p. 440-446.
217. Markovsky, Ela, Hemda Baabur-Cohen, and Ronit Satchi-Fainaro, Anticancer polymeric nanomedicine bearing synergistic drug combination is superior to a mixture of individually-conjugated drugs. Journal of Controlled Release, 2014. 187: p. 145-157.
218. Denis, I., L. Cellerin, M. Gregoire, and C. Blanquart, Cisplatin in combination with Phenethyl Isothiocyanate (PEITC), a potential new therapeutic strategy for malignant pleural mesothelioma. Oncotarget, 2014. 5(22): p. 11641-52.
219. Di Pasqua, Anthony J., Charles Hong, Mona Y. Wu, Erin McCracken, Xiantao Wang*, et al.*, Sensitization of Non-small Cell Lung Cancer Cells to Cisplatin by Naturally Occurring Isothiocyanates. Chemical Research in Toxicology, 2010. 23(8): p. 1307-1309.
220. Yin, Ping, Tomoya Kawamura, Meilan He, Donkena Krishna Vanaja, and Charles YF Young, Phenethyl isothiocyanate induces cell cycle arrest and reduction of α-and β-tubulin isotypes in human prostate cancer cells. Cell biology international, 2009. 33(1): p. 57-64.
221. Kaczyńska, Angelika, Joanna Świerczyńska, and Anna Herman-Antosiewicz, Sensitization of HER2 positive breast cancer cells to lapatinib using plants-derived isothiocyanates. Nutrition and cancer, 2015. 67(6): p. 976-986.
222. Li, Xinming, Yanan Hou, Jintao Zhao, Jin Li, Song Wang*, et al.*, Combination of chemotherapy and oxidative stress to enhance cancer cell apoptosis. Chemical Science, 2020. 11(12): p. 3215-3222.
223. Zhang, Yuesheng, Role of glutathione in the accumulation of anticarcinogenic isothiocyanates and their glutathione conjugates by murine hepatoma cells. Carcinogenesis, 2000. 21(6): p. 1175-1182.
224. Doudican, Nicole A., Benjamin Bowling, and Seth J. Orlow, Enhancement of arsenic trioxide cytotoxicity by dietary isothiocyanates in human leukemic cells via a reactive oxygen species-dependent mechanism. Leukemia Research, 2010. 34(2): p. 229-234.

225. Hanahan, Douglas, Hallmarks of Cancer: New Dimensions. Cancer Discovery, 2022. 12(1): p. 31-46.
226. Yamaguchi, Hideki, Jeffrey Wyckoff, and John Condeelis, Cell migration in tumors. Current opinion in cell biology, 2005. 17(5): p. 559-564.
227. Bhattacharya, Arup, Yun Li, Yi Shi, and Yuesheng Zhang, Enhanced inhibition of urinary bladder cancer growth and muscle invasion by allyl isothiocyanate and celecoxib in combination. Carcinogenesis, 2013. 34(11): p. 2593-2599.
228. Hanahan, D. and R. A. Weinberg, The hallmarks of cancer. Cell, 2000. 100(1): p. 57-70.
229. Groelly, Florian J., Matthew Fawkes, Rebecca A. Dagg, Andrew N. Blackford, and Madalena Tarsounas, Targeting DNA damage response pathways in cancer. Nature Reviews Cancer, 2023. 23(2): p. 78-94.
230. Raju, Uma, Faye Johnson, Bonnie Glisson, Oliver Riesterer, Luka Milas*, et al.*, Mechanisms of enhanced radiosensitivity of human head and neck squamous cell carcinomas by dasatinib (BMS-354825, an inhibitor of Src kinases) include induction of apoptosis and inhibition of DNA repair. Cancer Research, 2008. 68(9_Supplement): p. 642-642.
231. Peng, S., B. Sen, T. Mazumdar, L. A. Byers, L. Diao*, et al.*, Dasatinib induces DNA damage and activates DNA repair pathways leading to senescence in non-small cell lung cancer cell lines with kinase-inactivating BRAF mutations. Oncotarget, 2016. 7(1): p. 565-79.
232. Jia, Yaxun, Min Wang, Xiaolin Sang, Pixu Liu, Jingchun Gao*, et al.*, Phenethyl Isothiocyanate Enhances the Cytotoxic Effects of PARP Inhibitors in High-Grade Serous Ovarian Cancer Cells. Frontiers in Oncology, 2022. 11.
233. D'Arcy, Mark S., Cell death: a review of the major forms of apoptosis, necrosis and autophagy. Cell Biology International, 2019. 43(6): p. 582-592.
234. Satyan, K. S., Narasimha Swamy, Don S. Dizon, Rakesh Singh, Cornelius O. Granai*, et al.*, Phenethyl isothiocyanate (PEITC) inhibits growth of ovarian cancer cells by inducing apoptosis: Role of caspase and MAPK activation. Gynecologic Oncology, 2006. 103(1): p. 261-270.
235. Hu, Rong, Bok Ryang Kim, Chi Chen, Vidya Hebbar, and A. N. Tony Kong, The roles of JNK and apoptotic signaling pathways in PEITC-mediated responses in human HT-29 colon adenocarcinoma cells. Carcinogenesis, 2003. 24(8): p. 1361-1367.

236. Johnson, Faye M., Babita Saigal, Moshe Talpaz, and Nicholas J. Donato, Dasatinib (BMS-354825) Tyrosine Kinase Inhibitor Suppresses Invasion and Induces Cell Cycle Arrest and Apoptosis of Head and Neck Squamous Cell Carcinoma and Non–Small Cell Lung Cancer Cells. Clinical Cancer Research, 2005. 11(19): p. 6924-6932.
237. Song, Lanxi, Mark Morris, Tapan Bagui, Francis Y. Lee, Richard Jove*, et al.*, Dasatinib (BMS-354825) Selectively Induces Apoptosis in Lung Cancer Cells Dependent on Epidermal Growth Factor Receptor Signaling for Survival. Cancer Research, 2006. 66(11): p. 5542-5548.
238. Shor, Audrey C., Elizabeth A. Keschman, Francis Y. Lee, Carlos Muro-Cacho, G. Douglas Letson*, et al.*, Dasatinib Inhibits Migration and Invasion in Diverse Human Sarcoma Cell Lines and Induces Apoptosis in Bone Sarcoma Cells Dependent on Src Kinase for Survival. Cancer Research, 2007. 67(6): p. 2800-2808.
239. Dai, X., D. Wang, and J. Zhang, Programmed cell death, redox imbalance, and cancer therapeutics. Apoptosis, 2021. 26(7-8): p. 385-414.
240. Trachootham, Dunyaporn, Yan Zhou, Hui Zhang, Yusuke Demizu, Zhao Chen*, et al.*, Selective killing of oncogenically transformed cells through a ROS-mediated mechanism by β-phenylethyl isothiocyanate. Cancer Cell, 2006. 10(3): p. 241-252.
241. Hong, Yoon-hee, Md. Hafiz Uddin, Untek Jo, Boyun Kim, Dong Hoon Suh*, et al.*, ROS accumulation by PEITC selectively kills ovarian cancer cells via UPR-mediated apoptosis. Frontiers in Oncology, 2015. 5.
242. Wang, Huizhen, Yida Lu, Mingliang Wang, Aolin Shen, Youliang Wu*, et al.*, Src inhibitor dasatinib sensitized gastric cancer cells to cisplatin. Medical Oncology, 2022. 40(1): p. 49.
243. Narayan, Ravi S., Carlos A. Fedrigo, Eelke Brands, Rogier Dik, Lukas J. A. Stalpers*, et al.*, The allosteric AKT inhibitor MK2206 shows a synergistic interaction with chemotherapy and radiotherapy in glioblastoma spheroid cultures. BMC Cancer, 2017. 17(1): p. 204.
244. Mikus, Gerd and Kathrin Isabelle Foerster, Role of CYP3A4 in kinase inhibitor metabolism and assessment of CYP3A4 activity. Translational Cancer Research, 2017: p. S1592-S1599.
245. Xiaohai, Li, He Yuanjun, H. Ruiz Claudia, Koenig Marcel, and D. Cameron Michael, Characterization of Dasatinib and Its Structural Analogs as CYP3A4 Mechanism-Based Inactivators and the Proposed Bioactivation Pathways. Drug Metabolism and Disposition, 2009. 37(6): p. 1242.

246. Morris, M. E. and R. A. Dave, Pharmacokinetics and pharmacodynamics of phenethyl isothiocyanate: implications in breast cancer prevention. Aaps j, 2014. 16(4): p. 705-13.
247. Srinivas, Upadhyayula Sai, Bryce W. Q. Tan, Balamurugan A. Vellayappan, and Anand D. Jeyasekharan, ROS and the DNA damage response in cancer. Redox Biology, 2019. 25: p. 101084.
248. Hirao, A., Y. Y. Kong, S. Matsuoka, A. Wakeham, J. Ruland*, et al.*, DNA damage-induced activation of p53 by the checkpoint kinase Chk2. Science, 2000. 287(5459): p. 1824-7.
249. Bayraktepe, Dilek Eskiköy, A voltammetric study on drug-DNA interactions: Kinetic and thermodynamic aspects of the relations between the anticancer agent dasatinib and ds-DNA using a pencil lead graphite electrode. Microchemical Journal, 2020. 157: p. 104946.
250. Wang, Zhifeng, Fengli Wang, Tieshan Tang, and Caixia Guo, The role of PARP1 in the DNA damage response and its application in tumor therapy. Frontiers of Medicine, 2012. 6(2): p. 156-164.
251. Tang, N. Y., Y. T. Huang, C. S. Yu, Y. C. Ko, S. H. Wu*, et al.*, Phenethyl isothiocyanate (PEITC) promotes G2/M phase arrest via p53 expression and induces apoptosis through caspase- and mitochondria-dependent signaling pathways in human prostate cancer DU 145 cells. Anticancer Res, 2011. 31(5): p. 1691-702.
252. Sun, C., W. Jing, G. Xiong, D. Ma, Y. Lin*, et al.*, Inhibiting Src-mediated PARP1 tyrosine phosphorylation confers synthetic lethality to PARP1 inhibition in HCC. Cancer Lett, 2022. 526: p. 180-192.
253. Schwartz, Gary K. and Manish A. Shah, Targeting the Cell Cycle: A New Approach to Cancer Therapy. Journal of Clinical Oncology, 2005. 23(36): p. 9408-9421.
254. Zhang, Chan, Xinan Zhao, Zifeng Wang, Tao Gong, Hong Zhao*, et al.*, Dasatinib in combination with BMS-754807 induce synergistic cytotoxicity in lung cancer cells through inhibiting lung cancer cell growth, and inducing autophagy as well as cell cycle arrest at the G1 phase. Investigational New Drugs, 2023.
255. Song, Yan, Xin Sun, Wei-Liang Bai, and Wen-Yue Ji, Antitumor effects of Dasatinib on laryngeal squamous cell carcinoma in vivo and in vitro. European Archives of Oto-Rhino-Laryngology, 2013. 270(4): p. 1397-1404.
256. Wu, Chang-Lin, An-Cheng Huang, Jai-Sing Yang, Ching-Lung Liao, Hsu-Feng Lu*, et al.*, Benzyl isothiocyanate (BITC) and phenethyl isothiocyanate (PEITC)-mediated

generation of reactive oxygen species causes cell cycle arrest and induces apoptosis via activation of caspase-3, mitochondria dysfunction and nitric oxide (NO) in human osteogenic sarcoma U-2 OS cells. Journal of Orthopaedic Research, 2011. 29(8): p. 1199-1209.

257. Huang, S-H, M-H Hsu, S-C Hsu, J-S Yang, W-W Huang*, et al.*, Phenethyl isothiocyanate triggers apoptosis in human malignant melanoma A375.S2 cells through reactive oxygen species and the mitochondria-dependent pathways. Human & Experimental Toxicology, 2014. 33(3): p. 270-283.
258. Mi, L., Z. Xiao, B. L. Hood, S. Dakshanamurthy, X. Wang*, et al.*, Covalent binding to tubulin by isothiocyanates. A mechanism of cell growth arrest and apoptosis. J Biol Chem, 2008. 283(32): p. 22136-46.
259. Vermeulen, K., D. R. Van Bockstaele, and Z. N. Berneman, The cell cycle: a review of regulation, deregulation and therapeutic targets in cancer. Cell Prolif, 2003. 36(3): p. 131-49.
260. Castedo, M., J. L. Perfettini, T. Roumier, and G. Kroemer, Cyclin-dependent kinase-1: linking apoptosis to cell cycle and mitotic catastrophe. Cell Death & Differentiation, 2002. 9(12): p. 1287-1293.
261. Choi, H. J. and B. T. Zhu, Critical role of cyclin B1/Cdc2 up-regulation in the induction of mitotic prometaphase arrest in human breast cancer cells treated with 2-methoxyestradiol. Biochim Biophys Acta, 2012. 1823(8): p. 1306-15.
262. Shang, Z., L. Yu, Y. F. Lin, S. Matsunaga, C. Y. Shen*, et al.*, DNA-PKcs activates the Chk2–Brca1 pathway during mitosis to ensure chromosomal stability. Oncogenesis, 2014. 3(2): p. e85-e85.
263. Swift, L. H. and R. M. Golsteyn, Chapter 22 - The Relationship Between Checkpoint Adaptation and Mitotic Catastrophe in Genomic Changes in Cancer Cells, in Genome Stability, I. Kovalchuk and O. Kovalchuk, Editors. 2016, Academic Press: Boston. p. 373-389.
264. Carneiro, Benedito A. and Wafik S. El-Deiry, Targeting apoptosis in cancer therapy. Nature Reviews Clinical Oncology, 2020. 17(7): p. 395-417.
265. Shlomovitz, Inbar, Mary Speir, and Motti Gerlic, Flipping the dogma – phosphatidylserine in non-apoptotic cell death. Cell Communication and Signaling, 2019. 17(1): p. 139.

266. Holze, C., C. Michaudel, C. Mackowiak, D. A. Haas, C. Benda*, et al.*, Oxeiptosis, a ROS-induced caspase-independent apoptosis-like cell-death pathway. Nat Immunol, 2018. 19(2): p. 130-140.
267. Kang, Pan, Jianru Chen, Weigang Zhang, Ningning Guo, Xiuli Yi*, et al.*, Oxeiptosis: a novel pathway of melanocytes death in response to oxidative stress in vitiligo. Cell Death Discovery, 2022. 8(1): p. 70.
268. Zeb, A., V. Choubey, R. Gupta, M. Kuum, D. Safiulina*, et al.*, A novel role of KEAP1/PGAM5 complex: ROS sensor for inducing mitophagy. Redox Biol, 2021. 48: p. 102186.
269. Pallichankandy, Siraj, Faisal Thayyullathil, Anees Rahman Cheratta, Karthikeyan Subburayan, Ameer Alakkal*, et al.*, Targeting oxeiptosis-mediated tumor suppression: a novel approach to treat colorectal cancers by sanguinarine. Cell Death Discovery, 2023. 9(1): p. 94.
270. Cheng, Meiyu, Nan Lin, Delu Dong, Jiaoyan Ma, Jing Su*, et al.*, PGAM5: A crucial role in mitochondrial dynamics and programmed cell death. European Journal of Cell Biology, 2021. 100(1): p. 151144.
271. Wischhof, Lena, Enzo Scifo, Dan Ehninger, and Daniele Bano, AIFM1 beyond cell death: An overview of this OXPHOS-inducing factor in mitochondrial diseases. EBioMedicine, 2022. 83: p. 104231.
272. Sekine, S., Y. Kanamaru, M. Koike, A. Nishihara, M. Okada*, et al.*, Rhomboid protease PARL mediates the mitochondrial membrane potential loss-induced cleavage of PGAM5. J Biol Chem, 2012. 287(41): p. 34635-45.
273. Thiery, Jean Paul, Epithelial–mesenchymal transitions in tumour progression. Nature Reviews Cancer, 2002. 2(6): p. 442-454.
274. Schliekelman, Mark J, Ayumu Taguchi, Jun Zhu, Xudong Dai, Jaime Rodriguez*, et al.*, Molecular portraits of epithelial, mesenchymal, and hybrid states in lung adenocarcinoma and their relevance to survivalmolecular signatures of emt status in lung adenocarcinoma. Cancer research, 2015. 75(9): p. 1789-1800.
275. van Nimwegen, M. J. and B. van de Water, Focal adhesion kinase: a potential target in cancer therapy. Biochem Pharmacol, 2007. 73(5): p. 597-609.
276. Liu, X., X. Song, J. Zhang, Z. Xu, L. Che*, et al.*, Focal adhesion kinase activation limits efficacy of Dasatinib in c-Myc driven hepatocellular carcinoma. Cancer Med, 2018. 7(12): p. 6170-6181.

277. El Sayed, I., M. W. Helmy, and H. S. El-Abhar, Inhibition of SRC/FAK cue: A novel pathway for the synergistic effect of rosuvastatin on the anti-cancer effect of dasatinib in hepatocellular carcinoma. Life Sci, 2018. 213: p. 248-257.
278. Schlaepfer, D. D., S. K. Hanks, T. Hunter, and P. van der Geer, Integrin-mediated signal transduction linked to Ras pathway by GRB2 binding to focal adhesion kinase. Nature, 1994. 372(6508): p. 786-91.
279. Calalb, M. B., T. R. Polte, and S. K. Hanks, Tyrosine phosphorylation of focal adhesion kinase at sites in the catalytic domain regulates kinase activity: a role for Src family kinases. Mol Cell Biol, 1995. 15(2): p. 954-63.
280. Yang, M. D., K. C. Lai, T. Y. Lai, S. C. Hsu, C. L. Kuo*, et al.*, Phenethyl isothiocyanate inhibits migration and invasion of human gastric cancer AGS cells through suppressing MAPK and NF-kappaB signal pathways. Anticancer Res, 2010. 30(6): p. 2135-43.
281. Walsh, M. F., V. Thamilselvan, R. Grotelueschen, L. Farhana, and M. Basson, Absence of adhesion triggers differential FAK and SAPKp38 signals in SW620 human colon cancer cells that may inhibit adhesiveness and lead to cell death. Cell Physiol Biochem, 2003. 13(3): p. 135-46.
282. Finn, Richard S., Alexey Aleshin, Judy Dering, Peter Yang, Charles Ginther*, et al.*, Molecular subtype and response to dasatinib, an Src/Abl small molecule kinase inhibitor, in hepatocellular carcinoma cell lines in vitro. Hepatology, 2013. 57(5): p. 1838-1846.
283. Woodhouse, Elisa C., Rodrigo F. Chuaqui, and Lance A. Liotta, General mechanisms of metastasis. Cancer, 1997. 80(S8): p. 1529-1537.
284. Lokman, Noor A., Alison S. F. Elder, Carmela Ricciardelli, and Martin K. Oehler, Chick Chorioallantoic Membrane (CAM) Assay as an In Vivo Model to Study the Effect of Newly Identified Molecules on Ovarian Cancer Invasion and Metastasis. International Journal of Molecular Sciences, 2012. 13(8): p. 9959-9970.
285. Sys, Gwen, Mieke Van Bockstal, Ramses Forsyth, Maurice Balke, Bart Poffyn*, et al.*, Tumor grafts derived from sarcoma patients retain tumor morphology, viability, and invasion potential and indicate disease outcomes in the chick chorioallantoic membrane model. Cancer Letters, 2012. 326(1): p. 69-78.
286. Liu, Peng, Samuel J Atkinson, Sophia E Akbareian, Zhigang Zhou, Andrea Munsterberg*, et al.*, Sulforaphane exerts anti-angiogenesis effects against

hepatocellular carcinoma through inhibition of STAT3/HIF-1α/VEGF signalling. Scientific reports, 2017. 7(1): p. 12651.

287. Kanteti, R., S. K. Batra, F. E. Lennon, and R. Salgia, FAK and paxillin, two potential targets in pancreatic cancer. Oncotarget, 2016. 7(21): p. 31586-601.
288. Azios, Nicolas G. and Suranganie F. Dharmawardhane, Resveratrol and estradiol exert disparate effects on cell migration, cell surface actin structures, and focal adhesion assembly in MDA-MB-231 human breast cancer cells. Neoplasia (New York, N.Y.), 2005. 7(2): p. 128-140.
289. Zheng, Q., L. Han, Y. Dong, J. Tian, W. Huang*, et al.*, JAK2/STAT3 targeted therapy suppresses tumor invasion via disruption of the EGFRvIII/JAK2/STAT3 axis and associated focal adhesion in EGFRvIII-expressing glioblastoma. Neuro Oncol, 2014. 16(9): p. 1229-43.
290. Liang, Q., C. Ma, Y. Zhao, G. Gao, and J. Ma, Inhibition of STAT3 reduces astrocytoma cell invasion and constitutive activation of STAT3 predicts poor prognosis in human astrocytoma. PLoS One, 2013. 8(12): p. e84723.
291. Pei, G., Y. Lan, D. Chen, L. Ji, and Z. C. Hua, FAK regulates E-cadherin expression via p-SrcY416/p-ERK1/2/p-Stat3Y705 and PPARγ/miR-125b/Stat3 signaling pathway in B16F10 melanoma cells. Oncotarget, 2017. 8(8): p. 13898-13908.
292. Kaszak, Ilona, Olga Witkowska-Piłaszewicz, Zuzanna Niewiadomska, Bożena Dworecka-Kaszak, Felix Ngosa Toka*, et al.*, Role of Cadherins in Cancer—A Review. International Journal of Molecular Sciences, 2020. 21(20): p. 7624.
293. Bielenberg, Diane R and Bruce R Zetter, The contribution of angiogenesis to the process of metastasis. The Cancer Journal, 2015. 21(4): p. 267-273.
294. Bergers, Gabriele and Douglas Hanahan, Modes of resistance to anti-angiogenic therapy. Nature Reviews Cancer, 2008. 8(8): p. 592-603.
295. Kerbel, R. S. and B. A. Kamen, The anti-angiogenic basis of metronomic chemotherapy. Nat Rev Cancer, 2004. 4(6): p. 423-36.
296. Bodzioch, Mariusz, Piotr Bajger, and Urszula Foryś, Angiogenesis and chemotherapy resistance: optimizing chemotherapy scheduling using mathematical modeling. Journal of Cancer Research and Clinical Oncology, 2021. 147(8): p. 2281-2299.
297. Song, Ningning, Hulin Guo, Jia Ren, Suhong Hao, and Xinchao Wang, Synergistic anti-tumor effects of dasatinib and dendritic cell vaccine on metastatic breast cancer in a mouse model. Oncol Lett, 2018. 15(5): p. 6831-6838.

298. Wang, Xiu-Hong, Breeze E. Cavell, Sharifah S. Syed Alwi, and Graham Packham, Inhibition of hypoxia inducible factor by phenethyl isothiocyanate. Biochemical Pharmacology, 2009. 78(3): p. 261-272.
299. Gupta, Brinda, Linda Chiang, KyungMin Chae, and Dae-Hee Lee, Phenethyl isothiocyanate inhibits hypoxia-induced accumulation of HIF-1α and VEGF expression in human glioma cells. Food chemistry, 2013. 141(3): p. 1841-1846.
300. Fonseca, Belchiolina Beatriz, Murilo Vieira da Silva, and Lígia Nunes de Morais Ribeiro, The chicken embryo as an in vivo experimental model for drug testing: Advantages and limitations. Lab Animal, 2021. 50(6): p. 138-139.
301. Bárcena, Cristina, Milica Stefanovic, Anna Tutusaus, Guillermo A. Martinez-Nieto, Laura Martinez*, et al.*, Angiogenin Secretion From Hepatoma Cells Activates Hepatic Stellate Cells To Amplify A Self-Sustained Cycle Promoting Liver Cancer. Scientific Reports, 2015. 5(1): p. 7916.
302. Hisai, Hiroyuki, Junji Kato, Masayoshi Kobune, Tsuzuku Murakami, Koji Miyanishi*, et al.*, Increased expression of angiogenin in hepatocellular carcinoma in correlation with tumor vascularity. Clinical cancer research, 2003. 9(13): p. 4852-4859.
303. Mas, Valeria R, Daniel G Maluf, Kellie J Archer, Kenneth C Yanek, and Robert A Fisher, Angiogenesis soluble factors as hepatocellular carcinoma noninvasive markers for monitoring hepatitis C virus cirrhotic patients awaiting liver transplantation. Transplantation, 2007. 84(10): p. 1262-1271.
304. Li, Shuping and Guo-Fu Hu, Emerging role of angiogenin in stress response and cell survival under adverse conditions. Journal of cellular physiology, 2012. 227(7): p. 2822-2826.
305. Kawada, Manabu, Hiroyuki Inoue, Masayuki Arakawa, Kozo Takamoto, Tohru Masuda*, et al.*, Highly tumorigenic human androgen receptor-positive prostate cancer cells overexpress angiogenin. Cancer Science, 2007. 98(3): p. 350-356.
306. Kishimoto, Koji, Shoko Yoshida, Soichiro Ibaragi, Norie Yoshioka, Tatsuo Okui*, et al.*, Hypoxia-induced up-regulation of angiogenin, besides VEGF, is related to progression of oral cancer. Oral oncology, 2012. 48(11): p. 1120-1127.
307. Isozaki, Takeo, Ali S Arbab, Christian S Haas, M Asif Amin, Monica D Arendt*, et al.*, Evidence that CXCL16 is a potent mediator of angiogenesis and is involved in endothelial progenitor cell chemotaxis: studies in mice with K/BxN serum–induced arthritis. Arthritis & Rheumatism, 2013. 65(7): p. 1736-1746.

308. Zhuge, Xin, Toshinori Murayama, Hidenori Arai, Ryoko Yamauchi, Makoto Tanaka*, et al.*, CXCL16 is a novel angiogenic factor for human umbilical vein endothelial cells. Biochemical and Biophysical Research Communications, 2005. 331(4): p. 1295-1300.
309. Wang, Jianhua, Yi Lu, Jingchen Wang, Alisa E Koch, Jian Zhang*, et al.*, CXCR6 induces prostate cancer progression by the AKT/mammalian target of rapamycin signaling pathway. Cancer research, 2008. 68(24): p. 10367-10377.
310. Yu, Xiaowen, Renping Zhao, Sensen Lin, Xianshu Bai, Luyong Zhang*, et al.*, CXCL16 induces angiogenesis in autocrine signaling pathway involving hypoxia-inducible factor 1α in human umbilical vein endothelial cells. Oncology Reports, 2016. 35(3): p. 1557-1565.
311. Carmeliet, Peter, VEGF as a Key Mediator of Angiogenesis in Cancer. Oncology, 2005. 69(Suppl. 3): p. 4-10.
312. Niu, Guilian, Kenneth L. Wright, Mei Huang, Lanxi Song, Eric Haura*, et al.*, Constitutive Stat3 activity up-regulates VEGF expression and tumor angiogenesis. Oncogene, 2002. 21(13): p. 2000-2008.
313. Jung, Joo Eun, Hyun-Gyu Lee, Ik-Hyun Cho, Doo Hyun Chung, Sun-Hee Yoon*, et al.*, STAT3 is a potential modulator of HIF-1-mediated VEGF expression in human renal carcinoma cells. The FASEB Journal, 2005. 19(10): p. 1296-1298.
314. Sp, Nipin, Dong Young Kang, Youn Hee Joung, Jong Hwan Park, Wan Seop Kim*, et al.*, Nobiletin inhibits angiogenesis by regulating Src/FAK/STAT3-mediated signaling through PXN in ER+ breast cancer cells. International Journal of Molecular Sciences, 2017. 18(5): p. 935.
315. Park, Serk In, Ami N Shah, Jing Zhang, and Gary E Gallick, Regulation of angiogenesis and vascular permeability by Src family kinases: opportunities for therapeutic treatment of solid tumors. Expert opinion on therapeutic targets, 2007. 11(9): p. 1207-1217.
316. Lechertier, Tanguy and Kairbaan Hodivala-Dilke, Focal adhesion kinase and tumour angiogenesis. The Journal of pathology, 2012. 226(2): p. 404-412.
317. Ribatti, Domenico, The discovery of the placental growth factor and its role in angiogenesis: a historical review. Angiogenesis, 2008. 11(3): p. 215-221.
318. Eriksson, A., R. Cao, R. Pawliuk, S. M. Berg, M. Tsang*, et al.*, Placenta growth factor-1 antagonizes VEGF-induced angiogenesis and tumor growth by the formation of functionally inactive PlGF-1/VEGF heterodimers. Cancer Cell, 2002. 1(1): p. 99-108.

319. Xu, Lei, David M. Cochran, Ricky T. Tong, Frank Winkler, Satoshi Kashiwagi*, et al.*, Placenta Growth Factor Overexpression Inhibits Tumor Growth, Angiogenesis, and Metastasis by Depleting Vascular Endothelial Growth Factor Homodimers in Orthotopic Mouse Models. Cancer Research, 2006. 66(8): p. 3971-3977.
320. Yang, Xiaojuan, Yin Zhang, Yunlong Yang, Sharon Lim, Ziquan Cao*, et al.*, Vascular endothelial growth factor-dependent spatiotemporal dual roles of placental growth factor in modulation of angiogenesis and tumor growth. Proceedings of the National Academy of Sciences, 2013. 110(34): p. 13932-13937.
321. Cao, Yihai, Positive and negative modulation of angiogenesis by VEGFR1 ligands. Science signaling, 2009. 2(59): p. re1-re1.
322. Cudmore, M. J., P. W. Hewett, S. Ahmad, K. Q. Wang, M. Cai*, et al.*, The role of heterodimerization between VEGFR-1 and VEGFR-2 in the regulation of endothelial cell homeostasis. Nat Commun, 2012. 3: p. 972.
323. Gould, Stephen E, Melissa R Junttila, and Frederic J de Sauvage, Translational value of mouse models in oncology drug development. Nature medicine, 2015. 21(5): p. 431-439.
324. Perrin, Steve, Preclinical research: Make mouse studies work. Nature, 2014. 507(7493): p. 423-425.
325. Kröger, Andrea, Dörte Ortmann, Tim U Krohne, Leonhardt Mohr, Hubert E Blum*, et al.*, Growth suppression of the hepatocellular carcinoma cell line Hepa1-6 by an activatable interferon regulatory factor-1 in mice. Cancer research, 2001. 61(6): p. 2609-2617.
326. Torrens, Laura, Carla Montironi, Marc Puigvehí, Agavni Mesropian, Jack Leslie*, et al.*, Immunomodulatory effects of lenvatinib plus anti–programmed cell death protein 1 in mice and rationale for patient enrichment in hepatocellular carcinoma. Hepatology, 2021. 74(5): p. 2652-2669.
327. Han, Zhen, Shuo Liu, Hongsheng Lin, Anna L Trivett, Sean Hannifin*, et al.*, Inhibition of murine hepatoma tumor growth by cryptotanshinone involves TLR7-dependent activation of macrophages and induction of adaptive antitumor immune defenses. Cancer Immunology, Immunotherapy, 2019. 68: p. 1073-1085.
328. Grimm, Christian F, Dörte Ortmann, Leonhard Mohr, Sabine Michalak, Tim U Krohne*, et al.*, Mouse α-fetoprotein–specific DNA-based immunotherapy of hepatocellular carcinoma leads to tumor regression in mice. Gastroenterology, 2000. 119(4): p. 1104-1112.

329. Vitali, Roberta, Camillo Mancini, Vincenzo Cesi, Barbara Tanno, Marta Piscitelli*, et al.*, Activity of tyrosine kinase inhibitor Dasatinib in neuroblastoma cells in vitro and in orthotopic mouse model. International journal of cancer, 2009. 125(11): p. 2547-2555.
330. Nautiyal, Jyoti, Sanjeev Banerjee, Shailender S Kanwar, Yingjie Yu, Bhaumik B Patel*, et al.*, Curcumin enhances dasatinib-induced inhibition of growth and transformation of colon cancer cells. International Journal of Cancer, 2011. 128(4): p. 951-961.
331. Hekim, Can, Mette Ilander, Jun Yan, Erin Michaud, Richard Smykla*, et al.*, Dasatinib Changes Immune Cell Profiles Concomitant with Reduced Tumor Growth in Several Murine Solid Tumor ModelsDasatinib-Induced Antitumor Immunomodulation in Mouse Models. Cancer immunology research, 2017. 5(2): p. 157-169.
332. Luo, Feng, Yu Chen Barrett, Zheng Yang, Amy Camuso, Kelly McGlinchey*, et al.*, Identification and validation of phospho-SRC, a novel and potential pharmacodynamic biomarker for dasatinib (SPRYCEL™), a multi-targeted kinase inhibitor. Cancer chemotherapy and pharmacology, 2008. 62: p. 1065-1074.
333. Le, Xiao-Feng, Weiqun Mao, Zhen Lu, Bing Z Carter, and Robert C Bast Jr, Dasatinib induces autophagic cell death in human ovarian cancer. Cancer, 2010. 116(21): p. 4980-4990.
334. Karim, Saadia A, Helen Creedon, Hitesh Patel, Neil O Carragher, Jennifer P Morton*, et al.*, Dasatinib inhibits mammary tumour development in a genetically engineered mouse model. The Journal of pathology, 2013. 230(4): p. 430-440.
335. Redin, Esther, Irati Garmendia, Teresa Lozano, Diego Serrano, Yaiza Senent*, et al.*, SRC family kinase (SFK) inhibitor dasatinib improves the antitumor activity of anti-PD-1 in NSCLC models by inhibiting Treg cell conversion and proliferation. Journal for immunotherapy of cancer, 2021. 9(3).
336. Dunn, Emily F, Mari Iida, Rebecca A Myers, DA Campbell, KA Hintz*, et al.*, Dasatinib sensitizes KRAS mutant colorectal tumors to cetuximab. Oncogene, 2011. 30(5): p. 561-574.
337. Xiao, Dong and Shivendra Vikram Singh, Phenethyl isothiocyanate sensitizes androgen-independent human prostate cancer cells to docetaxel-induced apoptosis in vitro and in vivo. Pharmaceutical research, 2010. 27: p. 722-731.
338. Gupta, Parul and Sanjay K Srivastava, Antitumor activity of phenethyl isothiocyanate in HER2-positive breast cancer models. BMC medicine, 2012. 10(1): p. 1-18.

339. Gupta, Parul, Stephen E Wright, and Sanjay K Srivastava, PEITC treatment suppresses myeloid derived tumor suppressor cells to inhibit breast tumor growth. Oncoimmunology, 2015. 4(2): p. e981449.
340. Eisa, Nada H, Nehal M ElSherbiny, Abdelhadi M Shebl, Laila A Eissa, and Mamdouh M El-Shishtawy, Phenethyl isothiocyanate potentiates anti-tumour effect of doxorubicin through Akt-dependent pathway. Cell Biochemistry and Function, 2015. 33(8): p. 541-551.
341. Chou, Yu-Cheng, Meng-Ya Chang, Hsu-Tung Lee, Chiung-Chyi Shen, Tomor Harnod*, et al.*, Phenethyl isothiocyanate inhibits in vivo growth of xenograft tumors of human glioblastoma cells. Molecules, 2018. 23(9): p. 2305.
342. Li, Enya, Li Lin, Chia-Wei Chen, and Da-Liang Ou, Mouse models for immunotherapy in hepatocellular carcinoma. Cancers, 2019. 11(11): p. 1800.
343. Ma, Chao, Yansong Peng, Hongtong Li, and Weiqiang Chen, Organ-on-a-Chip: A New Paradigm for Drug Development. Trends in Pharmacological Sciences, 2021. 42(2): p. 119-133.
344. Tosca, Elena M, Davide Ronchi, Daniele Facciolo, and Paolo Magni, Replacement, Reduction, and Refinement of Animal Experiments in Anticancer Drug Development: The Contribution of 3D In Vitro Cancer Models in the Drug Efficacy Assessment. Biomedicines, 2023. 11(4): p. 1058.
345. Hartleb, M., L. Biernat, and A. Kochel, Drug-induced liver damage -- a three-year study of patients from one gastroenterological department. Med Sci Monit, 2002. 8(4): p. Cr292-6.
346. Oprea, T. I. and J. Mestres, Drug Repurposing: Far Beyond New Targets for Old Drugs. The AAPS Journal, 2012. 14(4): p. 759-763.
347. Jabbour, E, M Deininger, and A Hochhaus, Management of adverse events associated with tyrosine kinase inhibitors in the treatment of chronic myeloid leukemia. Leukemia, 2011. 25(2): p. 201-210.
348. Yang, Xiaochun, Jincheng Wang, Jiabin Dai, Jinjin Shao, Jian Ma*, et al.*, Autophagy protects against dasatinib-induced hepatotoxicity via p38 signaling. Oncotarget, 2015. 6(8): p. 6203.
349. Li, Yan, Er-Jia Wang, Laishun Chen, Adam P Stein, Kenneth R Reuhl*, et al.*, Effects of phenethyl isothiocyanate on acetaminophen metabolism and hepatotoxicity in mice. Toxicology and applied pharmacology, 1997. 144(2): p. 306-314.

350. Atici, Bugrahan, Ayse Burcin Uyumlu, and Asli Taslidere, The role of Nrf2/SIRT1 pathway in the hepatoprotective effect of PEITC against HFD/STZ-induced diabetic liver disease. 2022.
351. Abdel-Moneim, Ashraf M., Mohammed A. Al-Kahtani, Mohamed A. El-Kersh, and Mohammed A. Al-Omair, Free Radical-Scavenging, Anti-Inflammatory/Anti-Fibrotic and Hepatoprotective Actions of Taurine and Silymarin against CCl4 Induced Rat Liver Damage. PLOS ONE, 2015. 10(12): p. e0144509.
352. Hu, Y. L., S. Lu, K. W. Szeto, J. Sun, Y. Wang*, et al.*, FAK and paxillin dynamics at focal adhesions in the protrusions of migrating cells. Sci Rep, 2014. 4: p. 6024.
353. Barry, Seán P., Paul A. Townsend, Richard A. Knight, Tiziano M. Scarabelli, David S. Latchman*, et al.*, STAT3 modulates the DNA damage response pathway. International Journal of Experimental Pathology, 2010. 91(6): p. 506-514.
354. Wei, Saisai, Xiangwei Gao, Juan Du, Jinfeng Su, and Zhengping Xu, Angiogenin Enhances Cell Migration by Regulating Stress Fiber Assembly and Focal Adhesion Dynamics. PLOS ONE, 2011. 6(12): p. e28797.
355. Dutta, S., C. Bandyopadhyay, V. Bottero, M. V. Veettil, L. Wilson*, et al.*, Angiogenin interacts with the plasminogen activation system at the cell surface of breast cancer cells to regulate plasmin formation and cell migration. Mol Oncol, 2014. 8(3): p. 483-507.
356. Arzumanian, V. A., O. I. Kiseleva, and E. V. Poverennaya, The Curious Case of the HepG2 Cell Line: 40 Years of Expertise. Int J Mol Sci, 2021. 22(23).
357. ATCC Hep G2 [HEPG2]. Accessed September 2023; Available from: https://www.atcc.org/products/hb-8065.
358. López-Terrada, D., S. W. Cheung, M. J. Finegold, and B. B. Knowles, Hep G2 is a hepatoblastoma-derived cell line. Hum Pathol, 2009. 40(10): p. 1512-5.
359. Kudo, Yotaro, Masayuki Sugimoto, Esperanza Arias, Hiroaki Kasashima, Thekla Cordes*, et al.*, PKCλ/ι loss induces autophagy, oxidative phosphorylation, and NRF2 to promote liver cancer progression. Cancer Cell, 2020. 38(2): p. 247-262. e11.
360. Makol, A., H. Kaur, S. Sharma, S. Kanthaje, R. Kaur*, et al.*, Vimentin as a potential therapeutic target in sorafenib resistant HepG2, a HCC model cell line. Clin Mol Hepatol, 2020. 26(1): p. 45-53.
361. Chen, Mingyue, Lei Jia, Xiaofeng Zheng, Mingshu Han, Lin Li*, et al.*, Ancient Human Endogenous Retroviruses Contribute to Genetic Evolution and Regulate Cancer Cell Type–Specific Gene Expression. Cancer Research, 2022. 82(19): p. 3457-3473.

362. Suzuki, Sawako, Divya Venkatesh, Hiroaki Kanda, Akitoshi Nakayama, Hiroyuki Hosokawa*, et al.*, GLS2 is a tumor suppressor and a regulator of ferroptosis in hepatocellular carcinoma. Cancer Research, 2022. 82(18): p. 3209-3222.
363. Wu, Kejia, Yiqi Zhang, Yuxin Liu, Qingxiu Li, Yong Chen*, et al.*, Phosphorylation of UHRF2 affects malignant phenotypes of HCC and HBV replication by blocking DHX9 ubiquitylation. Cell Death Discovery, 2023. 9(1): p. 27.
364. Xia, Anliang, Qi Yue, Mingming Zhu, Jianbo Xu, Siyuan Liu*, et al.*, The cancer-testis lncRNA LINC01977 promotes HCC progression by interacting with RBM39 to prevent Notch2 ubiquitination. Cell Death Discovery, 2023. 9(1): p. 169.
365. Shan, Ge, RNA interference as a gene knockdown technique. The International Journal of Biochemistry & Cell Biology, 2010. 42(8): p. 1243-1251.
366. Vakifahmetoglu, H., M. Olsson, and B. Zhivotovsky, Death through a tragedy: mitotic catastrophe. Cell Death & Differentiation, 2008. 15(7): p. 1153-1162.
367. Mansilla, S., W. Priebe, and J. Portugal, Mitotic catastrophe results in cell death by caspase-dependent and caspase-independent mechanisms. Cell Cycle, 2006. 5(1): p. 53-60.
368. Liu, Reng-Yun, Yuanyuan Zeng, Zhe Lei, Longqiang Wang, Haiping Yang*, et al.*, JAK/STAT3 signaling is required for TGF-β-induced epithelial-mesenchymal transition in lung cancer cells. International journal of oncology, 2014. 44(5): p. 1643-1651.
369. Zhang, Chuanhai, Fenglin Guo, Geliang Xu, Jie Ma, and Feng Shao, STAT3 cooperates with Twist to mediate epithelial-mesenchymal transition in human hepatocellular carcinoma cells. Oncology reports, 2015. 33(4): p. 1872-1882.
370. Hasin, Yehudit, Marcus Seldin, and Aldons Lusis, Multi-omics approaches to disease. Genome Biology, 2017. 18(1): p. 83.
371. Hassan, Md Imtaiyaz, Multi-omics approaches to therapeutic target identification. 2023, Oxford University Press. p. 75-75.
372. Dopazo, Joaquin, Genomics and transcriptomics in drug discovery. Drug Discovery Today, 2014. 19(2): p. 126-132.
373. Frantzi, Maria, Agnieszka Latosinska, and Harald Mischak, Proteomics in Drug Development: The Dawn of a New Era? PROTEOMICS – Clinical Applications, 2019. 13(2): p. 1800087.
374. Heath, James R., Antoni Ribas, and Paul S. Mischel, Single-cell analysis tools for drug discovery and development. Nature Reviews Drug Discovery, 2016. 15(3): p. 204-216.